Synchronisation, détection et égalisation de modulation à phase continue dans des canaux sélectifs en temps et en fréquence

Romain Chayot

THÈSE

En vue de l'obtention du

DOCTORAT DE L'UNIVERSITÉ DE TOULOUSE

Délivré par :

Institut National Polytechnique de Toulouse (Toulouse INP)

Discipline ou spécialité :

Informatique et Télécommunication

Présentée et soutenue par :

M. ROMAIN CHAYOT

le mardi 15 janvier 2019

Titre :

Synchronisation, détection et égalisation de modulation à phase continue dans des canaux sélectifs en temps et en fréquence

---

Ecole doctorale :

Mathématiques, Informatique, Télécommunications de Toulouse (MITT)

Unité de recherche :

Institut de Recherche en Informatique de Toulouse (I.R.I.T.)

Directeur(s) de Thèse :

M. CHARLY POULLIAT

MME MARIE LAURE BOUCHERET

Rapporteurs :

M. DANIEL ROVIRAS, CNAM PARIS

M. YVES LOUET, SUPELEC RENNES

Membre(s) du jury :

Mme MARYLINE HELARD, INSA DE RENNES, Président

M. CHARLY POULLIAT, INP TOULOUSE, Membre

M. CHRISTOPHE JEGO, UNIVERSITÉ DE BORDEAUX, Membre

Mme MARIE LAURE BOUCHERET, INP TOULOUSE, Membre

Mme NATHALIE THOMAS, INP TOULOUSE, Membre

Remerciements

Je souhaite remercier en premier lieu toutes les personnes qui, au quotidien, m'ont accompagné pendant ces trois années. Votre soutien a beaucoup compté et je vous en remercie chaleureusement.

Merci à mes directeurs de thèse, Charly Poulliat, Marie-Laure Boucheret et Nathalie Thomas pour leurs confiances, leurs encouragements et leurs soutiens au cours de ces années. Sans eux, ce travail ne se serait pas déroulé dans ces conditions quasi-optimal. Merci pour leurs conseils et les discussions qui ont permis de résoudre bien des problèmes auxquelles j'ai été confronté. Merci particulièrement à Charly qui a su me pousser pour réussir, comme tout bon mentor doit savoir faire.

Je tiens également à remercier mes encadrements « industriels » Guy Lesthievent (CNES) et Nicolas Van Wambeke (Thales Alenia Space) pour leur soutien durant la thèse.

Je remercie également toutes les personnes que j'ai pu côtoyer durant ces trois ans au laboratoire TéSA. Les discussions (plus ou moins pertinentes), la pause-café et la bonne ambiance ont été des facteurs déterminants à la réussite de cette thèse. Corinne, Jean-Yves, Philippe, David, Raoul, Patrice (et nos discussions passionnées d'Histoire), Sylvain, Quentin, Julien, Barbara, Selma (la liste est longue), Fabio, Adrien, Lorenzo (aka Chorizo), Isabelle... J'arrête la liste-là (puisqu'elle est en réalité bien trop longue) mais sachez que je vous remercie tous pour votre compagnie.

Je tiens particulièrement remercier Charles-Ugo et Simone, mes fidèles camarades de bureau, qui m'ont suivi lors de mon déménagement dans la bibliothèque de TéSA. Nos discussions, les blagues et votre bonne humeur me manquent. Ces derniers mois, lors de la préparation de la soutenance, j'ai été accompagné par de nouveaux collègues (et amis) à Thales. Merci à eux pour leur aide dans les répétitions mais également pour leur humour des plus fins et délicats. Puisqu'ils pimentent ma vie en dehors du travail, je remercie également tous mes amis qui ont aussi su m'accompagner durant ces trois ans dans les bons comme dans les mauvais moments.

Pour finir, mes remerciements vont à ma famille, mes sœurs et mes parents qui m'ont toujours soutenu dans mes choix scolaires et de carrière. Je leur dois ce que je suis devenu et je les remercie énormément.

Success always demands a greater effort. Wintson Churchill – 13 Décembre 1940

Contents

List of Figures

List of Tables

Table des sigles et acronymes

ASK	*Amplitude Shift Keying*
AWGN	Additive White Gaussian Noise
BCJR	Bahl, Cocke, Jelinek and Raviv
BEM	Basis Expansion Model
BER	Bit Error Rate
BICM	Bit Interleaved Coded Modulation
CFO	Carrier Frequency Offset
CNPC	Command and Non Payload Communication
CP	Cyclic Prefix
CPM	Continuous Phase Modulation
CRB	Cramer Rao Bound
DA	Data Aided
(I)DFT	(Inverse) Discrete Fourier Transform
EXIT	EXtrinsic Information Transfer
FD	Frequency Domain
FIR	Finite Impulse Response
FS	Fractionally-Spaced
FWD	ForWarD Link
GMSK	Gaussian Minimum Shift Keying
GPS	Global Positionning System
GSM	Global System for Mobile Communications
IR	Information Rate
LDPC	Low Density Parity Check code
LLR	Log Likelihood Ratio
LP	Laurent Pulses

LPF	Low Pass Filter
LS	Least Squares
LTV	Linear Time Varying
MAP	Maximum A Posteriori
ML	Maximum Likelihood
MSE	Mean Square Error
MMSE	Minimum Mean Square Error
MMSE-FDE	MMSE Frequency Domain Equalizer
OFDM	Orthogonal Frequency-Division Multiplexing
PAM	Pulse Amplitude Modulation
PSD	Power Spectral Density
PSK	Phase Shift Keying
RC	Raised Cosine
REC	RECtangular
RTN	ReTurN link
SC-FDE	Single Carrier Frequency Domain Equalization
SE	Spectral Efficiency
SISO	Soft Input Soft Output
SNR	Signal to Noise Ratio
SOQPSK	Shaped Offset Quadrature Phase Shift Keying
SVD	Singular Value Decomposition
TD	Time-Domain
TIV	Time InVariant
TV	Time Variant
UAV	Unmanned Aerial Vehicle
UW	Unique Word
ZF	Zero Forcing

Introduction (Français)

Contexte de la thèse

Alors que l'idée des drones (ou UAV pour son acronyme anglais) est apparue au début du siècle dernier avec le premier vol sur 100 kilomètres d'un avion équipé d'un système de pilotage automatique, les drones ne sont devenus populaires que depuis une poignée d'années pour des applications nombreuses et diverses. En effet, maintenant, les drones sont considérés pour des problématiques de télémesure, d'observation (surveillance des frontières et des forêts, inspections de ponts et de bâtiments), de télédétection, de communications (en cas de catastrophes naturelles par exemple), de divertissement (spectacles nocturnes), de livraison de marchandises, etc. Comme la présence d'un réseau de communication terrestre n'est pas garantie pour de nombreux cas d'usages, un lien de communication par satellite fiabiliserait les communications avec les drones, et particulièrement le lien de commande et contrôle. Enfin, il faut s'assurer de l'intégration complète et sûre des drones dans le trafic aérien actuel.

Pour le moment, les systèmes de communications de drone utilisent la bande KU Fixed Satellite Service (*FSS*) pour communiquer avec la station au sol à distance (RPS). L'organisation internationale de l'aviation civile (*ICAO*) et l'Union internationale des télécommunications (*ITU*) cherchent à standardiser un système de communications dans la bande C. L'annexe 10 de la Convention de Chicago relative à l'aviation civile internationale porte spécifiquement sur les télécommunications aéronautiques et récemment le Radio Technical Commission for Aeronautics (*RTCA*) a commencé à développer des exigences et des standards pour le lien de contrôle des drones (Control and Non-Payload Communication *CNPC*) avec en premier le lien terrestre [RCT16]. Concernant la couche physique, ils ont proposé une modulation à phase continue, la GMSK (Gaussian Minimum-Shift Keying), à cause de ses propriétés intéressantes, comme son efficacité énergétique, son occupation spectrale ou sa robustesse au bruit. Ainsi, dans l'optique de réduire l'encombrement des drones, des modulations à phase continue sont également considérées pour le lien satellitaire (comme illustré dans la Figure.1) et nous proposons dans cette thèse d'étudier cette famille de modulations non-linéaires.

L'ITU propose d'utiliser la bande de fréquence des 5030-5091 MHz (la bande C) pour le Aeronautical Mobile en-Route Service (AM(R)S) du lien de contrôle. Ce nouveau lien de communication ne devrait pas interférer avec l'infrastructure déjà en place. La Figure 2 résume les allocations de fréquence autour la bande C.

Dans ce scénario, le signal transmis est sujet à de fortes perturbations dues au canal aéronautique par satellite. De plus, à cause du contexte spatial, le signal sera également perturbé par les amplificateurs embarqués travaillant dans des régimes proches de la saturation. Différentes solutions ont été étudiées pour lutter contre ces problèmes comme la pré-distorsion (qui consiste à inverser la fonction de transfert des différentes distorsions), ou l'égalisation du signal à la réception. Des modulations sont par nature robustes à ces non-linéarités comme

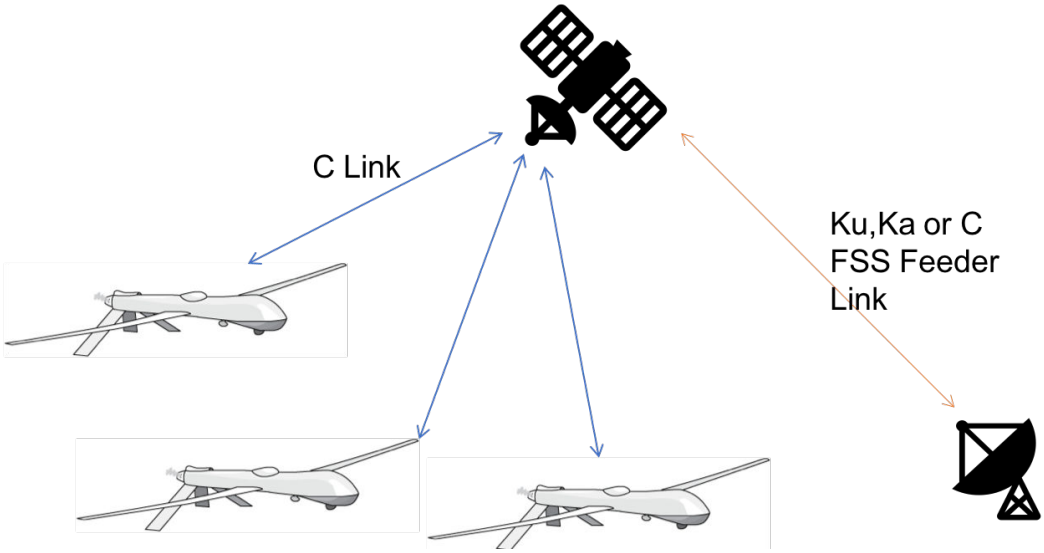

FIGURE 1 – Lien de commande et contrôle par satellite

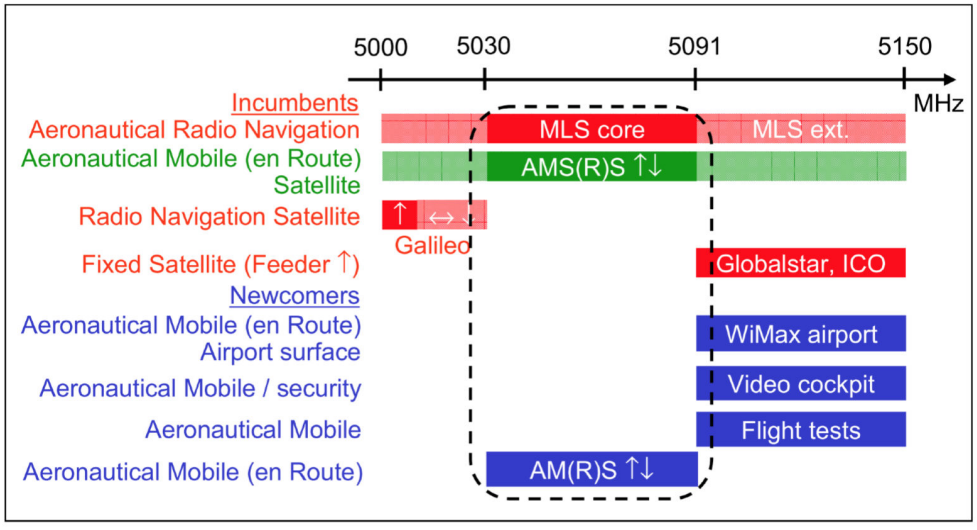

FIGURE 2 – Vue d'ensemble du spectre autour des 5GHz (de [Ben15]

les modulations Interplex ou les modulations à phase continue.

Dans ce thèse, nous allons considérer les modulations à phase continue puisque ces derniers présentent des propriétés intéressantes en terme d'occupation spectrale, de consommation énergétique et que leur structure est facilement utilisable dans le cadre d'une concaténation en série avec un code correcteur d'erreur.

Modulation à Phase Continue

Les modulations à phase continue (ou *CPM* pour *Continuous Phase Modulation*) sont considérées pour de nombreuses et diverses applications comme les communications avec l'espace lointain (deep space) [Sim05] [Yue06] ou plus récemment pour des applications de télémesure où la modulation SOQPSK (Shaped Offset Quadrature Phase Shift Keying) a été standardisée [IRI17]. Elles ont également été utilisées pour les communication mobiles (GSM) [DCTS97], les communications militaires [CFC10] [CFC10], communications sur ondes millimétriques [DHJ07] [Nse+07] et les communications équipement à équipement (Device to Device) dans la 5G [WGPS11] [Boc+16].

La CPM est une candidate en lice pour le lien de communication d'un drone à un satellite. En effet, son enveloppe complexe constante la rend robuste aux non-linéarités introduites par les amplificateurs embarqués travaillant à un régime saturé et ainsi améliore le bilan de liaison globale puisqu'elle ne nécessite pas de diminuer la puissance en entrée pour les HPA (High Power Amplifiers). De plus, son occupation spectrale est meilleure que celles de certaines modulations linéaires comme les modulations PSK (Phase Shift Keying), ce qui améliore la capacité du système de communication.

Les signaux CPM ont été grandement étudiés dans le cas de transmission sur des canaux à bruit blanc additif Gaussien (ou *AWGN*) et ont montré leur efficacité lors de leur concaténation en série avec un code correcteur (comme un code convolutif ou un code LDPC). Si un code LDPC est bien conçu, une CPM concaténée à ce code LDPC peut être proche de la capacité avec une complexité de décodage faible [Ben15].

De façon étonnante, pour des transmissions sur des canaux sélectifs en fréquence, le peu de travaux réalisés montre la difficulté de traiter cette famille de modulations non-linéaires dans ce contexte. [TS05], [PV06] et [VT+09] proposent des égaliseurs dans le domaine fréquentiel minimisant un critère d'erreur moyenne quadratique (*MMSE-FDE* pour Minimum Mean Square Error -Frequency-Domain Equalizers (*MMSE-FDE*)) dans le contexte de transmissions de signaux CPM sur des canaux sélectifs en fréquence. Cependant, comme montré dans cette thèse, [TS05] repose sur des hypothèses trop restrictives sur le canal de propagation pour en faire un schéma utilisable en pratique tandis que [PV06] et [VT+09] qui proposent deux approches différentes pour égaliser le signal (le premier repose sur la décomposition de Laurent) ont en fait les mêmes performances et sont équivalents (théoriquement prouvé dans [Cha+17a]). Dans les deux cas, ces méthodes par bloc ont une complexité calculatoire importante puisqu'elles requièrent d'inverser des matrix pleines, contrairement aux cas des

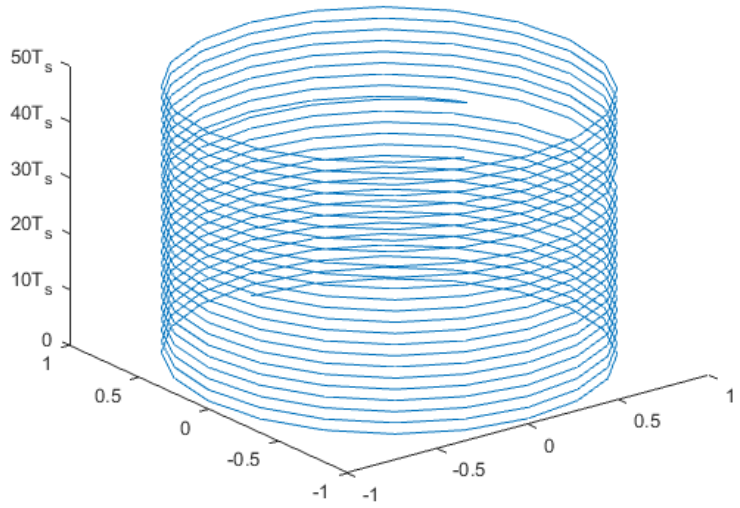

FIGURE 3 – Signal CPM dans le plan polaire (CPM quaternaire, L=2, h=1/4, RC

modulations linéaires (Single Carrier Frequency Domain Equalizer *SC-FDE*).

Les problématiques de synchronisation pour CPM sur canal AWGN ont été étudiées dans [MD97] où plusieurs chapitres lui sont entièrement consacrés. Une étude complète de la synchronisation temporelle, fréquentielle et trame pour CPM sur canal AWGN a été conduite au début des années 2010 dans [Hos13] où les bornes théoriques ont également été calculées. Cependant, à notre connaissance, la synchronisation pour signaux CPM tranmis sur des canaux sélectifs en fréquence ou doublement sélectifs n'a pas été étudiée. De plus, l'estimation canal est également une problématique fastidieuse qui a été très peu abordée.

Sans surprise, l'égalisation et la synchronisation pour CPM sur canaux doublement sélectifs ont été très étudiées dans des articles comme [Dar+16] pour l'égalisation ou plus récemment [OLS18] pour l'égalisation et une estimation canal aveugle conjointe.

Plan et contibutions principales

Pendant cette thèse, notre objectif a été d'étudier des récepteurs pour modulations à phase continue dans le cas de canaux sélectifs en fréquence ou doublement sélectifs. La principale application est le lien communication des drones par satellite (avec le canal dit aéronautique par satellite). Le plan du manuscrit de thèse et les principales contributions de la thèse sont résumés ci-dessous :

Chapitre 1 : Dans ce chapitre, nous donnons une description des signaux CPM. Nous définissons ces principaux paramètres et nous montrons leurs influences sur le signal. Quelques

notations utiles pour la suite sont également données. Nous introduisons également une représentation en treillis des signaux CPM [Lau86] et décrivons le récepteur associé dans le cas d'une transmission sur canal AWGN [CB05]. Finalement la structure globale d'un récepteur est décrite. Nous donnons également quelques pistes de réflexion sur des méthodes de précodage qui permettent soit d'augmenter l'efficacité spectrale [Mes+16] ; [OSL17] soit d'éviter d'itérer entre le détecteur et le code correcteur d'erreur [Per+10].

Chapitre 2 : Ce chapitre traite des transmissions de signaux CPM sur des canaux sélectifs en fréquence. Nous nous intéressons dans un premier temps à la problématique d'égalisation qui est plus complexe que dans le cas des modulations linéaires. En effet, dans le cas des modulations linéaires, nous avons un modèle linéaire gaussien par rapport aux symboles transmis ; ce n'est pas le cas avec les CPM. Cependant, un modèle linéaire Gaussien peut être obtenu par rapport à un vecteur de pseudo-symboles (provenant de la décomposition de Laurent [Lau86]) ou à un vecteur des échantillons de l'enveloppe complexe. Ainsi, dans ce chapitre, nous présentons les principaux égaliseurs de la littérature ([TS05] ; [PV06] ; [VT+09] et montrons leurs différences. Nous présentons également un nouvel égaliseur de faible complexité pour CPM qui est exact (i.e. qui ne fait aucune approximation sur le signal) et qui exploite les propriétés statistiques périodiques du signal dû à sa transmission par bloc étendu circulairement.

Dans un second temps, nous présentons des méthodes d'estimation canal pour CPM qui sont compatibles avec les précédents égaliseurs. De plus, nous développons un estimateur conjoint du canal et de l'erreur de fréquence résiduel (Carrier Frequency Offset) pour CPM, et montrons que sa variance atteint la borne de Cramér Rao Bound.

Les résultats de ce chapitre ont été publiés dans :

- Article de journal : R. Chayot, N. Thomas, C. Poulliat, M.-L. Boucheret, G. Lesthievent, N. Van Wambeke, "A New Exact Low-Complexity MMSE Equalizer for Continuous Phase Modulation", *IEEE Communications Letters*, 2018
- Article de conférence : R. Chayot, N. Thomas, C. Poulliat, M.-L. Boucheret, N. Van Wambeke, G. Lesthievent, "Channel Estimation and Equalization for CPM with application for aeronautical communications via a satellite link", *IEEE Int. Military Communications Conference (MILCOM)*, Baltimore (MD), U.S.A, 2017
- Article de conférence : R. Chayot, M.-L. Boucheret, C. Poulliat, N. Thomas, N. Van Wambeke, G. Lesthievent, "Joint Channel and Carrier Frequency Estimation for M-ary CPM over frequency-selective channel using PAM decomposition", *IEEE Int. Conf. Acoust., Speech, and Signal Proc. (ICASSP)*, New Orleans LA, U.S.A, 2017
- Article de conférence : R. Chayot, N. Thomas, C. Poulliat, M.-L. Boucheret, N. Van Wambeke, G. Lesthivent, "Sur l'égalisation fréquentielle des modulations à phase continue", *Colloque GRETSI sur le traitement du Signal*, Juan-les-pins, France, 2017

Chapitre 3 : Dans ce chapitre, nous nous consacrons au récepteur pour signaux CPM transmis sur des canaux doublement sélectifs. Après une courte description du modèle du

signal reçu, nous dérivons un nouvel égaliseur dans le domaine fréquentiel, qui exploite la structure en "bande" de la matrice canal dans le domaine fréquentiel pour réduire sa complexité au prix d'une approximation. A notre connaissance, l'égalisation de signaux CPM sur canal doublement-sélectifs a été très peu abordée avec par exemple [Dar+16] qui présente un égaliseur dans le domaine temporel.

Ensuite, nous présentons une méthode pour estimer ce canal doublement-sélectif grâce au Basis Expansion Model. Nous exploitons la structure de la trame du signal pour estimer ce canal et ensuite égaliser le signal reçu. Enfin, une extension de notre précèdent estimateur conjoint du canal et de fréquence est introduit.

Les différents résultats de ce chapitre ont été présentés dans :

- Article de conférence : R. Chayot, N. Thomas, C. Poulliat, M.-L. Boucheret, N. Van Wambeke, G. Lesthievent, "Doubly-Selective Channel Estimation for Continuous Phase Modulation", *IEEE Int. Military Communications Conference (MILCOM)*, Los Angeles (CA), U.S.A, 2018
- Article de conférence : R. Chayot, N. Thomas, C. Poulliat, M.-L. Boucheret, G. Lesthievent, N. Van Wambeke, "A Frequency-Domain Band-MMSE Equalizer for Continuous Phase Modulation over Frequency-Selective Time-Varying Channels", *European Signal Processing Conference (EUSIPCO)*, Rome, Italy, 2018

Chapitre 4 : Ce chapitre présente le système de communication pour le contexte de cette thèse, qui est le lien de commande et contrôle des drones par satellite. Dans un premier temps, nous décrivons les schémas de transmissions considérés pour la standardisation et faisons une analyse asymptotique de leurs performances (en donnant également des pistes pour une amélioration future). De plus, nous appliquons les méthodes présentées dans les chapitres précédents (détection, égalisation, estimation de paramètre) pour montrer leurs validités dans le contexte de la thèse.

Conclusion et Perspectives : Pour finir, nous résumons les résultats obtenus de cette thèse et nous tirons une conclusion sur ces deniers. De plus, nous identifions des pistes de travail pour de futurs travaux dans ce contexte.

Introduction

Context of the thesis

Even if the idea of Unmanned Aerial Vehicle (*UAV*) appears a century ago, with a first 100 kilometers-long flight of a plane with a remote/autonomous pilot system, UAVs became a very popular solution for a wide range of applications only since a few years. Indeed, UAVs are now considered for teledetection, earth observation (forest and border surveillance, buildings and bridges inspections), remote sensing, for communications (in case of natural disasters for instance), for entertainment (nighttime shows), for goods delivery, etc. Since the presence of terrestrial networks is not certain in a lot of those applications, a satellite communication link would ensure the reliability of the communication system with the UAV, and especially of the Command & Control link. Moreover, we have to ensure the complete and safe integration of UAV in the air traffic.

For the moment, UAV communication systems use the Ku-band Fixed Satellite Service (*FSS*) to communicate with the remote pilot station (RPS). However, the International Civil Aviation Organization (*ICAO*) and the International Telecommunication Union (*ITU*) want to standardize the UAV communication system in the C band. Annex 10 of the *Chicago Convention on International Civil Aviation* specifically deals with *Aeronautical Telecommunications* and recently the Radio Technical Commission for Aeronautics (*RTCA*) started to develop requirements and standards for the Control and Non-Payload Communication (*CNPC*) with a terrestrial link [RCT16]. Regarding the physical layer, they proposed a Gaussian Minimum-Shift Keying (*GMSK*) modulation, due to its many favorable properties, such as low-power consumption, high spectral efficiency, and noise robustness. Hence, in order to reduce the weight of UAV, Continuous Phase Modulation are also considered for the satellite link (as illustrated in Fig.4) and we will only study this link in this thesis.

The ITU proposes to use the the 5030-5091 MHz frequency band (C-band) especially for the Aeronautical Mobile en-Route Service (AM(R)S) for the CNPC. This new established communication link should not interfere with the existing infrastructure. Figure 5 summarizes the main frequency allocations within the targeted 5GHz band.

The transmitted signal would be subject to strong disturbance due to aeronautical channel by satellite. Furthermore, due to the satellite context, it would also be disturbed when embedded amplifiers are working near saturation. Different solutions can be considered to mitigate this issue as pre-distortion (which consists in inverting the transfer function of the distortions), or counterbalancing those distortions of the received signal by equalizing the signal. Others can also considered modulations schemes which are by nature robust to those non-linearities such as Interplex modulation or Continuous Phase Modulation.

In this thesis, we will consider Continuous Phase Modulation as it offers interesting power and spectral efficiency but also for its structure easily adaptable for serially concatenated

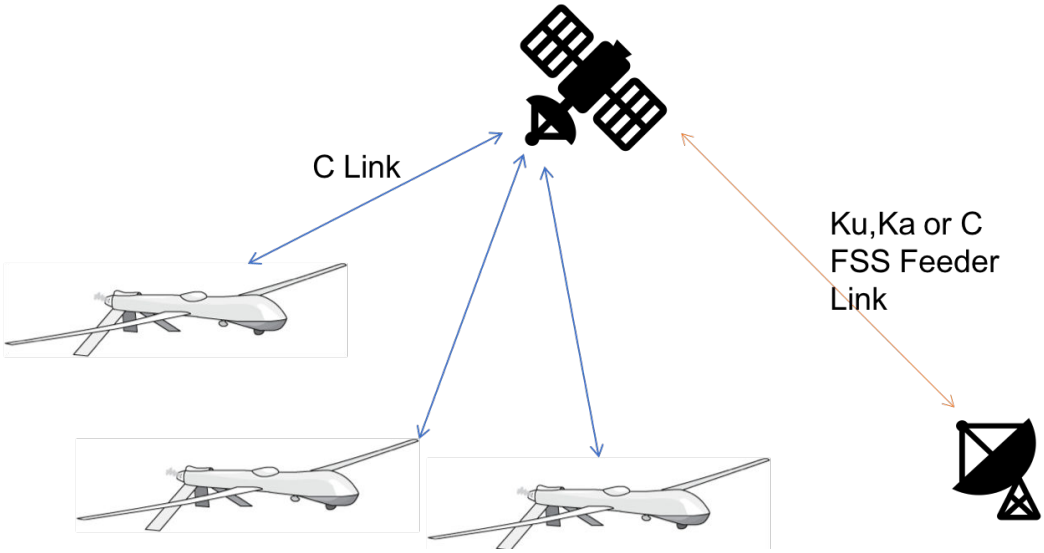

Figure 4 – CNPC by satellite

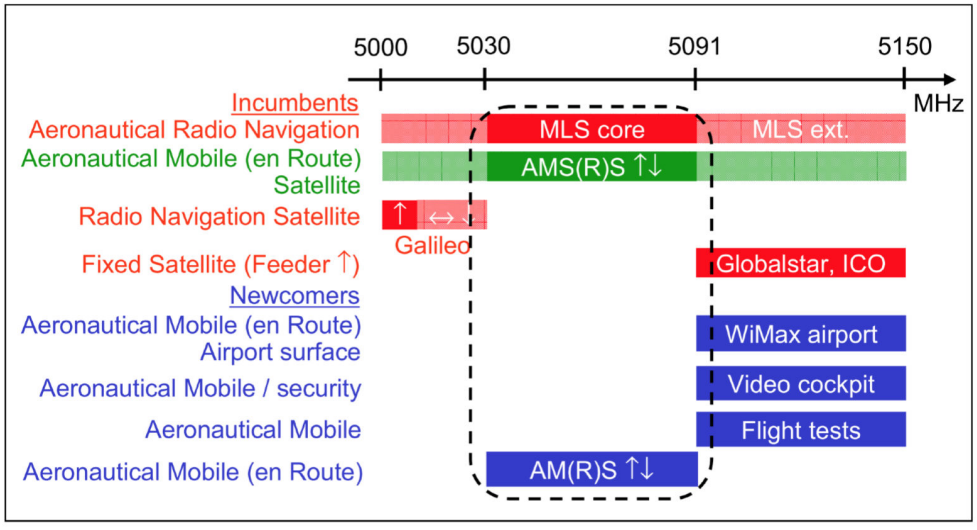

Figure 5 – Overview of the 5GHz Spectrum (from [Ben15]

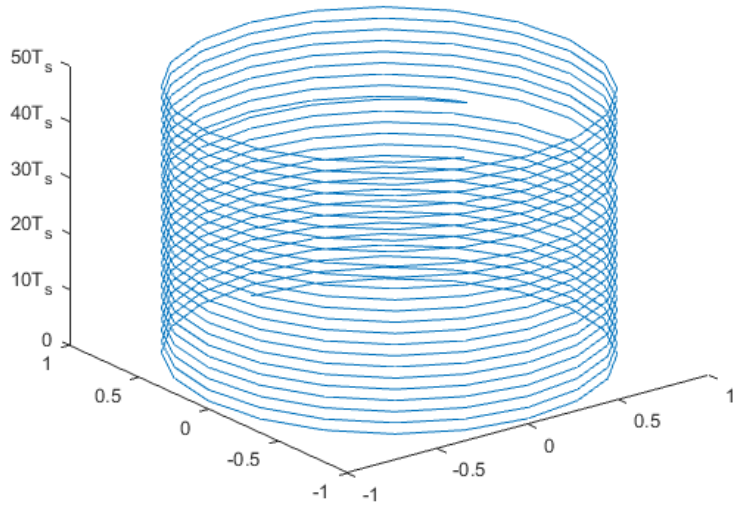

Figure 6 – CPM signal in a polar plan (Quaternary CPM, L=2, h=1/4, RC pulse shape

schemes with an outer code.

Continuous Phase Modulation

Continuous Phase Modulation (*CPM*) are considered for a lot of different applications such as deep-space communications [Sim05] [Yue06] and more recently for telemetry applications where SOQPSK (Shaped Offset Quadrature Phase Shift Keying) modulation are standardized [IRI17]. They have been used or are currently considered also for mobile communications (GSM) [DCTS97], military communications [CFC10] [CFC10], millimeter communications [DHJ07] [Nse+07] and machine-type communications in 5G [WGPS11] [Boc+16].

CPM is a suitable candidate for the communication link between a satellite and a UAV. Indeed, the constant complex envelop makes them robust to non-linearities introduced by embedded amplifiers working at the saturation regime and therefore improves the overall link budget as it does not require back-off for High Power Amplifiers (*HPA*). Moreover, it has a better spectral occupancy than linear modulations such as Phase Shift Keying (*PSK*) modulation, which will also increase the system capacity.

CPM signals have been well studied for transmission over Additive White Gaussian Noise (*AWGN*) channel and also prove to be efficient when used with serially concatenated schemes (a convolutional code or a LPDC code as an outer code for example). If properly designed, a Low-Density Parity-Check (*LDPC*) code concatenated with a CPM can be close to the capacity with low decoding complexity [Ben15].

Surprisingly, for transmission over frequency-selective channels, few papers show that this kind of non-linear modulation are more difficult to handle, compared to linear modulation schemes. [TS05], [PV06] and [VT+09] propose different Minimum Mean Square Error - Frequency-Domain Equalizers (*MMSE-FDE*) for CPM transmission over frequency-selective channels. However, as we will see in this thesis, [TS05] made some hypothesis on the channel which make its practical interest limited, whereas [PV06] and [VT+09] proposed two different approaches (the first one capitalizes on the Laurent Decomposition) but in fact reached the same performance as shown theoretically and by simulation in [Cha+17a]. In both cases, they proposed block methods requiring an important computational complexity as it does require a *full*-matrix inversion, unlike the Single Carrier Frequency Domain Equalizer (*SC-FDE*) for linear modulations.

Synchronization for CPM signals over AWGN channels have been studied in [MD97] where several chapters of this book are dedicated to this family of modulation. A full study of timing, carrier and frame synchronization for CPM over AWGN channel has been carried out in 2012 in [Hos13] where also theoretical bounds are derived. But, to our knowledge, the case of a transmission over frequency-selective or doubly-selective channels has not been considered for the synchronization. Moreover, channel estimation is also a tedious issue which has not been well studied.

With no genuine surprise, equalization and synchronization for a CPM transmission over a doubly-selective channel have been studied in a very few papers such as [Dar+16] for equalization or [OLS18] for joint equalization and blind channel estimation.

Dissertation outline and main contributions

In this thesis, we aim to study different receiver techniques for Continuous Phase Modulation over frequency-selective and doubly-selective channels. The main application will be the aeronautical channel for UAV communications by satellite. The dissertation outline and the main contributions are summarized bellow:

Chapter 1: In this chapter, we give an introduction to CPM signals. We define its main parameters, show their influences on the signal and also give some notations. We also introduce a trellis representation of the CPM signals [Lau86], and its associated detector [CB05] for a transmission over an AWGN channel, to finally describe the overall receiver structure. We give some clues about how to use precoding to enhance the Spectral Efficiency of legacy CPM scheme [Mes+16]; [OSL17] and also how to avoid turbo-detection/decoding [Per+10] in case of serially concatenated CPM schemes.

Chapter 2: This chapter deals with CPM transmissions over frequency-selective channels (also called time-invariant channels). We will first address channel equalization, which is a little more tedious than for the linear modulation case. Indeed, if in the case of linear modulation, we have a Gaussian linear model of the received signal regarding the transmitted data symbols, this is not the case for CPM signals. However, we do have a Gaussian linear

model of the received signal with respect to a vector of pseudo-symbols (coming from the Laurent decomposition [Lau86]) or to a vector of collected samples of the received complex envelop. Hence, in this chapter, we will present the main equalizers from the literature ([TS05]; [PV06]; [VT+09] and point out their similitude and differences. We will also present a new *exact* low-complexity equalizer for CPM which exploits the periodic statistics of the signal in case of circular-extended block-based transmissions.

In a second time, we will present some channel estimation methods for CPM which are compatible with the latter equalizers. We will also present a joint channel and carrier frequency estimation for CPM, and show that the variance achieves the derived Cramér Rao Bound (*CRB*).

The results of this chapter are published in:

- Journal: R. Chayot, N. Thomas, C. Poulliat, M.-L. Boucheret, G. Lesthievent, N. Van Wambeke, "A New Exact Low-Complexity MMSE Equalizer for Continuous Phase Modulation", *IEEE Communications Letters*, 2018
- Paper: R. Chayot, N. Thomas, C. Poulliat, M.-L. Boucheret, N. Van Wambeke, G. Lesthievent, "Channel Estimation and Equalization for CPM with application for aeronautical communications via a satellite link", *IEEE Int. Military Communications Conference (MILCOM)*, Baltimore (MD), U.S.A, 2017
- Paper: R. Chayot, M.-L. Boucheret, C. Poulliat, N. Thomas, N. Van Wambeke, G. Lesthievent, "Joint Channel and Carrier Frequency Estimation for M-ary CPM over frequency-selective channel using PAM decomposition", *IEEE Int. Conf. Acoust., Speech, and Signal Proc. (ICASSP)*, New Orleans LA, U.S.A, 2017
- Paper: R. Chayot, N. Thomas, C. Poulliat, M.-L. Boucheret, N. Van Wambeke, G. Lesthivent, "Sur l'égalisation fréquentielle des modulations à phase continue", *Colloque GRETSI sur le traitement du Signal*, Juan-les-pins, France, 2017

Chapter 3: In this chapter, we will oversee receivers techniques for CPM transmission over doubly-selective channels. First, after a short presentation of the system model, we will derive an *approximate* frequency-domain equalizer for CPM over doubly-selective channels, which exploits the *band* structure of the channel matrix in the frequency-domain to reduce its computational complexity. To our knowledge, only a few equalizers consider the case of doubly-selective channels such as the one in [Dar+16] which is in the Time-Domain.

Then, we will also present how to estimate a doubly-selective channel using the well-known Basis Expansion Model. We will use the particular block-based structure of our CPM transmission to perform such channel estimation and then equalize the received signal. Last, an extension of our previous joint channel and carrier frequency estimation for CPM over doubly-selective channels will be introduced.

The different results of this chapter are published in:

- Paper: R. Chayot, N. Thomas, C. Poulliat, M.-L. Boucheret, N. Van Wambeke, G. Lesthievent, "Doubly-Selective Channel Estimation for Continuous Phase Modulation", *IEEE Int. Military Communications Conference (MILCOM)*, Los Angeles (CA), U.S.A, 2018

- Paper: R. Chayot, N. Thomas, C. Poulliat, M.-L. Boucheret, G. Lesthievent, N. Van Wambeke, "A Frequency-Domain Band-MMSE Equalizer for Continuous Phase Modulation over Frequency-Selective Time-Varying Channels", *European Signal Processing Conference (EUSIPCO)*, Rome, Italy, 2018

Chapter 4: This chapter presents the system for the context of this thesis, which is the CNPC of UAV using a satellite communication link. We will first present the transmission schemes which are currently considered for standardization and also provide an asymptotic analysis of those links (giving some clues on their improvements). Also, we will assess our proposed methods (detection, channel equalization and parameters estimation) in order to show their validity in such contexts.

Conclusion and Perspective: Finally we summarize the main results of this thesis and conclusion is drawn. Moreover, we identify potential future work.

List of publications

Journal Papers

1. R. Chayot, N. Thomas, C. Poulliat, M.-L. Boucheret, G. Lesthievent, N. Van Wambeke, "A New Exact Low-Complexity MMSE Equalizer for Continuous Phase Modulation", *IEEE Communications Letters*, 2018

International conference papers

2. R. Chayot, N. Thomas, C. Poulliat, M.-L. Boucheret, N. Van Wambeke, G. Lesthievent, "Doubly-Selective Channel Estimation for Continuous Phase Modulation", *IEEE Int. Military Communications Conference (MILCOM)*, Los Angeles (CA), U.S.A, 2018

3. R. Chayot, N. Thomas, C. Poulliat, M.-L. Boucheret, G. Lesthievent, N. Van Wambeke, "A Frequency-Domain Band-MMSE Equalizer for Continuous Phase Modulation over Frequency-Selective Time-Varying Channels", *European Signal Processing Conference (EUSIPCO)*, Rome, Italy, 2018

4. R. Chayot, N. Thomas, C. Poulliat, M.-L. Boucheret, N. Van Wambeke, G. Lesthievent, "Channel Estimation and Equalization for CPM with application for aeronautical communications via a satellite link", *IEEE Int. Military Communications Conference (MILCOM)*, Baltimore (MD), U.S.A, 2017

5. R. Chayot, M.-L. Boucheret, C. Poulliat, N. Thomas, N. Van Wambeke, G. Lesthievent, "Joint Channel and Carrier Frequency Estimation for M-ary CPM over frequency-selective channel using PAM decomposition", *IEEE Int. Conf. Acoust., Speech, and Signal Proc. (ICASSP)*, New Orleans LA, U.S.A, 2017

National conference papers

6. R. Chayot, N. Thomas, C. Poulliat, M.-L. Boucheret, N. Van Wambeke, G. Lesthivent, "Sur l'égalisation fréquentielle des modulations à phase continue", *Colloque GRETSI sur le traitement du Signal*, Juan-les-pins, France, 2017

Chapter 1

Communication systems using CPM Signals

Contents

Résumé

Dans ce chapitre, nous donnons une description rapide des Modulations à Phase Continue (*CPM*). Les modulations à phase continue sont une classe de modulation non linéaire qui a la particularité d'avoir une enveloppe complexe constante, les rendant robustes aux non-linéarités comme celles introduites par les amplificateurs embarqués. De plus, les signaux CPM ont généralement un lobe spectral principal plus étroit que les modulations linéaires de type *PSK* (Phase Shift Keying). Pour les CPM, les symboles de données sont filtrés par une fonction de mise en forme de la phase assurant la continuité de cette dernière.

Le nom de modulation à phase continue a été introduit dans les papiers fondateurs [ARS81a] [ARS81b] de Tor Aulin, sous la supervision de Carl-Erik Sundberg où une étude théorique de ces signaux a été réalisée et leur structure en treillis exhibée. Cependant, les premières CPM sont apparues avant dans les années 70 avec les modulations Minimum Shift Keying (*MSK*) et Frequency Shift Keying (*FSK*).

Les signaux CPM sont envisagés pour de nombreuses applications comme les communications militaires [CFC10], les communications à 60Ghz [Nse+07], l'Internet des Objets [DL12], la télémesure aéronautique [Ran15] [IRI17] ou encore les communications aéronautiques [RCT16].

Dans un premier temps, nous donnons une définition des signaux CPM et exposons leurs paramètres et leurs influences sur le signal émis. Ensuite, nous décrivons les récepteurs associés de type Maximum A Posteriori (MAP) aux signaux CPM dans le cas d'une transmission sur canal AWGN utilisant la décomposition de Laurent, qui permet d'écrire un signal CPM comme la somme de modulations PAM modulés par des pseudo-symboles (corrélés et ayant une relation non-linéaire entre eux). Nous en profitons également pour montrer comment cette décomposition peut être utilisée pour calculer la fonction d'auto-corrélation d'un signal CPM. Enfin, nous présentons deux techniques de pré-codage qui permettent soit d'améliorer l'efficacité spectrale d'un schéma considéré soit de rendre inutile les itérations entre code correcteur d'erreur et détecteur CPM.

1.1 Introduction

Continuous Phase Modulation (CPM) signals are a class of non-linear modulations which have the property of having a constant complex envelop, making them robust to non-linearities such as the ones introduced by embedded amplifiers. For CPM signals, the data symbols are filtered by a phase shaping function which ensures continuous phase from one symbol to another.

The name Continuous Phase Modulation has been introduced in the two seminal papers [ARS81a] [ARS81b] where Tor Aulin, under the supervision of Carl-Erik Sundberg, finalized the theoretical study of CPM signals and of their underlying trellis representations. However, the first CPM system traces back to the 70's with the Minimum Shift Keying (MSK) and Frequency Shift Keying (FSK) modulations. Later, by exploiting the trellis structure of those two modulations, and with the objective of improving the euclidean distance properties, the Continuous Phase Frequency Shift Keying ($CPFSK$) has been introduced, which consists of a different modulation index.

CPM signals are considered for a lot of applications such as military communications [CFC10], 60Ghz communications [Nse+07], Internet of Things [DL12], aeronautical telemetry [Ran15] [IRI17] and also aeronautical communications [RCT16]. Indeed, their constant envelop made them suitable to transmissions through non-linear channels where the amplitude of the signal is distorted. Moreover, as the phase transition are continuous, CPM signals benefit from a narrow spectral main lobe (compared to Phase Shift Keying (PSK) linear modulations).

Last, as we will show in this chapter, their Markov structure makes them suitable for serially concatenated schemes. Several works were conducted on serial concatenated schemes with convolutional codes or other short block codes (see [AAS13] [AS06] and [MA01]). More

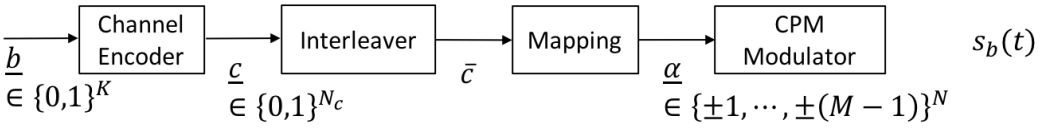

Figure 1.1 – BICM for CPM signals

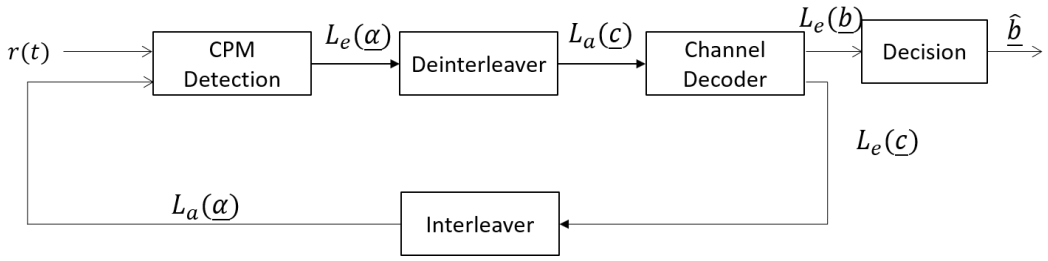

Figure 1.2 – Overall CPM receiver

recently, [Ben15] proposed the asymptotic analysis and the design of turbo-CPM systems based on the optimization of sparse graph-based codes.

1.2 Communication systems for CPM over AWGN channels

1.2.1 CPM transmitter

In this thesis, we will consider a Bit Interleaved Coded Modulation (*BICM*) for CPM, as illustrated in Fig.1.1. At the transmitter side, a binary message $\underline{\boldsymbol{b}}$ of length K is encoded to a codeword $\underline{\boldsymbol{c}}$ of length N_c using a error correcting code of rate $R = K/N_c$ and, after being interleaved, sent to a M-ary mapper to obtain a sequence $\underline{\boldsymbol{\alpha}} \in \{\pm 1, \pm 3, \ldots, \pm(M-1)\}^N$. This data symbols sequence is then given to the CPM modulator. The transmitted complex envelop of the CPM signals is described in Section 1.3.

1.2.2 Receiver Structure

In this chapter, we only consider a transmission over an AWGN channel and perfect synchronization is assumed (Phase noise is not included ; carrier frequency offset, time offset and Doppler spread are not considered either). Hence, at the receiver side, the complex envelope of the received signal is:

$$r(t) = s_b(t) + w(t) \tag{1.1}$$

where $w(t)$ is a complex white gaussian noise with two-sided power spectral density $2N_0$.

The received signal is fed to a soft CPM receiver (as the one described in 1.3.3) and

we perform Soft Input-Soft Output (*SISO*) channel decoding, based on the BCJR algorithm [Bah+74]. If iterative turbo detection is used, iterations are performed on extrinsic log likelihood ratio between the CPM detection and the channel decoder. As we will show, later in Section 1.3.4, in most legacy CPM schemes, turbo-detection is mandatory to avoid any loss of performance and to achieve code capacity. The overall receiver is illustrated in Fig.1.2.

1.3 CPM signals

1.3.1 Definition of CPM signals

Let $\underline{\boldsymbol{\alpha}} = \{\alpha_n\}_{0 \leq n \leq N-1} \in \{\pm 1, \pm 3, \ldots, \pm M-1\}^N$ be a sequence of N symbols taken from a M-ary alphabet . The complex envelope $s_b(t)$ associated with the transmitted CPM signal is written as follows

$$s_b(t) = \sqrt{\frac{2E_s}{T_s}} \exp\left(j\theta(t, \underline{\boldsymbol{\alpha}})\right) \tag{1.2}$$

where

$$\theta(t, \underline{\boldsymbol{\alpha}}) = 2\pi h \sum_{i=0}^{N-1} \alpha_i q(t - iT_s)$$

and

$$q(t) = \begin{cases} \int_0^t g(\tau)d\tau, t \leq LT_s \\ 1/2, t > LT_s \end{cases}$$

E_s is the symbol energy, T_s is the symbol period, $\theta(t, \underline{\boldsymbol{\alpha}})$ is the information phase, $g(t)$ is the pulse response, h is the modulation index and L is the CPM memory.

All those parameters and how they affect the CPM properties are discussed in the following.

1.3.1.1 The Pulse Response $q(t)$

The pulse response is defined as the primitive function of the frequency pulse $g(t)$: and

$$q(t) = \begin{cases} \int_0^t g(\tau)d\tau, t \leq LT_s \\ 1/2, t > LT_s \end{cases}$$

It ensures the continuity of the modulation phase as it defines the shape of the phase trajectory. Different shapes have been studied since several years allowing the signal to achieve different properties. We choose to focus on different shapes: Raised Cosine (RC) Shape,

Name	Frequency Pulse	Support	Parameters
REC	$g(t) = \frac{1}{2LT_s}$	$[0, LT_s]$	L
RC	$g(t) = \frac{1}{2LT_s}(1 - \cos(\frac{2\pi t}{LT_s}))$	$[0, LT_s]$	L
Mixed RC-REC	$(1-\alpha)g_{\text{REC}}(t) + \alpha g_{\text{RC}}(t)$	$[0, LT_s]$	L, α
GMSK	$g(t) = \frac{1}{LT_s}\left\{Q(2\pi B\frac{t-T_s/2}{\sqrt{ln(2)}}) - Q(2\pi B\frac{t+T_s/2}{\sqrt{ln(2)}})\right\}$	Infinite	L, $0 < BT_s < 1$

Table 1.1 – Pulse Shape Table

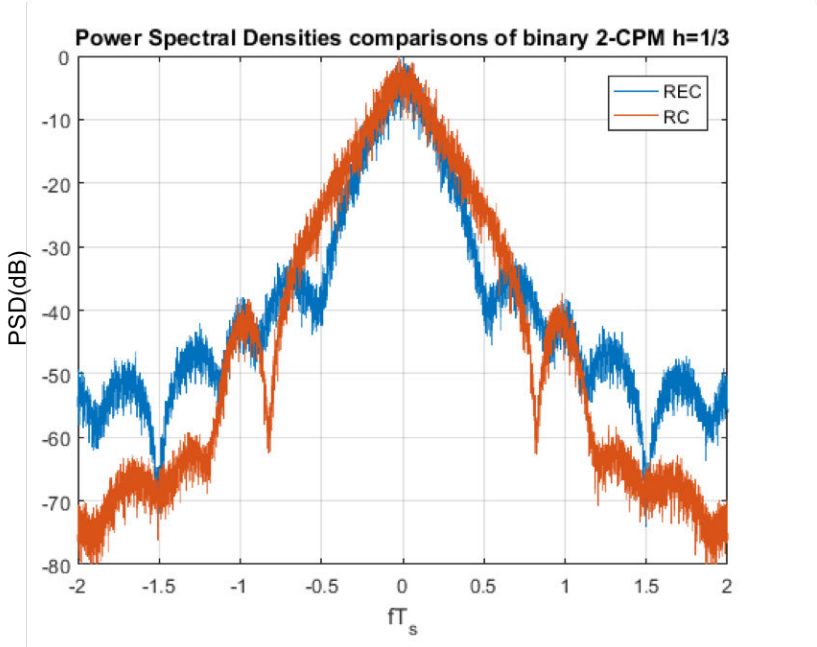

Figure 1.3 – Power Spectral Densities for a RC and REC pulse shape CPM schemes, $h = 1/3$ and $L = 2$

Rectangular (*REC*) Shape, Mixed Raised Cosine and Rectangular (*Mixed RC-REC*) shape and the Gaussian Minimum Shift Keying (*GMSK*) shape. Table 1.1 defines those commonly used shapes.

As illustrated in Fig.1.3 where the Power Spectral Densities (*PSD*) are plotted, the REC pulse shape has a narrower main lobe compared to the RC pulse shape, but it has a greater out-of-band power leakage.

1.3.1.2 The Modulation Index h

This a real number, usually smaller than 1. Generally, it is a constant although in CPM schemes known as *multi*-h CPM [PT87], it can change cyclically during the transmission (multi-h CPM signals are out of the scope of this thesis). h can also take irrational values, but it leads to a high complexity receiver and then it is not the case in most legacy CPM

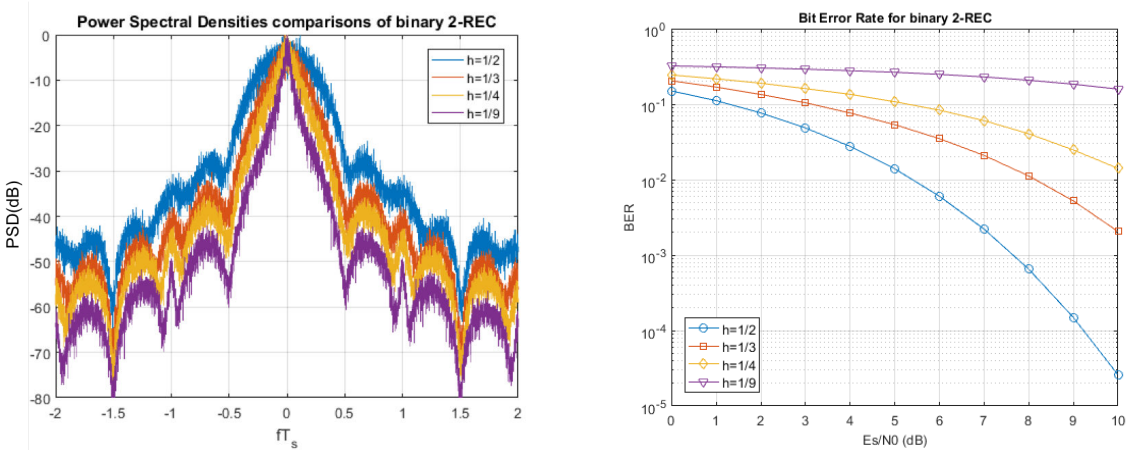

Figure 1.4 – Influence of h on the Power Spectral Density and on the Bit Error Rate

schemes.

A smaller h results in a narrower occupied bandwidth, but at the price of a smaller minimal distance as illustrated in Fig.1.4. Generally, h is a rational number such as $h = \frac{k}{p}$.

1.3.1.3 The CPM Memory L

The CPM Memory L is defined as the support length of $g(t)$. It is also the size of the memory associated to the trellis representation of a CPM signal. In the case where $L = 1$, CPM signals are called *total response* CPMs. For instance, Continuous-Phase Frequency-Shift Keying (*CPFSK*) modulation and Minimum-Shift Keying (*MSK*) modulation are total response CPMs.

In the case where $L > 1$, we refer to *partial response* CPMs, as the one defined in the DVB-RCS2 standard or the ones considered for standardization for the UAV communication link by satellite.

As L increases, the spectrum occupancy decreases. However, it will increase complexity for the CPM detection as shown latter.

1.3.2 PAM Representation

CPM signals are a non-linear modulation scheme with memory. Hence, it can be represented as a finite-state machine. This structure implies the existence of a trellis representation of the CPM signal. First, [ARS81b] has proposed a time-variant trellis with a number of states that depends on the modulation index. To simplify this structure, [Rim88] introduced a time-invariant trellis. Its associated receiver is composed of a bank of pM^L filters and a non-linear Soft Input Soft Output MAP detector. This representation is often used in the study of

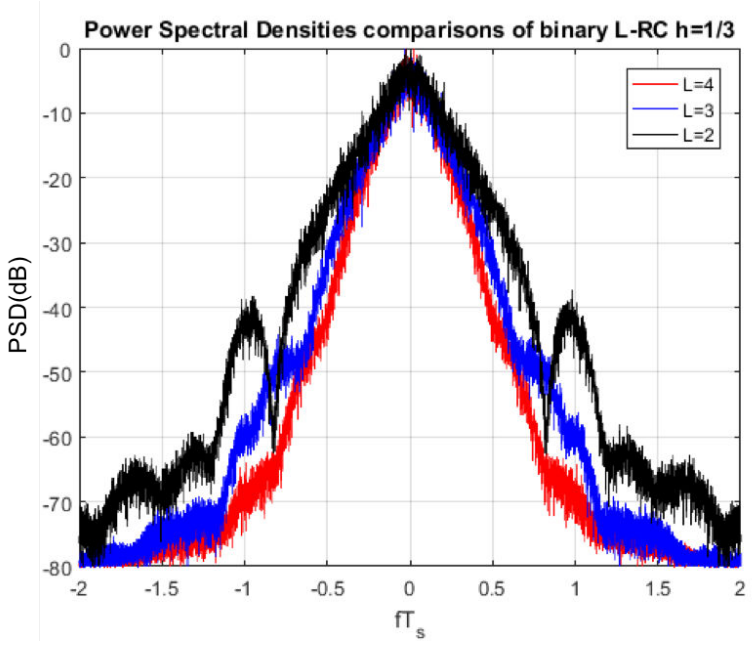

Figure 1.5 – Influence of the CPM memory L on the PSD

CPM schemes serially concatenated with an outer channel coder. However, in the literature, low-complexity CPM detectors have been developed [Kal89] [CB05] by capitalizing on the Laurent Decomposition.

The Laurent Decomposition has been introduced in [Lau86] for binary CPM signals with non-integer modulation index. This decomposition allows us to write the CPM signal as a sum of modulated PAM, where the non-linearity is within the complex pseudo-symbols dependency. In this section, we will present this decomposition and exhibits the underlying trellis structure of the CPM signal.

For more details on the influence of the parameters, readers may refer to [AAS13] and [Cha+04].

1.3.2.1 Derivation

We recall that a CPM signal is given in Eq.(1.2). In this part, we only consider binary CPMs with non-integer modulation index. Using the Laurent Decomposition, the complex baseband signal $s_b(t)$ can be expressed as the sum of $K = 2^{L-1}$ pulse amplitude-modulated

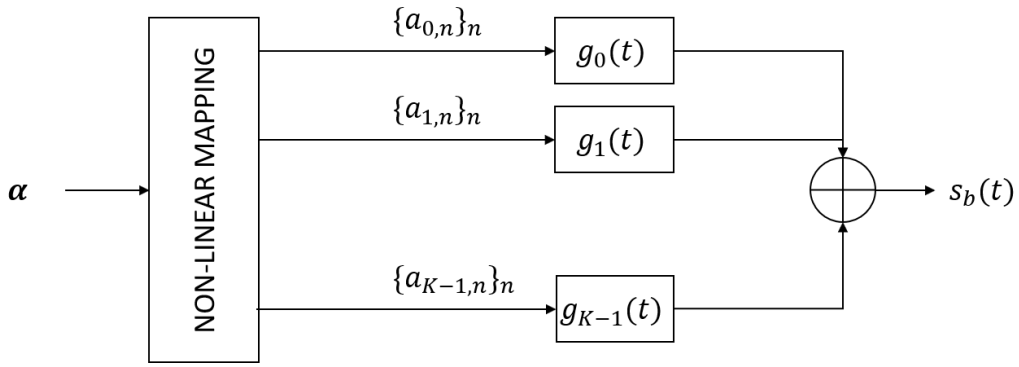

Figure 1.6 – Laurent Representation of a CPM signal

signals (PAM), modulated by complex pseudo-symbols $a_{k,n}$:

$$s_b(t) = \sum_{k=0}^{K-1} \sum_{n=0}^{N-1} a_{k,n} g_k(t - nT_s) \tag{1.3}$$

$$g_k(t) = s_0(t) \prod_{j=1}^{L-1} s_{j+L\beta_{k,j}}(t), 0 < k \leq K-1$$

$$a_{k,n} = e^{j2\pi h A_{k,n}}$$

$$A_{k,n} = \sum_{i=0}^{n} \alpha_i - \sum_{j=1}^{L-1} \alpha_{n-j}\beta_{k,j}$$

$$s_j(t) = \frac{\sin(\psi(t + jT_s))}{\sin(h\pi)}$$

$$\psi(t) = \begin{cases} 2\pi h q(t), & 0 \leq t \leq LT_s \\ \pi h - 2\pi h q(t - LT_s), & LT_s \leq t \leq 2LT_s \\ 0, & \text{elsewhere} \end{cases} \tag{1.4}$$

where $\beta_{k,j}$ refers to the j^{th} bit in the binary representation of k, $k \in 0, 1, \ldots, K-1$:

$$k = \sum_{j=1}^{L-1} \beta_{k,j} 2^{j-1}$$

Using this representation, a CPM signal can be seen as a sum of linear modulations with correlated pseudo-symbols as shown in Fig.1.6. The K Laurent Pulses $\{g_k(t)\}_{0 \leq k \leq K-1}$ have different duration lengths by construction, as reported in Table 1.2.

An example of the Laurent Pulses (LP) is given in Fig.1.7 for a binary CPM with a RC pulse shape, $h = 1/2$ and a memory $L = 3$. This CPM signals can be represented by four pulses.

As we can see in Fig.1.7, by considering only the first LP which contains most of the energy, a rather good approximation of binary CPM signals with non-integer modulation

Laurent Pulse	Duration
$g_0(t)$	$(L+1)T_s$
$g_1(t)$	$(L-1)T_s$
$g_2(t)$,$g_3(t)$	$(L-2)T_s$
$\vdots$	$\vdots$
$g_{K/2}$, $\cdots$, g_{K-1}	T_s

Table 1.2 – Duration of the Laurent Pulses

index is obtained:

$$s_b(t) \approx \sum_{n=0}^{N-1} a_{0,n} g_0(t - nT_s) \tag{1.5}$$
$$a_{0,n} = e^{j2\pi h \sum_{i=0}^{n} \alpha_i}$$

This properties is often used for CPM detection as it allows to design low-complexity receivers without a noticeable loss of performance.

Extension of the Laurent Decomposition The Laurent decomposition only considers the case of binary CPM with non-integer modulation index. [MM95] extends this decomposition to M-ary CPM, by writing a M-ary CPM signal as a product of binary CPM signals and by applying the Laurent Decomposition on them. Indeed, in this case, a symbol from the M-ary alphabet $\{\pm 1, \pm 3, \ldots, \pm(M-1)\}$ is written as $\alpha_i = \sum_{p=0}^{P-1} 2^p b_i^p$ with $\{b_i^p\}_p \in \{\pm 1\}^P$ and $P = \log_2(M)$. Therefore, the transmitted CPM signal is given by:

$$s_b(t) = \exp\{\pi h \sum_{i=0}^{N-1} \alpha_i q(t - iT)\} \tag{1.6}$$
$$= \exp\{\pi h \sum_{i=0}^{N-1} (\sum_{p=0}^{P-1} 2^p b_i^p) q(t - iT)\} \tag{1.7}$$
$$= \sum_{p=0}^{P-1} \exp\{\pi h 2^p b_i^p q(t - iT)\} \tag{1.8}$$
$$= \sum_{p=0}^{P-1} s_{\text{bin}}(t; b^p, q, 2^p h) \tag{1.9}$$

where $s_{\text{bin}}(t; b^p, q, 2^p h)$ is a binary CPM with the pulse shape $q(.)$, an index modulation $2^p h$ and a binary input sequence $\{b_i^p\}_{0 \le i \le N-1}$. The Laurent decomposition is applied on those binary CPM signals to obtain the PAM decomposition of the M-ary CPM signal.

Also [HL03] extends this work for CPM signals with integer modulation index. [PR05] presents the PAM decomposition for multi-h CPM schemes. In this thesis, we will refer to all those decomposition as the PAM Decomposition of a CPM signal.

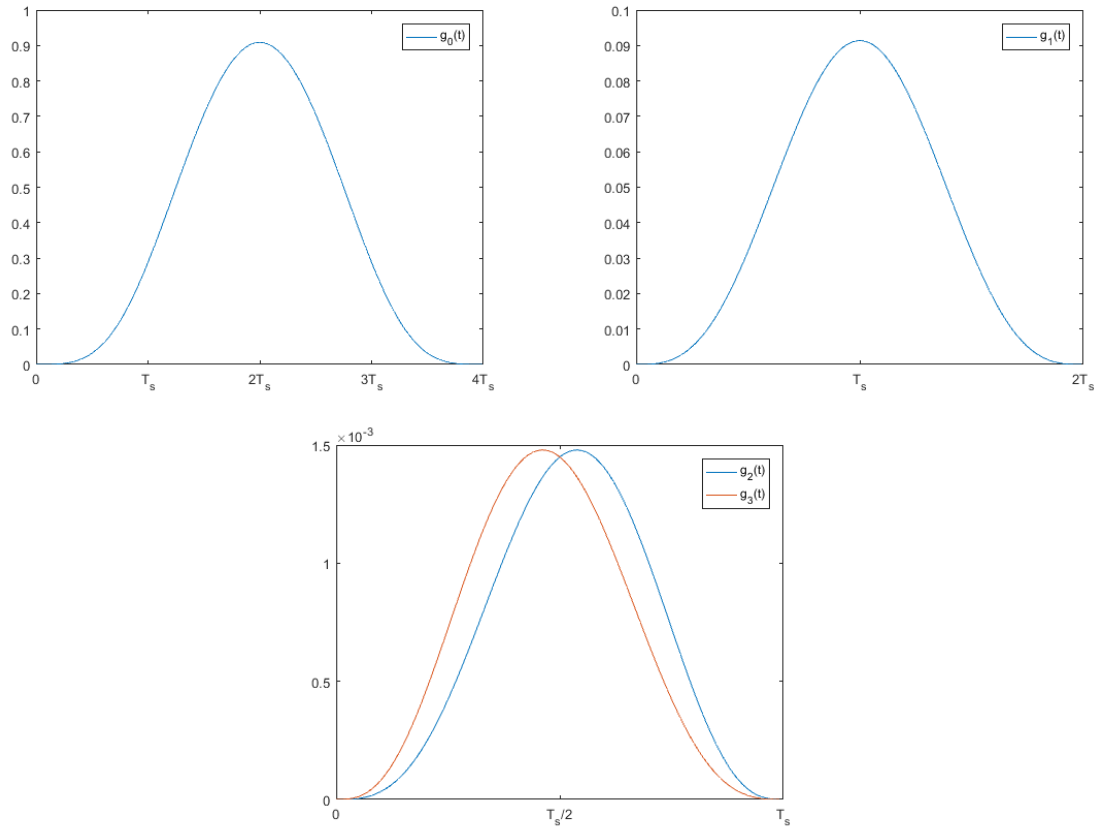

Figure 1.7 – Laurent Pulses for a binary CPM

1.3.2.2 Trellis Representation

[Kal89] exhibited the trellis structure of the Laurent Decomposition. Indeed, let us recall that:

$$A_{k,n} = \sum_{i=0}^{n} \alpha_i - \sum_{j=1}^{L-1} \alpha_{n-j}\beta_{k,j} \tag{1.10}$$

$$= A_{0,n-1} + \alpha_n - \sum_{j=1}^{L-1} \alpha_{n-j}\beta_{k,j} \tag{1.11}$$

Hence, at each nT_s, the pseudo-symbols can be computed from the input symbols α_n and the tuples $\{A_{0,n-1}, \alpha_{n-L+1}, \alpha_{n-L+2}, \ldots, \alpha_{n-1}\}$.

Hence, the trellis is given by the state $\sigma_n = \{A_{0,n-1}, \alpha_{n-L+1}, \alpha_{n-L+2}, \ldots, \alpha_{n-1}\}$ and the next state is $\sigma_{n+1} = \{A_{0,n} = A_{0,n-1} + \alpha_n, \alpha_{n-L+2}, \alpha_{n-L+3}, \ldots, \alpha_n\}$.

By using the approximation where only the first Laurent Pulse is considered, the current state is further reduced to $\sigma_n = \{A_{0,n-1}\}$, which will be exploited to reduce the computational

complexity of the detection.

1.3.2.3 Time-averaged auto-correlation function

An other useful tool provided by this Laurent Decomposition is the computation of the time-averaged auto-correlation function of the CPM signals. Indeed, this auto-correlation function is used later in this manuscript when MMSE equalizers are derived in Chapters 2 and 3.

For a time lag τ, the auto-correlation function is defined as

$$R(\tau) = \sum_{i=0}^{K-1} \sum_{j=0}^{K-1} \sum_{p=-\infty}^{\infty} E_{ij}^{p} C_{ij}(\tau - pT_s) \tag{1.12}$$

where $C_{ij}(\theta)$ is the inter-correlation of the Laurent Pulses given by

$$C_{ij}(\theta) = \int g_i(t) g_j(t+\tau) dt \tag{1.13}$$

and E_{ij}^{p} is the inter-correlation of the complex pseudo-symbols given by

$$E_{ij}^{p} = C^{\Delta(i,j,p)} \tag{1.14}$$

$$\text{and } C = \cos(h\pi) \tag{1.15}$$

$\Delta(i,j,p)$ is the number of terms in the algebraic expressions of $A_{i,n} - A_{j,n+p}$. The computation of this term is tedious, and therefore we invite the readers to refer to [Lau86] (Eq.526, pp.155) for the details.

One case of interest is when $h = 1/2$ as in this case $C = 0$. Therefore, the time-averaged auto-correlation function becomes:

$$R(\tau) = \begin{cases} \sum_{k=0}^{K-1} C_{ii}(\tau) & \text{for } 0 \leq |\tau| \leq (L+1)T \\ 0 & \text{elsewhere} \end{cases} \tag{1.16}$$

Others papers deal with the auto-correlation function of CPM signals. [NS01] derives its own decomposition in order to compute high-order statistics of CPM signals including the time-averaged auto-correlation function. [Dar+17] considers an one-sided CPM signal to derive a closed-form function of the time-averaged auto-correlation and cyclic auto-correlation functions.

1.3.3 Symbol-wise MAP detection

As there is no linear relation between the received signal and the data symbols, we need to use a non-linear detector to retrieve them. As we have presented a trellis-based representation of

CPM signals, we are interested here in trellis-based decoders: the Viterbi algorithm [Vit67] and the *BCJR* algorithm [Bah+74] are two main representatives of such receivers. The Viterbi algorithm is a Maximum Likelihood Sequence Estimator (*MLSE*) which means that it outputs the most likely sequence of data symbols whereas the BCJR is a bit/symbol-wise algorithm which produces a Maximum A Posteriori (*MAP*) probability for each symbols/bits given the whole observation sequence. [Kal89] presents a MLSE and, capitalizing on the Laurent Decomposition, designs a low-complexity detector by taking into account the main Laurent Pulse. Using the metric issued from the MLSE, [CB05] presents a soft MAP detector for CPM over an AWGN channel and also designs a low-complexity receiver by taking into account the main components of the PAM representation.

In this section, we will present the soft MAP decoder of [CB05] as, at the receiver, we are interested in performing turbo-decoding. This MAP decoder capitalizes on the trellis structure resulting from the PAM representation of the CPM signal.

To develop this detector, we have to consider a transmission over an AWGN channel. Therefore, the received signal is given by:

$$r(t) = s_b(t) + w(t) \tag{1.17}$$

Let us consider the compact representation of the observation, resulting from the PAM decomposition, and represented in Fig.1.8.

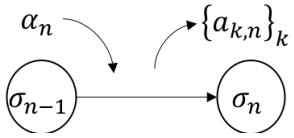

Figure 1.8 – Trellis using PAM Decomposition

The overall structure of the SISO MAP detector using the PAM Decomposition is given in Fig.1.9 where $r_{k,n}$ is the output of the matched filter to the k^{th} component of the Laurent Decomposition sampled at nT_s and $\{r_{k,n}\}_{k,n}$ and proven to be sufficient statistics to estimate the data symbols $\underline{\boldsymbol{\alpha}}$. They are given by:

$$r_{k,n} = \int_0^{(L+1)T_s} r(t + nT_s) g_k^*(-t) dt \tag{1.18}$$

The MAP criterion for the bit α_n is given by:

$$\widehat{\alpha}_n = \underset{\alpha_n}{\text{argmax}}\ p(\alpha_n | \{\underline{\boldsymbol{r}}_{k,n}\}_{k,n}) \tag{1.19}$$

$$= \underset{\alpha_n}{\text{argmax}}\ p(\alpha_n; \{\underline{\boldsymbol{r}}_{k,n}\}_{k,n}) \tag{1.20}$$

$$p(\alpha_n; \{\underline{\boldsymbol{r}}_{k,n}\}_{k,n}) = \sum_{S_{\alpha_n}} p(\sigma_{n-1} = s_{n-1}, \sigma_n = s_n, \{\underline{\boldsymbol{r}}_{k,n}\}_{k,n}) \tag{1.21}$$

where S_{α_n} is the set of transition corresponding to the symbols α_n, i.e.
$S_{\alpha_n} = \{(s_{n-1}, s_n) \text{where} (\sigma_{n-1} = s_{n-1}) \rightarrow (\sigma_n = s_n) | \alpha_n\}$.

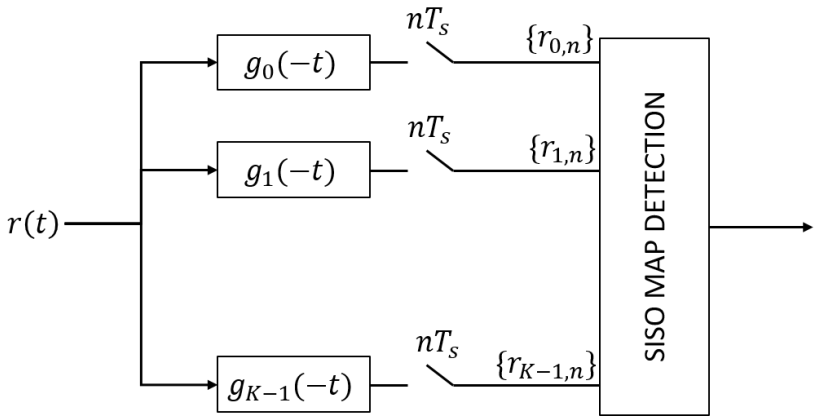

Figure 1.9 – CPM SISO MAP using PAM Decomposition

Let us denote r_l^m a set of the sufficient statistics such as
$r_l^m = [\{r_{k,l}\}_{0\leq k\leq K-1}, \{r_{k,l+1}\}_{0\leq k\leq K-1}, \ldots, \{r_{k,m}\}_{0\leq k\leq K-1}]$ and $r_n = \{r_{k,n}\}_{0\leq k\leq K-1}$

$$
\begin{aligned}
P &= p(\sigma_{n-1} = s_{n-1}, \sigma_n = s_n, \{\underline{\boldsymbol{r}}_{k,n}\}_{k,n}) && (1.22)\\
&= p(\sigma_{n-1} = s_{n-1}, \sigma_n = s_n, r_0^{n-1}, r_n, r_{n+1}^{N-1})\\
&= p(\underline{\boldsymbol{r}}_{n+1}^{N-1} | \sigma_{n-1} = s_{n-1}, \sigma_n = s_n, r_0^{n-1}, r_n) p(\sigma_{n-1} = s_{n-1}, \sigma_n = s_n, r_0^{n-1}, r_n)\\
&= p(\underline{\boldsymbol{r}}_{n+1}^{N-1} | \sigma_{n-1} = s_{n-1}, \sigma_n = s_n, r_0^{n-1}, r_n) p(\sigma_n = s_n, r_n | \sigma_{n-1} = s_{n-1}, r_0^{n-1}) p(\sigma_{n-1} = s_{n-1}, r_0^{n-1})\\
&= p(r_{n+1}^{N-1} | \sigma_n = s_n) p(\sigma_n = s_n, r_n | \sigma_{n-1} = s_{n-1}) p(\sigma_{n-1} = s_{n-1}, r_0^{n-1})\\
&= p(r_{n+1}^{N-1} | \sigma_n = s_n) p(\sigma_n = s_n, r_n | \sigma_{n-1} = s_{n-1}) p(r_n | \sigma_{n-1} = s_{n-1}, \sigma_n = s_n) p(\sigma_{n-1} = s_{n-1}, r_0^{n-1})\\
&= p(r_{n+1}^{N-1} | \sigma_n = s_n) p(\sigma_n = s_n, r_n | \sigma_{n-1} = s_{n-1}) p(\sigma_{n-1} = s_{n-1}, r_0^{n-1}) && (1.23)
\end{aligned}
$$

In Eq.(1.23), we can see three terms:

- $p(\sigma_{n-1} = s_{n-1}, r_0^{n-1})$ which only depends on the previous channel observations. This metric is referred to as the forward metric, and will be denoted as $\mathcal{A}_n(s_{n-1})$;
- $p(r_{n+1}^{N-1} | \sigma_n = s_n)$ which only depends on the future observation. This one is referred to as the backward metric, and will be denoted as $\mathcal{B}_n(s_n)$;
- $p(\sigma_n = s_n, r_n | \sigma_{n-1} = s_{n-1})$ is the transition metric, which depends on the current channel observation and on the *a priori* probability of the symbol α_n. It will be denoted as $\mathcal{G}_n(s_{n-1}, s_n)$.

The transition metric for the AWGN channel can be shown to be proportional to

$$\mathcal{G}_n(s_{n-1}, s_n) \propto \exp\left\{ \frac{2}{N_0} \Re\{ \sum_{k=0}^{K-1} r_{k,n} a_{k,n}^* \} \right\} \pi(\alpha_n) \qquad (1.24)$$

where $\Re\{.\}$ is the real part operator and $\pi(\alpha_n)$ is the *a priori* probability of the symbol α_n.

The *a priori* probability of a symbol can be computed straightforwardly from the *a priori* probability of the bits if considered independent as in BICM systems. Indeed, by considering a symbol from a M-ary alphabet such as $\alpha_n = \sum_{p=0}^{P-1} 2^p b_n^p$, where $\{b_i^p\}_p \in \{\pm 1\}^P$ and $P = \log_2(M)$, the probability of this symbol is equal to the product of the probability of its bits if considered independent as in BICM systems.

The forward and backward metrics can be computed recursively such as:

$$\mathcal{A}_n(s) = \sum_{s'} \mathcal{G}_n(s', s)\mathcal{A}_{n-1}(s') \tag{1.25}$$

$$\mathcal{B}_{n-1}(s) = \sum_{s'} \mathcal{G}_n(s, s')\mathcal{B}_n(s) \tag{1.26}$$

The last step of our detector is to compute the extrinsic probability of a bit from the previous *a posteriori* probability of a symbol. To do so, we have to first compute the *a posteriori* probability of each bits from the *a posteriori* probability (APP) of the symbols. Let us consider that a symbol from a M-ary alphabet can be written as:

$$\alpha_n = \sum_{p=0}^{P-1} 2^p b_n^p \tag{1.27}$$

with $\{b_i^p\}_p \in \{\pm 1\}^P$ and $P = \log_2(M)$.

Let define by $S_{b_p^+}$ (resp. $S_{b_p^-}$) the set of symbols where the p^{th} bit is equal to 1 (resp. -1), i.e. $b_n^p = +1$ (resp. $b_n^p = -1$). The *a posteriori* probability (APP) of this bit is given by:

$$p(b_n^p = +1; \{\underline{\boldsymbol{r}}_{k,n}\}_{k,n}) = \sum_{S_{b_p^+}} p(\alpha_n; \{\underline{\boldsymbol{r}}_{k,n}\}_{k,n}) \tag{1.28}$$

$$p(b_n^p = -1; \{\underline{\boldsymbol{r}}_{k,n}\}_{k,n}) = \sum_{S_{b_p^-}} p(\alpha_n; \{\underline{\boldsymbol{r}}_{k,n}\}_{k,n}) \tag{1.29}$$

Then the log-likelihood ratio (llr) of the APP is defined as:

$$\text{llr}_{\text{APP}}(b_n^p) = \log\left(\frac{p(b_n^p = +1; \{\underline{\boldsymbol{r}}_{k,n}\}_{k,n})}{p(b_n^p = -1; \{\underline{\boldsymbol{r}}_{k,n}\}_{k,n})}\right) \tag{1.30}$$

The *extrinsic* llr is obtained by removing the *a priori* llr (denoted as $\text{llr}_{\text{a}}(b_n^p)$):

$$\text{llr}_{\text{ext}}(b_n^p) = \text{llr}_{\text{APP}}(b_n^p) - \text{llr}_{\text{a}}(b_n^p) \tag{1.31}$$

where

$$\text{llr}_{\text{a}}(b_n^p) = \log\left(\frac{\pi(b_n^p = +1)}{\pi(b_n^p = -1)}\right) \tag{1.32}$$

with $\pi(.)$ corresponds to the bit *a priori* probability.

In order to avoid numerical issues as the absolute values of the different metrics can grow to infinity quickly, we use the BCJR algorithm in the *log* domain by defining the following:

$$\begin{aligned}
\widetilde{\mathcal{G}}_n(s_{n-1}, s_n) &= \log(\mathcal{G}_n(s_{n-1}, s_n)) \\
\widetilde{\mathcal{A}}_n(s) &= \log(\mathcal{A}_n(s)) \\
&= \max^*_{s'}(\widetilde{\mathcal{G}}_n(s', s)\widetilde{\mathcal{A}}_{n-1}(s')) \\
\text{and } \widetilde{\mathcal{B}}_{n-1}(s) &= \log(B_{n-1}(s)) \\
&= \max^*_{s'}(\widetilde{\mathcal{G}}_n(s, s')\widetilde{\mathcal{B}}_n(s))
\end{aligned}$$

where the operator max* is:

$$\max^*(a, b) = \max(a, b) + \log(1 + e^{-|a-b|}) \tag{1.33}$$

To further reduce the complexity of the algorithm, one can use a look-up table to approximate the log part of the operator. Others can also replaced this operator by the max operation at the prize of a slight performance loss.

The main advantage of those receivers is that we can easily reduce their computational complexity. Indeed, as explained in Section 1.3.2.2, binary CPM with non-integer modulation index can be well-approximated by only the first Laurent Pulse, therefore the branch metric in Eq.(1.24) becomes:

$$\mathcal{G}_n(s_{n-1}, s_n) \propto \exp\left\{\frac{2}{N_0}\Re\{r_{0,n}a^*_{0,n}\}\right\}\pi(\alpha_n) \tag{1.34}$$

$$\tag{1.35}$$

where the trellis state is reduced to $\sigma_n = \{a_{0,n-1}\}$.

In this thesis, we only consider this soft MAP decoder in the *log* domain for simulations. However, our results concerning equalization or parameters estimation do not depend on the used CPM detector (Laurent-based or Rimoldi-based). A complete study of the soft MAP detection using the Rimoldi decomposition and the Laurent decomposition is available to readers in [Ben15].

1.3.4 EXIT Charts and asymptotic analysis

For the study of the behaviour of SISO components with or without iterative detection, such as the previous CPM detector, one may be interested in computing the input-output EXtrinsic Information Transfer (*EXIT*) characteristic. At the input, a general SISO block (as represented in Fig.1.10) can have some channel observations and some a priori Log-Likelihood Ratios (*LLR*). For a given signal to noise ratio (SNR), extrinsic information is computed at

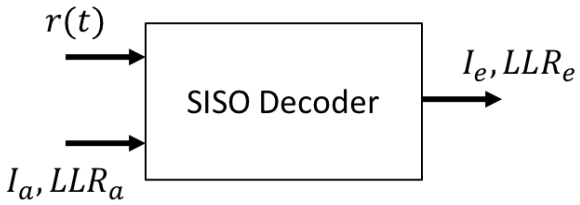

Figure 1.10 – SISO receiver

the output. We recall that the LLR for the n^{th} bit b_n is defined as:

$$\text{LLR}(b_n) = \log\left(\frac{p(b_n = +1)}{p(b_n = -1)}\right) \tag{1.36}$$

The EXIT transfer function, denoted here by $T(.)$, computes the mutual information I_e between the sent bits and the extrinsic LLRs versus the mutual information I_a between the a priori LLRs and the corresponding bits such that:

$$I_e = T(I_a) \tag{1.37}$$

The mutual information between a binary random variable $X \in \{\pm 1\}$ and the corresponding LLRs is given by:

$$I(X, \text{LLR}) = \frac{1}{2}\sum_{x\in\pm 1}\int p(\text{llr}|x)\log_2\left(\frac{2p(\text{llr}|x)}{p(\text{llr}|x=+1)+p(\text{llr}|x=-1)}\right)d\text{llr} \tag{1.38}$$

The computation of $p(\text{llr}|x)$ is not straightforward and so we compute it by Monte Carlo. For each SNR point, for each I_a, we generate a CPM signal. The corresponding *a priori* llr is the generated through a Gaussian distribution of mean $m_{\text{llr}} = \frac{\sigma^2_{\text{llr}}}{2}$ and variance σ^2_{llr} such that for the $n^{\text{th}}bit$:

$$\text{llr}_a(b_n) = \sigma^2_{\text{llr}}/2b_n + n_a \tag{1.39}$$

where n_a is an independent Gaussian random variable with zero mean and variance σ^2_{llr}.

We fed the SISO MAP receiver with the received signal and with this computed *a priori* llr. At the output, we compute the corresponding mutual information through the means of a histogram of the *extrinsic* llr. Readers may refer to [Ben15] for more details.

Moreover, by computing it by simulation, it allows us to take into account the effect of other components such as the equalizer for instance. An example of EXIT curve is given for a binary CPM with a RC pulse shape, a memory of $L = 2$ and $h = 1/4$ in Fig.1.11.

It has been shown that the area under the EXIT curve of an iterative component corresponds to its maximal achievable rate over the Binary Erasure Channel in [AKB04]. This

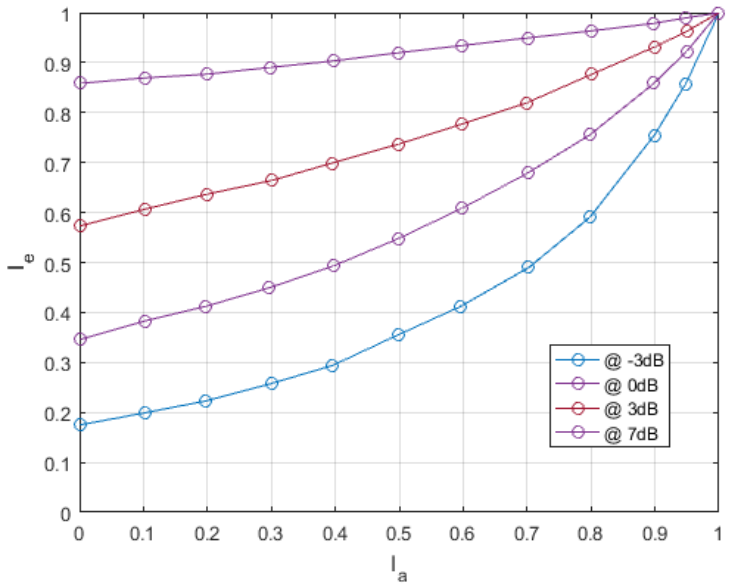

Figure 1.11 – EXIT charts for a binary CPM with a RC pulse shape, a memory of $L = 2$ and $h = 1/4$

area is also considered as a good approximation for others channels and detectors [Hag04]; [LSL06]. Hence, this can be also used to estimate a lower bound of the maximum achievable rate R^* for the inner code and for a given signal to noise ratio. This lower bound is given by:

$$R^* \leq \int_0^1 T(x)dx \tag{1.40}$$

Readers unfamiliar with EXIT charts may refer to the tutorial by [Hag04].

EXIT charts analysis can be also used to compute by simulation the Spectral Efficiency (SE) of a CPM scheme. Indeed, the SE correspond to the achievable Information Rate (IR, noted I) for a given bandwidth. 1Hz is usually taken.

We can evaluate the SE by using:

$$\widehat{\text{SE}} = \frac{\log_2(M) \times R^*}{B_\rho T} \tag{1.41}$$

where T is taken equal to 1 and B_ρ is the considered bandwidth. We need a suitable definition of the bandwidth. In fact, the Power Spectral Density (PSD) of CPM signals has an infinite support. However, almost all of the power is located only in a small portion. The most common definition is based on this power concentration, which assumes that the CPM signal bandwidth is the spectrum area that contains a given fraction ρ of the total power (usually $\rho \in \{0.99, 0.999\}$, in this thesis we consider $\rho = 0.99$). If we note $\Gamma(f)$ the PSD, the bandwidth

is given by

$$B_\rho = \int_{-B_\rho/2}^{B_\rho/2} \Gamma(f)df = \rho \int_{-\infty}^{+\infty} \Gamma(f)df \tag{1.42}$$

1.4 Precoded CPM

1.4.1 CPM with duo-binary encoder

In [Mes+16], the authors present a precoder improving the Spectral Efficiency of a binary CPM scheme. The main idea is to improve the Information Rate (*IR*) without increasing significantly the spectral occupancy. One simple way to increase the IR is to increase the modulation order to ternary CPM schemes, but this yields to a bandwidth expansion. Indeed, the bandwidth expansion is mainly due to the transition from symbols '+2' to '-2'. Hence, the role of the precoder is to map the input bits into ternary symbols, but without any transition between the symbols '+2' to '-2' (and vice versa) to avoid the phase hopping yielding to the increased bandwidth occupation.

Let us denote α_n the n^{th} ternary symbols and b_n the n^{th} input bits. The precoder proposed by [Mes+16] is:

$$\alpha_n = b_n \alpha_{n-d}(-1)^{d+1} \tag{1.43}$$

where α_{n-d} is the latest symbols such that $|\alpha_{n-d}| = 2$.

This proposed precoder does avoid any transition to '+2' to '-2' (and vice versa) and so it increases the SE of the original CPM scheme. However, it is tedious to use at the receiver. In [OSL17], the authors proposed an other precoder which also map bits into ternary symbols without any transition between the symbols '+2' to '-2' (and vice versa). We want to point out that this kind of duo-binary encoder are already in used in some legacy CPM schemes as the Shaped Offset Quadrature Phase-Shift Keying (*SO-QPSK*) modulation. It has been shown that the duo-binary encoder achieves the same SE as the precoder in [Mes+16]. However, it is more tractable as it allows us to write the Ternary CPM schemes as a binary CPM and therefore, by using the Laurent Decomposition, to design a low-complexity receiver.

In the following, we will present briefly the PAM decomposition of ternary CPM with duo-binary encoding by only exhibiting the main result of [OSL17].

Let us consider a binary input sequence $\underline{\boldsymbol{b}} = \{b_0, b_1, \ldots, b_{N-1}\}$. The ternary symbol is obtained thanks to the following duo-binary encoder:

$$\alpha_n = \frac{b_n + b_{n-1}}{2} \tag{1.44}$$

which can been seen as a 2-radix decomposition of the ternary symbols α_n. Those symbols are then given to a CPM modulator. This CPM has a memory L_{cpm} and a pulse shape $q(t)$.

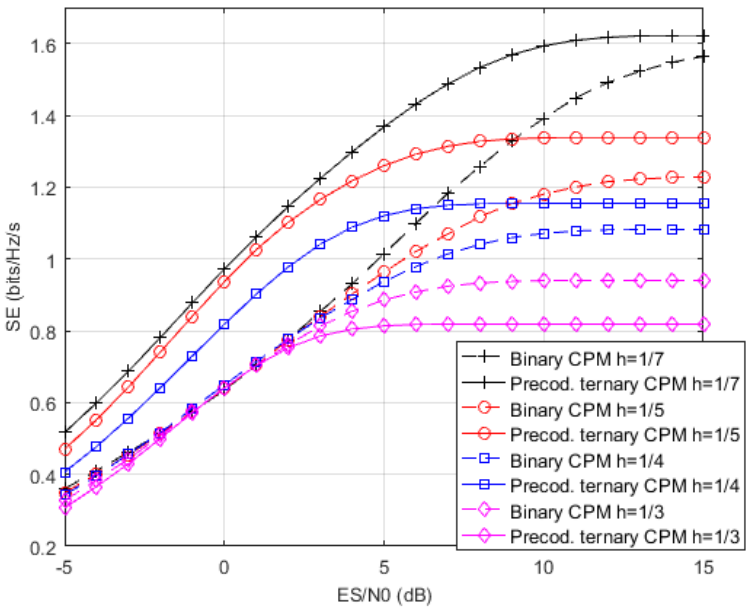

Figure 1.12 – SE for 1-REC with different modulation indices

Then the information phase of the ternary CPM is given by:

$$\Phi(t, \underline{\boldsymbol{\alpha}}) = 2\pi h \sum_{n=0}^{N-1} \alpha_n q(t - nT_s) \tag{1.45}$$

$$= \pi h \sum_{i=-\infty}^{N-L_d} b_i + 2h\pi \sum_{i=N-L_d+1}^{N} b_i \widetilde{q}(t - iT_s) \tag{1.46}$$

where $L_d = L_{\text{cpm}} + 1$ and $\widetilde{q}(t)$ is a continuous function defined as:

$$\widetilde{q}(t) = \frac{q(t) + q(t - T)}{2} \tag{1.47}$$

$$= \begin{cases} 0, \text{ if } t < 0 \\ 1/2, t > L_d T_s \end{cases} \tag{1.48}$$

Equation (1.46) corresponds to the definition of the information phase of a binary CPM. Hence, the ternary CPM scheme with duo-binary encoding can be seen as a binary CPM, and the Laurent Decomposition can be applied allowing us to design a low-complexity receiver.

In Fig.1.12 and in Fig.1.13, we have computed the Spectral Efficiency (SE) by simulations using a Laurent-based MAP receiver for different schemes and obtained the same results as in [Mes+16]; [OSL17]. Even if ternary CPMs with duo-binary encoder have a lot of benefits (as it improves the SE without increasing the complexity at the transmitter/receiver), in order to be compliant with most CPM schemes, we choose not to study this CPM scheme in this thesis.

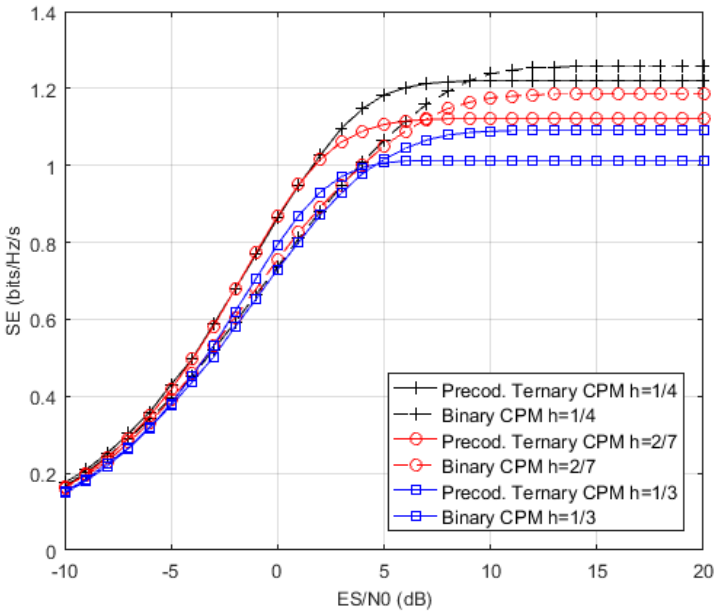

Figure 1.13 – SE for 2-RC with different modulation indices

We have tried to expand this concept to see if it we can achieve better SE by increasing the modulation order while still using a precoder. This straightforward extension is presented in Annex A. However, our approach shows that the increasing modulation order leads to a bandwidth expansion which is not well compensated (resulting in a low increase of the SE). Hence, it seems that this precoder takes benefit from a low modulation order (ans shows its best performance in the case of ternary symbols) and from a low modulation index.

1.4.2 *Pragmatic* CPM

[Per+10] presents a new CPM scheme, referred to as Pragmatic CPM (*P-CPM*), which reduces greatly the complexity of the receiver by making the iteration between the CPM detector and the outer code decoder useless. P-CPM consists of a non-linear precoding applied to legacy CPM schemes, by mainly adding a non-linear precoding device to the Continuous Phase Encoder using from the Rimoldi representation (see [Rim88]).

Some CPM schemes have, by nature, a flat exit chart, making turbo-iterations useless. For instance, in [Rim88], it is shown that the CPFSK can have a non-recursive implementation. Using both recursive or non-recursive implementation leads to the same asymptotic performance.

A study of those P-CPM has been done recently in [LNJP17], and it has been shown that in most case, binary P-CPMs have a flat exit chart, which means that iterations between the detector and the channel decoder are no more crucial in this case.

In [LNJP17], all considered binary P-CPMs present flat EXIT charts, which makes the iteration between the CPM detector and the outer code decoder useless, and moreover the area under the EXIT curves of both P-CPM and legacy CPM are almost identical. Hence, P-CPM can achieve the same coding rate as legacy CPM.

As a conclusion, P-CPM shall be used for an efficient design of a serially concatenated coded CPM scheme without iterative decoding in case of binary CPM. The extension of this work for M-ary CPM has been shown to be sub-optimal.

Chapter 2

Receiver techniques for CPM signals over TIV Channels

Contents

Résumé

Dans ce chapitre, nous nous proposons d'étudier le récepteur adapté à des transmissions de signaux CPM sur des canaux sélectifs en fréquence.

Dans un premier temps, nous nous concentrons sur l'égalisation qui vise à attenuer l'effet du canal de propagation. Le traitement optimal consiste en une égalisation et détection conjointe. Cependant, sa complexité est prohibitive puisqu'elle augmente exponentiellement avec la taille de la mémoire de la CPM et avec la mémoire du canal de propagation. Ainsi, la solution la plus adoptée est de séparer égalisation et détection. Nous nous intéressons pour la suite uniquement aux égaliseurs dans le domaine fréquentiel. [PV06] propose d'égaliser les pseudo-symboles de la décomposition de Laurent tandis que [VT+09] égalise l'envelope complexe sur-échantillonnée du signal CPM reçu. Nous avons pu démontrer mathématiquement et par simulations que ces deux approches sont équivalentes (à un traitement linéaire près). De plus, ces deux approches n'exploitent pas entièrement la structure circulaire du signal (liée à l'utilisation d'Unique Word ou de Préfixe Cyclique pour circulariser le canal afin de permettre de réaliser des traitements dans le domaine fréquentiel). Nous avons ainsi pu développer un nouvel égaliseur qui, exploitant cette structure, atteint les mêmes performances que les égaliseurs de l'état de l'art mais avec une complexité bien moindre.

Enfin, les travaux précédents ont été réalisés sous hypothèse de synchronisation parfaite et de connaisance parfaite du canal. Nous avons donc proposé un nouvel estimateur de canal adapté aux schémas d'égalisation ainsi qu'un estimateur conjoint du canal et de la fréquence porteuse. La borne de Cramér Rao pour la récupération de la porteuse a été dérivée dans ce contexte de transmission sur canal sélectif en fréquence.

2.1 Introduction

In this chapter, we present some receiver techniques for CPM over frequency-selective channels.

First, we will consider some equalization techniques. We choose to work only in the Frequency-Domain in order to reduce the computational complexity of this equalization and so we will focus on two Minimum Mean Square Error (*MMSE*) Frequency-Domain Equalizer (*FDE*) of the literature ([PV06] and [VT+09]) working on the over-sampled received signal. We will show mathematically and by simulations that those two approaches are equivalent up to a linear post-processing. Then, by fully exploiting the circular-extended block structure of the CPM, we will develop a new MMSE-FDE which reaches the same performance but with a significant lower complexity.

We will also discuss some parameters estimation techniques such as channel estimation or some transmission parameters as the Carrier Frequency-Offset. In order to be compliant with the model used for the equalization, we need to develop a channel estimation working on the same over-sampled received signal. Moreover, we will present a joint channel and carrier frequency estimation and Cramér Rao Bound (*CRB*) for the carrier recovery will be derived.

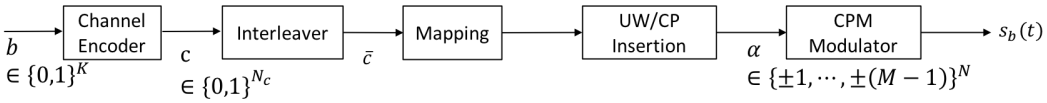

Figure 2.1 – BICM for CPM with CP or UW insertion

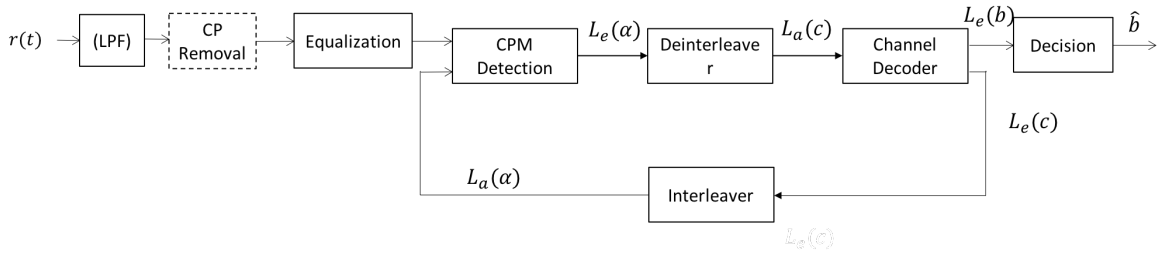

Figure 2.2 – Receiver structure (with CP removal in dotted lines, if CP is used)

2.2 Transmission over a TIV channel

2.2.1 Communication system description

We will consider a Bit Interleaved Coded Modulation ($BICM$) using CPM, as illustrated in Fig.2.1. At the transmitter side, a binary message $\underline{\boldsymbol{b}}$ of length K is encoded to a codeword $\underline{\boldsymbol{c}}$ of length N_c and sent to a M-ary mapper to obtain a sequence $\underline{\boldsymbol{\alpha}} \in \{\pm 1, \pm 3, \ldots, \pm(M-1)\}^N$. After the insertion of a Unique Word (UW) or a Cyclic Prefix (CP), the data symbols sequence is then given to the CPM modulator.

The only difference between the CPM transmitter considered in this chapter and the one presented in Chapter 1 is the insertion of a CP or a UW which is needed to *circularize* the channel, in order to perform efficient frequency-domain equalization. As for linear modulations, we can derive a block-based model by using a CP or a known UW, also called training sequence. At the receiver, in order to obtain the circular block-based model, the CP must be removed before the equalization such as only the data block is processed as depicted in Fig.2.2 with the dotted lines. In our thesis, we will only consider the use of a UW and the block of interest to process is the data block concatenated to the UW.

First, let us recall the complex envelop definition of a CPM signal. Let $\alpha = [\alpha_0, \cdots, \alpha_{N-1}] \in \{\pm 1, \pm 3, \ldots, \pm(M-1)\}^N$ be a block of N independent and identically distributed symbols from a M-ary alphabet. The equivalent baseband complex envelope $s_b(t)$ of the transmitted CPM signal is given by:

$$s_b(t) = \sqrt{\frac{2E_s}{T_s}} \exp\left(j\theta(t, \boldsymbol{\alpha})\right) \tag{2.1}$$

where E_s is the symbol energy, the information phase is $\theta(t, \boldsymbol{\alpha}) = 2\pi h \sum_{i=0}^{N-1} \alpha_i q(t - iT_s)$, T_s

is the symbol duration,

$$q(t) = \begin{cases} \int_0^t g(\tau)d\tau, t \leq L_{\text{cpm}}T_s \\ 1/2, t > L_{\text{cpm}}T_s \end{cases}$$

$g(t)$ is the pulse response, h is the modulation index and L_{cpm} is the CPM memory.

The CPM signal is then transmitted over a frequency-selective channel with equivalent baseband impulse response

$$h_c(t) = \sum_{l=0}^{L_c-1} a_l \delta(t - \tau_l) \tag{2.2}$$

where L_c is the number of paths, τ_l and a_l are the delay and the complex attenuation of the l^{th} path.

The received signal is the linear convolution between the channel and the transmitted complex envelope of the CPM signal given by

$$r(t) = h_c(t) * s_b(t) + w'(t) \tag{2.3}$$

where $w'(t)$ is a white Gaussian Noise with power spectral density $2N_0$.

2.2.2 On the use of a CP or a UW

First, as for linear modulation, the use of a UW or a CP introduces an equivalence between the linear convolution and a circular convolution in Eq.(2.3) as illustrated in Fig.2.3.

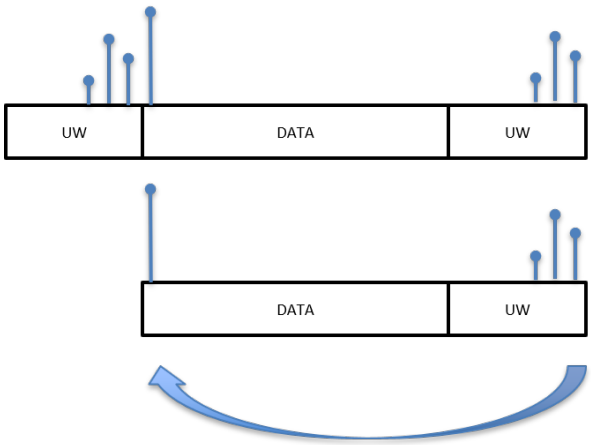

Figure 2.3 – Equivalence between linear and circular convolution thanks to the UW

However, the use of a CP or an UW to obtain a circular block model leads to a constant loss of bandwidth efficiency. In this section, we present briefly the CP and UW insertion techniques and we provide a comparison of those techniques in term of bandwidth efficiency loss and their possible use in the receiver.

First, unlike for linear modulations, due to the CPM memory, we need to add some termination symbols at the end of the data block in order to ensure the phase continuity and the return to the *zero* state after encoding. In our system, we will assume that the UW contains already the termination symbol sequence to return to the zero state of the encoder. Fig.2.4 resumes the CP insertion technique whereas Fig.2.5 presents the UW insertion technique. Moreover, the length of a UW/CP must be larger than the time dispersion of the channel to avoid interference between CPM blocks (generally known as Inter Block Interference or *IBI*).

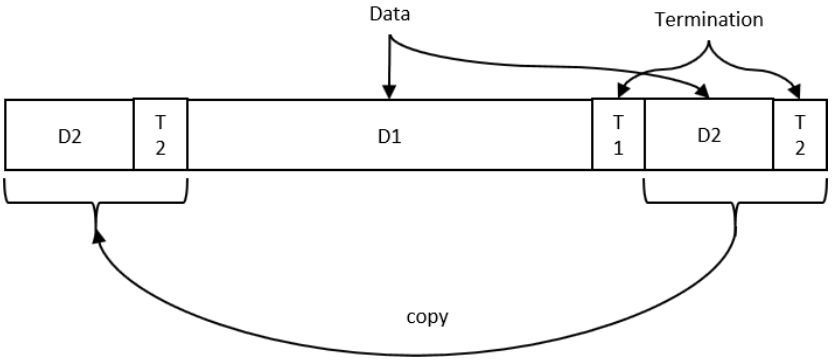

Figure 2.4 – Block-based structure of the CPM signal using a CP

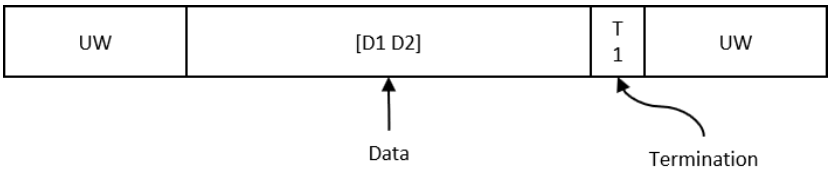

Figure 2.5 – Block-based structure of the CPM signal using a UW

Let us denote by N_{X} the size of the block 'x' in Fig.2.4 and Fig.2.5. We will consider that all termination symbols sequence have the same lengths. Let us denote by N_{B} the size of the block of interest for the equalizer. In the case of a CP, $N_{\mathrm{B}} = N_{\mathrm{D1}} + N_{\mathrm{D2}} + 2N_{\mathrm{T}}$ whereas for the UW, $N_{\mathrm{B}} = N_{\mathrm{D1}} + N_{\mathrm{D2}} + N_{\mathrm{T}} + N_{\mathrm{UW}}$. To make a fair comparison, we assume that the size of the UW and the size of the CP are equals, i.e. $N_{\mathrm{CP}} = N_{\mathrm{UW}} = N_{\mathrm{D2}} + N_{\mathrm{T}}$. Thus, the bandwidth efficiency is reduced respectively by a factor:

$$\rho_{\mathrm{UW}} = \frac{N_{\mathrm{B}} - N_{\mathrm{CP}}}{N_{\mathrm{B}}} \tag{2.4}$$

$$\rho_{\mathrm{CP}} = \frac{N_{\mathrm{B}}}{N_{\mathrm{B}} + N_{\mathrm{CP}}} \tag{2.5}$$

We give some values of this degradation in term of bandwidth efficiency for classical values in Table 2.1 for the UW insertion scheme and in Table 2.2 for the CP insertion scheme. We can see that the additional degradation in case of the use of an UW can be negligible in some case and is very-well compensated by the advantages for parameters estimation (without introducing furthermore overhead, as the UW is known unlike the CP) and could increase the performance of the Block Decision Feedback Equalizer [Wit+02]. Similar results has been

$N_B/\ N_{UW}$	8	16	32
128	93.75%	87.5%	75%
256	96.87%	93.75%	87.5%
512	98.44 %	96.88%	93.7%
1024	99.22%	98.44%	96.88%

Table 2.1 – Bandwidth efficiency loss with the UW

$N_B/\ N_{CP}$	8	16	32
128	94.12%	88.89%	80%
256	96.97%	94.12%	88.89%
512	98.46 %	96.97%	94.12%
1024	99.22%	98.46%	96.97%

Table 2.2 – Bandwidth efficiency loss with a CP

obtained for linear modulations in [Wit+02].

Through this manuscript, and motivated by the previous explanations, we choose to study a circular block-based structure using the UW insertion technique, even if the introduction of a UW brings a higher loss of spectral efficiency compared to the introduction of a CP. Concerning equalization, obtained results can still be extended to a CP-based approach. Furthermore, those UW will be used in Chapter 3 to perform channel estimation in case of Time-Varying channels.

2.2.3 Received signal representation

As in [Thi+09], we assume that the transmitted CPM is roughly bandlimited to $B \simeq \frac{k}{2T_s}$, $k \geq 2$. Then it can be sampled uniformly at a rate of $T_e = T_s/k$, without a significant loss of information.

Hence, this signal can be reconstructed from its samples using the *sinc* basis expansion defined as:

$$\text{sinc}_{T_e}(t) \triangleq \frac{\sin(\pi t/T_e)}{\pi t/T_e} \tag{2.6}$$

$$\text{and } s_b(t) = \sum_n s_b(nT_e)\text{sinc}_{T_e}(t - nT_e) \tag{2.7}$$

We recall that the *sinc*(.) function is the impulse response of the ideal low-pass filter (*LPF*) with bandwidth $\frac{kR_s}{2}$ ($R_s = 1/T_s$), that we denoted by $\Psi(t)$ and the CPM signal can be written as:

$$s_b(t) \simeq \sum_n s_b(nT_e)\Psi(t - nT_e) \tag{2.8}$$

At the receiver, we consider the matched filter to the ideal low-pass filtering using the front-end filter $\Psi(t)$, which is also $\Psi(t)$. We define $h(t) = \Psi(t) * h_c(t) * \Psi(t)$, where $*$ is the linear convolution operator. Hence, the received signal, also denoted by $r(t)$ by ease of presentation, can be written as [Thi+09]:

$$r(t) = e^{j(2\pi ft+\theta)}\Psi(t) * h_c(t) * s_b(t) + \underbrace{\Psi(t) * w'(t)}_{\triangleq w(t)} \tag{2.9}$$

$$= e^{j(2\pi ft+\theta)} \sum_m s(m\frac{T_s}{k})h(t - m\frac{T_s}{k}) + w(t) \tag{2.10}$$

where f is the carrier frequency offset (CFO), θ the initial phase and $w(t) = \Psi(t) * w'(t)$ is still a complex baseband additive white Gaussian noise with power spectral density $2N_0$. For ease of presentation, we will not differentiate the filtered noise and the noise in the following as they have the same statistical properties.

As we will mainly discuss equalization techniques in this chapter, we will assume now perfect synchronization at the receiver, i.e. $f = 0$ and $\theta = 0$, which gives us the following received signal:

$$r(t) = \sum_m s(m\frac{T_s}{k})h(t - m\frac{T_s}{k}) + w(t) \tag{2.11}$$

Hence, the received signal can be written as the linear convolution between the filtered channel impulse response and the transmitted complex envelope of the CPM signal. We will now show that the insertion of a UW gives us an equivalence between this linear convolution and a circular convolution of the periodized version of the channel and the circular-extended transmitted complex envelope. This property holds true in the case of a CP, even if we only consider the use of a UW in the following.

We define N_{data} the number of data symbols (including the termination), N_{UW} the number of symbols in the UW and $N = N_{\text{data}} + N_{\text{UW}}$. We also define L the span of the channel in number of symbols (with $L < N_{\text{UW}}$), i.e. $h(t) = 0$ if $t < 0$ and $h(t) = 0$ if $t > LT_s$. In this case, by taking $t_0 = 0$ at the beginning of the data block, for $0 < t < N_{\text{UW}}T_s$, we have

$$s_b(-t) = s_b(NT_s - t) \tag{2.12}$$

The received signal for $0 \leq t \leq NT_s$ is given by the linear convolution between the

transmitted signal $s_b(t)$ and the filtered channel impulse response $h(t)$:

$$r(t) = h(t) * s_b(t) + w(t) \tag{2.13}$$
$$= \int_{\mathbb{R}} s_b(t-x)h(x)dx + w(t) \tag{2.14}$$
$$= \int_0^{LT_s} s_b(t-x)h(x)dx + w(t) \tag{2.15}$$
$$= \int_0^{t} s_b(t-x)h(x)dx + \int_t^{LT_s} s_b(t-x)h(x)dx + w(t) \tag{2.16}$$

In the second integral, we have:

$$t \leq x \leq LT_s \tag{2.17}$$
$$0 \geq t - x \geq t - LT_s \geq -N_{\mathrm{UW}}T_s \tag{2.18}$$

Hence, we obtain:

$$r(t) = \int_0^{t} s_b(t-x)h(x)dx + \int_t^{LT_s} s_b(NT_s + t - x)h(x)dx + w(t) \tag{2.19}$$

Let us now define $s_{NT_s}(t)$ (resp. $h_{NT_s}(t)$) the periodized version of $s_b(t)$ (resp. $h(t)$) of period NT_s such that $\forall l \in \mathbb{Z}$, for $0 \leq t \leq NT_s$, $s_{NT_s}(t+lNT_s) = s_b(t)$ (resp. $\forall l \in \mathbb{Z}, h_{NT_s}(t+lNT_s) = h(t)$). The linear convolution becomes:

$$r(t) = \int_0^{t} s_{NT_s}(t-x)h(x)dx + \int_t^{LT_s} s_{NT_s}(NTs + t - x)h(x)dx + w(t) \tag{2.20}$$
$$= \int_0^{t} s_{NT_s}(t-x)h_{NT_s}(x)dx + \int_t^{LT_s} s_{NT_s}(t-x)h_{NT_s}(x)dx + w(t) \tag{2.21}$$
$$= \int_{\mathbb{R}} s_{NT_s}(t-x)h_{NT_s}(x)dx + w(t) \tag{2.22}$$
$$= s_{NT_s}(t) \otimes h_{NT_s}(t) + w(t) \tag{2.23}$$

where the operator $\otimes$ is the circular convolution, as given in [VKG14] (pp.358-359).

This equivalence between the linear convolution and the circular convolution thanks to the circular extension (based on a UW or a CP) is widely known and used to design Single Carrier Frequency Domain Equalizer (*SC-FDE*) systems for linear modulation [Ben+10]. For CPM signals, the FDE methods also exploits this property to make the channel circular. However, as we will show latter, they do not exploit carefully this model to design a low complexity MMSE-FDE.

By sampling the signal at kR_s, we obtain the following discrete circular convolution, for

$0 \leq n \leq kN-1$:

$$r[n] = r(nT_e) \tag{2.24}$$
$$= \sum_m h_{NT_s}[m] s_{NT_S}[n-m] \tag{2.25}$$
$$= \sum_m h[m] s_b[\text{mod}(n-m, kN)] \tag{2.26}$$

2.3 FD-MMSE Equalizers for TIV channels

2.3.1 Introduction

Compared to linear modulations, CPM transmission over frequency-selective channels is a challenging task.

Optimal joint channel equalization and detection using a Maximum A Posteriori (*MAP*) trellis based detector is prohibitive as its complexity grows exponentially with both the CPM and the channel memory. Contrary to the single carrier (SC) case using linear modulation, as the received signal is not a linear function of the transmitted data symbols, sub-optimal linear equalization and detection using the minimum mean square error (MMSE) criterion should be performed into two steps: first linear equalization is usually performed over the over-sampled complex signal envelop, then the output is fed to a non linear detector for CPM for Gaussian channels.

SC-FDE using linear modulations leads to a circular linear Gaussian model, linear with respect to the transmitted data symbols whose Time-Domain (*TD*) and Frequency-Domain (*FD*) auto-correlation matrices are usually both diagonals, leading to, with some abuse of terminology, the so-called 'one-tap' or 'per-tone' FD equalizer.

FDE for CPM signals also ends up with a circular linear Gaussian model, but with respect to a vector of samples of the over-sampled complex signal or a vector of pseudo-symbols resulting from the PAM decomposition, which are correlated by nature. Therefore, without any further hypothesis, both TD and FD auto-correlation matrices of those vectors are not diagonal matrices anymore, and having a 'one-tap' FD equalizer highly depends on the structure of the model used at the reciver to perform equalization.

The use of SC-FDE blindly drawn from the linear case is a rough approximation leading to some heavy performance degradations.

In this section, we will hence focus on channel equalization. We will present some MMSE-FDE methods proposed in the literature. Then, we will show that by exploiting carefully the model and the representation of the received over-sampled CPM signal, a 'one-tap' FD equalizer is achievable without making any approximation, by using the cyclic statistical properties of the signal in case of circular block-based transmission and a Fractionally-Spaced (*FS*) representation of the signal.

2.3.2 State of the Art Equalizers

Several papers deal with equalization for CPM over TIV channels and propose different MMSE-FDE.

In [TS05], the authors proposed two baud-rate equalizers using an orthogonal representation of the signal space or the Laurent representation. However, due to hypothesis made on the propagation channel, the practical interest is limited and therefore, we will present those equalizers in Annex B.

[PV06] proposed a MMSE-FDE capitalizing on the Laurent decomposition and equalizes both channel and Laurent Pulses contribution, using a Fractionally-spaced representation of the over-sampled received signal. [VT+09] proposed to only consider the channel contribution when deriving its equalizer, using a polyphase/multi-channel representation of the over-sampled received signal. However, as we will see later, this approach requires "full" matrix inversion (and so has a computational complexity cubic with the number of data symbols). [VT+09] also proposed a low-complexity version of its equalizer by making some approximation and therefore resulting in a loss of performance. [VT+09] and [RP17] (which considers those equalizers for telemetry application) failed to make the link with the previous equalizer and claimed that the two equalizers have different performance. In [Cha+17a], we have shown that in fact those two equalizers achieve the same performance, if a proper linear processing is used.

Other MMSE-FDEs have been proposed. [OKD09] for instance derived a turbo-equalizer for CPM taking into account only the channel contribution, and by not taking into account the auto-correlation of the over-sampled transmitted complex envelop. [Xu+09], [CW14] or [Has+09], to cite a few, use the same approximation to develop low-complexity MMSE-FDE. It corresponds to a 'blind' application of SC-FDE for linear modulation, without taking into account that CPM signals are correlated.

As we are only interested in an exact derivation of a MMSE-FDE equalizer, we will only present in details the equalizers proposed in [PV06] and [VT+09].

2.3.2.1 Channel MMSE Equalizer

In [VT+09], the authors present a MMSE-FDE which only considers the channel (i.e. the propagation channel filtered by the LPF). They consider the polyphase representation in order to design their equalizer and a sample rate of $2R_s$ ($k = 2$). The extension to a higher sample rate is straightforward and presented in [Cha+17a].

Let us recall that the received signal is, for $0 \leq n \leq kN-1$:

$$r[n] = \sum_{m=0}^{kN-1} h[m]s(\text{mod } (n-m, kN)) + w[m] \tag{2.27}$$

$$= \sum_{m=0}^{kN-1} s[m]h(\text{mod } (n-m, kN)) + w[m] \tag{2.28}$$

Moreover, let also recall the PAM decomposition of CPM signals:

$$s_b(t) = \sum_{p=0}^{K-1} a_{p,n} g_p(t - nT_s) \tag{2.29}$$

where $\{a_{p,n}\}$ are the pseudo-symbols and $\{g_p(t)\}$ the components of the PAM decomposition. Hence, by considering the periodized version of $s_b(t)$, we obtain:

$$s[m] = s_b(mT_e) \tag{2.30}$$

$$= \sum_{p=0}^{K-1} a_{p,n} g_p[\text{mod } (m-kn, kN)] \tag{2.31}$$

The corresponding polyphase component is:

$$s_m^i = s[km+i] \tag{2.32}$$

$$= s((km+i)T_e) \tag{2.33}$$

$$= \sum_{p=0}^{K-1} a_{p,n} g_p[\text{mod } (km+i-pn, kN)] \tag{2.34}$$

$$= \sum_{p=0}^{K-1} a_{p,n} g_p[\text{mod } (k(m-n)+i, kN)] \tag{2.35}$$

$$= \sum_{p=0}^{K-1} a_{p,n} g_{p,m-n}^i \tag{2.36}$$

where $g_{p,m-n}^i = g_p[\text{mod } (k(m-n)+i, kN)]$.

To describe this discrete circular convolution between the Laurent Pulses $\{g_p(t)\}$ and the vector of pseudo-symbols $\{a_{p,n}\}$, we define the following circulant matrices:

$$[\underline{\underline{\boldsymbol{l}}}_p^i]_{m,n} = g_p[\text{mod } (k(m-n)+i, kN)] \tag{2.37}$$

and so the circular-extended over-sampled complex envelope of the transmitted signal is:

$$\underline{\boldsymbol{s}}_p = [s_0^0, s_1^0, \ldots, s_{N-1}^0, s_0^1, s_1^1, \ldots, s_{N-1}^1]^T \tag{2.38}$$

$$= \underbrace{\begin{bmatrix} \underline{\underline{\boldsymbol{l}}}_0^0 & \underline{\underline{\boldsymbol{l}}}_1^0 & \cdots & \underline{\underline{\boldsymbol{l}}}_{P-1}^0 \\ \underline{\underline{\boldsymbol{l}}}_0^1 & \underline{\underline{\boldsymbol{l}}}_1^1 & \cdots & \underline{\underline{\boldsymbol{l}}}_{P-1}^1 \end{bmatrix}}_{=\underline{\underline{\boldsymbol{l}}}_p} \underline{\boldsymbol{b}} \tag{2.39}$$

$$= \underline{\underline{\boldsymbol{l}}}_p \underline{\boldsymbol{b}} \tag{2.40}$$

where $\underline{\boldsymbol{b}}$ is a vector collecting the pseudo-symbols of the PAM decomposition, such as $\underline{\boldsymbol{b}} = [a_{0,0}, a_{0,1}, \ldots, a_{0,N-1}, a_{1,0}, \ldots, a_{K-1,0}, \ldots, a_{K-1,N-1}]^T$.

The received over-sampled signal is split into two *polyphase* components ($i \in \{0, 1\}$):

$$r_n^i = r(nT_s + iT_e) \tag{2.41}$$

$$= \sum_m s_m^0 h_{n-m}^i + \sum_m s_m^1 h_{n-m-1+i}^{1-i} + w_n^i \tag{2.42}$$

where

$$h_n^i = h_p[nT_s + iT_e] = h_p[(2n+i)T_e] \tag{2.43}$$

$$w_n^i = w[nT_s + iT_e] \tag{2.44}$$

$$\text{and } s_n^i = s_p[nT_s + iT_e] \tag{2.45}$$

Let us recall that h_p is the periodic version of the filtered channel $h(t)$ obtained thanks to the circular-extended block signal model.

We now define the following circulant matrices, which corresponds to the polyphase components of the channels, for $i \in \{0, 1\}$ with generic terms:

$$[\underline{\underline{\boldsymbol{h}}}^0]_{n,m} = h^0_{\text{mod}(n-m,N)} \tag{2.46}$$

$$[\underline{\underline{\boldsymbol{h}}}^1]_{n,m} = h^1_{\text{mod}(n-m,N)} \tag{2.47}$$

$$[\underline{\underline{\boldsymbol{h}}}^{1'}]_{n,m} = h^1_{\text{mod}(n-m-1,N)} \tag{2.48}$$

Therefore, the received signal can be written matrix-wise as

$$\underline{\boldsymbol{r}}_p = [r_0^0, r_1^0, \ldots, r_{N-1}^0, r_0^1, r_1^1, \ldots, r_{N-1}^1]^T \tag{2.49}$$

$$\underbrace{\begin{bmatrix} \underline{\underline{\boldsymbol{h}}}^0 & \underline{\underline{\boldsymbol{h}}}^{1'} \\ \underline{\underline{\boldsymbol{h}}}^1 & \underline{\underline{\boldsymbol{h}}}^0 \end{bmatrix}}_{=\underline{\underline{\boldsymbol{h}}}_p} \underline{\boldsymbol{s}}_p + \underline{\boldsymbol{w}}_p \tag{2.50}$$

$$= \underline{\underline{\boldsymbol{h}}}_p \underline{\boldsymbol{s}}_p + \underline{\boldsymbol{w}}_p \tag{2.51}$$

$$= \underline{\underline{\boldsymbol{h}}}_p \underline{\underline{\boldsymbol{l}}}_p \underline{\boldsymbol{b}} + \underline{\boldsymbol{w}}_p \tag{2.52}$$

We now apply a Discrete Fourier Transform (DFT) of size $N \times N$ to each polyphase compo-

nents. Let us define $\underline{\underline{\boldsymbol{F}}}_{N,q}$ a matrix of size $qN \times qN$, such as $\underline{\underline{\boldsymbol{F}}}_{N,q} = \underline{\underline{\boldsymbol{I}}}_q \otimes \underline{\underline{\boldsymbol{F}}}_N$ where $\underline{\underline{\boldsymbol{F}}}_N$ is the unitary Fourier matrix of size $N \times N$ with generic term $[\underline{\underline{\boldsymbol{F}}}_N]_{k,n} = \exp(-j2\pi/N)^{kn}/\mathrm{sqrt}(N)$ and the operator $\otimes$ is the Kronecker product. Therefore, applying a DFT to each polyphase components can be seen as the following matrix-wise operation:

$$\begin{aligned}
\underline{\boldsymbol{R}}_p &= \underline{\underline{\boldsymbol{F}}}_{N,2}\underline{\boldsymbol{r}}_p && (2.53)\\
&= \underline{\underline{\boldsymbol{F}}}_{N,2}\underline{\underline{\boldsymbol{h}}}_p\underline{\underline{\boldsymbol{l}}}_p\underline{\boldsymbol{b}} + \underline{\underline{\boldsymbol{F}}}_{N,2}\underline{\boldsymbol{w}}_p && (2.54)\\
&= \underbrace{\underline{\underline{\boldsymbol{F}}}_{N,2}\underline{\underline{\boldsymbol{h}}}_p\underline{\underline{\boldsymbol{F}}}^H_{N,2}}_{=\underline{\underline{\boldsymbol{H}}}_p}\underbrace{\underline{\underline{\boldsymbol{F}}}_{N,2}\underline{\underline{\boldsymbol{l}}}_p\underline{\underline{\boldsymbol{F}}}^H_{N,P}}_{=\underline{\underline{\boldsymbol{L}}}_p}\underbrace{\underline{\underline{\boldsymbol{F}}}_{N,P}\underline{\boldsymbol{b}}}_{=\underline{\boldsymbol{B}}} + \underbrace{\underline{\underline{\boldsymbol{F}}}_{N,2}\underline{\boldsymbol{w}}_p}_{=\underline{\boldsymbol{W}}_p} && (2.55)\\
&= \underline{\underline{\boldsymbol{H}}}_p\underline{\underline{\boldsymbol{L}}}_p\underline{\boldsymbol{B}} + \underline{\boldsymbol{W}}_p && (2.56)
\end{aligned}$$

We point out that as all submatrices of $\underline{\underline{\boldsymbol{h}}}_p$ and $\underline{\underline{\boldsymbol{l}}}_p$ are circulant by definition (thanks to the circular extension of our data block), and therefore by DFT properties, all their equivalent FD counterparts are diagonals.

As we are only interested in mitigating the contribution of the channel (given by $\underline{\underline{\boldsymbol{H}}}_p$), we have to define the vector $\underline{\boldsymbol{S}}_p = \underline{\underline{\boldsymbol{L}}}_p\underline{\boldsymbol{B}}$. This vector corresponds to the polyphase vector of the over-sampled complex envelope of the transmitted signal in the Frequency Domain.

The equalization is performed by the block equalizer matrix $\underline{\underline{\boldsymbol{G}}}_{\mathrm{MMSE}}$ of size $2N \times 2N$ such as the equalized signal is:

$$\widehat{\underline{\boldsymbol{S}}}_p = \underline{\underline{\boldsymbol{G}}}_{\mathrm{MMSE}}\underline{\boldsymbol{R}}_p \tag{2.57}$$

The matrix $\underline{\underline{\boldsymbol{G}}}_{\mathrm{MMSE}}$ of size $2N \times 2N$ minimizes the following Mean Square Error (MSE) criterion:

$$\mathrm{MSE} = \mathbb{E}\{(\underline{\boldsymbol{S}}_p - \underline{\underline{\boldsymbol{G}}}_{\mathrm{MMSE}}\underline{\boldsymbol{R}}_p)^H(\underline{\boldsymbol{S}}_p - \underline{\underline{\boldsymbol{G}}}_{\mathrm{MMSE}}\underline{\boldsymbol{R}}_p)\} \tag{2.58}$$

A straightforward derivation shows that the matrix $\underline{\underline{\boldsymbol{G}}}_{\mathrm{MMSE}}$ is given by [VT+09]:

$$\underline{\underline{\boldsymbol{G}}}_{\mathrm{MMSE}} = \underline{\underline{\boldsymbol{R}}}_{\mathrm{SS,p}}\underline{\underline{\boldsymbol{H}}}^H_p\underline{\underline{\boldsymbol{K}}}^{-1} \tag{2.59}$$

where $\underline{\underline{\boldsymbol{R}}}_{\mathrm{SS,p}}$ is the auto-correlation matrix of the FD vector $\underline{\boldsymbol{S}}$, $\underline{\underline{\boldsymbol{K}}} = \underline{\underline{\boldsymbol{H}}}_p\underline{\underline{\boldsymbol{R}}}_{\mathrm{SS,p}}\underline{\underline{\boldsymbol{H}}}^H_p + \sigma_n^2\underline{\underline{\boldsymbol{I}}}_{2N}$ and σ_n^2 is the noise variance.

We can note that the correlation matrix $\underline{\underline{\boldsymbol{R}}}_{\mathrm{SS,p}}$ can be computed using the PAM decomposition as

$$\begin{aligned}
\underline{\underline{\boldsymbol{R}}}_{\mathrm{SS,p}} &= \mathbb{E}\{\underline{\boldsymbol{S}}_p\underline{\boldsymbol{S}}^H_p\} && (2.60)\\
&= \underline{\underline{\boldsymbol{L}}}_p\mathbb{E}\{\underline{\boldsymbol{B}}\underline{\boldsymbol{B}}^H\}\underline{\underline{\boldsymbol{L}}}^H_p && (2.61)\\
&= \underline{\underline{\boldsymbol{L}}}_p\underline{\underline{\boldsymbol{R}}}_{\mathrm{BB}}\underline{\underline{\boldsymbol{L}}}^H_p && (2.62)
\end{aligned}$$

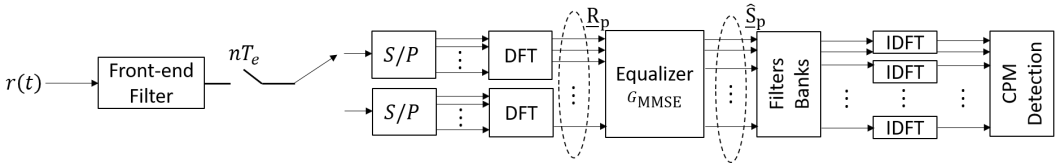

Figure 2.6 – MMSE-FDE of [VT+09]

The time-averaged auto-correlation matrix $\underline{\underline{\boldsymbol{R}}}_{\mathrm{BB}}$ of the pseudo-symbols vector $\underline{\boldsymbol{B}}$ and the auto-correlation matrix $\underline{\underline{\boldsymbol{R}}}_{\mathrm{SS,p}}$ of the vector $\underline{\boldsymbol{S}}_p$ can be precomputed and stored using the Laurent Decomposition [Lau86] for binary CPM with non-integer modulation indices. Even if not considered in [VT+09], this can be extended to the M-ary CPM and for CPM with integer modulation indices. Using the PAM decomposition, this auto-correlation matrix of the pseudo-symbols in the FD is given by

$$\underline{\underline{\boldsymbol{R}}}_{\mathrm{BB}} = \mathbb{E}\{\underline{\boldsymbol{B}}\underline{\boldsymbol{B}}^H\} \tag{2.63}$$

$$= \mathbb{E}\{\underline{\underline{\boldsymbol{F}}}_N \underline{\boldsymbol{b}}\underline{\boldsymbol{b}}^H \underline{\underline{\boldsymbol{F}}}_N^H\} \tag{2.64}$$

$$= \underline{\underline{\boldsymbol{F}}}_N \mathbb{E}\{\underline{\boldsymbol{b}}\underline{\boldsymbol{b}}^H\} \underline{\underline{\boldsymbol{F}}}_N^H \tag{2.65}$$

After equalization, $\widehat{\underline{\boldsymbol{S}}}_p$ is filtered by the over-sampled matched filters of the Laurent components, this operation is equivalent to multiply $\widehat{\underline{\boldsymbol{S}}}_p$ by $\underline{\underline{\boldsymbol{L}}}_p^H$. Those outputs then feds a conventional CPM detector as the ones presented in [CB05]. The overall structure of this equalizer is presented in Fig.2.6.

2.3.2.2 Channel and Laurent Pulse MMSE Equalizer

In [PV06], it turns out that the derived structure performs joint equalization of both the channel (filtered by the LPF) and the Laurent pulses on the Fractionally-Spaced received signal: each filter linked to the PAM representation is jointly considered with the channel.

We consider a time-invariant multi-path channel modeled as:

$$h(t) = \sum_{l=0}^{L_c-1} a_l \delta(t - \tau_l) \tag{2.66}$$

and we recall that the received signal can be written as the circular convolution of periodized versions of the FIR channel and the over-sampled transmitted complex envelope:

$$r(t) = s_{NT_s}(t) \otimes h_{NT_s}(t) + w(t) \tag{2.67}$$

As we consider a periodic version of the channel impulse response, we can compute its

associated Fourier series (and the associated Fourier series coefficients):

$$H(f) = \frac{1}{NT_s} \int_0^{NT_s} h_{NT_s}(t) e^{j2\pi f T_s} \tag{2.68}$$

$$\text{and } H_k = H(k/NT_s) = \sum_{l=0}^{L_c-1} a_l e^{-j2\pi k \tau_l / T_s} \tag{2.69}$$

Furthermore, through the same circular convolution, we also consider a periodic version of the transmitted over-sampled complex envelop of the CPM signal s_{NT_s}. Let us consider the PAM decomposition as described in Chapter 1 and we obtain

$$s_{NT_s}(t) = \sum_{n=0}^{N-1} \sum_{p=0}^{P-1} a_{p,n} g_p(\text{mod}(t - nT_s, NT_s)) \tag{2.70}$$

where $a_{p,n}$ (resp. $g_p(t)$) are the pseudo-symbols (resp. components) of the PAM Decomposition. Hence, as we consider periodic version (of period NT_s) of the P Laurent Pulses $g_p(t)$, we can compute its Fourier Series and the Fourier Series Coefficients:

$$L_p(f) = \frac{1}{NT_s} \int_0^{NT_s} g_p(t) e^{j2\pi f T_s} \tag{2.71}$$

$$\text{and } L_{p,k} = L_p(k/NT_s) \tag{2.72}$$

Let us point out that the Fourier series coefficients $\{H_k\}_k$ (resp. $\{L_{p,k}\}_{p,k}$) of periodized version of the channel $h_{NT_s}(t)$ (resp. of the Laurent Pulses $g_p(t)$) are given by the coefficient of the normalized DFT of one period of the samples of $h(t)$ (resp. $g_p(t)$).

Hence, the received signal is given by:

$$r(t) = \frac{1}{\sqrt{NT_s}} \sum_{k=-N}^{N} \sum_{p=0}^{P-1} L_{p,k} H_k B_{p,k} e^{j2\pi k t / T_s} + w(t) \tag{2.73}$$

where $B_{p,k}$ is the k^{th} elements of the DFT of $\underline{\underline{\boldsymbol{B}}}_{p,N} = \underline{\underline{\boldsymbol{F}}}_N \underline{\boldsymbol{b}}_{p,N}$ where $\underline{\boldsymbol{b}}_{p,N} = [b_{p,0}, b_{p,1}, \ldots, b_{p,N-1}]^T$ and $\underline{\underline{\boldsymbol{F}}}_N$ is the Fourier matrix of size $N \times N$ with generic term $[\underline{\underline{\boldsymbol{F}}}_N]_{k,n} = \exp(-j2\pi/N)^{kn}/\text{sqrt}(N)$

After sampling at $t_i = iT_s/2$, we obtain:

$$r_i = \sqrt{T_s/2} r(t_i) \tag{2.74}$$

$$= \sqrt{\frac{T_s}{2NT_s}} \sum_{k=-N}^{N} \sum_{p=0}^{P-1} L_{p,k} H_k B_{p,k} e^{j2\pi k (iT_s/2)/T} + w_i \tag{2.75}$$

$$= \frac{1}{\sqrt{2N}} \sum_{k=-N}^{N} \sum_{p=0}^{P-1} L_{p,k} H_k B_{p,k} e^{j2\pi k i / 2N} + w_i \tag{2.76}$$

By defining $W_N = \exp(j2\pi/N)$, we have then $W_{2N}^{-ki} = \exp(-j\pi ki/2N)$ and the previous

equation becomes:

$$r_i = \frac{1}{\sqrt{2N}} \sum_{k=-N}^{N} \sum_{p=0}^{P-1} L_{p,k} H_k B_{p,k} W_{2N}^{-ki} + w_i \tag{2.77}$$

The vector $\underline{\boldsymbol{r}} = [r_0, r_1, \ldots, r_{2N-1}]^T$ feeds a 2N-point DFT, producing the vector $\underline{\boldsymbol{R}} = [R_0, R_1, \ldots, R_{2N-1}]^T$. By remarking that $B_{p,k+N} = B_{p,k}$ due to the periodicity of the DFT, we obtain:

$$\underline{\boldsymbol{R}} = \underline{\underline{\boldsymbol{M}}}\,\underline{\boldsymbol{B}}_{2N} + \underline{\boldsymbol{N}} \tag{2.78}$$

where:

$$\underline{\boldsymbol{B}}_{2N} = [\underline{\boldsymbol{B}}_{0,2N}^T, \underline{\boldsymbol{B}}_{1,2N}^T, \ldots, \underline{\boldsymbol{B}}_{P-1,2N}^T]^T \tag{2.79}$$

$$\underline{\boldsymbol{B}}_{p,2N} = [\underline{\boldsymbol{B}}_{p,N}^T, \underline{\boldsymbol{B}}_{p,N}^T]^T \tag{2.80}$$

$$\underline{\underline{\boldsymbol{M}}} = [\underline{\underline{\boldsymbol{M}}}_0, \underline{\underline{\boldsymbol{M}}}_1, \ldots, \underline{\underline{\boldsymbol{M}}}_{P-1}] \tag{2.81}$$

$$\underline{\underline{\boldsymbol{M}}}_p = \mathrm{diag}(M_{p,k}) \tag{2.82}$$

where $M_{p,k} = L_{p,k} H_k (\mathrm{resp.} L_{p,k-2N} H_{k-2N})$ for $k \in \{0, 1, \ldots, N-1\}$ (resp. $k \in \{N, N+1, \ldots, 2N-1\}$).

[PV06] performs an equalization in the Frequency-Domain, defined by the matrix $\underline{\underline{\boldsymbol{D}}}_{LE}$ of size $PN \times 2N$, using the MMSE criterion such as the equalized pseudo-symbols in FD $\underline{\boldsymbol{T}}$ are given by:

$$\underline{\boldsymbol{T}} = \underline{\underline{\boldsymbol{D}}}_{LE} \underline{\boldsymbol{R}} \tag{2.83}$$

and where the equalization matrix $\underline{\underline{\boldsymbol{D}}}_{LE}$ minimizes the MSE as follows:

$$\underline{\underline{\boldsymbol{D}}}_{LE} = \underset{\underline{\underline{\boldsymbol{D}}}}{\mathrm{argmax}}\ \mathbb{E}\{(\underline{\underline{\boldsymbol{D}}}\,\underline{\boldsymbol{R}} - \underline{\boldsymbol{B}})^H (\underline{\underline{\boldsymbol{D}}}\,\underline{\boldsymbol{R}} - \underline{\boldsymbol{B}})\} \tag{2.84}$$

The vector $\underline{\boldsymbol{B}}$ is the vector of collected pseudo-symbols in the FD, i.e. $\underline{\boldsymbol{B}} = [\underline{\boldsymbol{B}}_{0,N}^T, \underline{\boldsymbol{B}}_{1,N}^T, \ldots, \underline{\boldsymbol{B}}_{P-1,N}^T]^T$

This MMSE-FDE is given by [PV06]:

$$\underline{\underline{\boldsymbol{D}}}_{LE} = \underline{\underline{\boldsymbol{J}}}\,\underline{\underline{\boldsymbol{M}}}^H \underline{\underline{\boldsymbol{K}}} \tag{2.85}$$

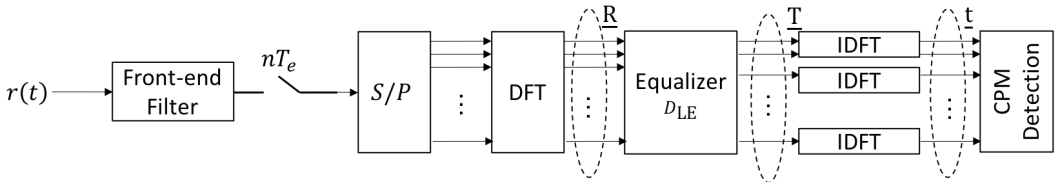

Figure 2.7 – MMSE-FDE of [PV06]

where

$$\underline{\underline{\boldsymbol{G}}}_{r,c} = \mathbb{E}\{\underline{\boldsymbol{B}}_{r,N}\underline{\boldsymbol{B}}_{c,N}^{H}\} \tag{2.86}$$
$$= \mathbb{E}\{\underline{\underline{\boldsymbol{F}}}_{N}\underline{\boldsymbol{b}}_{r,N}\underline{\boldsymbol{b}}_{c,N}^{H}\underline{\underline{\boldsymbol{F}}}_{N}^{H}\}$$
$$= \underline{\underline{\boldsymbol{F}}}_{N}\mathbb{E}\{\underline{\boldsymbol{b}}_{r,N}\underline{\boldsymbol{b}}_{c,N}^{H}\}\underline{\underline{\boldsymbol{F}}}_{N}^{H}$$
$$\underline{\boldsymbol{J}} = [\underline{\underline{\boldsymbol{G}}}_{r,c}\underline{\underline{\boldsymbol{G}}}_{r,c}] \tag{2.87}$$
$$\underline{\underline{\boldsymbol{\Phi}}} = [\underline{\underline{\boldsymbol{G}}}_{r,c}\underline{\underline{\boldsymbol{G}}}_{r,c}; \underline{\underline{\boldsymbol{G}}}_{r,c}\underline{\underline{\boldsymbol{G}}}_{r,c}] \tag{2.88}$$
$$\underline{\underline{\boldsymbol{K}}} = [\underline{\underline{\boldsymbol{M}\boldsymbol{\Phi}\boldsymbol{M}}}^{H} + \sigma_n^2\underline{\underline{\boldsymbol{I}}}_{k,N}]^{-1} \tag{2.89}$$

Hence, the equalized pseudo-symbols $\underline{\boldsymbol{t}}$ are obtained by inverse DFT for each PAM, ie $\underline{\boldsymbol{t}} = \underline{\underline{\boldsymbol{F}}}_{P,N}^{H}\underline{\boldsymbol{T}}$. The overall structure of this equalizer is illustrated in Fig.2.7.

The main disadvantage of this equalizer is the use of a non-conventional detector. Indeed, the equalized pseudo-symbols $\underline{\boldsymbol{t}}$ cannot be used in a conventional trellis-based MAP detector as in [CB05] and we have to use the modified detector introduced by [PV06] and based on [MFG97]. By analogy with the previous equalizer, we can derive a quite simple yet efficient method to compensate for this disadvantage: we can reconstruct an equalized over-sampled complex envelope by using the equalized pseudo-symbols.

2.3.2.3 Equivalence of the Joint Channel and Laurent Pulses Equalizer [PV06] and the FDE Channel equalizer from [VT+09]

Contrary to what has been claimed in [VT+09], we will show that both equalizers [VT+09] and [PV06] propose the same performance if a proper linear processing is done after equalization.

Indeed, let us recall the matrix-wise representation of the received signal using the polyphase representation of [VT+09]:

$$\underline{\boldsymbol{R}}_p = \underbrace{\underline{\underline{\boldsymbol{H}}}_p\underline{\underline{\boldsymbol{L}}}_p}_{=\underline{\underline{\boldsymbol{P}}}}\underline{\boldsymbol{S}}_p + \underline{\boldsymbol{W}}_p \tag{2.90}$$
$$= \underline{\underline{\boldsymbol{P}}}\underline{\boldsymbol{S}}_p + \underline{\boldsymbol{W}}_p \tag{2.91}$$

Using the joint channel and Laurent Pulses equalizer of [PV06] and the polyphase represen-

ation, the equalized pseudo-symbols are:

$$\underline{\widehat{\boldsymbol{B}}} = \underline{\underline{\boldsymbol{D}}}_{LE}\underline{\boldsymbol{R}}_p \tag{2.92}$$

with

$$\underline{\underline{\boldsymbol{D}}}_{LE} = \underline{\underline{\boldsymbol{R}}}_{\mathrm{BB}}\underline{\underline{\boldsymbol{P}}}^H[\underline{\underline{\underline{\boldsymbol{P}}\boldsymbol{R}}}_{\mathrm{BB}}\underline{\underline{\boldsymbol{P}}}^H + \sigma_n^2\underline{\underline{\boldsymbol{I}}}_{2N}]^{-1} \tag{2.93}$$

Using the channel equalizer of [VT+09], we recall that the equalized signal is given by:

$$\underline{\widehat{\boldsymbol{S}}} = \underline{\underline{\boldsymbol{G}}}_{\mathrm{MMSE}}\underline{\boldsymbol{R}} \tag{2.94}$$

where

$$\underline{\underline{\boldsymbol{G}}}_{\mathrm{MMSE}} = \underline{\underline{\boldsymbol{R}}}_{\mathrm{SS,p}}\underline{\underline{\boldsymbol{H}}}_p^H[\underline{\underline{\boldsymbol{H}}}_p\underline{\underline{\boldsymbol{R}}}_{\mathrm{SS,p}}\underline{\underline{\boldsymbol{H}}}_p^H + \sigma_n^2\underline{\underline{\boldsymbol{I}}}_{2N}]^{-1} \tag{2.95}$$

with $\underline{\underline{\boldsymbol{R}}}_{\mathrm{SS,p}} = \underline{\underline{\boldsymbol{L}}}_p\underline{\underline{\boldsymbol{R}}}_{\mathrm{BB}}\underline{\underline{\boldsymbol{L}}}_p^H$ as defined in Section 2.3.2.1.

It can been easily shown that the two equalizers are linked by a simple linear relation:

$$\begin{aligned}
\underline{\underline{\boldsymbol{G}}}_{\mathrm{MMSE}} &= \underline{\underline{\boldsymbol{L}}}_p\underline{\underline{\boldsymbol{R}}}_{\mathrm{BB}}\underline{\underline{\boldsymbol{L}}}_p^H\underline{\underline{\boldsymbol{H}}}_p^H[\underline{\underline{\boldsymbol{H}}}_p\underline{\underline{\boldsymbol{L}}}_p\underline{\underline{\boldsymbol{R}}}_{\mathrm{BB}}\underline{\underline{\boldsymbol{L}}}_p^H\underline{\underline{\boldsymbol{H}}}_p^H + \sigma_n^2\underline{\underline{\boldsymbol{I}}}_{2N}]^{-1} && (2.96)\\
&= \underline{\underline{\boldsymbol{L}}}_p\underline{\underline{\boldsymbol{R}}}_{\mathrm{BB}}\underline{\underline{\boldsymbol{P}}}^H[\underline{\underline{\underline{\boldsymbol{P}}\boldsymbol{R}}}_{\mathrm{BB}}\underline{\underline{\boldsymbol{P}}}^H + \sigma_n^2\underline{\underline{\boldsymbol{I}}}_{2N}]^{-1} && (2.97)\\
&= \underline{\underline{\boldsymbol{L}}}_p\underline{\underline{\boldsymbol{D}}}_{LE} && (2.98)
\end{aligned}$$

and so the equalized pseudo-symbols and the equalized over-sampled complex envelop of the transmitted signal are also linked by a linear relation:

$$\begin{aligned}
\underline{\widetilde{\boldsymbol{S}}} &= \underline{\underline{\boldsymbol{L}}}_p\underline{\widehat{\boldsymbol{B}}} && (2.99)\\
&= \underline{\underline{\boldsymbol{L}}}_p\underline{\underline{\boldsymbol{D}}}_{\mathrm{LE}}\underline{\boldsymbol{R}}_p && (2.100)\\
&= \underline{\underline{\boldsymbol{G}}}_{\mathrm{MMSE}}\underline{\boldsymbol{R}}_p && (2.101)\\
\text{as } \underline{\underline{\boldsymbol{G}}}_{\mathrm{MMSE}} &= \underline{\underline{\boldsymbol{L}}}_p\underline{\underline{\boldsymbol{D}}}_{LE} && (2.102)
\end{aligned}$$

Hence, by reconstructing the signal, we show that both equalizers are finally strictly equivalent when used with a conventional detector if the proper processing is done on the equalized pseudo-symbols, contrary to what has been claimed in [VT+09].

To conclude, the difference of performance between the two equalizers does not come from increased noise power by equalizing the Laurent Pulses in addition to the channel as stated in [VT+09]. Indeed, by using the same SISO MAP detector, both equalizers achieve the same performance as shown by simulation in Section 2.3.5 (in order to be the more complete, we have also implemented this equalizer using the polyphase representation for simulations purpose).

2.3.3 A new exact low-complexity FD-MMSE Equalizer for CPM over TIV Channels

In this section, we derive an *exact low-complexity* MMSE equalizer in the Frequency-Domain based on the fractionally-spaced representation of the CPM waveforms, only considering time-invariant frequency-selective channels. As in [VT+09], we perform a linear MMSE-FDE over the over-sampled complex envelope of the CPM signals, but by using the FS representation, we can fully benefit from the properties of circular block-based CPM and reduce the complexity, without making any kind of approximation in the equalizer derivation.

While performing the same as the equalizer proposed by [PV06] and the "full complexity" polyphase domain equalizer of [VT+09], we will show that the proposed approach has a significant lower complexity, of the same order as the *approximated low complexity* version of [VT+09]. Moreover, we will also prove that the MMSE-FDE from [OKD09] is an approximation of the proposed FS equalizer.

2.3.3.1 Derivation of the MMSE-FDE

Let us recall that the received signal is given by the circular convolution:

$$r(t) = h_{NT_s}(t) \otimes s_{NT_s}(t) + w(t) \tag{2.103}$$

After sampling at kR_s, we obtain the following matrix-wise representation:

$$\underline{\boldsymbol{r}} = \begin{bmatrix} r[0] \\ r[1] \\ \vdots \\ \vdots \\ \vdots \\ r[kN-1] \end{bmatrix} = \begin{bmatrix} h[0] & 0 & \dots & h[L-1] & \dots & h[1] \\ h[1] & h[0] & 0 & \dots & h[L-1] & \ddots \\ \ddots & \ddots & \ddots & \ddots & \ddots & \ddots \\ h[L-1] & \dots & h[0] & 0 & \dots & 0 \\ \ddots & \ddots & \ddots & \ddots & \ddots & \ddots \\ 0 & \dots & h[L-1] & \dots & h[1] & h[0] \end{bmatrix} \begin{bmatrix} s[0] \\ s[1] \\ \vdots \\ \vdots \\ \vdots \\ s[kN-1] \end{bmatrix} + \begin{bmatrix} w[0] \\ w[1] \\ \vdots \\ \vdots \\ \vdots \\ w[kN-1] \end{bmatrix} \tag{2.104}$$

$$= \underline{\underline{\boldsymbol{h}}}\,\underline{\boldsymbol{s}} + \underline{\boldsymbol{w}} \tag{2.105}$$

We define the matrix $\underline{\underline{\boldsymbol{F}}}_{kN}$ the unitary Fourier matrix of size $kN \times kN$ with generic term $[\underline{\underline{\boldsymbol{F}}}_N]_{l,m} = \exp(-j2\pi/(kN))^{lm}/\mathrm{sqrt}(kN)$. Then, the FD counterpart of Eq.(2.105) is:

$$\underline{\boldsymbol{R}} = \underline{\underline{\boldsymbol{F}}}_{kN}\underline{\boldsymbol{r}} \tag{2.106}$$

$$= \underbrace{\underline{\underline{\boldsymbol{F}}}_{kN}\underline{\underline{\boldsymbol{h}}}\underline{\underline{\boldsymbol{F}}}_{kN}^{H}}_{=\underline{\underline{\boldsymbol{H}}}} \underbrace{\underline{\underline{\boldsymbol{F}}}_{kN}\underline{\boldsymbol{s}}}_{=\underline{\boldsymbol{S}}} + \underbrace{\underline{\underline{\boldsymbol{F}}}_{kN}\underline{\boldsymbol{w}}}_{=\underline{\boldsymbol{W}}} \tag{2.107}$$

$$= \underline{\underline{\boldsymbol{H}}}\,\underline{\boldsymbol{S}} + \underline{\boldsymbol{W}} \tag{2.108}$$

By DFT properties, the matrix $\underline{\underline{\boldsymbol{H}}}$ is a diagonal matrix as $\underline{\underline{\boldsymbol{h}}}$ is circulant.

The equalization is performed using the block equalizer matrix $\underline{\underline{\boldsymbol{J}}}_{\mathrm{MMSE}}$ of size $kN \times kN$ such as the equalized signal is:

$$\underline{\widehat{\boldsymbol{S}}} = \underline{\underline{\boldsymbol{J}}}_{\mathrm{MMSE}} \underline{\boldsymbol{R}} \tag{2.109}$$

and $\underline{\underline{\boldsymbol{J}}}_{\mathrm{MMSE}}$ minimizes the following Mean Square Error (*MSE*) criterion:

$$\underline{\underline{\boldsymbol{J}}}_{\mathrm{MMSE}} = \underset{\underline{\underline{\boldsymbol{J}}}}{\mathrm{argmax}}\ \mathbb{E}\Big\{(\underline{\boldsymbol{S}} - \underline{\underline{\boldsymbol{J}}}\,\underline{\boldsymbol{R}})^H (\underline{\boldsymbol{S}} - \underline{\underline{\boldsymbol{J}}}\,\underline{\boldsymbol{R}})\Big\}. \tag{2.110}$$

A straightforward derivation [HMV95] shows that the matrix $\underline{\underline{\boldsymbol{J}}}_{\mathrm{MMSE}}$ minimizing the MSE is given by:

$$\underline{\underline{\boldsymbol{J}}}_{\mathrm{MMSE}} = \underline{\underline{\boldsymbol{R}}}_{\mathrm{SS}} \underline{\underline{\boldsymbol{H}}}^H \underline{\underline{\boldsymbol{K}}}^{-1} \tag{2.111}$$

with $\underline{\underline{\boldsymbol{K}}} = \underline{\underline{\boldsymbol{H}}}\,\underline{\underline{\boldsymbol{R}}}_{\mathrm{SS}} \underline{\underline{\boldsymbol{H}}}^H + \sigma_n^2 \underline{\underline{\boldsymbol{I}}}_{kN}$, σ_n^2 the noise variance and $\underline{\underline{\boldsymbol{R}}}_{\mathrm{SS}}$ is the time-averaged auto-correlation matrix of $\underline{\boldsymbol{S}}$, defined as:

$$\begin{aligned}
\underline{\underline{\boldsymbol{R}}}_{\mathrm{SS}} &= \mathbb{E}\{\underline{\boldsymbol{S}}\underline{\boldsymbol{S}}^H\} && (2.112)\\
&= \mathbb{E}\{\underline{\underline{\boldsymbol{F}}}_{kN} \underline{\boldsymbol{s}}\underline{\boldsymbol{s}}^H \underline{\underline{\boldsymbol{F}}}_{kN}^H\} && (2.113)\\
&= \underline{\underline{\boldsymbol{F}}}_{kN} \underbrace{\mathbb{E}\{\underline{\boldsymbol{s}}\underline{\boldsymbol{s}}^H\}}_{=\underline{\underline{\boldsymbol{r}}}_{\mathrm{ss}}} \underline{\underline{\boldsymbol{F}}}_{kN}^H && (2.114)\\
&= \underline{\underline{\boldsymbol{F}}}_{kN} \underline{\underline{\boldsymbol{r}}}_{\mathrm{ss}} \underline{\underline{\boldsymbol{F}}}_{kN}^H && (2.115)
\end{aligned}$$

The matrix $\underline{\underline{\boldsymbol{r}}}_{\mathrm{ss}}$ corresponds to the time-averaged discrete auto-correlation function of the over-sampled complex envelope of the transmitted CPM signal. Moreover, this matrix $\underline{\underline{\boldsymbol{r}}}_{\mathrm{ss}}$ (and therefore $\underline{\underline{\boldsymbol{R}}}_{\mathrm{SS}}$) can be precomputed using the Laurent decomposition [Lau86] for binary CPM with non-integer modulation indices as shown in [VT+09] and thus stored at the receiver side. This can be extended to the M-ary case and to CPM with integer modulation indices.

This equalizer is equivalent in its derivation to the one using the polyphase representation presented in [VT+09]. The only difference is within the use of the FS representation: it leads to a different ordering of the matrices elements implied in equation (2.111), exhibiting nice properties. Indeed, we will show in the following that $\underline{\underline{\boldsymbol{R}}}_{\mathrm{SS}}$, as $\underline{\underline{\boldsymbol{H}}}$, is a diagonal matrix for the FS representation (contrary to the polyphase representation), which enables a lower complexity for the equalizer.

First, we recall that the received sequence corresponds to the circular convolution of the circularly extended transmitted sequence (composed by the data block and the UW) and the channel impulse response. Therefore, over a finite-time observation window corresponding to this block, this circular convolution can be seen as a linear convolution of $\underline{\boldsymbol{h}}$ and a periodic version of $\underline{\boldsymbol{s}}$. Hence, by considering this periodic version of $\underline{\boldsymbol{s}}$ while deriving the statistical properties, the time-averaged auto-correlation function of $\underline{\boldsymbol{s}}$ is periodic of period kN over

this block. As $s(t)$ is a complex signal, the auto-correlation is Hermitian, i.e. $r_{\text{ss}}^*(l) = r_{\text{ss}}(-l)$ (where $r_{\text{ss}}(.)$ is the discrete time-averaged auto-correlation function). We now obtain: $r_{\text{ss}}^*(l) = r_{\text{ss}}(-l) = r_{\text{ss}}(kN - l)$. This property is illustrated in Fig.2.8.

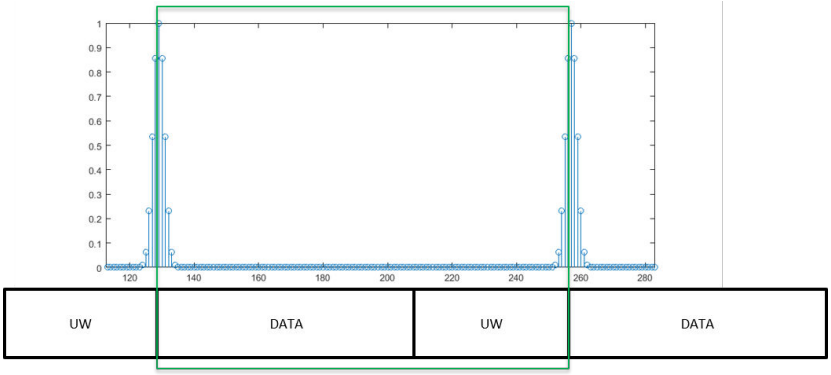

Figure 2.8 – Periodization of the time-averaged auto-correlation function

Then, we can show that the time-domain time-averaged auto-correlation matrix is circulant:

$$\underline{\underline{\boldsymbol{r}}}_{\text{ss}} = \begin{bmatrix} r_{\text{ss}}(0) & r_{\text{ss}}^*(1) & r_{\text{ss}}^*(2) & \dots & r_{\text{ss}}^*(kN-1) \\ r_{\text{ss}}(1) & r_{\text{ss}}(0) & r_{\text{ss}}^*(1) & \dots & r_{\text{ss}}^*(kN-2) \\ r_{\text{ss}}(2) & r_{\text{ss}}(1) & r_{\text{ss}}(0) & \dots & r_{\text{ss}}^*(kN-3) \\ \vdots & \vdots & \vdots & \ddots & \vdots \\ r_{\text{ss}}(kN-1) & r_{\text{ss}}(kN-2) & r_{\text{ss}}(kN-3) & \dots & r_{\text{ss}}(0) \end{bmatrix} \tag{2.116}$$

$$= \begin{bmatrix} r_{\text{ss}}(0) & r_{\text{ss}}(kN-1) & r_{\text{ss}}(kN-2) & \dots & r_{\text{ss}}(1) \\ r_{\text{ss}}(1) & r_{\text{ss}}(0) & r_{\text{ss}}(kN-1) & \dots & r_{\text{ss}}(2) \\ r_{\text{ss}}(2) & r_{\text{ss}}(1) & r_{\text{ss}}(0) & \dots & r_{\text{ss}}(3) \\ \vdots & \vdots & \vdots & \ddots & \vdots \\ r_{\text{ss}}(kN-1) & r_{\text{ss}}(kN-2) & r_{\text{ss}}(kN-3) & \dots & r_{\text{ss}}(0) \end{bmatrix} \tag{2.117}$$

We can see that $\underline{\underline{\boldsymbol{r}}}_{\text{ss}}$ is finally circulant with first column $\underline{\underline{\boldsymbol{r}}}_{\text{ss}}$ being $[r_{\text{ss}}(0), r_{\text{ss}}(1), \dots, r_{\text{ss}}(kN-1)]^T$. The auto-correlation matrix in the frequency domain $\underline{\underline{\boldsymbol{R}}}_{\text{SS}}$ is thus diagonal by DFT property. Moreover all the diagonal terms are real numbers. We point out that this diagonalization is not possible in the case of [VT+09] as they do not use a FS representation of the received signal resulting in a different auto-correlation matrix in the time-domain.

Hence, the equalizer $\underline{\underline{\boldsymbol{J}}}_{\text{MMSE}}$ is simply a diagonal matrix with generic term given by:

$$J[l] = \frac{R_{\text{SS}}[l]H^*[l]}{R_{\text{SS}}[l]|H[l]|^2 + \sigma_n^2} \tag{2.118}$$

The overall architecture of our proposed low-complexity MMSE-FDE is depicted in Fig.2.9.

Note that, if we approximate the correlation matrix $\underline{\underline{\boldsymbol{R}}}_{\text{SS}}$ by an identity matrix (ie. ne-

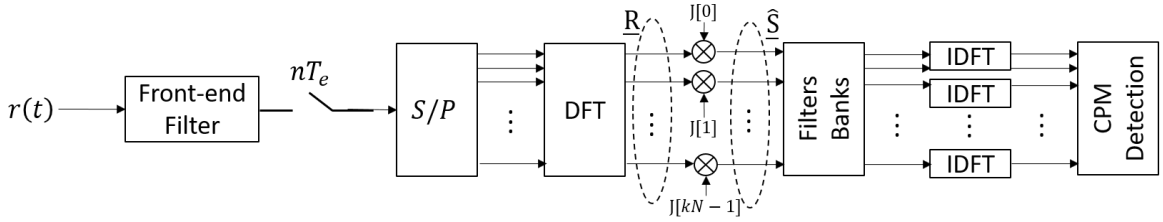

Figure 2.9 – Proposed Exact Low-complexity MMSE-FDE

glecting the signal correlation and assuming the signal energy normalized to 1), the equalizer becomes:

$$J_{\text{approx}}[l] = \frac{H^*[l]}{|H[l]|^2 + \sigma_n^2} \tag{2.119}$$

which corresponds to the equalizer proposed in [OKD09] with $k = 2$.

2.3.3.2 Difference between the proposed equalizer and the MMSE-FDE [VT+09]

As we derive a similar MMSE-FDE as the one in [VT+09], one may ask why it could not achieve a low-complexity structure.

As previously said, the main difference between our equalizer and the one in [VT+09] is the representation of the over-sampled received signal. Indeed, [VT+09] uses the polyphase/multi-channel representation whereas we use a FS representation which are linked by a permutation matrix $\underline{\underline{\boldsymbol{P}}}_M = [\underline{\underline{\boldsymbol{I}}}_N \otimes [1,0]; \underline{\underline{\boldsymbol{I}}}_N \otimes [0,1]]$ ($\otimes$ is the Kronecker product) and so $\underline{\boldsymbol{s}}_{\text{p}} = \underline{\underline{\boldsymbol{P}}}_M \underline{\boldsymbol{s}}$.

However, when using the polyphase representation, the time-domain auto-correlation matrix of the over-sampled complex envelope does not have anymore a circular structure per block. Indeed, this matrix is given by:

$$\underline{\underline{\boldsymbol{r}}}_{\text{ss,p}} = \mathbb{E}[\underline{\boldsymbol{s}}_p \underline{\boldsymbol{s}}_p^H] \tag{2.120}$$

$$= \begin{bmatrix} r_{\text{ss}}(0) & r_{\text{ss}}^*(2) & r_{\text{ss}}^*(4) & \dots & r_{\text{ss}}^*(2N-2) & r_{\text{ss}}^*(1) & r_{\text{ss}}^*(3) & \dots & r_{\text{ss}}^*(2N-1) \\ r_{\text{ss}}(2) & r_{\text{ss}}(0) & r_{\text{ss}}^*(2) & \dots & r_{\text{ss}}^*(2N-4) & r_{\text{ss}}(3) & r_{\text{ss}}^*(1) & \dots & r_{\text{ss}}^*(2N-3) \\ \vdots & \vdots & \vdots & \vdots & \vdots & \vdots & \vdots & \vdots & \vdots \end{bmatrix} \tag{2.121}$$

where $\mathbb{E}[.]$ is the expectation operator and $r_{\text{ss}}(.)$ is the discrete time-averaged auto-correlation function. By using the property of periodicity of this function, we obtain

$$\underline{\underline{\boldsymbol{r}}}_{\text{ss,p}} = \begin{bmatrix} r_{\text{ss}}(0) & r_{\text{ss}}(2N-2) & r_{\text{ss}}(2N-4) & \dots & r_{\text{ss}}(2) & r_{\text{ss}}(2N-1) & r_{\text{ss}}(2N-3) & \dots & r_{\text{ss}}(1) \\ r_{\text{ss}}(2) & r_{\text{ss}}(0) & r_{\text{ss}}(2N-2) & \dots & r_{\text{ss}}(4) & r_{\text{ss}}(3) & r_{\text{ss}}(2N-1) & \dots & r_{\text{ss}}(3) \\ \vdots & \vdots & \vdots & \vdots & \vdots & \vdots & \vdots & \vdots & \vdots \end{bmatrix} \tag{2.122}$$

Therefore, in this system, no diagonalization is possible by DFT and we cannot design the same low-complexity equalizer structure as the one we proposed.

2.3.4 Summary and Complexity Analysis

In the following, we will compare the proposed equalizer (called "FS-MMSE-FDE", see Section 2.3.3) with the other exact MMSE-FDE equalizers: (a) the equalizer proposed in [VT+09] (see Section 2.3.2.1). This equalizer uses the polyphase representation and produces an estimated signal by only considering the channel contribution. It will be called "PP-MMSE-FDE"; (b) the equalizer proposed in [PV06]. This equalizer both considers the contribution of the channel and the LD to produce an estimate of the LD pseudo-symbols using the FS representation. It will be called "LD-FS-MMSE-FDE" (see Section 2.3.2.2); (c) a modified version of the equalizer proposed in [PV06], using a polyphase representation instead of a FS. It will be called "LD-PP-MMSE-FDE".

The main features of those equalizers are resumed in Table 2.3.

Notation	Reference	Equalizer	Signal Rep.
LD-FS-MMSE-FDE	[PV06]	$\widehat{\underline{\underline{\boldsymbol{B}}}} = \underline{\underline{\boldsymbol{J}}}\underline{\underline{\boldsymbol{M}}}^H[\underline{\underline{\boldsymbol{M}}}\underline{\underline{\boldsymbol{\Phi}}}\underline{\underline{\boldsymbol{M}}}^H + \sigma_n^2 I_{2N}]^{-1}\underline{\underline{\boldsymbol{R}}}$	FS
PP-MMSE-FDE	[VT+09]	$\widehat{\underline{\underline{\boldsymbol{S}}}}_p = \underline{\underline{\boldsymbol{R}}}_{\mathrm{SS,p}}\underline{\underline{\boldsymbol{H}}}_p^H[\underline{\underline{\boldsymbol{H}}}_p\underline{\underline{\boldsymbol{R}}}_{\mathrm{SS,p}}\underline{\underline{\boldsymbol{H}}}_p^H + \sigma_n^2\underline{\underline{\boldsymbol{I}}}_{2N}]^{-1}\underline{\underline{\boldsymbol{R}}}_p$	Polyphase
LD-PP-MMSE-FDE	[Cha+17a]	$\widehat{\underline{\underline{\boldsymbol{B}}}} = \underline{\underline{\boldsymbol{R}}}_{\mathrm{BB}}\underline{\underline{\boldsymbol{P}}}^H[\underline{\underline{\boldsymbol{P}}}\underline{\underline{\boldsymbol{R}}}_{\mathrm{BB}}\underline{\underline{\boldsymbol{P}}}^H + \sigma_n^2\underline{\underline{\boldsymbol{I}}}_{2N}]^{-1}\underline{\underline{\boldsymbol{R}}}_p$	Polyphase
FS-MMSE-FDE	[Cha+18]	$\widehat{\underline{\underline{\boldsymbol{S}}}} = \underline{\underline{\boldsymbol{R}}}_{\mathrm{SS}}\underline{\underline{\boldsymbol{H}}}^H[\underline{\underline{\boldsymbol{H}}}\underline{\underline{\boldsymbol{R}}}_{\mathrm{SS}}\underline{\underline{\boldsymbol{H}}}^H + \sigma_n^2\underline{\underline{\boldsymbol{I}}}_{2N}]^{-1}\underline{\underline{\boldsymbol{R}}}$	FS

Table 2.3 – Relation between the TIV-MMSE-FDE

We now analyze the complexity of our proposed MMSE-FDE in order to compare it with the others over-sampled MMSE-FDEs proposed in the literature.

The complexity will be expressed in number of floating-point operations (flops) per block as in [VT+09], where a flop corresponds to one real multiplication plus one real addition [PV06].

Thanks to the circular block-based structure of the CPM transmission, we have shown that $\underline{\underline{\boldsymbol{R}}}_{\mathrm{ss}}$ and $\underline{\underline{\boldsymbol{K}}}$ are diagonal matrices. Hence, the computation of $\underline{\underline{\boldsymbol{K}}}^{-1}$ requires $4kN$ real multiplications and $2kN$ real additions, plus kN real divisions for the inversion. The product $\underline{\underline{\boldsymbol{R}}}_{\mathrm{ss}}\underline{\underline{\boldsymbol{H}}}^H\underline{\underline{\boldsymbol{K}}}^{-1}$ is done with $3kN$ real multiplications. Thus, the computation of $\underline{\underline{\boldsymbol{J}}}_{\mathrm{MMSE}}$ requires $2kN$ real additions, $7kN$ real multiplications and kN real divisions. The equalization is then performed with kN complex multiplications as we only deal with a diagonal matrix of size kN.

So, we can conclude that the complexity of our receiver is dominated by the DFT and IDFTs operations and is in $O\big(kN\log(kN) + PN\log(N)\big)$. This is the same for the low complexity MMSE-FDE proposed in [OKD09] (only removing $2kN$ real multiplications), and comparing our equalizer with equalizers leading to the same performance (as it will be shown in the following section), TABLE 2.4 highlights that the computational complexity of our

Receiver Type	FFTs and IFFTs	Equalizer Calc.	Equalization
Linear MMSE-TDE [PV06]	0	$+8N^3$	$+\mathcal{O}(PN^3)$
LD-FS-MMSE-FDE [PV06]	$2N\log(2N) + PN\log(N)$	$+8N^3$	$+\mathcal{O}(PN^3)$
PP-MMSE-FDE [VT+09]	$2N\log(N) + PN\log(N)$	$+8N^3$	$+\mathcal{O}(PN^3)$
Approx. PP-MMSE-FDE [VT+09]	$2N\log(N) + PN\log(N)$	$+\mathcal{O}(2N)$	$+\mathcal{O}(PN)$
FS-MMSE-FDE	$2N\log(2N) + PN\log(N)$	$+\mathcal{O}(2N)$	$+\mathcal{O}(PN)$

Table 2.4 – Computational complexity comparison between the over-sampled MMSE-FDE equalizers

receiver is lower (in the equalization procedure, we also take into account the computational complexity of the filtering).

2.3.5 Results and Discussion

We present in this section different results obtained with those equalizers by simulation. As explained previously, we will show that the equalizers of [PV06], denoted LD-FS-MMSE-FDE, and [VT+09], denoted PP-MMSE-FDE, have the same performance if a proper post-processing is used before feeding the CPM detector. Moreover, we will show that our equalizer also has the same performance but with a lower computational complexity. Last, we will point out by simulation that the equalizer in [TS05] does not work in case of paths' delays that are not multiple of the symbol duration.

We present in Fig 2.10 the uncoded BER obtained by simulation for a generic frequency-selective channel. We use the channel (chan 1) proposed in [TS05]. However, instead of considering delays which are multiples of T_s, we consider the same Power Delay Profile with delays multiples of $T_s/2$. No difference can be seen for the LD-FS-MMSE-FDE and the PP-MMSE-FDE for both CPM schemes as theoretically proved. In order to be as much complete as possible, we have also implemented the joint channel and LPs equalizer using a polyphase representation (LD-PP-MMSE-FDE) of the over-sampled received signal of the equalizer [PV06] and there is no difference of performance. We can see that the Tan and Stüber's equalizer exhibits a floor as it does not take into account all the interference between signal components due to the frequency-selective channel.

Let us now consider two binary CPM schemes with a raised-cosine pulse shape (noted *RC*), a memory of $L_{\text{cpm}} = 3$ and a modulation index $h \in \{\frac{1}{4}, \frac{1}{2}\}$. The transmitted signal is composed of 8 blocks of 512 symbols, where each block is composed of data symbols, termination symbols and a Unique Word of size 16. The channel is the generic frequency channel proposed in [TS05] as *chan 1*, but with modified delays: multiples of $T_s/2$ instead of T_s and the same Power Delay Profile.

Fig. 2.11 plots the obtained achievable rates for the four schemes using MMSE-FDE. The achievable coding rate is estimated by computing the area under the Extrinsic Information Transfer Chart (*EXIT chart*) of the detector [Hag04] (see Chapter 1). Achievable

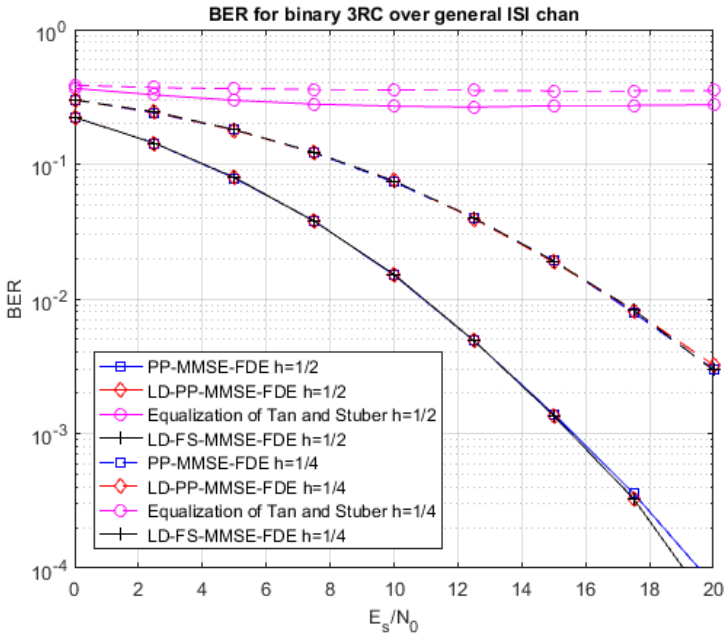

Figure 2.10 – Uncoded BER over general ISI channel

coded spectral efficiency can then be derived by multiplying the obtained achievable rate with the spectral efficiency of the inner CPM waveform [Hag04]. The results show that the proposed equalizer has the same performance as the equalizers proposed by [VT+09] and [PV06] (actually both having the same performance, as it has been shown in [Cha+17a], up to post-processing which is applied here).

Fig. 2.12 plots bit error rates, considering now a coded transmission and an iterative concatenated scheme between the CPM MAP detector and the channel MAP decoder. Used channel for simulations is an aeronautical channel, modeled as a two-paths channel with a second path delayed by $3.7T_s$ compared to the first one. A convolutional code with polynomial generators $(5, 7)_8$ has been added and 20 iterations have been done in the iterative procedure between the CPM MAP detector and the channel MAP decoder. For the same complexity, the fact that we do not approximate the auto-correlation matrix, as it is done in [OKD09], allows our equalizer to increase the performance of 2dB at a BER of 10^{-3} and to achieve the same performance than other state-of-the-art approaches.

2.4 TIV Channel estimation

Generally, for study of equalization schemes, all those works have been done under the hypothesis of perfect channel knowledge and perfect carrier recovery. Only [VT+09] presents simulation results for equalization with channel estimation errors and [BV], [BV11] perform a frequency-domain channel estimation with interpolation (using B-spline functions). [PHR09] performs frequency-domain channel estimation with superimposed pilots.

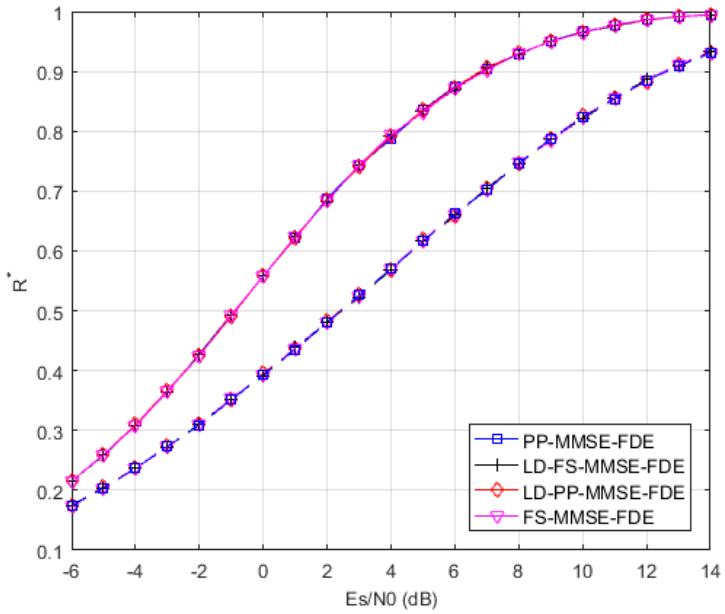

Figure 2.11 – Maximum achievable coding rate for the different MMSE-FDE

In this section, we will present a Least Squares (LS) channel estimation for over-sampled received signal. Indeed, as most of the equalizers works on an over-sampled version of the transmitted complex envelope, we need to estimate the over-sampled filtered channel.

As previously, we will consider a transmission over a frequency-selective channel defined by:

$$h_c(t) = \sum_{l=0}^{L_c-1} h_l \delta(t - \tau_l) \tag{2.123}$$

After ideal low-pass filtering using $\Psi(t)$, we recall that the received signal is:

$$r(t) = \sum_m s(m\frac{T_s}{k}) h(t - m\frac{T_s}{k}) + w(t) \tag{2.124}$$

$$\text{where } h(t) = \Psi(t) * h_c(t) * \Psi(t) \tag{2.125}$$

and $w(t)$ is an additive White Gaussian noise. After sampling at nT_e, we obtain

$$r[n] = r(nT_e) = \sum_m s(m\frac{T_s}{k}) h(nT_e - m\frac{T_s}{k}) + w(nT_e) \tag{2.126}$$

$$= \sum_m s[m]h[n-m] + w[n] \tag{2.127}$$

By denoting L_h the span of the filtered channel $h(t)$ in number of samples and considering the J first received symbols, we have the following matrix-wise representation of the received

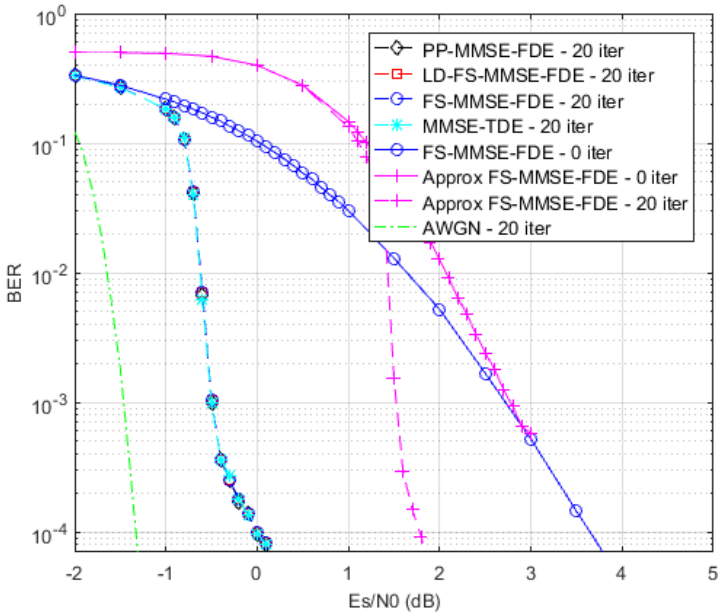

Figure 2.12 – BER over frequency-selective channel

signal:

$$\begin{bmatrix} r[0] \\ r[1] \\ \vdots \\ \vdots \\ r[kJ-1] \end{bmatrix} = \begin{bmatrix} s[0] & s[-1] & \dots & s[-L_h+1] \\ s[1] & s[0] & s[-1] & \dots \\ s[L_h-1] & \dots & s[1] & s[0] \\ \ddots & \ddots & \ddots & \ddots \\ s[kJ-1] & \dots & s[kJ-L_h+1] & s[kJ-L_h] \end{bmatrix} \begin{bmatrix} h[0] \\ h[1] \\ \vdots \\ \vdots \\ h[L_h-1] \end{bmatrix} + \underline{\boldsymbol{w}} \quad (2.128)$$

$$= \underline{\underline{\boldsymbol{s}}}\,\underline{\boldsymbol{h}} + \underline{\boldsymbol{w}} \quad (2.129)$$

where the matrix $\underline{\underline{\boldsymbol{s}}}$ is of size $kJ \times L_h$ and the vector $\underline{\boldsymbol{h}}$ is the channel vector of length L_h to estimate.

The major difference between our model and the one generally considered for channel estimation in case of linear modulation is that we do not estimate a discrete equivalent channel (at baud rate) but an over-sampled channel filtered by a LPF at the receiver. We illustrate the effect of the LPF on the channel $h_c(t)$ in Fig.2.13. To plot it, we consider a down-sampling from 10 samples per symbols to 2 samples per symbol, and $h_c(t) = h_0\delta(t) + h_1\delta(t - 2.7T_s)$. We can see how the LPF filter *interpolates* the different paths of the channel.

Different scenarios can be considered:

- There is no prior transmission, i.e. $s[-1] = s[-2] = \dots = s[1 - L_h] = 0$
- There is a prior transmission:
  - $[s[-1], [-2], \dots, s[1 - L_h]]$ are unknown. In this case, we have to remove the first

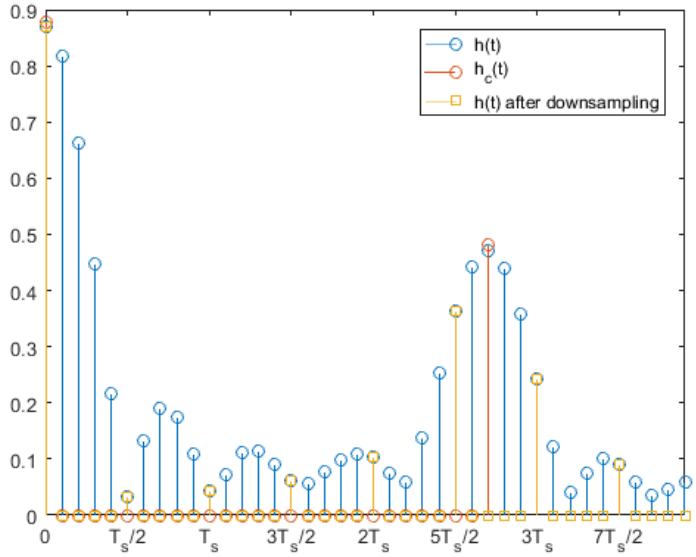

Figure 2.13 – Finite impulse responses of $h_c(t)$ and $h(t)$

L_h samples to the received vector;

- $[s[-1], [-2], \ldots, s[1-L_h]]$ are known (for example, it can correspond to the end of a previous UW).

In the following, we will consider a known sequence of J symbols at the receiver and we consider the first case (without loss of generality), where $s[-1] = s[-2] = \cdots = s[1-L_h] = 0$, and therefore our system model is:

$$\begin{bmatrix} r[0] \\ r[1] \\ \vdots \\ \vdots \\ r[kJ-1] \end{bmatrix} = \begin{bmatrix} s[0] & 0 & \ldots & 0 \\ s[1] & s[0] & 0 & \ddots \\ s[L_h-1] & \ldots & s[1] & s[0] \\ \ddots & \ddots & \ddots & \ddots \\ s[kJ-1] & \ldots & s[kJ-L_h+1] & s[kJ-L_h] \end{bmatrix} \begin{bmatrix} h[0] \\ h[1] \\ \vdots \\ \vdots \\ h[L_h-1] \end{bmatrix} + \underline{\boldsymbol{w}} \tag{2.130}$$

$$= \underline{\underline{\boldsymbol{s}}}\boldsymbol{h} + \underline{\boldsymbol{w}} \tag{2.131}$$

Last, as we work with block-based CPM, we can notice that in the case where our channel impulse channel has a length larger than the size of our UW, the model does not hold (as we have inter-block interference). Hence, the maximum length of our estimated channel can be chosen equal to the size of the UW. The size of the block-matrix can so be reduced to $N \times L_{\text{UW}}$. One can also choose a different estimated channel length L_h as long as $L_h < J$. In our simulation we choose to consider $L_h = L_{\text{UW}}$.

2.4.1 Least Squares Estimation

A standard approach to perform channel as in the case of linear modulations is to perform a well-known LS estimation. The main difference is that, instead of estimating a discrete channel model as for linear modulation, for CPM signals, we have to estimate an over-sampled version of the filtered propagation channel $h(t)$ (not $h_c(t)$). An other difference between this estimation and the classical one for linear modulations is the sampling rate which has to be superior to $2R_s$.

As the noise in our system model is a white Gaussian noise, the LS estimate of the channel $\underline{\boldsymbol{h}}$ is given by:

$$\underline{\widehat{\boldsymbol{h}}}_{\mathrm{LS}} = (\underline{\underline{\boldsymbol{s}}}^H \underline{\underline{\boldsymbol{s}}})^{-1} \underline{\underline{\boldsymbol{s}}}^H \underline{\boldsymbol{r}} \tag{2.132}$$

The LS operator needs a matrix inversion where the square matrix to inverse is of size $L_h \times L_h$, which will depend on the delay span of the channel $h_c(t)$ and on the Low-Pass Filter $\Psi(t)$. However, it can be pre-computed at the receiver side and so the operator will only consist in a matrix multiplication between a matrix of size $L_h \times kJ$ and a vector of size kJ.

2.4.2 Parametric Least Squares Estimation

A different approach can be considered to perform channel equalization. Indeed, instead of performing the estimation of the sampled filtered channel $h(t) = \Psi(t) * h_c(t) * \Psi(t)$, as the low-pass filter $\Psi(t)$ is known at the receiver, we could directly estimate the attenuations $\{h_l\}_l$ and the delays $\{\tau_l\}_l$ of the different path of the channel as in [CVM07] [BM96] and [SS08] where they considered sparse channel estimation for linear modulation. However, the overall performance of this joint estimation depends greatly on the quality of the estimation of the delays.

In case of the aeronautical channel, [Rad+15] shows that the channel is also sparse for linear modulation and moreover that the delays $\{\tau_l\}_l$ are known by geometrical consideration at the receiver thanks to the GPS positioning of the UAV. Following this approach, we can simplify the channel estimation for CPM by using a parametric model of the filtered channel $h(t)$ by considering the delays known at the receiver.

We define the vector $\underline{\boldsymbol{\tau}} = [\tau_0, \ldots, \tau_{L_c-1}]$ which contains the delay of the different paths and $\underline{\boldsymbol{a}} = [h[0], \ldots, h[L_c - 1]]^H$ the complex attenuations. We recall that the over-sampled received signal is:

$$r[n] = \sum_m s[m]h[n-m] + w[n] \tag{2.133}$$

where $h[n-m]$ is the sample of the filtered channel given by:

$$h(t) = \Psi(t) * h_c(t) * \Psi(t) \tag{2.134}$$

$$= \sum_{l=0}^{L_c-1} h_l \Psi(t-\tau_l) \text{as } \Psi(t) * \Psi(t) = \Psi(t) \tag{2.135}$$

$$\text{and so } h[k] = h(kT_e) = \sum_{l=0}^{L_c-1} h_l \Psi(kT_e - \tau_l) \tag{2.136}$$

as $\Psi(t) * \Psi(t) = \Psi(t)$ using an ideal LPF.

In this case, in order to introduce a parametric dependence on the delays, we can introduce the matrix $\underline{\underline{\boldsymbol{P}}}(\underline{\boldsymbol{\tau}})$ of size $kN \times L_c$ such as:

$$\underline{\underline{\boldsymbol{P}}}(\underline{\boldsymbol{\tau}}) = \begin{bmatrix} \Psi(0-\tau_0) & \dots & \Psi(0-\tau_{L_c-1}) \\ \Psi(T_e-\tau_0) & \dots & \Psi(T_e-\tau_{L_c-1}) \\ \vdots & \dots & \vdots \\ \Psi(kNT_e-\tau_0) & \dots & \Psi(kNT_e-\tau_{L_c-1}) \end{bmatrix} \tag{2.137}$$

$$\text{and so } \underline{\boldsymbol{h}} = \underline{\underline{\boldsymbol{P}}}(\underline{\boldsymbol{\tau}})\underline{\boldsymbol{a}} \tag{2.138}$$

Hence, our received signal is:

$$\underline{\boldsymbol{r}} = \underline{\underline{\boldsymbol{s}}}\underline{\boldsymbol{h}} + \underline{\boldsymbol{w}} \tag{2.139}$$

$$= \underbrace{\underline{\underline{\boldsymbol{s}}}\underline{\underline{\boldsymbol{P}}}(\underline{\boldsymbol{\tau}})}_{=\underline{\underline{\boldsymbol{s}}}(\underline{\boldsymbol{\tau}})} \underline{\boldsymbol{a}} + \underline{\boldsymbol{w}} \tag{2.140}$$

$$= \underline{\underline{\boldsymbol{s}}}(\underline{\boldsymbol{\tau}})\underline{\boldsymbol{a}} + \underline{\boldsymbol{w}} \tag{2.141}$$

We have introduced a parametric dependence on the delays in our model thanks to the matrix $\underline{\underline{\boldsymbol{s}}}(\underline{\boldsymbol{\tau}}) = \underline{\underline{\boldsymbol{s}}}\underline{\underline{\boldsymbol{P}}}(\underline{\boldsymbol{\tau}})$ of size $kJ \times L_c$.

Hence, as the noise in our system is still a white Gaussian noise, the LS channel estimation of $\underline{\boldsymbol{a}}$ can be reduced to:

$$\widehat{\underline{\boldsymbol{a}}} = (\underline{\underline{\boldsymbol{s}}}(\tau)^H \underline{\underline{\boldsymbol{s}}}(\tau))^{-1} \underline{\underline{\boldsymbol{s}}}(\tau)^H \underline{\boldsymbol{r}} \tag{2.142}$$

$$\text{and } \widehat{\underline{\boldsymbol{h}}} = \underline{\underline{\boldsymbol{P}}}(\tau)\widehat{\underline{\boldsymbol{a}}} \tag{2.143}$$

As previously stated, as we consider the paths' delays known at the receiver, this parametric LS estimation is a lower bound of the more generic case where a joint delays and attenuations estimation is performed.

The complexity of this operator is lower compared to the LS estimation presented in the previous section for any channel, as $L \leq L_h$. First, we only need to inverse the square matrix $\underline{\underline{\boldsymbol{s}}}(\underline{\boldsymbol{\tau}})^H \underline{\underline{\boldsymbol{s}}}(\underline{\boldsymbol{\tau}})$ of size $L_c \times L_c$ and we will only estimate a vector of L_c values instead of a vector of size L_h. The gain of such method will increase with the sampling factor k. However, we

will need to compute this operator as soon as the vector $\underline{\boldsymbol{\tau}}$ changes significantly. In the case of a aeronautical sparse channel where $L_c = 2$, we only inverse a square matrix of size 2×2.

2.4.3 Results and Discussion

In this part, we will consider the 3-RC CPM signals with $h_{\text{cpm}} = \frac{1}{2}$ for the uncoded case. In Fig 2.14, we show the Mean Square Error (MSE) for channel estimation for different size of training sequence and also with or without a priori information on the second path delay. With no surprise, we can see that the use of a priori information outperforms the classical LS

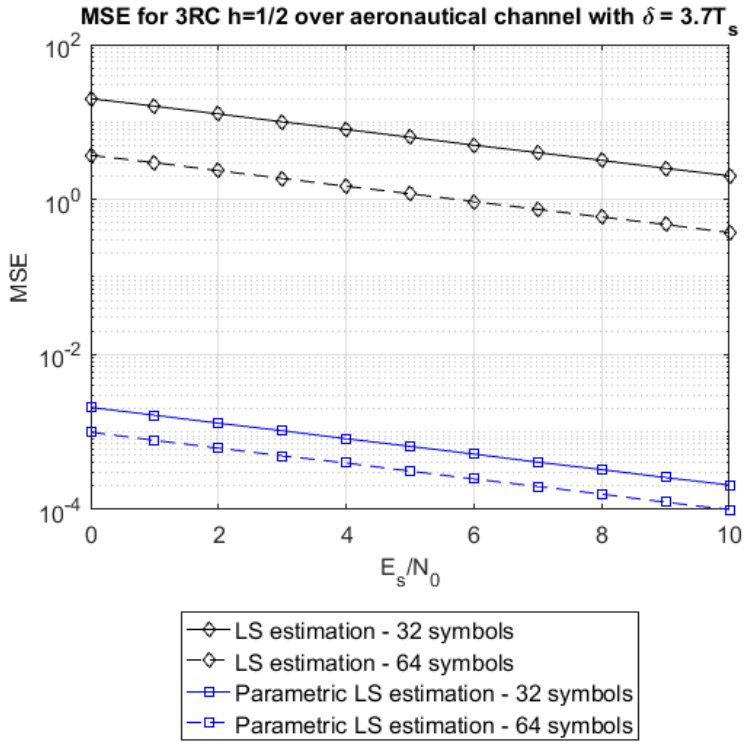

Figure 2.14 – Channel estimation MSE over the aeronautical channel

estimation. Also, we remark that we obtain performance similar to [BV11] for the classical LS estimate. When we double the number of symbols in the training sequence, we obtain a gain of almost 6dB which seems obvious as for the same numbers of path attenuation to be estimated, we have four times more observations. However, with the parametric LS, the gain is only of 3 dB. Fig 2.15 shows the Bit Error Rate for the channel equalizer with channel estimation. We can see that with the parametric LS estimation, our receiver shows a degradation less than 0.5dB. Furthermore, the performance with a classical LS estimation on 64 symbols presents a degradation of 2dB for a BER of 10^{-3}. Finally, Fig 2.16 shows some results with turbo-detection for the 3-RC CPM with $h = 1/4$. Prior to the CPM modulator, the information bits are encoded using a rate one-half convolutional code with octal representations $(5, 7)_8$ leading

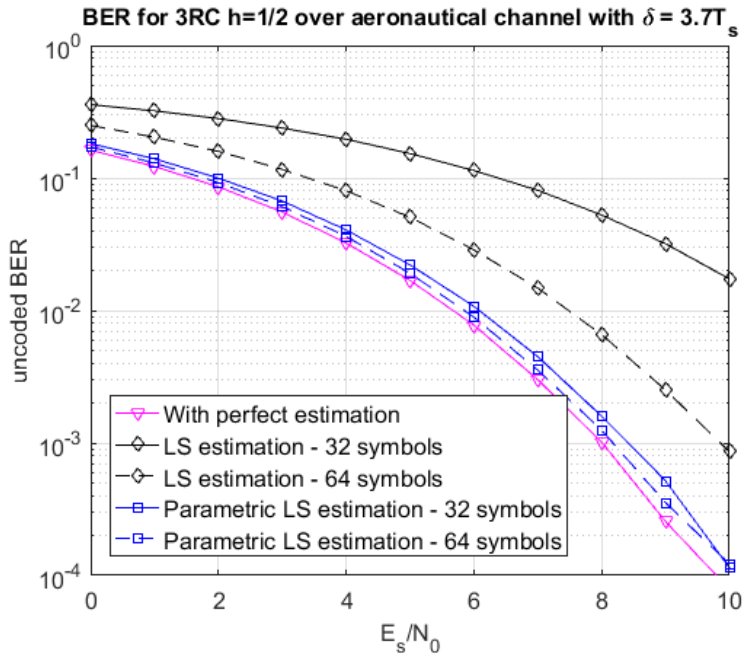

Figure 2.15 – Uncoded BER over the aeronautical channel with channel estimation

to codewords of size 1170. Random interleaving is applied between the channel encoder and the CPM modulator. We then divide these codewords into 5 subframes for which we add a termination and a UW of 16 symbols and of total size 256. We also consider three cases for channel estimation: perfect knowledge, parametric LS estimation with 32 or 64 symbols. At a BER of 10^{-3}, the channel estimation over 64 symbols introduces a degradation of 0.75dB. However, with a channel estimation over 32 symbols, the introduced error is more important (degradation of around 1.5dB at a BER of 10^{-2}).

2.5 Joint channel and carrier frequency estimation

In the previous section, we have presented equalization and channel estimation methods for CPM over frequency-channels. In order to fully study our receiver, we also need to perform transmission parameters estimation.

We recall that the received signal is:

$$r(t) = e^{j(2\pi ft+\theta)}(h(t) * s(t)) + w(t) \tag{2.144}$$

where f is the carrier frequency offset (CFO) and θ the carrier phase (considered constant over a frame). The phase θ can be taken into account directly in the channel by defining $h_\theta(t) = e^{j\theta}h(t)$ and then it will be processed during the equalization. Thus, our received

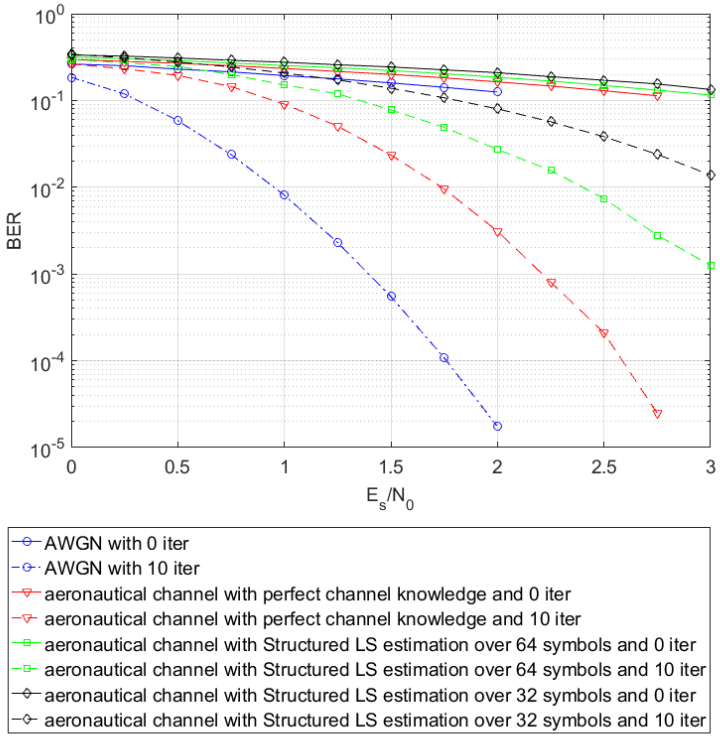

Figure 2.16 – BER over aeronautical channel with channel estimation and turbo-detection

signal is:

$$r(t) = e^{j2\pi ft}(h_\theta(t) * s(t)) + w(t) \tag{2.145}$$

For ease of presentation, we will remove the subscript for all the following part.

2.5.1 Carrier Frequency Estimation for CPM over AWGN channel

First, in this section, in order to do some comparison, we will discuss CFO estimation in the case of a transmission over an AWGN channel, i.e. $h(t) = \delta(t)$. Therefore, the received signal is:

$$r(t) = e^{j2\pi ft}s_b(t) + w(t) \tag{2.146}$$

This is a well-known problem in signal processing. Indeed, in case of Data-Aided (DA) estimation (with J known symbols), this problem can be bring back to the estimation of a single-frequency complex tone.

In 1974, [RB74] presents the ML estimation of the parameters of a single-frequency com-

plex tone from a finite number of noisy discrete-time observations. Moreover, it is shown how to compute this estimate through the mean of a DFT.

Let us consider the discrete version of Eq.(2.146) at kR_s, we obtain:

$$r[n] = e^{j2\pi fnT_e}s[n] + w[n] \tag{2.147}$$

$$\text{and } r[n]s^*[n] = e^{j2\pi fnT_e} + \widetilde{w}[n] \tag{2.148}$$

The ML criterion to maximize is given by [RB74]:

$$\Delta(\widetilde{f}) = \Re\Big\{ \sum_{l=0}^{kJ-1} r[l]s^*[l]e^{-j2\pi lT_e} \Big\} \tag{2.149}$$

More recently, in 2013, [HP13b]; [HP13a] have studied parameters estimation for CPM transmission over an AWGN channel. They develop a joint estimation of the CFO, initial phase and timing offset and design a preamble which allows this estimation to reach the CRB. The obtained log-likelihood function is:

$$\Delta(\underline{\boldsymbol{r}}; \widetilde{f}, \widetilde{\theta}, \widetilde{\epsilon}) = \Re\Big\{ \sum_{l=0}^{kJ-1} e^{-j(2\pi l\widetilde{f}T_e + \widetilde{\theta})} r[l]s^*_{\widetilde{\epsilon}}[l] \Big\} \tag{2.150}$$

In this section, we only consider the case of a CFO estimation and therefore $\widetilde{\theta} = 0$ and $s_{\widetilde{\epsilon}}[l] = s[l]$. The LLF becomes:

$$\Delta(\underline{\boldsymbol{r}}; \widetilde{f}) = \Re\Big\{ \sum_{l=0}^{kJ-1} e^{-j(2\pi l\widetilde{f}T_e)} r[l]s^*[l] \Big\} \tag{2.151}$$

which corresponds, without any surprise, to the one obtained previously in [RB74].

However, the main difference comes from the implementation of this estimation as it capitalizes on the designed preamble as explained more deeply in Annex C, which could result in a negligible degradation performance.

From Eq.(2.149) and as pointed out in [HP13a], it can be seen that the CFO estimation does not depend on the CPM parameters, as the only properties used is $s[l]s^*[l] = 1$, which comes form the exponential function.

In Fig.2.17, we present some simulation results for a binary CPM and different sizes of preamble. We can see that after a threshold, the estimators reach the CRB.

Those two estimators are based on a transmission of a CPM over an AWGN channel, hence we need to develop a method which also consider the channel estimation.

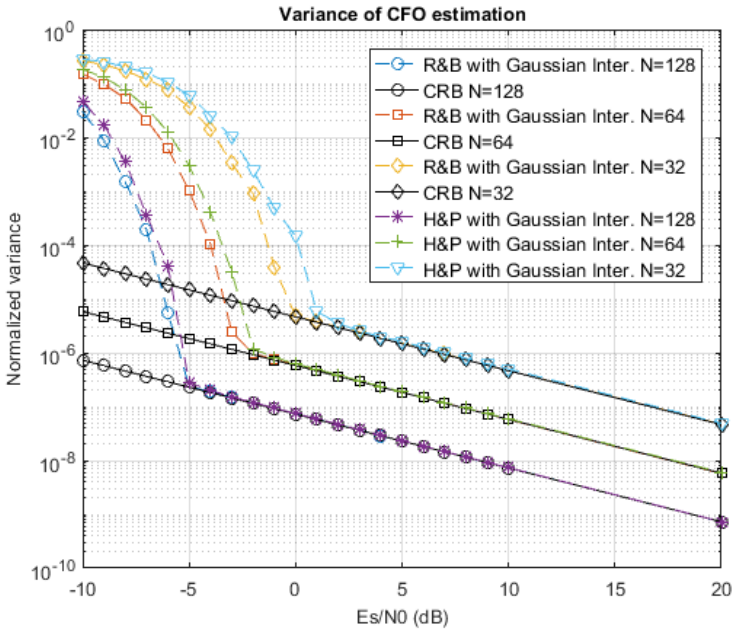

Figure 2.17 – CFO Estimation over AWGN channel

2.5.2 Baud-Rate Joint Channel and Carrier frequency estimation

In order to obtain a representation of the signal sampled at the symbol rate, we follow the example of [MM00]. In this paper, the authors used the well-known PAM decomposition introduced by [Lau86] for binary CPMs. With this decomposition, a CPM signal can be seen as a sum of linear modulation and can be approximated as a single linear modulation. However, they did not consider the case of M-ary CPM signals, where the CPM signal cannot be seen as a single linear modulation anymore. In [Cha+17b], we have extended this work by also using PAM decomposition extended for M-ary CPM in [MM95]. Contrary to [MM00], a M-ary CPM cannot be represented with one linear modulation and so a new baud rate linear representation has been introduced.

2.5.2.1 Linear representation of the signal using PAM decomposition

First, let us recall the PAM decomposition:

$$s_b(t) = \sum_{n=0}^{J-1} \sum_{k=0}^{K-1} a_{k,n} g_k(t - nT_s) \tag{2.152}$$

where $g_k(t)$ are the components of this decomposition (also called Laurent Pulses), $a_{k,n}$ are pseudo-symbols, K is the number of components and J is the number of known transmitted symbols. More details on those pseudo-symbols and components can be found in [Lau86] and [MM95].

Hence, by using Eq.(2.152) in Eq.(2.145), the received signal can now be written as

$$r(t) = e^{j2\pi ft}h(t) * (\sum_{n=0}^{J-1}\sum_{k=0}^{K-1} a_{k,n}g_k(t-nT_s)) + w(t) \tag{2.153}$$

$$= e^{j2\pi ft}(\sum_{k=0}^{K-1}\sum_{n=0}^{J-1} a_{k,n}\underbrace{(h*g_k)(t-nT_s))}_{\triangleq h_k(t)} + w(t) \tag{2.154}$$

$$= e^{j2\pi ft}(\sum_{k=0}^{K-1}\sum_{n=0}^{J-1} a_{k,n}h_k(t-nT_s) + w(t) \tag{2.155}$$

As we assume perfect timing and frame synchronization, the sampled received signal at $t = mT_S$ is given by

$$r[m] = r(mT_s) = e^{j2\pi fmT_s}(\sum_{k=0}^{K-1}\sum_{n=0}^{J-1} a_{k,n}h_k((m-n)T_s)) + w[m] \tag{2.156}$$

We can see from the previous equation that our received signal can be considered as the sum of linear modulations with some equivalent multi-path channels $h_k(t)$. Rewriting Eq.(2.156) in vector notations we have

$$\underline{\boldsymbol{r}} = \underline{\underline{\boldsymbol{\Gamma}}}(f)\sum_{k=0}^{K-1}\underline{\underline{\boldsymbol{A_k}}}\underline{\boldsymbol{h_k}} + \underline{\boldsymbol{w}} \tag{2.157}$$

where

$$\begin{aligned}
\underline{\boldsymbol{r}} &= [r[0], r[1], \ldots, r[J-1]]^T \\
\underline{\underline{\boldsymbol{\Gamma}}}(f) &= \mathrm{diag}(1, e^{j2\pi f}, \ldots, e^{j2\pi f(J-1)}) \\
\underline{\boldsymbol{h_k}} &= [h_k(0), h_k(T_s), \ldots, h_k((L-1)T_s)]^T \\
\underline{\boldsymbol{w}} &= [w[0], \ldots, w[J-1]]^T
\end{aligned}$$

and $\underline{\underline{\boldsymbol{A_k}}}$ is a (J-L)*L matrix with entries $[\underline{\underline{\boldsymbol{A_k}}}]_{i,j} = a_{k,i-j}$.

In this section, we consider a Data-Aided algorithm so $\{\underline{\underline{\boldsymbol{A_k}}}\}$ are known matrix. Using notations $\underline{\underline{\boldsymbol{A}}} = [\underline{\underline{\boldsymbol{A_0}}}, \ldots, \underline{\underline{\boldsymbol{A_{K'-1}}}}]$ and $\underline{\boldsymbol{h}}_{\mathrm{eq}} = [\underline{\boldsymbol{h_0}}, \ldots, \underline{\boldsymbol{h_{K'-1}}}]^T$, our system becomes:

$$\underline{\boldsymbol{r}} = \underline{\underline{\boldsymbol{\Gamma}}}(f)\underline{\underline{\boldsymbol{A}}}\underline{\boldsymbol{h}}_{\mathrm{eq}} + \underline{\boldsymbol{w}} \tag{2.158}$$

2.5.2.2 ML Estimation

Similarly to [MM00], for a fixed $(f, \underline{\boldsymbol{h}})$, $\underline{\boldsymbol{r}}$ is a Gaussian vector with mean $\underline{\underline{\boldsymbol{\Gamma}}}(f)\underline{\underline{\boldsymbol{A}}}\underline{\boldsymbol{h}}_{\mathrm{eq}}$ and co-variance matrix $\sigma_n^2\underline{\underline{\boldsymbol{I}}}_J$, where $\underline{\underline{\boldsymbol{I}}}_J$ is the identity matrix of size $J \times J$. Hence, the likelihood

function for the parameters $(f, \underline{\boldsymbol{h}}_{\text{eq}})$ to maximize is

$$\Delta(\underline{\boldsymbol{r}}; \widetilde{\underline{\boldsymbol{h}}}_{\text{eq}}, \widetilde{f}) = \frac{1}{(\pi\sigma_n^2)^J} \exp\Big\{ \frac{-1}{\sigma_n^2} [\underline{\boldsymbol{r}} - \underline{\underline{\boldsymbol{\Gamma}}}(\widetilde{f}) \underline{\underline{\boldsymbol{A}}} \widetilde{\underline{\boldsymbol{h}}}_{\text{eq}}][\underline{\boldsymbol{r}} - \underline{\underline{\boldsymbol{\Gamma}}}(\widetilde{f}) \underline{\underline{\boldsymbol{A}}} \widetilde{\underline{\boldsymbol{h}}}_{\text{eq}}]^H \Big\} \tag{2.159}$$

where $.^H$ stands for the Hermitian transposition.

We choose to maximize Δ over $\widetilde{\underline{\boldsymbol{h}}}_{\text{eq}}$ and $\widetilde{f}$ to obtain the joint ML estimates of $\underline{\boldsymbol{h}_{\text{eq}}}$ and f. The estimate of $\underline{\boldsymbol{h}}_{\text{eq}}$ for a given $\widetilde{f}$ is

$$\widehat{\underline{\boldsymbol{h}}}_{\text{eq}}(\widetilde{f}) = (\underline{\underline{\boldsymbol{A}}}^H \underline{\underline{\boldsymbol{A}}})^{-1} \underline{\underline{\boldsymbol{A}}}^H \underline{\underline{\boldsymbol{\Gamma}}}^H(\widetilde{f}) \underline{\boldsymbol{r}}. \tag{2.160}$$

Using this estimate in Eq.(2.159), we obtain the following CFO estimator:

$$\widehat{f} = \arg\max_{\widetilde{f}} g(\widetilde{f}) \tag{2.161}$$

where

$$g(\widetilde{f}) = \underline{\boldsymbol{r}}^H \underline{\underline{\boldsymbol{\Gamma}}}(\widetilde{f}) \underline{\underline{\underline{\boldsymbol{B}}}} \underline{\underline{\boldsymbol{\Gamma}}}^H(\widetilde{f}) \underline{\boldsymbol{r}} \tag{2.162}$$

and

$$\underline{\underline{\underline{\boldsymbol{B}}}} \triangleq \underline{\underline{\boldsymbol{A}}} (\underline{\underline{\boldsymbol{A}}}^H \underline{\underline{\boldsymbol{A}}})^{-1} \underline{\underline{\boldsymbol{A}}}^H \tag{2.163}$$

$g(\widetilde{f})$ can be written as:

$$g(\widetilde{f}) = -\rho(0) + 2\Re\Big\{ \sum_{m=0}^{J-1} \rho(m) e^{-j2\pi m \widetilde{f}} \Big\} \tag{2.164}$$

$$\text{with } \rho(m) = \sum_{k=m}^{J-1} [\underline{\underline{\underline{\boldsymbol{B}}}}]_{k-m,k} r(k) r^*(k-m) \tag{2.165}$$

$\Re(.)$ is the real part operator and $[\underline{\underline{\underline{\boldsymbol{B}}}}]_{k-m,k}$ is the element $(k-m, m)$ of the matrix $\underline{\underline{\underline{\boldsymbol{B}}}}$. This matrix can be pre-computed and the grid search of Eq.(2.162) can be performed by the mean of a Fast Fourier Transform (FFT) followed by a parabolic interpolation.

Thus, the following procedure can be applied at the receiver:

- Compute $\widehat{f}$ using Eq.(2.162);
- Compute $\widehat{\underline{\boldsymbol{h}}}_{\text{eq}}$ using the LS estimation on the counter-rotated received samples (according to $\widehat{f}$) using Eq.(2.160).

In the next section, we present some simulation results for this baud-rate joint channel and carrier frequency estimation.

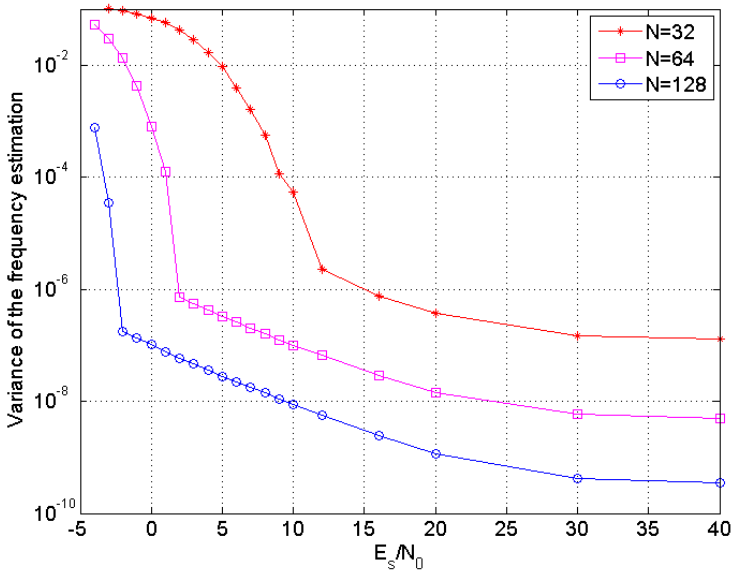

Figure 2.18 – Performance of the carrier recovery

2.5.2.3 Results and Discussion

We first consider a preamble of 64 symbols modulated by a GMSK with $M = 4$, $h = 1/4$, $L_{\text{cpm}} = 3$ and $BT = 0.3$. We consider a random preamble taken in the M-ary alphabet defined in section 2.2.

The true normalized frequency offset $\frac{f}{R_s}$, where R_s is the symbol rate, is taken as an uniformly random variable between -0.5 and 0.5. The SNR is defined as the average received energy per transmitted symbols over the noise variance.

We consider the following frequency-selective channel:

$$h_c(t) = \sum_{l=0}^{5} a_l \delta(t - \tau_l) \tag{2.166}$$

The normalized delays $\{\tau_l/T\}$ are $\{0, 0.054, 0.135, 0.432, 0.621, 1.351\}$.

The attenuation $\{a_l\}$ are complex random Gaussian variables with zero mean and variances (in decibel (dB)) $\{-3, 0, -2, -6, -8, -10\}$. For those simulations, we consider that all equivalent discrete channel have a length $L = 8$.

Performance of the carrier-frequency recovery: Fig.2.18. illustrates the influence of the size of the preamble for carrier-frequency recovery. We choose three training sequences of size J=32, J=64 and J=128. In this case, the selected FFT sizes are respectively 512, 1024 and 2048. We can see that when the size of the preamble increases, the threshold gets lower

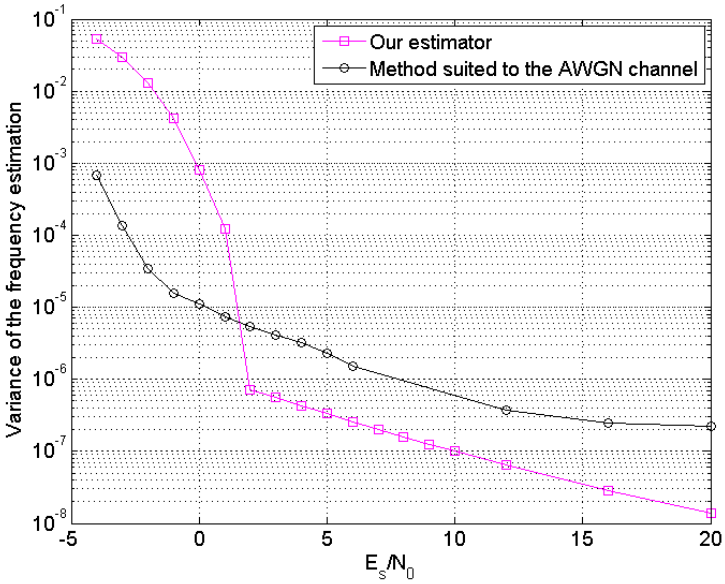

Figure 2.19 – Comparison with the method suited to the AWGN channel

and lower. For our estimator, the thresholds are respectively around 12dB, 2dB and -2dB for J=32, J=64 and J=128.

Fig.2.19. compares the estimation developed in this article with the method suited to the AWGN channel presented in [HP13b]. We can see that after the estimator threshold (around 2 dB), our estimator outperforms the other one, which is logical as it does not take into account the channel.

Fig.2.20. shows the value of the variance for frequency recovery in the case of a perfect channel estimation for $J = 128$.

Performance of the channel estimation: Fig.2.21. shows the variance of the estimation of the discrete equivalent channel $\boldsymbol{h_0}$ for the same set of parameters. The curve for $J = 32$ shows poor accuracy as we estimate three discrete channels of length $L = 8$, with only 32 observations.

In Fig.2.22. we plot the ideal Mean Square Error (MSE) value for channel estimation in case of perfect frequency recovery for $J = 128$. We can see that the loss due to the frequency estimation is less than 1dB. Hence, the overall performance of those estimates are mainly due to the channel estimation residual error.

Major Drawback: Even if this baud rate estimation gives us, as expected, better results than the ones developed for AWGN channel, it suffers from its channel model. Indeed, the estimated *equivalent* channel cannot be easily used in any equalizers presented in Section

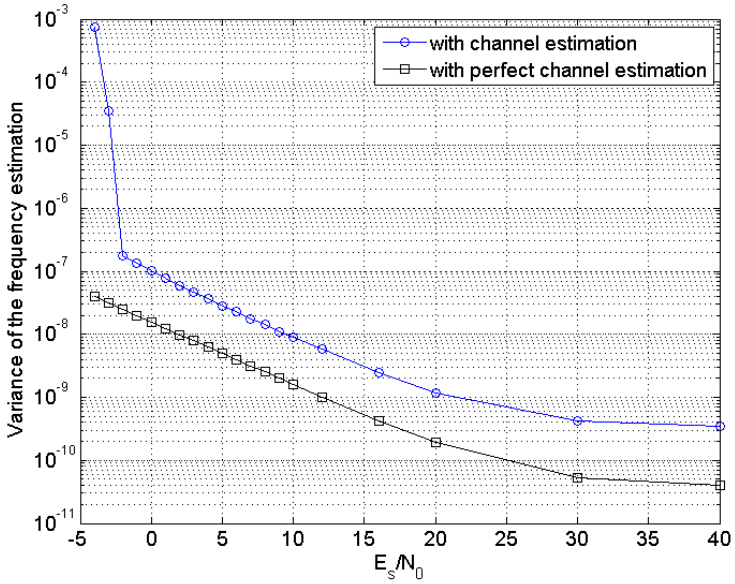

Figure 2.20 – Performance of the carrier recovery with perfect channel knowledge

2.3. Hence, we need to develop an estimator working on a over-sampled representation of the received signal.

2.5.3 Over-sampled Signal based Estimation

To be compliant with the model used for equalization (over-sampled received signal using FS or polyphase/multi-channel representation), we present a new joint channel and carrier frequency estimation for CPM transmission over frequency-selective channel. As previously, we will consider the transmission of J known data symbols and a data-aided estimation at the receiver.

Let us derive a classical fractionally-spaced (FS) representation without loss of generally with an other over-sampled representation (indeed, we recall that the polyphase representation can be obtained through a permutation matrix). In this case, we do not suppose any structure of the transmitted signal (as the block-based transmission used for equalization).

By denoting $T_e = T_s/k$, the received signal can be written as the following discrete linear convolution:

$$\begin{aligned} r[l] &= r[lT_e] && (2.167)\\ &= e^{j2\pi f l T_e} \sum_m s[m] h\Big((l-m)\frac{T_s}{k}\Big) + w[l] \\ &= e^{j2\pi f l T_e} \sum_m s[m] h[l-m] + w[l] && (2.168) \end{aligned}$$

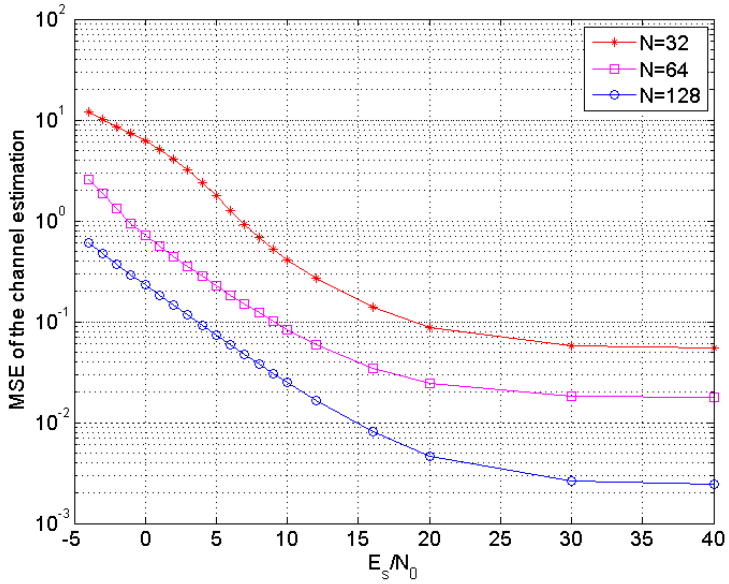

Figure 2.21 – MSE of the channel estimate

Therefore, by defining the vector $\underline{\boldsymbol{r}} = [r(0), r(T_e), r(2T_e), \ldots, r((k-1)JT_e)]^T$, we obtain the following matrix-wise representation, similar to the ones in Eq.(2.131) plus the additional term $\underline{\underline{\boldsymbol{\Gamma}}}(f)$:

$$\begin{bmatrix} r[0] \\ r[1] \\ \vdots \\ \vdots \\ r[kJ-1] \end{bmatrix} = \underline{\underline{\boldsymbol{\Gamma}}}(f) \begin{bmatrix} s[0] & 0 & \ldots & 0 \\ s[1] & s[0] & 0 & \ddots \\ s[L_h-1] & \ldots & s[1] & s[0] \\ \ddots & \ddots & \ddots & \ddots \\ s[kJ-1] & \ldots & s[kJ-L_h+1] & s[kJ-L_h] \end{bmatrix} \begin{bmatrix} h[0] \\ h[1] \\ \vdots \\ \vdots \\ h[L_h-1] \end{bmatrix} + \underline{\boldsymbol{w}} \tag{2.169}$$

$$= \underline{\underline{\boldsymbol{\Gamma}}}(f)\underline{\underline{\boldsymbol{s}}}\underline{\boldsymbol{h}} + \underline{\boldsymbol{w}} \tag{2.170}$$

where L_h is over-sampled estimated channel impulse length, $\underline{\underline{\boldsymbol{s}}}$ is a matrix of size $kJ \times L_h$ and $\underline{\underline{\boldsymbol{\Gamma}}}(f)$ is a diagonal matrix of size $kJ \times kJ$ defined as:

$$\underline{\underline{\boldsymbol{\Gamma}}}(f) = \text{diag}\{1, e^{j2\pi f T_e}, e^{j2\pi f 2T_e}, \ldots, e^{j2\pi f(kJ-1)T_e}\} \tag{2.171}$$

2.5.3.1 Joint ML channel and carrier frequency estimation

For a given $(\underline{\boldsymbol{h}}, f)$, we can note that $\underline{\boldsymbol{r}}$ is Gaussian with mean $\underline{\underline{\boldsymbol{\Gamma}}}(f)\underline{\underline{\boldsymbol{s}}}\underline{\boldsymbol{h}}$ and co-variance matrix $\sigma_n^2 \underline{\underline{\boldsymbol{I}}}_{kJ}$ where $\underline{\underline{\boldsymbol{I}}}_{kJ}$ is the identity matrix of size $kJ \times kJ$. Hence, the log-likelihood function

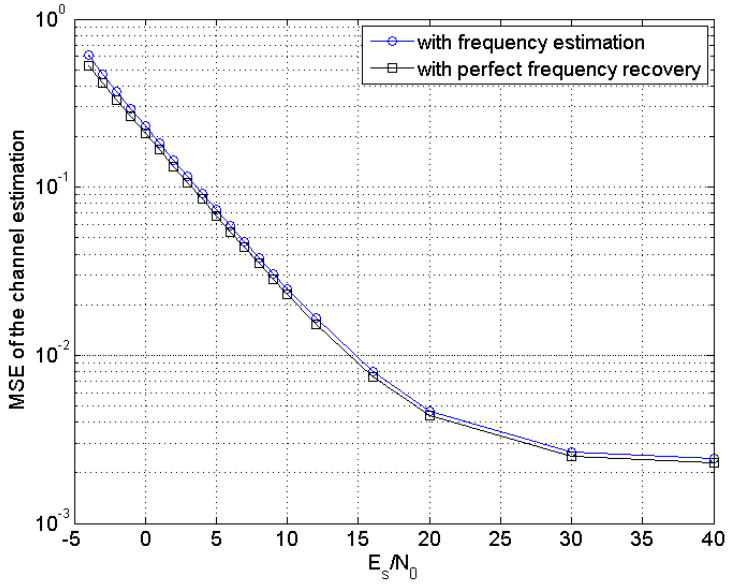

Figure 2.22 – MSE of the channel estimate with perfect carrier recovery

for the parameters $\underline{\boldsymbol{h}}$ and f is:

$$\Delta(\underline{\widetilde{\boldsymbol{h}}}, \widetilde{f}) = -\frac{1}{\sigma_n^2}[\underline{\boldsymbol{r}} - \underline{\underline{\boldsymbol{\Gamma}}}(\widetilde{f})\underline{\underline{\boldsymbol{s}}}\underline{\widetilde{\boldsymbol{h}}}]^H[\underline{\boldsymbol{r}} - \underline{\underline{\boldsymbol{\Gamma}}}(\widetilde{f})\underline{\underline{\boldsymbol{s}}}\underline{\widetilde{\boldsymbol{h}}}] \tag{2.172}$$

We choose to maximize Δ over $\underline{\widetilde{\boldsymbol{h}}}$ and $\widetilde{f}$ to obtain the joint ML estimates of $\underline{\boldsymbol{h}}$ and f. The estimate of $\underline{\boldsymbol{h}}$ for a given $\widetilde{f}$ is

$$\underline{\widehat{\boldsymbol{h}}}(\widetilde{f}) = (\underline{\underline{\boldsymbol{s}}}^H\underline{\underline{\boldsymbol{s}}})^{-1}\underline{\underline{\boldsymbol{s}}}^H\underline{\underline{\boldsymbol{\Gamma}}}^H(\widetilde{f})\underline{\boldsymbol{r}}. \tag{2.173}$$

Using this estimate in Eq.(2.172), we obtain the following carrier-frequency estimator:

$$\widehat{f} = \arg\max_{\widetilde{f}} g(\widetilde{f}) \tag{2.174}$$

where

$$g(\widetilde{f}) = \underline{\boldsymbol{r}}^H\underline{\underline{\boldsymbol{\Gamma}}}(\widetilde{f})\underline{\underline{\boldsymbol{B}}}\underline{\underline{\boldsymbol{\Gamma}}}^H(\widetilde{f})\underline{\boldsymbol{r}} \tag{2.175}$$

and

$$\underline{\underline{\boldsymbol{B}}} \triangleq \underline{\underline{\boldsymbol{s}}}(\underline{\underline{\boldsymbol{s}}}^H\underline{\underline{\boldsymbol{s}}})^{-1}\underline{\underline{\boldsymbol{s}}}^H \tag{2.176}$$

As for the baud-rate estimation presented in Section 2.5.2, this estimation can be performed

effectively with a DFT and a grid search. Indeed, it can be shown that

$$g(\widetilde{f}) = -\rho(0) + 2\Re\Big\{ \sum_{m=0}^{kJ-1} \rho(m) e^{-j2\pi \widetilde{f} m} \Big\} \tag{2.177}$$

where $\rho(m)$ is the weighted discrete auto-correlation of $\underline{\boldsymbol{r}}$ such as:

$$\rho(m) = \sum_{l=0}^{kJ-1} [\underline{\underline{\boldsymbol{B}}}]_{l-m,l} r[l] r^*[l-m] \tag{2.178}$$

Once again, the procedure to jointly estimate the CFO and the Channel is the following:

- Compute $\widehat{f}$ using Eq.(2.177);

- Compute $\underline{\widehat{\boldsymbol{h}}_{\text{eq}}}$ using the LS estimate on the counter-rotated received samples (according to $\widehat{f}$) using Eq.(2.173).

2.5.3.2 AWGN case

In the this section, we will consider the case where the CPM signal in transmitted over an AWGN channel and show that our estimation corresponds to a classical ML estimation of the CFO presented in [RB74]. Moreover, we will also prove that our estimator asymptotically reaches the CRB for carrier recovery. In this case, the channel does not introduce interference between the samples as $\underline{\boldsymbol{h}} = [1]$ and $L_c = L = 1$. Therefore, the Carrier Frequency Offset estimation becomes:

$$\begin{aligned}
\text{and so } g(\widetilde{f}) &= \underline{\boldsymbol{r}}^H \Gamma(\widetilde{f}) \underline{\boldsymbol{s}} (\underline{\boldsymbol{s}}^H \underline{\boldsymbol{s}})^{-1} \underline{\boldsymbol{s}}^H \Gamma^H(\widetilde{f}) \underline{\boldsymbol{r}} && (2.179)\\
&= \frac{1}{\sum_{i=0}^{kJ-1} |s[i]|^2} \underline{\boldsymbol{r}}^H \Gamma(\widetilde{f}) \underline{\boldsymbol{s}}\underline{\boldsymbol{s}}^H \Gamma^H(\widetilde{f}) \underline{\boldsymbol{r}} && (2.180)\\
&= \frac{1}{\sum_{i=0}^{kJ-1} |s[i]|^2} |\underline{\boldsymbol{r}}^H \Gamma(\widetilde{f}) \underline{\boldsymbol{s}}|^2 && (2.181)\\
&= \frac{1}{\sum_{i=0}^{kJ-1} |s[i]|^2} \sum_{l=0}^{kJ-1} r[l] s^*[l] e^{-j2\pi f l} && (2.182)
\end{aligned}$$

which can be efficiently computed through a DFT and corresponds to the classical ML frequency estimation for AWGN channels [HP13b] [RB74].

2.5.3.3 Performance Analysis

Following the same method as previously, we compute the bias and the variance of our estimator according to [MM00]. They can be approximated by:

$$E(\widehat{f}) \approx f - \frac{E[\dot{g}(f)]}{E[\ddot{g}(f)]} \tag{2.183}$$

$$\mathrm{var}(\widehat{f}) \approx \frac{E([\dot{g}(f)]^2)}{E(\ddot{g}(f))^2} \tag{2.184}$$

where $\dot{g}(f)$ and $\ddot{g}(f)$ are the first and second derivatives of $g(\widetilde{f})$ at $\widetilde{f} = f$.

The derivation of those equations are tedious and does not differ from the ones in [MM00] and here only the results are given:

$$E(\widehat{f}) \approx f \tag{2.185}$$

$$\mathrm{var}(\widehat{f}) \approx \frac{E([\dot{g}(f)]^2)}{E(\ddot{g}(f))^2} \tag{2.186}$$

$$= \frac{1}{2J} \frac{\underline{\boldsymbol{s}}^H \underline{\boldsymbol{s}}}{\underline{\boldsymbol{y}}^H (\underline{\underline{\boldsymbol{I}}}_{kJ} - \underline{\underline{\boldsymbol{B}}}) \underline{\boldsymbol{y}}} \mathrm{SNR}^{-1} \tag{2.187}$$

with

$$\underline{\boldsymbol{s}} = \underline{\underline{\boldsymbol{s}}} \underline{\boldsymbol{h}} \tag{2.188}$$

$$\underline{\boldsymbol{y}} = 2\pi \underline{\underline{\underline{\boldsymbol{M}}}} \underline{\underline{\boldsymbol{s}}} \underline{\boldsymbol{h}} \tag{2.189}$$

$$\text{and } \underline{\underline{\underline{\boldsymbol{M}}}} = \mathrm{diag}(0, 1, \ldots, kJ-1) \tag{2.190}$$

2.5.3.4 Cramér Rao Bound

We use the same procedure than the annex of [MM00] to compute the CRB. To begin, we call $\underline{\boldsymbol{h}}_r$ and $\underline{\boldsymbol{h}}_i$ the real and imaginary components of the channel response and define $u = (\underline{\boldsymbol{h}}_r, \underline{\boldsymbol{h}}_i, f)$the set of the unknown parameters. Then, the components of the Fisher information matrix are:

$$[\underline{\underline{\boldsymbol{F}}}]_{i,j} = -E\Big[\frac{\partial^2 \ln \Delta(\underline{\boldsymbol{r}}, u)}{\partial u(i) \partial u(j)}\Big] \tag{2.191}$$

We can see that:

$$-\ln \Delta(\underline{\boldsymbol{r}}, u) = \frac{1}{\sigma_n^2} [\underline{\boldsymbol{r}} - \underline{\underline{\boldsymbol{\Gamma}}}(f) \underline{\underline{\boldsymbol{s}}} (\underline{\boldsymbol{h}}_r + j \underline{\boldsymbol{h}}_i)]^H [\underline{\boldsymbol{r}} - \underline{\underline{\boldsymbol{\Gamma}}}(f) \underline{\underline{\boldsymbol{s}}} (\underline{\boldsymbol{h}}_r + j \underline{\boldsymbol{h}}_i)] \tag{2.192}$$

$$\underline{\underline{\boldsymbol{F}}} = \frac{2}{\sigma_n^2}\begin{pmatrix} \Re\{\underline{\boldsymbol{s}}^H\underline{\boldsymbol{s}}\} & -\Im\{\underline{\boldsymbol{s}}^H\underline{\boldsymbol{s}}\} & -\Im\{\boldsymbol{y}^H\underline{\boldsymbol{s}}\} \\ \Im\{\underline{\boldsymbol{s}}^H\underline{\boldsymbol{s}}\} & \Re\{\underline{\boldsymbol{s}}^H\underline{\boldsymbol{s}}\} & \Re\{\boldsymbol{y}^H\underline{\boldsymbol{s}}\} \\ \Im\{\underline{\boldsymbol{y}}^H\underline{\boldsymbol{s}}\} & \Re\{\underline{\boldsymbol{y}}^H\underline{\boldsymbol{s}}\} & \underline{\boldsymbol{y}}^H\underline{\boldsymbol{y}} \end{pmatrix} \tag{2.193}$$

where $\Re\{.\}$ and $\Im\{.\}$ are the real and imaginary part operators.

Following [MM00], and after a similar tedious derivation, it can be shown that the CRB on carrier frequency estimation is:

$$CRB(f) = \frac{\sigma_n^2}{2\underline{\boldsymbol{y}}^H(\underline{\underline{\boldsymbol{I}}}_{kJ} - \underline{\underline{\boldsymbol{B}}})\underline{\boldsymbol{y}}} \tag{2.194}$$

with

$$\underline{\boldsymbol{y}} = 2\pi\underline{\underline{\boldsymbol{M}}}\underline{\boldsymbol{s}}\boldsymbol{h} \tag{2.195}$$

$$\text{with } \underline{\underline{\boldsymbol{M}}} = \text{diag}(0, 1, \ldots, kJ-1) \tag{2.196}$$

In the case where the transmission is over an AWGN channel, the CRB can be simplified. Indeed, in this case, we recall that:

$$\underline{\boldsymbol{h}} = [1] \tag{2.197}$$

$$\text{and } \underline{\boldsymbol{s}} = \underline{\underline{\boldsymbol{s}}}\boldsymbol{h} \tag{2.198}$$

$$= [s(0), s(T_e), s(2T_e), \ldots, s(kJT_e - 1)]^T \tag{2.199}$$

$$\underline{\underline{\boldsymbol{B}}} = \frac{1}{kJ}\underline{\underline{\boldsymbol{s}}}\underline{\underline{\boldsymbol{s}}}^H \tag{2.200}$$

Hence, Eq.(2.189) becomes:

$$\underline{\boldsymbol{y}} = 2\pi[0, s(T_e), 2s(2T_e), \ldots, kJs(kJT_e - 1)]^T \tag{2.201}$$

The Cramér Rao Bound for carrier-recovery over AWGN channel is therefore:

$$CRB(f) = \frac{\sigma_n^2}{2\underline{\boldsymbol{y}}^H(\underline{\underline{\boldsymbol{I}}}_{kJ} - \underline{\underline{\boldsymbol{B}}})\underline{\boldsymbol{y}}} \tag{2.202}$$

$$\approx \frac{3}{2\pi^2 J^3}(SNR)^{-1} \tag{2.203}$$

which corresponds to the Modified CRB presented in [DMR94] and recently redeveloped for CPM in [HP13a].

2.5.3.5 Results and Discussion

In the following, we present some simulation results for our joint carrier frequency offset and channel estimation.

First, we evaluate its performance in the case of an AWGN channel. Without surprise,

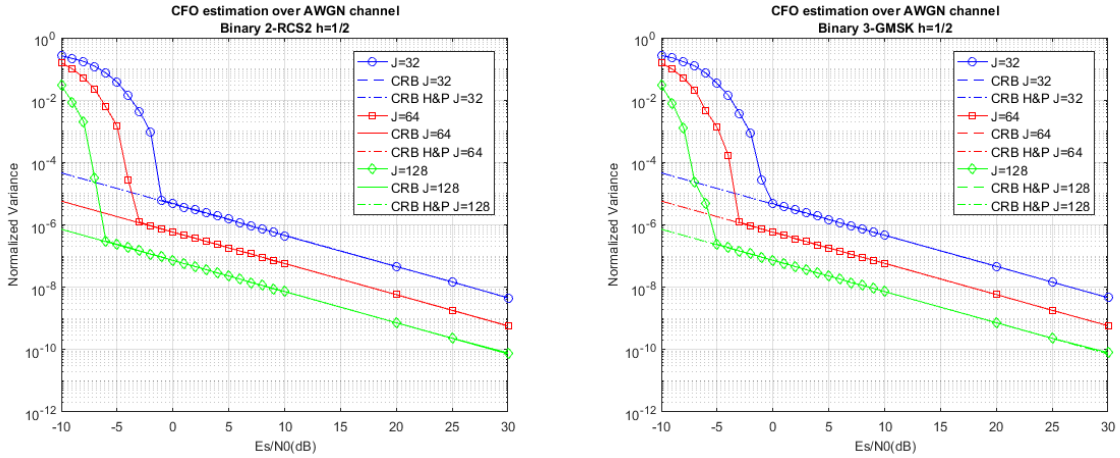

Figure 2.23 – Carrier Recovery for binary CPMs over AWGN channel

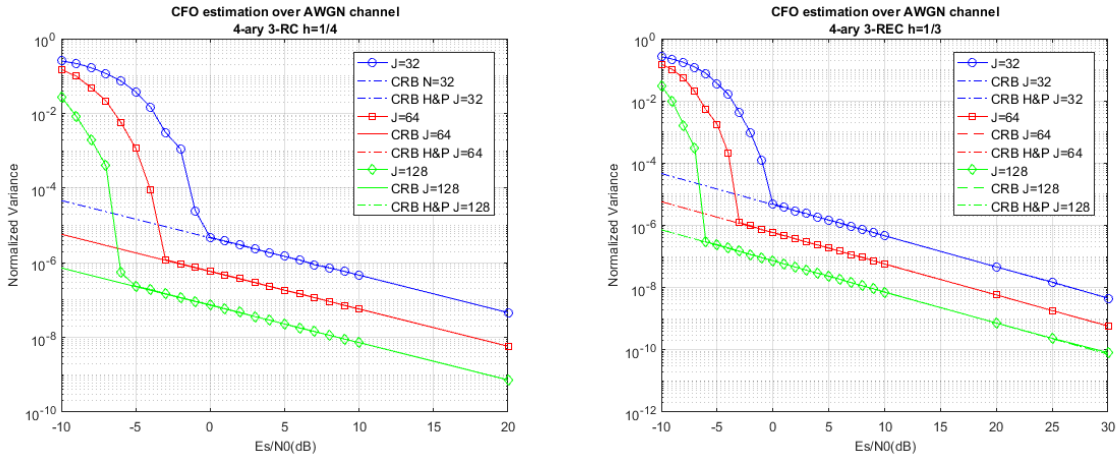

Figure 2.24 – Carrier Recovery for 4-ary CPMs over AWGN channel

we obtain the same results that the carrier recovery algorithms presented in section 2.5.1. Moreover, we can see that the CRB developed in the case of frequency-selective channels does correspond to the one for transmission over AWGN channel in this special case for both binary (see Fig.2.23) and 4-ary CPM schemes (see Fig.2.24). As previously stated, as we used the same preamble for each CPM schemes, the performance does not depend on the CPM parameters. We also checked that our CRB bound corresponds to the one in [HP13a] for AWGN channels.

We now assess the performance in the case of TIV channels for different binary and 4-ary CPM schemes. We consider the GSM urban channel, which is generally used for simulation in the CPM field and we also used the optimal preamble for synchronization over AWGN channel (*H&P*) from [HP13b].

In Fig.2.25 and Fig.2.26, we present some results in the case of binary CPM schemes. We have plotted the maximum and minimum CRB for each case as it does depend on the current

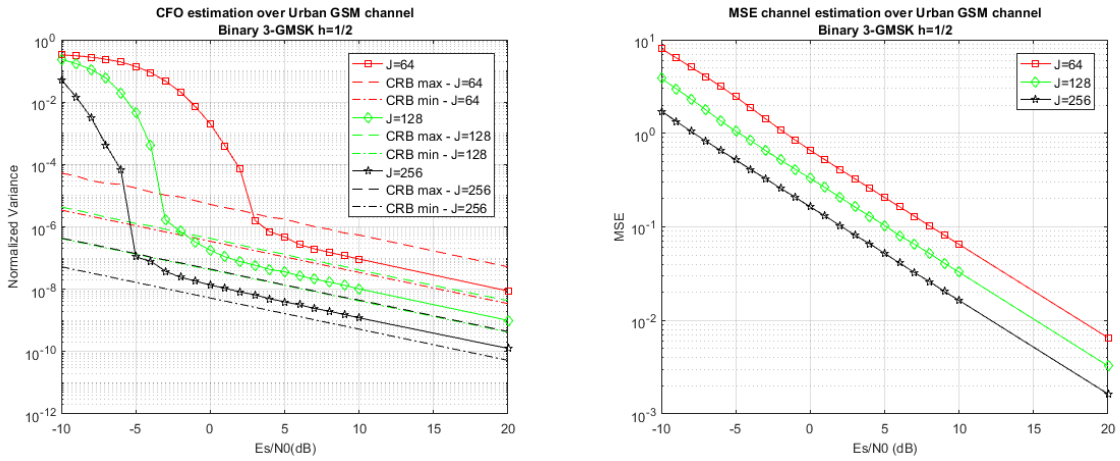

Figure 2.25 – Carrier Recovery for Binary 3-GMSK h=1/3 over Urban GSM channel

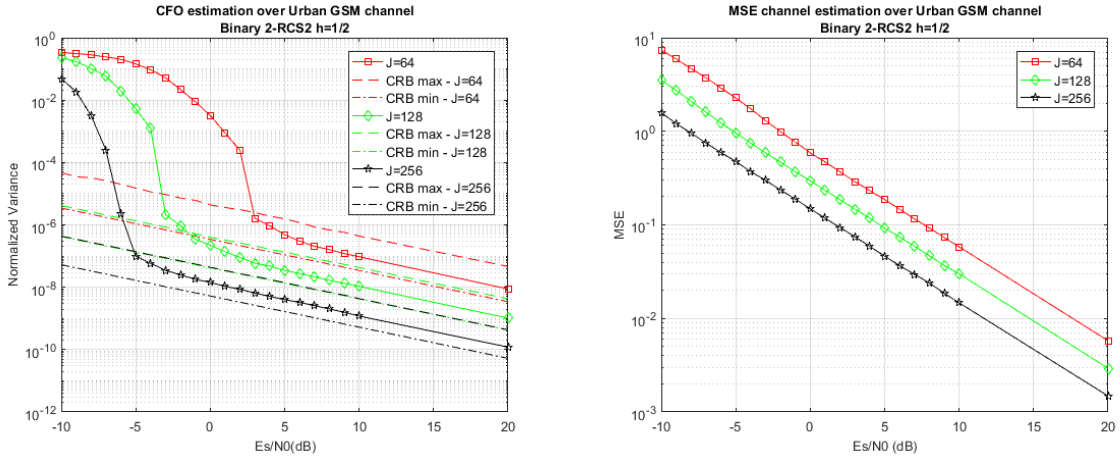

Figure 2.26 – Carrier Recovery for Binary 2-RCS2 h=1/2 over Urban GSM channel

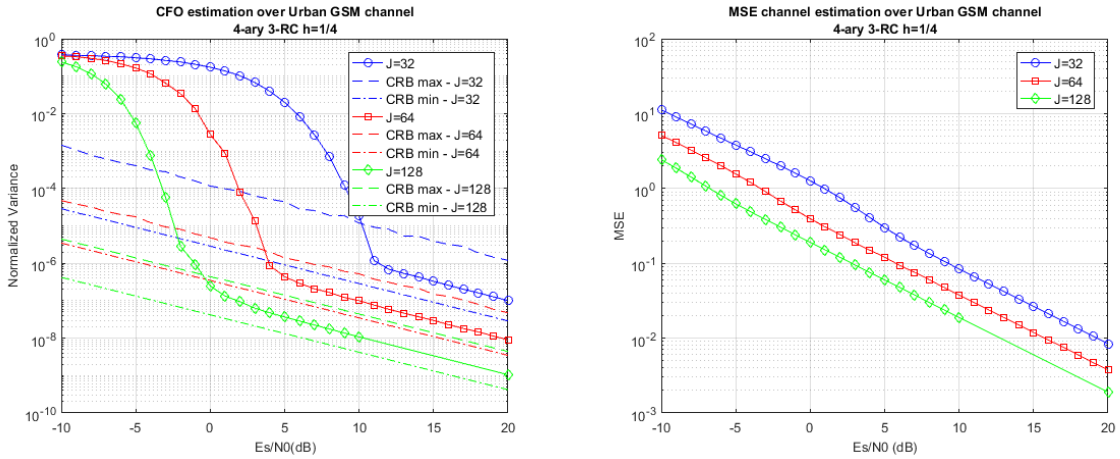

Figure 2.27 – Carrier Recovery for Quaternary 3-RC h=1/4 over Urban GSM channel

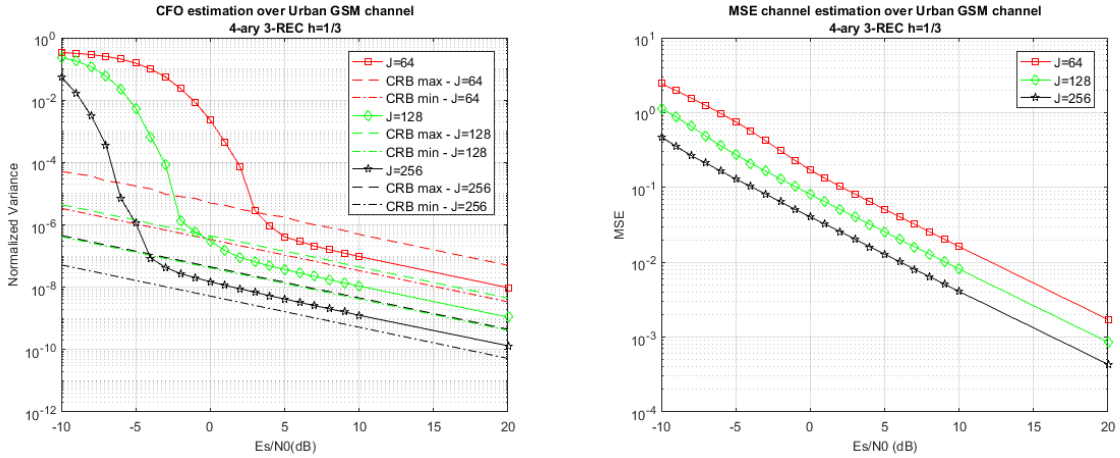

Figure 2.28 – Carrier Recovery for Quaternary 3-REC h=1/3 over Urban GSM channel

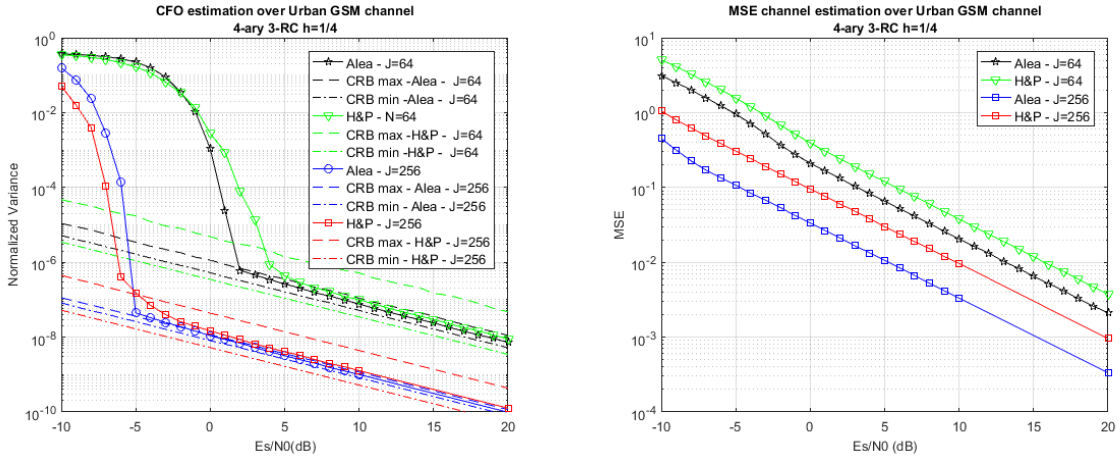

Figure 2.29 – Comparison between H&P and random sequence preamble for Quaternary 3-REC h=1/3 over Urban GSM channel

channel. It can been seen that now the performance of the joint channel and CFO estimation does depend on the CPM parameters, as it affects the channel estimation (the transmitted signal is correlated and with non-negligible sidelobes).

Hence, the preamble design may have a critical impact on the performance of the synchronization and channel estimation. Indeed, as shown in Section 2.5.3.4, the CRB depends on the chosen preamble in case of a transmission over a TIV channel. Therefore, by simulation, we compare the H&P preamble with a random preamble in Fig.2.29. We emphasize the fact that even if the transmitted symbols are random (i.i.d.), the transmitted signal is not as CPM signals are correlated by nature. As expected, the optimal preamble for CPM signals over AWGN channel is not optimal anymore and a random sequence preamble outperforms it of a few dBs for carrier recovery and up to 5dB for channel estimation. In future work, it will be interesting to design a preamble for CPM over TIV channels.

2.6 Conclusion

In this chapter, we have presented several equalizers for CPM over Time-Invariant Channels and also some synchronization techniques for CPM.

We have developed a new exact low-complexity equalizer which exploits "fully" the block-circular transmission scheme and presents the same performance than the other equalizers but with a smaller complexity.

We have also shown how to estimate the channel and how to perform a joint channel and carrier frequency estimation. This last estimator is proved to reach asymptotically the Cramér Rao Bound.

Chapter 3

Receiver techniques for CPM signals over TV Channels

Contents

Résumé

Dans le chapitre précédent, nous avons étudié des schémas d'égalisation, de synchronisation et d'estimation canal pour des signaux CPM transmis sur des canaux sélectifs en fréquence (et

ainsi considérés comme constant pendant la durée de la transmission). Nous nous proposons maintenant d'étudier les mêmes techniques pour des transmissions sur des canaux sélectifs en temps et fréquence.

Concernant l'égalisation, nous perdons la diagonalisation de la matrice "canal" dans le domaine fréquentiel et ainsi, les égalisations dans le domaine fréquentiel sont donc souvent jugées trop complexes et le domaine temporel est privilégié [Dar+16]. Cependant, comme nous allons le voir, la matrice canal dans le domaine fréquentiel possède une structure en "bande" qui peut être exploitée pour développer un égaliseur dans le domaine fréquentiel à complexité réduite, au prix d'une approximation entrainant une dégradation de performance.

Enfin, nous allons également étudier l'estimation canal dans le contexte de canaux doublement sélectifs grâce à l'utilisation des 'Basis Expansion Models'. Nous allons voir que les performances de tels estimateurs sont fortement dépendantes du modèle choisi. De plus, nous développerons également une estimation du canal et de la fréquence porteuse coinjointe et la borne de Cramér Rao sera dérivée dans ce nouveau contexte.

3.1 Introduction

In this chapter, we will discuss receiver techniques for Continuous Phase Modulation over doubly-selective channels.

To our knowledge, only a few papers deals with CPM transmission over time-varying (TV) channels. Indeed, the optimal approach would consist into a Maximum A Posteriori (MAP) detection taking into account both channel and CPM memory. However, this is computationally prohibitive as the associated time-varying trellis grows exponentially with the delay spread of the channel and with the CPM memory. Moreover, the techniques presented in Chapter 2 cannot be applied. For instance, to design an equalizer in the Frequency-Domain (FD), we use the fact that a Time InVariant (TIV) channel is a diagonal matrix in the FD, which is not the case for a TV channel. Hence, new receiver techniques are needed.

First, we will briefly introduce the system model used in case of a transmission over a TV channels. Then, we will present a State of the Art Linear Time-Varying Equalizer, which is to our knowledge one of the few equalizers dealing with CPM transmission over doubly-selective channels which has been first proposed in [Dar+16] for full response CPM signals and later extended to partial response CPM scheme in [Dar+18]. Both papers develop a Linear Time Varying (LTV) Equalizer in the Time-Domain which capitalizes on the Laurent Decomposition using both Zero Forcing (ZF) or Minimum Mean Square Error ($MMSE$) criterion under the hypothesis of perfectly known channel. More recently, [OLS18] has developed a joint channel estimation and data detector if no Training Sequence is known at the receiver. By capitalizing on the PAM decomposition for SOQPSK (presented in [OSL17]), they have adapted the Per Survivor Processing (PSP) algorithm (see [RPT95]) to design their receiver that outperforms classical receiver such as the Constant Modulus Algorithm [CRR14]. However, in this thesis, as we have a block based transmission scheme using Unique Word, we will

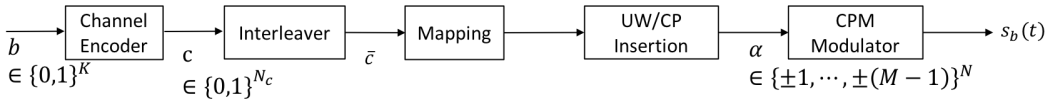

Figure 3.1 – Transmitter structure with CP or UW insertion

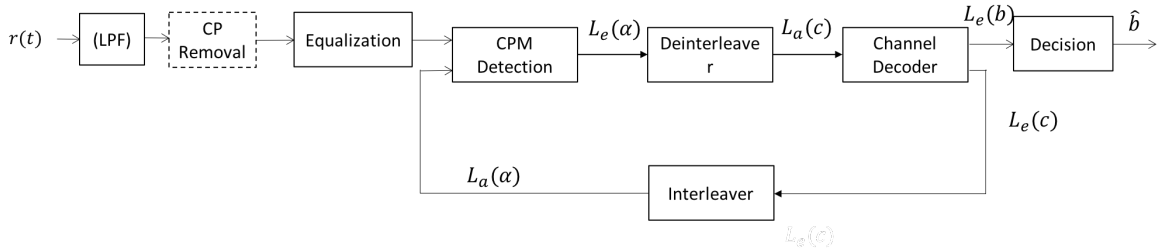

Figure 3.2 – Receiver structure (with CP removal in dotted lines, if CP is used)

capitalize on those known symbols to perform channel estimation and therefore semi-blind or blind joint channel and data estimation algorithms are out of scope.

We will also present a new low-complexity Minimum Mean Square Error Frequency-Domain Equalizer (*MMSE-FDE*) which exploits the 'band' structure of the channel in the FD. The main idea is to only consider the main diagonals of the FD channel matrix and, by doing a Cholesky Decomposition, to reduce the computational complexity of the required matrix inversion. However, as we approximate our channel matrix, this equalizer will suffer from some degradation in terms of performance.

As in Chapter 2, we will present some channel and carrier-frequency estimators which exploit the well-known Basis Expansion Model (*BEM*) and compliant with the previous equalization schemes. We will also present a joint TV channel and carrier frequency estimation for CPM over doubly-selective channel and Cramér Rao Bound (*CRB*) will be derived.

3.2 Transmission over doubly-selective channels

As in Chapter 2, we will consider a Bit Interleaved Coded Modulation (*BICM*) using CPM, as illustrated in Fig.3.1. At the transmitter side, a binary message $\underline{\boldsymbol{b}}$ of length K is encoded to a codeword $\underline{\boldsymbol{c}}$ of length N_c and sent to a M-ary mapper to obtain a sequence $\underline{\boldsymbol{\alpha}} \in \{\pm 1, \pm 3, \ldots, \pm(M-1)\}^N$. After the insertion of a Unique Word (*UW*) or a Cyclic Prefix (*CP*), the data symbols sequence is then given to the CPM modulator.

The overall receiver structure (with the CP removal) is described in Fig.3.2.

There is no difference between this CPM communication system and the one used in Chapter 2. For the rest of this chapter, we will only consider the UW insertion technique (as shown in Fig.3.3) as the UW will be used to perform data-aided channel estimation.

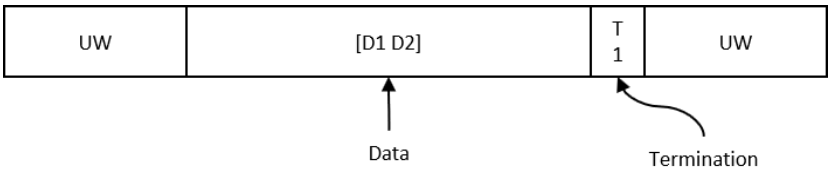

Figure 3.3 – Block-based structure of the CPM signal using a UW

Let us now consider a transmission over a TV channel $h_c(t,\tau)$. At the receiver, we assume ideal low-pass filtering using the front-end filter $\Psi(t)$ and ideal synchronization. Denoting $h(t,\tau) = \Psi(t) * h_c(t,\tau) * \Psi(t)$, where $*$ is the convolution operator, the received signal can be written as:

$$r(t) = e^{j(2\pi f t+\theta)} \sum_m s(m\frac{T_s}{k}) h(t, t - m\frac{T_s}{k}) + w(t) \tag{3.1}$$

where f is the Carrier Frequency Offset, θ the initial phase and $w(t)$ is a complex baseband additive white Gaussian noise with power spectral density $2N_0$ and k is the oversampling factor.

3.3 Equalizers for CPM over TV channels

As in this section we are only interested in mitigating the effect of the TV channels, we will assume perfect synchronization at the receiver, i.e. $f = 0$ and $\theta = 0$.

By sampling the received signal at kR_s (with $R_s = 1/T_s$), from Eq.(3.1) we obtain the following discrete linear convolution, for $0 \leq l \leq kN - 1$:

$$\begin{aligned} r[l] \triangleq r\left(\frac{lT_s}{k}\right) &= \sum_m s(m\frac{T_s}{k}) h\Big(l\frac{T_s}{k}, (l-m)\frac{T_s}{k}\Big) + w\left(l\frac{T_s}{k}\right) \\ &= \sum_m s[m] h[l; l-m] + w[l] \end{aligned} \tag{3.2}$$

3.3.1 Time-Domain Linear Time Varying Equalizer

In case of TV channels, [Dar+18] develops a time-domain MMSE equalizer with the hypothesis of perfect channel knowledge.

In this section, we will present this equalizer working in the Time Domain (TD) on the over-sampled signal first introduced in [Dar+16] for full-response binary CPM signals and later for binary CPM signals in [Dar+18], which is described as a potential candidate for Command and Control Link in UAV system. We will refer to it as a Linear Time-Varying (LTV) Equalizer.

3.3.2 System Model

First, this LTV Equalizer uses the polyphase representation of the received signal, as presented previously in Chapter 2, for the study of the equalizer [VT+09] (see Section 2.3.2.1 for more details). The received signal is sampled at $t = nT_s + \nu T_e$ ($n \in \mathbb{Z}$ and $\nu \in \{0, 1, \ldots, k-1\}$) and we obtain the following polyphase representation:

$$r^\nu(n) \triangleq r(\nu T_e + nT_s) \tag{3.3}$$

$$= \sum_{l=0}^{L_c-1} \sum_{i=0}^{k-1} h^\nu(n, lk + \nu - i) s^i(n-l) + w^\nu(n) \tag{3.4}$$

where $T_e = T_s/k$ and $h^\nu(a, b) = h(ak + \nu; b)$. We gather k consecutive samples into a vector such as:

$$\underline{\boldsymbol{r}}(n) = [r^0(n), r^1(n), \ldots, r^{k-1}(n)]^T \tag{3.5}$$

By denoting the matrix $\underline{\underline{\boldsymbol{H}}}_l(n)$ of size $k \times k$ with entries $[\underline{\underline{\boldsymbol{H}}}_l(n)]_{i_1,i_2} = h^{i_1}(n, lk + i_1 - i_2)$, we obtain a closed form of the received sampled signal given by:

$$\underline{\boldsymbol{r}}(n) = \sum_{l=0}^{L_h-1} \underline{\underline{\boldsymbol{H}}}_l(n) \underline{\boldsymbol{s}}(n-l) + \underline{\boldsymbol{w}}(n) \tag{3.6}$$

where $\underline{\boldsymbol{s}}(n) = [s^0(n), s^1(n), \ldots, s^{k-1}(n)]^T$ of length k and L_h is the channel span in number of samples.

As in [PV06], this LTV equalizer enables to recover the pseudo-symbols of the Laurent Decomposition (described in Chapter 1, Section 1.3.2). Let us recall the PAM decomposition:

$$s(t) = \sum_{n=0}^{N-1} \sum_{q=0}^{K-1} a_{q,n} l_q(t - nT_s) \tag{3.7}$$

where $\{a_{q,n}\}$ are the pseudo symbols, $\{l_q(t)\}$ the Laurent Pulses (LP) and K the number of LP.

The sampled complex envelope of the CPM signal is therefore:

$$\underline{\boldsymbol{s}}(n) = \sum_{q=0}^{K-1} \underline{\boldsymbol{a}}_{q,n} \underline{\underline{\boldsymbol{L}}}_q \tag{3.8}$$

where $\underline{\boldsymbol{a}}_{q,n}$ is the vector of pseudo-symbols such as $\underline{\boldsymbol{a}}_{q,n} = [a_{q,n}, a_{q,n-1}, \ldots, a_{q,n-L_a-L_q+1}]^T$, $L_a = L_e + L_h + 1$ (L_e is the order of the equalizer and therefore defined later) and last, the matrix $\underline{\underline{\boldsymbol{L}}}_q$ of size $k \times L_q$ stands for the over-sampled LP and has the generic term $[\underline{\underline{\boldsymbol{L}}}_q]_{i_1,i_2} = l_q^{i_1}(i_2) = l_q(i_2 T_s + i_1 T_e)$.

Finally, the received samples are:

$$\underline{\boldsymbol{r}}(n) = \sum_{l=0}^{L_h-1} \underline{\underline{\boldsymbol{H}}}_l(n) \sum_{q=0}^{K-1} \boldsymbol{a}_{q,n-l} \underline{\underline{\boldsymbol{L}}}_q + \underline{\boldsymbol{w}}(n) \tag{3.9}$$

Let us now consider a MMSE LTV Equalizer of order L_e (in number of symbols). Its input is a vector of size $k(L_e+1)$:

$$\underline{\boldsymbol{z}}(n) = [\underline{\boldsymbol{r}}^T(n), \underline{\boldsymbol{r}}^T(n-1), \ldots, \underline{\boldsymbol{r}}^T(n-L_e)]^T \tag{3.10}$$

$$= \underline{\underline{\boldsymbol{H}}}(n) \underline{\bar{\underline{\boldsymbol{L}}}} \underline{\boldsymbol{b}}(n) + \underline{\boldsymbol{w}}(n) \tag{3.11}$$

where the matrix $\underline{\underline{\boldsymbol{H}}}(n)$ is a time-varying channel matrix of size $k(L_e+1) \times k(L_e+1)$ given by:

$$\underline{\underline{\boldsymbol{H}}}(n) = \begin{bmatrix} \underline{\underline{\boldsymbol{H}}}_0(n) & \underline{\underline{\boldsymbol{H}}}_1(n) & \cdots & \underline{\underline{\boldsymbol{H}}}_{L_h-1}(n) & \underline{\underline{\boldsymbol{0}}}_{k\times k} & \cdots & \underline{\underline{\boldsymbol{0}}}_{k\times k} \\ \underline{\underline{\boldsymbol{0}}}_{k\times k} & \underline{\underline{\boldsymbol{H}}}_0(n-1) & \underline{\underline{\boldsymbol{H}}}_1(n-1) & \cdots & \underline{\underline{\boldsymbol{H}}}_{L_h-1}(n-1) & \ddots & \underline{\underline{\boldsymbol{0}}}_{k\times k} \\ \vdots & \ddots & \ddots & \ddots & \ddots & \ddots & \vdots \\ \underline{\underline{\boldsymbol{0}}}_{k\times k} & \cdots & \cdots & \underline{\underline{\boldsymbol{H}}}_0(n-L_e) & \underline{\underline{\boldsymbol{H}}}_1(n-L_e) & \cdots & \underline{\underline{\boldsymbol{H}}}_{L_h-1}(n-L_e) \end{bmatrix} \tag{3.12}$$

where $\underline{\underline{\boldsymbol{0}}}_{m\times n}$ is the null matrix of size $m \times n$. $\underline{\bar{\underline{\boldsymbol{L}}}}$ is matrix of size $k(L_e+L_h+1) \times K(L_e+L_h+L_c)$ which stands for the LP contribution and is given by:

$$\underline{\bar{\underline{\boldsymbol{L}}}} = [\underline{\bar{\underline{\boldsymbol{L}}}}_0, \underline{\bar{\underline{\boldsymbol{L}}}}_1, \ldots, \underline{\bar{\underline{\boldsymbol{L}}}}_{K-1}] \tag{3.13}$$

$$\text{and } \underline{\bar{\underline{\boldsymbol{L}}}}_q = \begin{bmatrix} \underline{\underline{\boldsymbol{L}}}_q & \underline{\underline{\boldsymbol{0}}}_{k,1} & \cdots & \underline{\underline{\boldsymbol{0}}}_{k,1} \\ \underline{\underline{\boldsymbol{0}}}_{k,1} & \underline{\underline{\boldsymbol{L}}}_q & \cdots & \underline{\underline{\boldsymbol{0}}}_{k,1} \\ \vdots & \ddots & \ddots & \vdots \\ \underline{\underline{\boldsymbol{0}}}_{k,1} & \cdots & \underline{\underline{\boldsymbol{0}}}_{k,1} & \underline{\underline{\boldsymbol{L}}}_q \end{bmatrix} \tag{3.14}$$

More details on the signal model can be found in [Dar+16] and [Dar+18].

3.3.3 Derivation of the equalizer

The equalizer is given by the matrices $\underline{\underline{\boldsymbol{F}}}(n)$ of size $k(L_e+1) \times K$, for $n \in \mathbb{Z}$:

$$\underline{\boldsymbol{y}}(n) = \underline{\underline{\boldsymbol{F}}}^H(n) \underline{\boldsymbol{z}}(n) \tag{3.15}$$

which are obtained by minimizing the following mean-square error cost function:

$$\text{MSE} = \mathbb{E}\{||\underline{\boldsymbol{y}}(n) - \underline{\boldsymbol{a}}(n-d)||^2\} \tag{3.16}$$

where $\underline{\boldsymbol{a}}(n-d)$ is the vector of pseudo-symbols of length K such as $\underline{\boldsymbol{a}}(n) = [a_{0,n}, a_{1,n}, \ldots, a_{K-1,n}]^T$ and d the equalizer delay. A straightforward derivation gives the following equalization matrix:

$$\underline{\underline{\boldsymbol{F}}}(n) = \underline{\underline{\boldsymbol{R}}}_{zs}^{H}(n)\underline{\underline{\boldsymbol{R}}}_{zz}^{-1}(n) \tag{3.17}$$

where $\underline{\underline{\boldsymbol{R}}}_{zz}(n) = \mathbb{E}\{\underline{\boldsymbol{z}}(n)\underline{\boldsymbol{z}}^H(n)\}$ and $\underline{\underline{\boldsymbol{R}}}_{zs} = \mathbb{E}\{\underline{\boldsymbol{z}}(n)\underline{\boldsymbol{s}}^H(n-d)\}$. Finally,

$$\underline{\underline{\boldsymbol{R}}}_{zs}(n) = \underline{\underline{\boldsymbol{H}}}(n)\underline{\bar{\underline{\boldsymbol{L}}}}\underline{\boldsymbol{r}}_{bs} \tag{3.18}$$

$$\text{and } \underline{\underline{\boldsymbol{R}}}_{zz}(n) = \underline{\underline{\boldsymbol{H}}}(n)\underline{\underline{\bar{\boldsymbol{L}}\boldsymbol{r}}}_{bb}[\underline{\underline{\boldsymbol{H}}}(n)\underline{\bar{\underline{\boldsymbol{L}}}}]^H + \sigma_n^2\underline{\underline{\boldsymbol{I}}}_{k(L_e+1)} \tag{3.19}$$

where $\underline{\boldsymbol{r}}_{\text{bs}} = \mathbb{E}\{\underline{\boldsymbol{b}}(n)\underline{\boldsymbol{s}}^H(n-d)\}$, $\underline{\boldsymbol{r}}_{\text{bb}} = \mathbb{E}\{\underline{\boldsymbol{b}}(n)\underline{\boldsymbol{b}}^H(n)\}$, $\underline{\underline{\boldsymbol{I}}}_{k(L_e+1)}$ the identity matrix of size $k(L_e+1) \times k(L_e+1)$ and σ_n^2 the noise variance.

The matrix $\underline{\underline{\boldsymbol{R}}}_{zs}(n)$ is of size $k(L_e+1) \times K$ whereas the matrix $\underline{\underline{\boldsymbol{R}}}_{zz}(n)$ (which has to be inverted at baud rate) is of size $k(L_e+1) \times k(L_e+1)$.

As for [PV06], this equalizer outputs a sequence of estimated pseudo-symbols, which requires to fed a non-conventional CPM detector as the one in [MFG97] or a sub-optimal one as in [Dar+18].

In [Dar+16], others LTV equalizers are presented for CPM over TV channel such as a ZF equalizer and a Widely Linear versions of those equalizers. Moreover, details on the implementation are given as the capitalization on the well-known Basis Expansion Model (*BEM*) used to represent TV channel with a few coefficients. BEM will be presented and used for channel estimation later in Section 3.4.

As for linear modulation and for both TV or TIV channels, the complexity of time-domain equalizers grows quickly with the channel span or the data rate (here both are represented in the parameter L_e).

In the case of a TIV channel, only one matrix inversion, for $\underline{\underline{\boldsymbol{R}}}_{\text{zz}}(n)$, is required in order to synthesize the time-domain MMSE equalizer. Once, this equalizer coefficients have been computed and stored, the equalizer consists in the product of a matrix of size $K \times k(L_e+1)$ by a vector of size $k(L_e+1)$ where L_e is the equalizer order (in number of symbols), k the oversampling factor and K the number of considered components of the Laurent decomposition (we consider $K = 1$ in the following). This operation must be done for each symbol. Hence, the overall complexity of this operation is in $O(Nk(L_e+1))$. If we consider that the computational complexity of the equalizer synthesis is dominated by the matrix inversion in $O\Big((k(L_e+1))^3\Big)$ as the matrix to inverse is of size $k(L_e+1) \times k(L_e+1)$, the equalizer has a complexity of the order $O\Big((k(L_e+1))^3 + Nk(L_e+1)\Big)$ growing linearly with the size of the data block and with the delay spread of the channel (or equivalently with the data rate).

In the case of a TV channel, we need to synthesis N times the MMSE equalizer matrix, where N is the number of transmitted data symbols. Therefore, the computational complexity

of the equalizer is in $O\Big(N(k(L_e+1))^3 + Nk(L_e+1)\Big)$.

For this reason, we propose to develop a new FD equalizer for CPM over TV channels where the complexity can be greatly reduced by exploiting the band structure of the FD channel matrix.

$$\underline{\underline{\boldsymbol{h}}} = \begin{bmatrix} h[0,0] & 0 & \dots & \dots & 0 \\ \vdots & \ddots & \ddots & & \vdots \\ h[L-1,L-1] & & \ddots & \ddots & \vdots \\ \vdots & \ddots & & \ddots & 0 \\ 0 & \dots & h[kN-1,L-1] & \dots & h[kN-1,0] \end{bmatrix} + \begin{bmatrix} 0 & \dots & h[0,L-1] & \dots & h[0,1] \\ \vdots & \ddots & & \ddots & \vdots \\ 0 & & \ddots & & h[L-2,L-1] \\ \vdots & \ddots & & \ddots & \vdots \\ 0 & \dots & 0 & \dots & 0 \end{bmatrix} \tag{3.22}$$

3.3.4 A new approximate low-complexity MMSE-FDE for TV Channels

For the following, we consider a block-transmission scheme as defined in section 3.2 in order to avoid any Inter-Block Interference. Let us recall that the received signal is given by the following linear convolution:

$$\begin{aligned} r[l] = r\left(\frac{lT}{k}\right) &= \sum_m s(m\frac{T}{k}) h\Big(l\frac{T}{k}, (l-m)\frac{T}{k}\Big) + w\left(l\frac{T}{k}\right) \\ &= \sum_m s[m]h[l;l-m] + w[l] \end{aligned} \tag{3.20}$$

By considering the circular block-based structure of the signal and by defining the channel matrix $\underline{\underline{\boldsymbol{h}}}$ as given in Eq.(3.22) where L is the channel span and by assuming that this channel span is shorter than the size of the UW, the received signal has the following matrix-wise representation:

$$\begin{aligned} &\underline{\boldsymbol{r}} = \underline{\underline{\boldsymbol{h}}}\underline{\boldsymbol{s}} + \underline{\boldsymbol{w}} \\ &\text{with } \underline{\boldsymbol{r}} = [r[0], r[1], \dots, r[kN-1]]^T \\ &\underline{\boldsymbol{s}} = [s[0], s[1], \dots, s[kN-1]]^T \\ &\text{and } \underline{\boldsymbol{w}} = [w[0], w[1], \dots, w[kN-1]]^T \end{aligned} \tag{3.21}$$

The first term in Eq.(3.22) corresponds to the channel over the data and UW block, whereas the second term corresponds to the channel over the previous UW.

Then, the received signal in the FD is now:

$$\begin{aligned} \underline{\boldsymbol{R}} &= \underline{\underline{\boldsymbol{F}}}_{kN}\underline{\boldsymbol{r}} \\ &= \underbrace{\underline{\underline{\boldsymbol{F}}}_{kN}\underline{\underline{\boldsymbol{h}}}\underline{\underline{\boldsymbol{F}}}_{kN}^H}_{=\underline{\underline{\boldsymbol{H}}}} \underbrace{\underline{\underline{\boldsymbol{F}}}_{kN}\underline{\boldsymbol{s}}}_{=\underline{\boldsymbol{S}}} + \underbrace{\underline{\underline{\boldsymbol{F}}}_{kN}\underline{\boldsymbol{w}}}_{=\underline{\boldsymbol{W}}} \end{aligned} \tag{3.23}$$

where $\underline{\underline{\boldsymbol{F}}}_{kN}$ is the unitary Fourier Matrix of size $kN \times kN$ with generic term $[\underline{\underline{\boldsymbol{F}}}_{kN}]_{l,m} = \exp(-j2\pi/(kN))^{lm}/\text{sqrt}(kN)$.

In the case where the channel is time-invariant, the matrix $\underline{\underline{\boldsymbol{h}}}$ is circulant. Therefore, $\underline{\underline{\boldsymbol{H}}}$ will be a diagonal matrix and we obtain the same model as in Chapter 2.

For time-varying channels, $\underline{\underline{\boldsymbol{H}}}$ is not a diagonal matrix. However, it can be well approximated using a band matrix [RBL06]. We note Q the number of lower and upper diagonals retained from $\underline{\underline{\boldsymbol{H}}}$. By defining the matrix $\underline{\underline{\boldsymbol{B}}}^{(Q)}$ as having only non-zeroes on the Q lower and upper diagonals, we approximate our matrix $\underline{\underline{\boldsymbol{H}}}$ by

$$\underline{\underline{\boldsymbol{H}}}_Q = \underline{\underline{\boldsymbol{B}}}^{(Q)} \circ \underline{\underline{\boldsymbol{H}}} \tag{3.24}$$

where $\circ$ is the element-wise product operator. The approximated received signal can be finally written as

$$\underline{\boldsymbol{R}}_Q = \underline{\underline{\boldsymbol{H}}}_Q \underline{\boldsymbol{S}} + \underline{\boldsymbol{W}} \tag{3.25}$$

This MMSE-FDE is defined by the matrix $\underline{\underline{\boldsymbol{J}}}_{\mathrm{MMSE},Q}$ of size $kN \times kN$ such as:

$$\widehat{\underline{\boldsymbol{S}}} = \underline{\underline{\boldsymbol{J}}}_{\mathrm{MMSE},Q} \underline{\boldsymbol{R}} \tag{3.26}$$

The matrix $\underline{\underline{\boldsymbol{J}}}_{\mathrm{MMSE},Q}$ minimizes the following Mean Square Error (*MSE*) criterion:

$$\mathrm{MSE} = \mathbb{E}\Big\{ (\underline{\boldsymbol{S}} - \underline{\underline{\boldsymbol{J}}}_{\mathrm{MMSE},Q} \underline{\boldsymbol{R}}_Q)^H (\underline{\boldsymbol{S}} - \underline{\underline{\boldsymbol{J}}}_{\mathrm{MMSE},Q} \underline{\boldsymbol{R}}_Q) \Big\} \tag{3.27}$$

The linear block MMSE equalizer is given by:

$$\underline{\underline{\boldsymbol{J}}}_{\mathrm{MMSE},Q} = \underline{\underline{\boldsymbol{R}}}_{\mathrm{SS}} \underline{\underline{\boldsymbol{H}}}_Q^H \underline{\underline{\boldsymbol{K}}}^{-1} \tag{3.28}$$

with $\underline{\underline{\boldsymbol{K}}} = \underline{\underline{\boldsymbol{H}}}_Q \underline{\underline{\boldsymbol{R}}}_{\mathrm{SS}} \underline{\underline{\boldsymbol{H}}}_Q^H + \sigma_n^2 \underline{\underline{\boldsymbol{I}}}_{kN}$, σ_n^2 is the noise variance and $\underline{\underline{\boldsymbol{R}}}_{\mathrm{SS}}$ is the auto-correlation matrix of $\underline{\boldsymbol{S}}$ given by:

$$\begin{aligned}
\underline{\underline{\boldsymbol{R}}}_{\mathrm{SS}} &= \mathbb{E}\{\underline{\boldsymbol{S}}\underline{\boldsymbol{S}}^H\} && (3.29)\\
&= \mathbb{E}\{\underline{\underline{\boldsymbol{L}}}\underline{\boldsymbol{B}}\underline{\boldsymbol{B}}^H\underline{\underline{\boldsymbol{L}}}^H\} && (3.30)\\
&= \underline{\underline{\boldsymbol{L}}}\mathbb{E}\{\underline{\boldsymbol{B}}\underline{\boldsymbol{B}}^H\}\underline{\underline{\boldsymbol{L}}}^H && (3.31)\\
&= \underline{\underline{\boldsymbol{L}}}\underline{\underline{\boldsymbol{F}}}_{kN}\mathbb{E}\{\underline{\boldsymbol{b}}\underline{\boldsymbol{b}}^H\}\underline{\underline{\boldsymbol{F}}}_{kN}^H\underline{\underline{\boldsymbol{L}}}^H && (3.32)\\
&= \underline{\underline{\boldsymbol{L}}}\underline{\underline{\boldsymbol{F}}}_{kN}\underline{\boldsymbol{r}}_{\mathrm{bb}}\underline{\underline{\boldsymbol{F}}}_{kN}^H\underline{\underline{\boldsymbol{L}}}^H && (3.33)\\
& && (3.34)
\end{aligned}$$

As explained in [VT+09], we can note that the time-averaged auto-correlation matrix $\underline{\boldsymbol{r}}_{\mathrm{bb}}$ of the pseudo-symbols vector $\underline{\boldsymbol{b}}$ and so the correlation matrix $\underline{\underline{\boldsymbol{R}}}_{\mathrm{SS}}$ can be precomputed using [Lau86] as shown in Eq.(3.33) where $\underline{\underline{\boldsymbol{L}}}$ is the Laurent Pulses matrix. This can be also extended to the M-ary case. As explained in Section 2.3.3, this time-averaged auto-correlation matrix $\underline{\underline{\boldsymbol{R}}}_{\mathrm{SS}}$ is a diagonal matrix thanks to the circular block struture of the signal.

Hence, as $\underline{\underline{\boldsymbol{H_Q}}}$ is a band matrix and $\underline{\underline{\boldsymbol{R}}}_{\mathrm{SS}}$ a diagonal matrix, the equalizer matrix is also a

Algorithm 1: Equalization Procedure

Data: $\underline{\underline{\boldsymbol{H}}}_Q$, $\underline{\underline{\boldsymbol{R}}}_{\mathrm{SS}}$, σ_n^2, $\underline{\boldsymbol{R}}$

Result: $\widehat{\underline{\boldsymbol{S}}}$

Compute the band matrix $\underline{\underline{\boldsymbol{K}}} = \underline{\underline{\boldsymbol{H}}}_Q \underline{\underline{\boldsymbol{R}}}_{\mathrm{SS}} \underline{\underline{\boldsymbol{H}}}_Q^H + \sigma_n^2 \underline{\underline{\boldsymbol{I}}}_{kN}$;

Compute the LDL decomposition of $\underline{\underline{\boldsymbol{K}}} = \underline{\underline{\boldsymbol{L}}}\,\underline{\underline{\boldsymbol{D}}}\,\underline{\underline{\boldsymbol{L}}}^H$ where $\underline{\underline{\boldsymbol{L}}}$ is a lower triangular matrix and $\underline{\underline{\boldsymbol{D}}}$ a diagonal matrix following [RBL05] ;

Solve the triangular system $\underline{\underline{\boldsymbol{L}}}\,\underline{\boldsymbol{f}} = \underline{\underline{\boldsymbol{R}}}$;

Solve the diagonal system $\underline{\underline{\boldsymbol{D}}}\,\underline{\boldsymbol{g}} = \underline{\boldsymbol{f}}$;

Solve the triangular system $\underline{\underline{\boldsymbol{L}}}^H \underline{\boldsymbol{d}} = \underline{\boldsymbol{g}}$;

Compute $\widehat{\underline{\boldsymbol{S}}} = \underline{\underline{\boldsymbol{R}}}_{\mathrm{SS}} \underline{\underline{\boldsymbol{H}}}_Q^H \underline{\boldsymbol{d}}$;

band-matrix by construction:

$$\underline{\underline{\boldsymbol{J}}}_{\mathrm{MMSE,Q}} = \underline{\underline{\boldsymbol{R}}}_{\mathrm{SS}} \underline{\underline{\boldsymbol{H}_{\boldsymbol{Q}}}}^H [\underline{\underline{\boldsymbol{H}}}_Q \underline{\underline{\boldsymbol{R}}}_{\mathrm{SS}} \underline{\underline{\boldsymbol{H}}}_Q^H + \sigma_n^2 \underline{\underline{\boldsymbol{I}}}_{kN}]^{-1} \tag{3.35}$$

The computation of the inverse of the matrix $\underline{\underline{\boldsymbol{K}}} = \underline{\underline{\boldsymbol{H}}}_Q \underline{\underline{\boldsymbol{R}}}_{\mathrm{SS}} \underline{\underline{\boldsymbol{H}}}_Q^H + \sigma_n^2 \underline{\underline{\boldsymbol{I}}}_{kN}$ can be seen at first sight as computationally prohibitive, which is often argued for FD equalization over TV channels. However, by enforcing this band structure, as done above, we can exploit it to perform low-complexity equalization. Indeed, following the idea of [RBL05], the equalization can be computationally efficient using the LDL Decomposition (where L (resp.D) stands for Lower triangular matrix (resp. Diagonal matrix)), which is an alternative form of the Cholesky Decomposition. Thus, the procedure which has to be applied to efficiently equalize the received signal is presented in Algorithm 1.

In the case of time-invariant channels, $\underline{\underline{\boldsymbol{H}}}$ is a diagonal matrix by DFT properties and therefore our equalizer is a diagonal matrix:

$$\underline{\underline{\boldsymbol{J}}}_{\mathrm{MMSE,\ TIV}} = \underline{\underline{\boldsymbol{R}}}_{\mathrm{SS}} \underline{\underline{\boldsymbol{H}}}^H [\underline{\underline{\boldsymbol{H}}}\,\underline{\underline{\boldsymbol{R}}}_{\mathrm{SS}} \underline{\underline{\boldsymbol{H}}}^H + \sigma_n^2 \underline{\underline{\boldsymbol{I}}}_{kN}]^{-1} \tag{3.36}$$

which corresponds to the MMSE-FDE designed in 2.3.3. Hence, the exact low-complexity Frequency-Domain Equalizer for TIV channels presented in 2.3.3 can be seen as a particular case of this new one.

3.3.5 Complexity Analysis

In this section, we discuss the computational complexity of the proposed Band MMSE-FDE. Due to the band structure of the matrix $\underline{\underline{\boldsymbol{K}}}$ and similarly to [RBL05], only $(2Q^2 + 3Q)kN$ complex multiplications, $(2Q^2 + Q)kN$ complex additions and $2QkN$ complex divisions are required. Then, only one diagonal and two triangular systems have to be solved in order to equalize the received signal. They can be solved by band forward and backward substitution [GVL12]. By taking into account the Fast Fourier Transform, the overall complexity of the

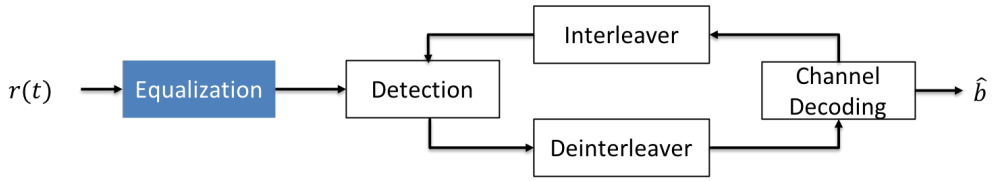

Figure 3.4 – Overall Receiver Structure

proposed equalizer is in the order of $O\big(kN(2Q^2+Q+\log(kN)\big)$.

In the special case where $Q=0$, the matrix $\underline{\underline{\boldsymbol{H}}}_Q$ and $\underline{\underline{\boldsymbol{R}}}_{\mathrm{SS}}$ are both diagonal matrices. Hence, our equalizer does not require the LDL factorization of $\underline{\underline{\boldsymbol{K}}}$ as the inversion has a lower complexity complexity. Then, the overall complexity of our equalizer is dominated by the complexity of the Fast Fourier Transform, which is in $O\big(kN\log(kN)\big)$.

We also evaluate the computational complexity of the LTV Equalizer [Dar+18]. For each symbols sent, this equalizer requires the inversion of a correlation matrix noted $\underline{\underline{\boldsymbol{R}}}_{\mathrm{zz}}$ of size kL_e where k is the oversampling factor and L_e is a parameter corresponding to the number of tap of the equalizer in number of symbols. Typical values of L_e used in [Dar+18] are in the set $\{2,3,4,5\}$. Hence, the LTV equalizer has a overall complexity of $O\big(N(kL_e)^3\big)$ which is of higher complexity compared to the proposed FD equalizer. However, the performance of the equalizer given in [Dar+18] does not suffer from the approximations we have done to ensure the band matrix structure. Thus, lower complexity is expected from our structure but at the price of some (hopefully) reasonable loss of performance.

3.3.6 Results and Discussion

In this section, we present some simulations results. We consider a binary CPM scheme with a raised-cosine (RC) pulse shape, a memory of $L_{\mathrm{CPM}}=3$ and a modulation index $h=1/2$ in the C-band. The transmitted signal is composed by 9 blocks of 512 symbols, where a block is divided into a data block and a Unique Word of 36 symbols. As we consider a BICM scheme, as an outer coding scheme, we use a convolutional code with polynomial generator $(5,7)_8$ given in octal. The overall structure of the receiver is illustrated in Fig.3.4.

The channel considered here is the "En Route" aeronautical channel by satellite with a $C/M=5$dB and a Doppler Spread of 500Hz [Haa02]. We assume that the channel is perfectly known at the receiver.

Fig.3.5 plots the obtained bit error rate as a function of E_s/N_0, for several values of Q and considering an iterative concatenated scheme using the proposed equalizer with 20 iterations between the CPM Detector and the MAP channel decoder. We can see that choosing $Q=1$ instead of $Q=0$ leads to a gain of almost 2dB at a BER of 2×10^{-2}. Then, the improvement is up to 4 dB at a BER of 10^{-2}.

The influence of the number of iterations between the CPM Detector and the Channel

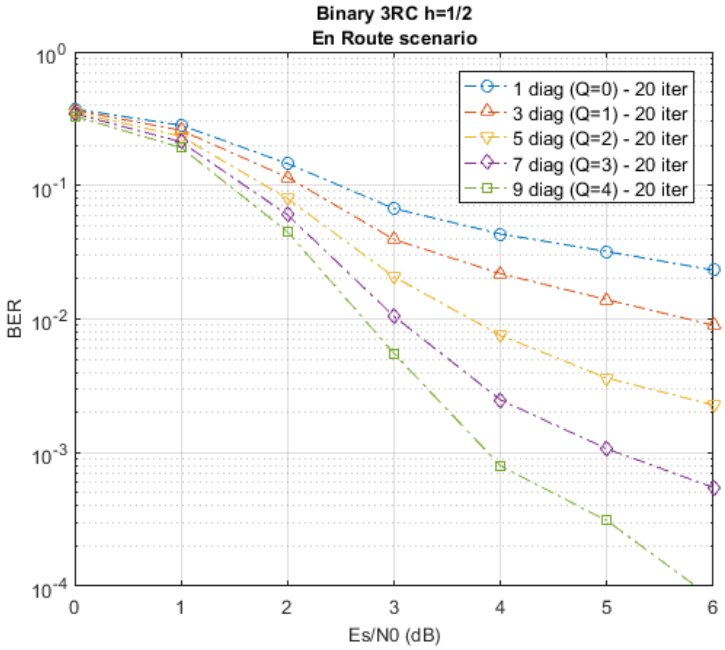

Figure 3.5 – Influence of the parameter Q

Decoder and of the parameter Q are shown in Fig.3.6 for several values of Q. We can see that the choice of those two parameters (number of iterations and Q) has a critical impact on the BER of the overall receiver. However, there is a trade-off to find between performance and computational complexity because increasing Q will increase the complexity of the equalizer, whereas increasing the number of iterations will increase the overall complexity and also the latency of our receiver.

Finally, Fig.3.7 shows the performance of our receiver in the context of [Dar+18] and we compare it to the LTV-MMSE receiver. We consider an uncoded binary GMSK with $h = 1/2$ and a memory of $L_{\text{CPM}} = 3$. We can see that by choosing $Q \geq 3$, our low complexity equalizer outperforms the MMSE-LTV equalizer in the low SNR region. However, at high SNR, the MMSE-LTV is performing better. It can be explained by the fact that our equalizer does not take into account all the Doppler spread, unlike [Dar+18], producing a residual interference between symbols. This drawback should be nevertheless balanced by the fact that, when considering iterative detection and decoding, low SNR behaviour of the detector mainly conditions the performance of the iterative receiver in the waterfall region. Thus having enhanced performance of the proposed detector in the low SNR regime is a good feature for the coded case when performing iterative detection and decoding.

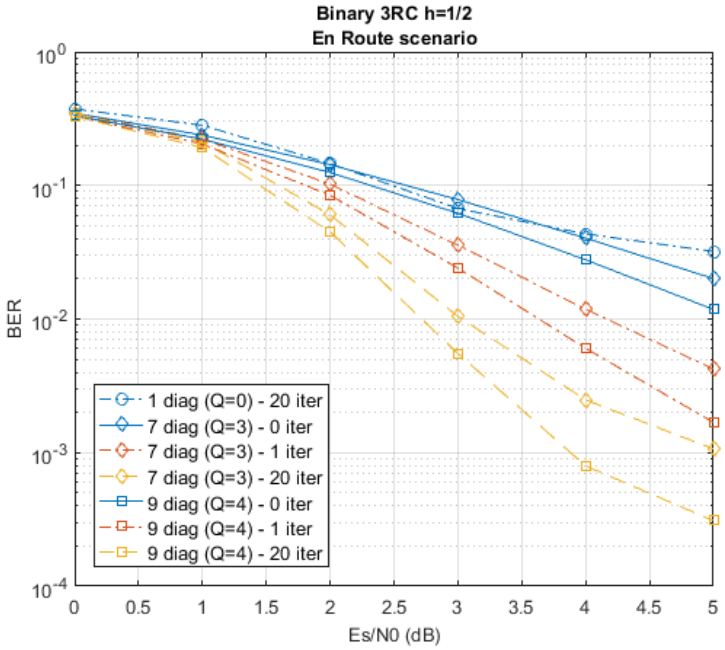

Figure 3.6 – Influence of the parameter Q and of the number of iteration

3.4 Time-Varying Channel estimation

In the previous section, we suppose that the channel is perfectly known at the receiver and it seems that the study of TV channel estimation is not widely addressed for Continuous Phase Modulation. However, for linear modulations and for OFDM, BEM-based channel estimation has been well studied using different Basis Expansion Models (*BEM*) [RBL06], [Vis96], [TO05], [TG96], [Leu04] and [LTB11] and so we propose, in this section, to adapt some of those methods for block-based CPM transmission over TV channels and to evaluate their performance.

We will see that a Least Squares estimation can be performed on the received signal using a fractionally-spaced representation and also that it can be improved by using an *a priori* knowledge on the paths delays (as in the case of aeronautical communication by satellite). We will also provide some performance for single-carrier block-based CPM transmission where we have to exploit the UW based block structure of the transmitted signal.

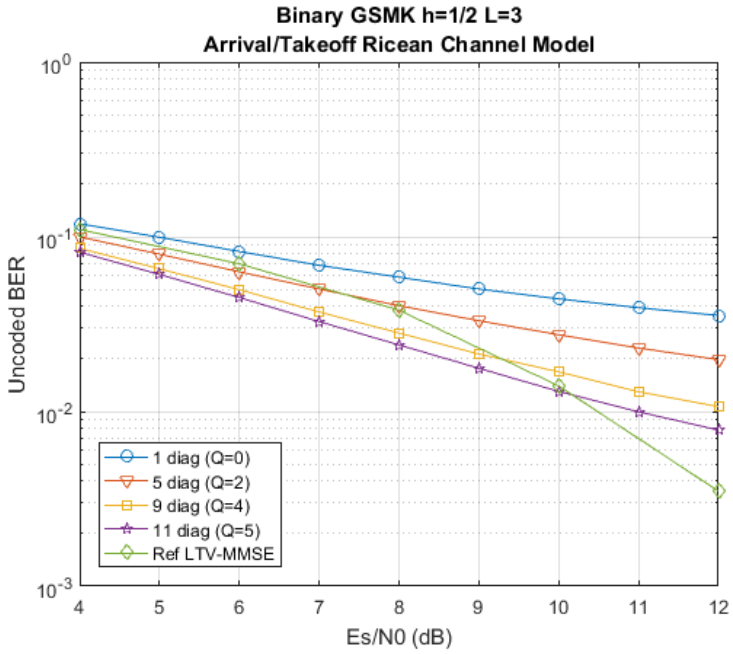

Figure 3.7 – Comparison with the LTV-MMSE [Dar+18]

3.4.1 System Model

3.4.1.1 Baseband representation

Using a Fractionally-Spaced representation of the received signal, we recall that the sampled received signal is:

$$\begin{aligned} r[l] = r\left(\frac{lT}{k}\right) &= \sum_m s(m\frac{T}{k})h\Big(l\frac{T}{k}, (l-m)\frac{T}{k}\Big) + w\left(l\frac{T}{k}\right) \\ &= \sum_m s[m]h[l; l-m] + w[l] \end{aligned} \tag{3.37}$$

By defining the channel matrix $\underline{\underline{\boldsymbol{h}}}$ in Eq.(3.39) where L is the channel span, and by neglecting the interference coming from the previous data block, the received signal has the following matrix-wise representation:

$$\begin{aligned} &\underline{\boldsymbol{r}} = \underline{\underline{\boldsymbol{h}}}\underline{\boldsymbol{s}} + \underline{\boldsymbol{w}} \\ &\text{with } \underline{\boldsymbol{r}} = [r[0], r[1], \ldots, r[kN-1]]^T \\ &\underline{\boldsymbol{s}} = [s[0], s[1], \ldots, s[kN-1]]^T \\ &\text{and } \underline{\boldsymbol{w}} = [w[0], w[1], \ldots, w[kN-1]]^T \end{aligned} \tag{3.38}$$

We point out that we can perfectly remove the interference from the previous data block (and hence, our hypothesis will be valid), by not taking into account the first L received samples (where L is the channel span).

$$\underline{\underline{\boldsymbol{h}}} = \begin{bmatrix} h[0,0] & 0 & \dots & \dots & 0 \\ \vdots & \ddots & \ddots & & \vdots \\ h[L-1,L-1] & & \ddots & \ddots & \vdots \\ \vdots & \ddots & & \ddots & 0 \\ 0 & \dots & h[kN-1,L-1] & \dots & h[kN-1,0] \end{bmatrix} \tag{3.39}$$

We now introduce the following representation:

$$\underline{\boldsymbol{h}}_l = \Big[h[0,l], h[1,l], \dots, h[kN-1,l]\Big]^T \tag{3.40}$$

where $\underline{\boldsymbol{h}}_l$ is a vector of size $kN \times 1$ corresponding to the complex attenuations of the l^{th} path. Then, our channel matrix $\underline{\underline{\boldsymbol{h}}}$ can be written as:

$$\underline{\underline{\boldsymbol{h}}} = \sum_{l=0}^{L-1} \underline{\underline{\boldsymbol{Z}}}_l \mathrm{diag}(\underline{\boldsymbol{h}}_l) \tag{3.41}$$

where $\underline{\underline{\boldsymbol{Z}}}_l$ is a matrix of size $kN \times kN$ which represents the delay of the l^{th} path in the *lag* domain, i.e. $[\underline{\underline{\boldsymbol{Z}}}_l]_{n,(n-l)} = 1$.

In terms of channel estimation, we can see that, by using those notations, the number of parameters to estimate can be too important (as there is kN complex coefficients per path). The Basis Expansion Model allows us to reduce the number of parameters to estimate as only a few coefficients are used to modelize the time-varying channels.

3.4.2 Basis Expansion Model

We now introduce the BEM which has been presented in [GT98]. However, in this section, our notations are inspired by the work of [RBL06] for OFDM systems in the case of Doppler Spread Channels.

3.4.3 Received signal using BEM

The complex attenuation corresponding to the l^{th} path is described as:

$$\underline{\boldsymbol{h}}_l = \underbrace{[\underline{\boldsymbol{\zeta}}_0, \underline{\boldsymbol{\zeta}}_1, \dots, \underline{\boldsymbol{\zeta}}_{P-1}]}_{\underline{\underline{\boldsymbol{\zeta}}}} \underbrace{[\eta_{l,0}, \eta_{l,1}, \dots, \eta_{l,P-1}]^T}_{=\underline{\boldsymbol{\eta}}_l} = \sum_{p=0}^{P-1} \eta_{l,p} \underline{\boldsymbol{\zeta}}_p \tag{3.42}$$

where P is the number of basis function, $\underline{\boldsymbol{\zeta}}_p$ is the (p+1)th deterministic base of size $kN \times 1$, and $\eta_{l,p}$ is the (p+1)th stochastic parameter for the (l+1)th path.

By introducing Eq.(3.42) in Eq.(3.41), we obtain:

$$\underline{\underline{\boldsymbol{h}}} = \sum_l \sum_p \eta_{l,p} \underbrace{\mathrm{diag}(\underline{\boldsymbol{\zeta}}_p)\underline{\underline{\boldsymbol{Z}}}_l}_{=\underline{\underline{\boldsymbol{\Omega}}}_{l,p}} = \sum_l \sum_p \eta_{l,p} \underline{\underline{\boldsymbol{\Omega}}}_{l,p} \tag{3.43}$$

$\underline{\underline{\boldsymbol{\Omega}}}_{l,p}$ is a deterministic matrix of size $kN \times kN$. We now define the matrix $\underline{\underline{\boldsymbol{\Omega}}}$ of size $kN \times PLkN$ by:
$\underline{\underline{\boldsymbol{\Omega}}} = [\underline{\underline{\boldsymbol{\Omega}}}_{0,0}, \ldots, \underline{\underline{\boldsymbol{\Omega}}}_{0,P-1}, \underline{\underline{\boldsymbol{\Omega}}}_{1,0}, \ldots, \underline{\underline{\boldsymbol{\Omega}}}_{1,P-1}, \ldots, \underline{\underline{\boldsymbol{\Omega}}}_{L-1,P-1}]$
and the vector $\underline{\boldsymbol{\eta}} = [\underline{\boldsymbol{\eta}}_0^T, \underline{\boldsymbol{\eta}}_1^T, \ldots, \underline{\boldsymbol{\eta}}_{L-1}^T]^T$ of size $LP \times 1$. Using the Kronecker product $\otimes$, we have:

$$\underline{\underline{\boldsymbol{h}}} = \underline{\underline{\boldsymbol{\Omega}}}(\underline{\boldsymbol{\eta}} \otimes \underline{\underline{\boldsymbol{I}}}_{kN}) \tag{3.44}$$

Finally, it can be shown that the received vector can be rewritten as:

$$\underline{\boldsymbol{r}} = \underline{\underline{\boldsymbol{\Omega}}}(\underline{\boldsymbol{\eta}} \otimes \underline{\underline{\boldsymbol{I}}}_{kN})\underline{\boldsymbol{s}} + \underline{\boldsymbol{w}} \tag{3.45}$$

$$= \underline{\underline{\boldsymbol{\Omega}}}(\underline{\underline{\boldsymbol{I}}}_{LP} \otimes \underline{\boldsymbol{s}})\underline{\boldsymbol{\eta}} + \underline{\boldsymbol{w}} \tag{3.46}$$

3.4.4 Case of a time-invariant channel

In the case of TIV channels, the BEM can be simplified. By taking $P = 1$ and $\underline{\boldsymbol{\zeta}}_0 = [1, 1, \ldots, 1]^T$, we obtain:

$$\underline{\boldsymbol{h}}_l = h[l]\underline{\boldsymbol{\zeta}}_0 \tag{3.47}$$

The BEM parameters are reduced to a vector of size $L \times 1$ such as

$$\underline{\boldsymbol{\eta}} = [\underline{\boldsymbol{\eta}}_0, \underline{\boldsymbol{\eta}}_1, \ldots, \underline{\boldsymbol{\eta}}_{L-1}]^T = [h[0], h[1], \ldots, h[L-1]]^T \tag{3.48}$$

$$\tag{3.49}$$

and therefore

$$\underline{\underline{\boldsymbol{\Omega}}}_{l,0} = \mathrm{diag}(\underline{\boldsymbol{\zeta}}_0)\underline{\underline{\boldsymbol{Z}}}_l = \underline{\underline{\boldsymbol{I}}}_N \underline{\underline{\boldsymbol{Z}}}_l = \underline{\underline{\boldsymbol{Z}}}_l \tag{3.50}$$

$$\text{and so } \underline{\underline{\boldsymbol{\Omega}}} = [\underline{\underline{\boldsymbol{Z}}}_0, \underline{\underline{\boldsymbol{Z}}}_1, \ldots, \underline{\underline{\boldsymbol{Z}}}_{L-1}] \tag{3.51}$$

Our received signal in Eq.(3.46) becomes:

$$\underline{\boldsymbol{r}} = \underbrace{\underline{\underline{\boldsymbol{\Omega}}}(\underline{\underline{\boldsymbol{I}}}_L \otimes \underline{\boldsymbol{s}})}_{=\underline{\underline{\boldsymbol{s}}}} \underline{\boldsymbol{h}} + \underline{\boldsymbol{w}} \tag{3.52}$$

which corresponds exactly to the model presented in Section 2.4 of Chapter 2 for TIV channel estimation.

3.4.4.1 BEM Design

In the State of the Art, various BEM are considered. We discuss here a few models, in a non-exhaustive way, that we will use later.

[Vis96] and [TO05] use the discrete Karhunen-Loeve expansion (*KL-BEM*). They assume that the auto-correlation function of the complex attenuation is the zeroth-order Bessel function (which is the case when the Doppler has a Jakes' Doppler Spectrum). With the knowledge of the maximum Doppler frequency and of the variance of the attenuation, this technique is optimal [TO05]. We note $\underline{\underline{\boldsymbol{R}}}$ the channel correlation matrix of a tap. By using a Singular Value Decomposition (*SVD*), we obtain $\underline{\underline{\boldsymbol{R}}} = \underline{\underline{\boldsymbol{V}}}\text{diag}(\underline{\boldsymbol{\Delta}})\underline{\underline{\boldsymbol{V}}}^H$. Then, the KL-BEM is designed by taking the P first columns of the matrix $\underline{\underline{\boldsymbol{V}}}$ as the basis functions $\{\underline{\boldsymbol{\zeta}}_p\}_p$.

[TG96] introduces a BEM based on Complex Exponential (*CE-BEM*) functions which has been "extended" to the over-sampled CE-BEM (*OCE-BEM*) in [TV00] and [Leu04]. In this case, no prior knowledge channel statistics is needed, reducing the problem of mismatched model. The basis function are defined by:

$$\zeta_p[n] = e^{j2\pi(p-P/2)n/(KkN)}, \text{ with } K \text{ a positive integer} \tag{3.53}$$

It is well-known that CE-BEM ($K = 1$) suffers from model error on the edge of the considered block (as it implies that the channel is periodic with a period equal to the duration of the block). OCE-BEM ($K \geq 2$) allows for a more accurate parametrization, but we loose the orthogonality of the base.

Other BEMs exist (such as polynomial BEM and discrete prolate spheroidal BEM) but they will not be discussed in this thesis. A comparison of some BEM in terms of modelling performance is given in [ZM05] and [Tan07].

3.4.5 Channel Estimation

In this section, we will present the Data-Aided Least Squares (*LS*) channel estimation of the BEM parameters $\underline{\boldsymbol{\eta}}$. Unlike for linear modulations, due to the use of the CPM, this estimation must be performed on the over-sampled received signal $\underline{\boldsymbol{r}}$. We will consider now the transmitted signal $\underline{\boldsymbol{s}}$ known at the receiver. Hence, the matrix $\underline{\underline{\boldsymbol{s}}} = \underline{\underline{\boldsymbol{\Omega}}}(\underline{\underline{\boldsymbol{I}}}_{LP} \otimes \underline{\boldsymbol{s}})$ of size $kN \times LP$ is also known.

3.4.5.1 Least Squares Estimation

As for linear modulations, the standard approach is to perform a LS estimation of the BEM parameters. We assume in this case that there is no model error. The Least Square estimation

is:

$$\widehat{\underline{\boldsymbol{\eta}}} = (\underline{\underline{\boldsymbol{s}}}^H \underline{\underline{\boldsymbol{s}}})^{-1} \underline{\underline{\boldsymbol{s}}}^H \underline{\boldsymbol{r}} \tag{3.54}$$

$$\text{and so } \widehat{\underline{\underline{\boldsymbol{h}}}} = \underline{\underline{\boldsymbol{\Omega}}} (\widehat{\underline{\boldsymbol{\eta}}} \otimes \underline{\underline{\boldsymbol{I}}}_{kN}) \tag{3.55}$$

as the additive noise in our system model is a white Gaussian noise.

The overall complexity of this estimation is dominated by the multiplication of the matrix $(\underline{\underline{\boldsymbol{s}}}^H \underline{\underline{\boldsymbol{s}}})^{-1} \underline{\underline{\boldsymbol{s}}}^H$ of size $LP \times kN$ by a vector of size kN. Indeed, this matrix can be pre-computed and stored at the receiver.

3.4.5.2 Least Squares Estimation with a priori positioning

As in case of TIV Channel estimation for linear modulations [Rad+15] and for CPM transmission over TIV channels (2.4.2), we can introduce a parametric dependence in the estimation of the BEM parameters and the delays of the L_c paths.

Let define the vector $\underline{\boldsymbol{\tau}} = [\tau_0, ..., \tau_{L_c-1}]^T$ which contains the delay of the different paths and $\underline{\boldsymbol{a}} = [\underline{\boldsymbol{a}}_0^T, ..., \underline{\boldsymbol{a}}_{L_c-1}^T]^T$ the associated BEM parameters such as $h_c(t, \tau) = \sum_{l=0}^{L_c-1} a_l(\tau)\delta(t - \tau_l)$. We now introduce the dependence on the delays $\underline{\boldsymbol{\tau}}$, and by using the BEM on the complex attenuation (we suppose $\underline{\boldsymbol{\tau}}$ constant during the frame transmission) and the same idea as previously done (see Eq.(3.44)), we obtain:

$$\underline{\underline{\boldsymbol{h}}} = \sum_{l=0}^{L_c-1} \sum_{p=0}^{P-1} \eta_{l,p} \text{diag}(\underline{\boldsymbol{\zeta}}_p) \underline{\underline{\boldsymbol{Z}}}_{\tau_l} \tag{3.56}$$

$$= \underline{\underline{\boldsymbol{\Omega}}}_{\underline{\boldsymbol{\tau}}} (\underline{\boldsymbol{\eta}}_P \otimes \underline{\underline{\boldsymbol{I}}}_{kN}) \tag{3.57}$$

$$\text{where } \underline{\underline{\boldsymbol{Z}}}_{\tau_l} \doteq \text{Toeplitz}(\underline{\boldsymbol{\Psi}}(\tau_l)) \tag{3.58}$$

$$\text{and } [\underline{\boldsymbol{\Psi}}(\tau_l)]_n \doteq \Psi(n\frac{T}{k} - \tau_l) \tag{3.59}$$

Let us now emphasize the difference between this parametric model and the one presented in Eq.(3.46). In this model, $\underline{\underline{\boldsymbol{\Omega}}}_{\underline{\boldsymbol{\tau}}}$ contains only the contribution of the front-end filter $\Psi(t)$ with the delays of the considered paths $\underline{\boldsymbol{\tau}}$. The vector $\underline{\boldsymbol{\eta}}_p$ of size $PL_c \times 1$ contains only the BEM parameters for each considered paths. Our received signal is now:

$$\underline{\boldsymbol{r}} = \underline{\underline{\boldsymbol{\Omega}}}_{\underline{\boldsymbol{\tau}}} (\underline{\underline{\boldsymbol{I}}}_{PL_c} \otimes \underline{\boldsymbol{s}}) \underline{\boldsymbol{\eta}}_P \ + \underline{\boldsymbol{w}} = \underline{\underline{\boldsymbol{s}}}_P \underline{\boldsymbol{\eta}}_P \ + \underline{\boldsymbol{w}} \tag{3.60}$$

where $\underline{\underline{\boldsymbol{s}}}_p$ is now a matrix of $kN \times PL_c$. This matrix $\underline{\underline{\boldsymbol{s}}}_p$ is known at the receiver as the vector τ is also known by geometrical consideration (see [Rad+15] and [Cha+17a]) or previously estimated as in [CVM07], [BM96] and [SS08].

As the noise in our system model is still a white Gaussian noise, the Least Squares esti-

mation of $\underline{\boldsymbol{\eta}}_P$ is given by:

$$\widehat{\underline{\boldsymbol{\eta}}}_P = (\underline{\underline{\boldsymbol{s}}}_p^H \underline{\underline{\boldsymbol{s}}}_p)^{-1} \underline{\underline{\boldsymbol{s}}}_p^H \underline{\boldsymbol{r}} \tag{3.61}$$

$$\text{and so } \widehat{\underline{\underline{\boldsymbol{h}}}}_P = \underline{\underline{\boldsymbol{\Omega}}}_{\underline{\boldsymbol{\tau}}} (\widehat{\underline{\boldsymbol{\eta}}}_P \otimes \underline{\underline{\boldsymbol{I}}}_{kN}) \tag{3.62}$$

By using this parametric estimator, we reduce the number of parameters to estimate from PL to PL_c parameters. We also reduce the computational complexity of the inverse as the matrix $\underline{\underline{\boldsymbol{s}}}_p^H \underline{\underline{\boldsymbol{s}}}_p$ is of size $L_c \times L_c$ instead of $L \times L$. For instance, in the case of the aeronautical channel, it is commonly admitted that $L_c = 2$

3.4.5.3 Block-based transmission

In case of block-based transmission as presented in Fig. 3.3, only the UW (composed of N_{UW} symbols) are known at the receiver, however we need to estimate the channel over both data block and UW in order to perform channel equalization as the one presented in [Dar+18] or in 3.3.4. To do so, we propose to consider the previous UW, the data block and the next UW as proposed in [LTB11]. In this case, we can separate the contribution of the UWs and of the data block. By considering, the vector $\underline{\boldsymbol{r}}_{\text{UW}} = [r[L], r[L+1], \ldots, r[kN_{\text{UW}} - 1], r[k(N - N_{\text{UW}}) + L], \ldots, r[kN-1]]^T$ of size $2k(N_{\text{UW}} - L) \times 1$ which contains only the received samples corresponding to the contribution of the UWs (we have removed the ISI coming from the data blocks), we can rewrite our system as [LTB11]:

$$\underline{\boldsymbol{r}}_{\text{UW}} = \underline{\underline{\boldsymbol{h}}}_{\text{UW}} \underbrace{[\underline{\boldsymbol{s}}_{\text{UW}}^T, \underline{\boldsymbol{s}}_{\text{UW}}^T]^T}_{\doteq \underline{\boldsymbol{s}}_{\text{UW},2}} + \underline{\boldsymbol{w}}_{\text{UW}} \tag{3.63}$$

where the matrix $\underline{\underline{\boldsymbol{h}}}_{\text{UW}}$ of size $k(N_{\text{UW}} - L) \times 2kN_{\text{UW}}$ is a concatenated sub-matrix of $\underline{\underline{\boldsymbol{h}}}$. We point out that this matrix $\underline{\underline{\boldsymbol{h}}}_{\text{UW}}$ depends on the same BEM parameters as the matrix $\underline{\underline{\boldsymbol{h}}}$ as it is only a partitioning of this former matrix. Hence, the LS estimation, based only on the UW, is given by:

$$\widehat{\underline{\boldsymbol{\eta}}}_{\text{UW}} = (\underline{\underline{\boldsymbol{s}}}_{\underline{\boldsymbol{UW}},2}^H \underline{\underline{\boldsymbol{s}}}_{\text{UW},2})^{-1} \underline{\underline{\boldsymbol{s}}}_{\text{UW},2}^H \underline{\boldsymbol{r}}_{\text{UW}} \tag{3.64}$$

$$\text{with } \underline{\underline{\boldsymbol{s}}}_{\text{UW},2} \doteq \underline{\underline{\boldsymbol{\Omega}}} (\underline{\underline{\boldsymbol{I}}}_{PL} \otimes \underline{\underline{\boldsymbol{s}}}_{\text{UW},2}) \tag{3.65}$$

This LS estimation can use *a priori* positioning as described in the previous section. Hence, our estimated channel is obtained by $\widehat{\underline{\underline{\boldsymbol{h}}}} = \underline{\underline{\boldsymbol{\Omega}}} (\widehat{\underline{\boldsymbol{\eta}}}_{\text{UW}} \otimes \underline{\underline{\boldsymbol{I}}}_{kN})$. The *interpolation* of our estimated channel over the data block is directly performed by the BEM. The partitioning of the time-domain channel matrix between Unique Word and Data block is illustrated in Fig.3.8.

3.4.6 Results and Discussion

For simulation, we consider a binary CPM scheme with $h = 1/2$, a CPM memory $L_{\text{CPM}} = 3$ and a REC pulse shape. We point out that, as our Unique Word can be independent of

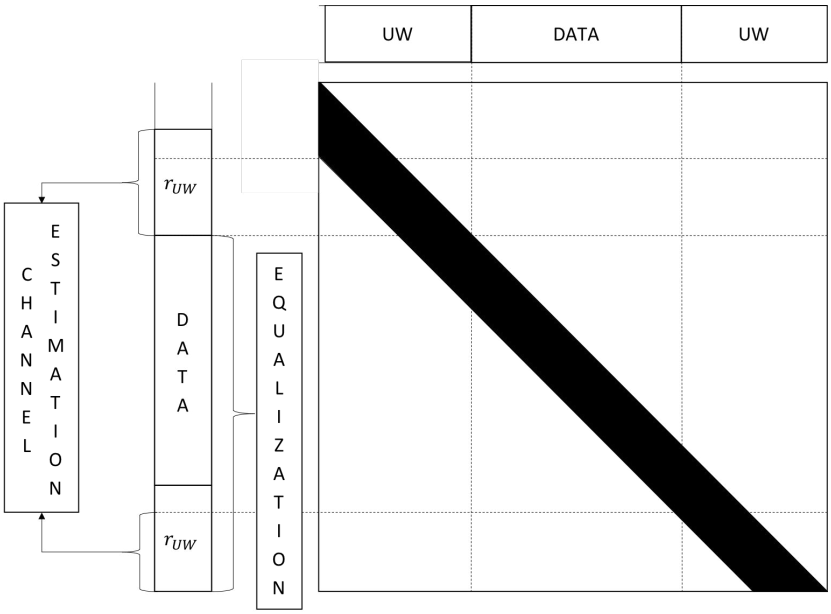

Figure 3.8 – Partitioning of the time-domain channel matrix

our CPM parameters, our results can be extended to other CPM schemes. We define the Normalized Mean Square Error *NMSE* as:

$$\mathrm{NMSE} = \mathbb{E}\Big\{ \frac{\sum_{l=0}^{L-1} |\underline{\boldsymbol{h}}_l - \widehat{\underline{\boldsymbol{h}}}_l|^2}{\sum_{l=0}^{L-1} |\underline{\boldsymbol{h}}_l|^2} \Big\} \tag{3.66}$$

This NMSE explicitly takes the BEM modeling error into account.

First, in Fig. 3.9, we consider a TIV channel and thus our model is the one presented in Chapter 2. The UW has a size of $N_{\mathrm{UW}} = 16$ and the data block is of size 48 symbols (which corresponds to a bandwidth efficiency of $\epsilon = 75\%$). However, as the channel is time-invariant, the performance of the channel estimators does not depend on the size of the data block, as illustrated in the simulation results. In both case, the estimation is done over 32 pilot symbols. We can see that our improved LS channel estimator (which uses the knowledge on the delays) outperforms the classic one with a gain of almost 25dB for a NMSE of 10^{-2}. Similar results have been already observed in [Cha+17a].

We now consider a time-varying channel. We examine our channel estimators for a Rayleigh channel with a Jakes' Doppler Spectrum and a maximum Doppler frequency of $0.0183R_s$ (where R_s is the symbol rate $R_s = 1/T$). This channel is composed of 2 paths with a delay of $1.5T$ between them. First, we consider the case where even the data block is known at the receiver in order to validate our methods. In our simulations, we perform the LS estimation with 128 known symbols.

In Fig. 3.10, we consider the KL-BEM and present simulation results for different numbers of basis functions. We can observe that by increasing the number of basis functions, the performance are improved, which is explained by the fact that our BEM is closer to the

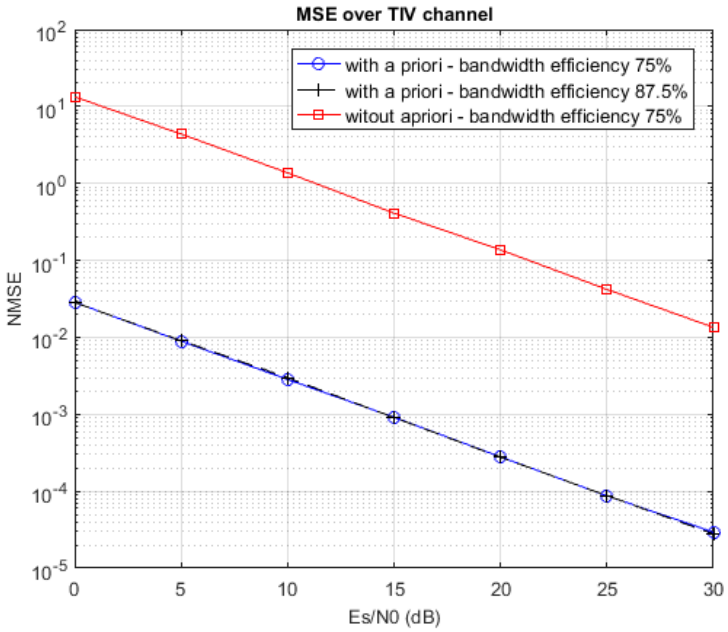

Figure 3.9 – NMSE over TIV channels

simulated channel. The floor error phenomenon is due to the BEM modeling error. It is acknowledged that a BEM is accurate when the modeling error is on the order of 10^{-4} [LTB11], which is the case when we use 7 basis functions. We do not consider the improved LS channel estimation using the knowledge of the delays due to the fact that the KL-BEM already uses this knowledge, by considering the variance of the attenuation. Nevertheless, the KL-BEM, described in subsection 3.4.4.1 requires an important knowledge on the channel such as the maximum Doppler frequency and the variance of the complex attenuation (which provides the knowledge on the delays). Hence, we investigate more robust BEM.

A common BEM is the (O)CE-BEM based only on complex exponentials. This model does not require any knowledge of the channel statistics. In this case, the BEM channel estimation suffers from the unknown *sparsity* of the channel. Indeed, we try to estimate a *null* path by a sum of weighted complex exponentials. Even the LS estimation with positioning *a priori* exhibits a large BEM modeling error as shown in Fig. 3.11. We can also observe that for the same number of basis function, the KL-BEM outperforms the chosen OCE-BEM, which can be explained by the optimality of the KL-BEM. However, as we can see in any of our chosen case, the OCE-BEM cannot be considered accurate as the error floor is around 10^{-3}, which can lead to further study to find an other suitable model based on the OCE-BEM (by changing the factor) or by considering a completely different BEM.

To conclude, we now present the performance of our algorithm in the case of a block-based transmission. As explained in subsection 3.4.5.3, only the UWs are known at receiver, and so the channel is *interpolated* over the data block thanks to the BEM.

We will consider different sizes N_{UW} of UW and different sizes of data block of N_{DATA}

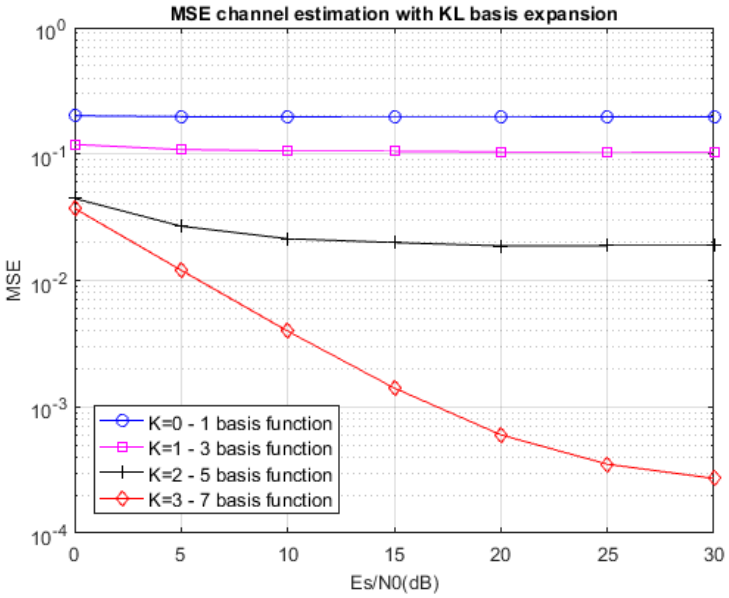

Figure 3.10 – NMSE over TV channels using KL-BEM

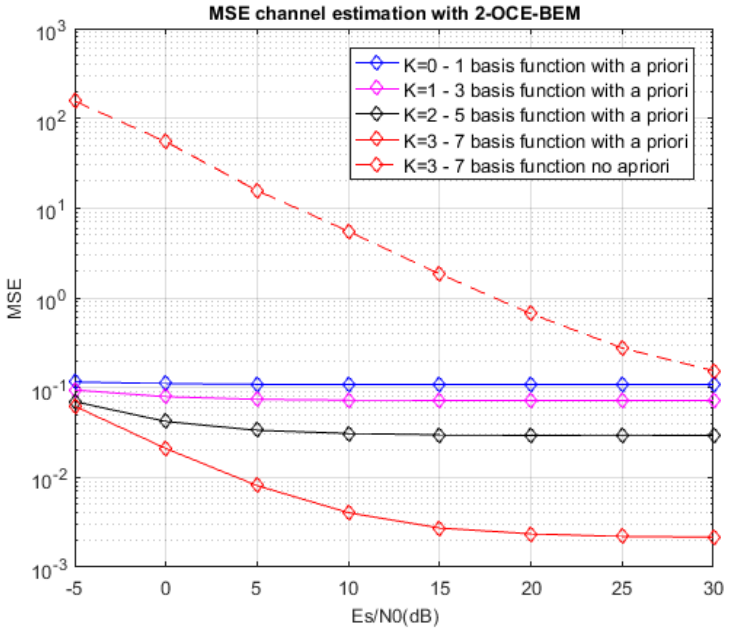

Figure 3.11 – NMSE over TV channels using OCE-BEM

(which give us a bandwidth efficiency of $1 - N_{\text{UW}}/(N_{\text{DATA}} + N_{\text{UW}})$). We choose for those simulations a normalized Doppler spread of $0.0008R_s$ and the KL-BEM to approximate our channel which supposes a maximum Doppler frequency of $0.002R_s$. Those parameters have been used in [LTB11]. Only 3 basis functions are considered, which gives us 6 BEM parameters to estimate as only 2 paths are considered. Simulations results are presented in Fig.3.12. We

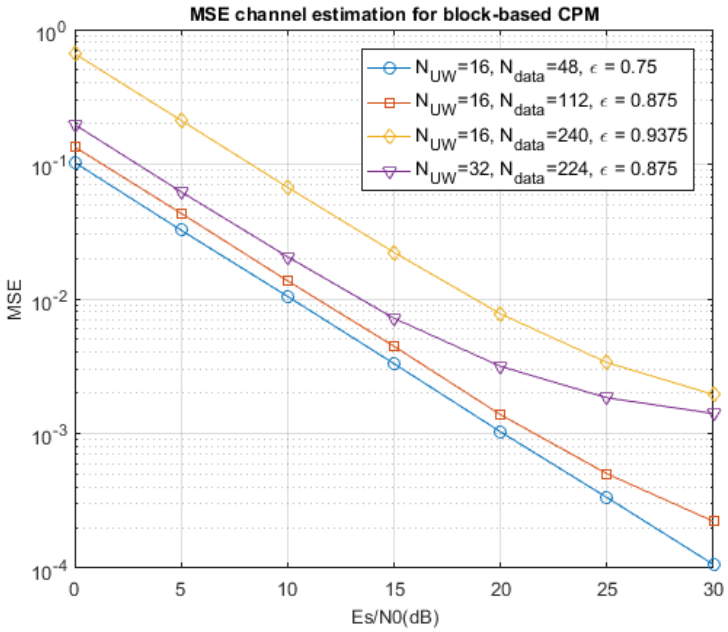

Figure 3.12 – NMSE over TV channels using KL-BEM for block-based CPM

obtain some performance comparable to the ones in [LTB11], which tends to validate our approach. We can observe that, when we increase the size of the data block while keeping the same size of UW, the performance are degraded which can be explained easily. Indeed, in this case, the *interpolation* of the channel over the data block is worse due to BEM modelling error.

3.5 Joint TV and Carrier Frequency Estimation

We have seen, in the previous sections, how to equalize a CPM signal in case of transmission over TV channels and also how to estimate the channel using the BEM Expansion. All this work has been done under the hypothesis of perfect synchronization at the receiver side.

We will now consider that there is a Carrier Frequency Offset and an initial phase to estimate. We recall that the received signal is (Eq.(3.1)):

$$r(t) = e^{j(2\pi ft+\theta)} \sum_m s(m\frac{T}{k})h(t, t - m\frac{T}{k}) + w(t)$$

For ease of presentation, we will put the initial phase in the channel by defining $h_\theta(t, t - m\frac{T}{k}) = e^{j\theta}h(t, t - m\frac{T}{k})$. However, for ease of notation, we will remove the subscript in the following.

After sampling at kR_s and by assuming a BEM for the TV channel of basis functions $\{\zeta_p\}$

and of parameters $\{\eta_{l,p}\}$, we obtain the following FS representation:

$$\underline{\boldsymbol{r}} = \underline{\underline{\boldsymbol{\Gamma}}}(f)\underline{\underline{\boldsymbol{\Omega}}}(\underline{\boldsymbol{\eta}} \otimes \underline{\underline{\boldsymbol{I}}}_{kN})\underline{\boldsymbol{s}} + \underline{\boldsymbol{w}} \tag{3.67}$$

$$= \underline{\underline{\boldsymbol{\Gamma}}}(f)\underbrace{\underline{\underline{\boldsymbol{\Omega}}}(\underline{\underline{\boldsymbol{I}}}_{LP} \otimes \underline{\boldsymbol{s}})}_{\doteq \underline{\underline{\boldsymbol{s}}}}\underline{\boldsymbol{\eta}} + \underline{\boldsymbol{w}} \tag{3.68}$$

$$= \underline{\underline{\boldsymbol{\Gamma}}}(f)\underline{\underline{\boldsymbol{s}}}\underline{\boldsymbol{\eta}} + \underline{\boldsymbol{w}} \tag{3.69}$$

where $\underline{\underline{\boldsymbol{\Omega}}}$ is a deterministic matrix of size $kN \times kN$ which depends on the BEM basis function $\{\zeta_p\}$ and $\underline{\boldsymbol{s}}$ is the transmitted signal of size $kN \times 1$. We can emphasize the fact that the matrix $\underline{\underline{\boldsymbol{s}}}$ of size $kN \times LP$ is perfectly known at the receiver. $\underline{\boldsymbol{\eta}}$ is the vector of parameters of the BEM to estimate and $\underline{\underline{\boldsymbol{\Gamma}}}(f)$ is a diagonal matrix which introduces the CFO f such as:

$$\underline{\underline{\boldsymbol{\Gamma}}}(f) = \mathrm{diag}(1, e^{j2\pi f T_e}, e^{j4\pi f T_e}, \ldots, e^{j2(kN-1)\pi f T_e})$$

We obtain a similar model to the one considered in Section 2.5.3. Instead of estimate the TIV channel taps, we now estimate the BEM parameters.

As in the previous chapter, we will derive a joint ML estimation for the BEM parameters and the CFO.

3.5.1 ML Estimation

For $(\underline{\boldsymbol{\eta}}, f)$, we can note that $\underline{\boldsymbol{r}}$ is Gaussian with mean $\underline{\underline{\boldsymbol{\Gamma}}}(f)\underline{\underline{\boldsymbol{s}}}\underline{\boldsymbol{\eta}}$ and covariance matrix $\sigma_n^2 \underline{\underline{\boldsymbol{I}}}_{kN}$. Hence, the log-likelihood function for the parameters $\underline{\boldsymbol{\eta}}$ and f is:

$$\Delta(\widetilde{\underline{\boldsymbol{\eta}}}, \widetilde{f}) = -\frac{1}{\sigma_n^2}[\underline{\boldsymbol{r}} - \underline{\underline{\boldsymbol{\Gamma}}}(\widetilde{f})\underline{\underline{\boldsymbol{s}}}\widetilde{\underline{\boldsymbol{\eta}}}]^H[\underline{\boldsymbol{r}} - \underline{\underline{\boldsymbol{\Gamma}}}(\widetilde{f})\underline{\underline{\boldsymbol{s}}}\widetilde{\underline{\boldsymbol{\eta}}}] \tag{3.70}$$

We choose to maximize Δ over $\widetilde{\underline{\boldsymbol{\eta}}}$ and $\widetilde{f}$ to obtain the joint ML estimates of $\underline{\boldsymbol{\eta}}$ and f. The estimate of $\underline{\boldsymbol{\eta}}$ for a given $\widetilde{f}$ is

$$\widehat{\underline{\boldsymbol{\eta}}}(\widetilde{f}) = (\underline{\underline{\boldsymbol{s}}}^H\underline{\underline{\boldsymbol{s}}})^{-1}\underline{\underline{\boldsymbol{s}}}^H\underline{\underline{\boldsymbol{\Gamma}}}^H(\widetilde{f})\underline{\boldsymbol{r}}. \tag{3.71}$$

Using this estimate in Eq.(2.159), we obtain the following carrier-frequency estimator:

$$\widehat{f} = \arg\max_{\widetilde{f}} g(\widetilde{f}) \tag{3.72}$$

where

$$g(\widetilde{f}) = \underline{\boldsymbol{r}}^H\underline{\underline{\boldsymbol{\Gamma}}}(\widetilde{f})\underline{\underline{\underline{\boldsymbol{B}}}}\underline{\underline{\boldsymbol{\Gamma}}}^H(\widetilde{f})\underline{\boldsymbol{r}} \tag{3.73}$$

and

$$\underline{\underline{\boldsymbol{B}}} \triangleq \underline{\underline{\boldsymbol{s}}}(\underline{\underline{\boldsymbol{s}}}^H\underline{\underline{\boldsymbol{s}}})^{-1}\underline{\underline{\boldsymbol{s}}}^H \tag{3.74}$$

Eq.(3.72) can be re-written as a the DFT of a weighed correlation of the over-sampled received signal:

$$g(\widetilde{f}) = -\rho(0) + 2\Re\Big\{\sum_{m=0}^{kN-1}\rho(m)e^{-j2\pi\widetilde{f}m}\Big\} \tag{3.75}$$

where $\rho(m)$ is the weighted discrete auto-correlation of $\underline{\boldsymbol{r}}$ such as:

$$\rho(m) = \sum_{l=0}^{kN-1}[\underline{\underline{\boldsymbol{B}}}]_{l-m,l}r[l]r^*[l-m] \tag{3.76}$$

As in Chapter 2, Section 2.4.2, the joint channel and carrier recovery can be performed using the following procedure:

- Compute $\widehat{f}$ using Eq.(3.73)
- Counter-rotate the received signal $\underline{\boldsymbol{r}}$ according to $\widehat{f}$
- Compute $\underline{\widehat{\boldsymbol{\eta}}}$ using the LS estimation of the BEM parameters Eq.(3.71)

3.5.2 TIV case

As in Section 3.4.4, we will exhibit the behaviour of our estimator in the case of a TIV channel. In this case, we recall that:

$$\underline{\boldsymbol{r}} = \underline{\underline{\boldsymbol{\Gamma}}}(f)\underline{\underline{\boldsymbol{s}}}\underline{\boldsymbol{h}} + \underline{\boldsymbol{w}} \tag{3.77}$$

where

$$\underline{\underline{\boldsymbol{s}}} = [\underline{\underline{\boldsymbol{Z}}}_0\underline{\underline{\boldsymbol{s}}}, \underline{\underline{\boldsymbol{Z}}}_1\underline{\underline{\boldsymbol{s}}}, \ldots, \underline{\underline{\boldsymbol{Z}}}_{L-1}\underline{\underline{\boldsymbol{s}}}] \tag{3.78}$$

$$= \begin{bmatrix} s[0] & 0 & \ldots 0 & \\ s[1] & s[0] & \ddots & \vdots \\ \vdots & \vdots & \vdots & \vdots \\ s[L-1] & \ldots & s[1] & s[0] \\ \vdots & \vdots & \vdots & \vdots \\ s[kN-1] & s[kN-2] & \ldots & s[kN-L] \end{bmatrix} \tag{3.79}$$

which corresponds exactly to the model used in Section 3.4.4 to derive our joint TIV channel and CFO estimator. Hence, it can been seen as a specific case of the estimator developed for

TV channels in this chapter.

3.5.3 Cramér Rao Bound

By assuming no modeling error (i.e. the channel fit perfectly the chosen BEM), and by following the same procedure as in Section 2.5.3.4 (and so as in [MM00]), we can derive the Modified CRB for carrier recovery over a TV channel.

To begin, we call $\underline{\boldsymbol{\eta}}_r$ and $\underline{\boldsymbol{\eta}}_i$ the real and imaginary components of the channel response and define $u = (\underline{\boldsymbol{\eta}}_r, \underline{\boldsymbol{\eta}}_i, f)$ the set of the unknown parameters. Then, the components of the Fisher information matrix are:

$$[\underline{\underline{\boldsymbol{F}}}]_{i,j} = -E\Big[\frac{\partial^2 \ln\Delta(\underline{\boldsymbol{r}}, u)}{\partial u(i)\partial u(j)}\Big] \tag{3.80}$$

We can see that:

$$-\ln\Delta(\underline{\boldsymbol{r}}, u) = \frac{1}{\sigma_n^2}[\underline{\boldsymbol{r}} - \underline{\underline{\boldsymbol{\Gamma}}}(f)\underline{\underline{\boldsymbol{s}}}(\underline{\boldsymbol{\eta}}_r + j\underline{\boldsymbol{\eta}}_i)]^H[\underline{\boldsymbol{r}} - \underline{\underline{\boldsymbol{\Gamma}}}(f)\underline{\underline{\boldsymbol{s}}}(\underline{\boldsymbol{\eta}}_r + j\underline{\boldsymbol{\eta}}_i)] \tag{3.81}$$

$$\underline{\underline{\boldsymbol{F}}} = \frac{2}{\sigma_n^2}\begin{pmatrix} \Re\{\underline{\underline{\boldsymbol{s}}}^H\underline{\underline{\boldsymbol{s}}}\} & -\Im\{\underline{\underline{\boldsymbol{s}}}^H\underline{\underline{\boldsymbol{s}}}\} & -\Im\{\underline{\boldsymbol{y}}^H\underline{\underline{\boldsymbol{s}}}\} \\ \Im\{\underline{\underline{\boldsymbol{s}}}^H\underline{\underline{\boldsymbol{s}}}\} & \Re\{\underline{\underline{\boldsymbol{s}}}^H\underline{\underline{\boldsymbol{s}}}\} & \Re\{\underline{\boldsymbol{y}}^H\underline{\underline{\boldsymbol{s}}}\} \\ \Im\{\underline{\boldsymbol{y}}^H\underline{\underline{\boldsymbol{s}}}\} & \Re\{\underline{\boldsymbol{y}}^H\underline{\underline{\boldsymbol{s}}}\} & \underline{\boldsymbol{y}}^H\underline{\boldsymbol{y}} \end{pmatrix} \tag{3.82}$$

where $\Re\{.\}$ and $\Im\{.\}$ are the real and imaginary part operators. Following [MM00], and after an equivalent tedious derivation, it can be shown that the CRB on carrier frequency estimation is:

$$CRB(f) = \frac{\sigma_n^2}{2\underline{\boldsymbol{y}}^H(\underline{\underline{\boldsymbol{I}}}_{kN} - \underline{\underline{\boldsymbol{B}}})\underline{\boldsymbol{y}}} \tag{3.83}$$

with

$$\underline{\boldsymbol{y}} = 2\pi\underline{\underline{\boldsymbol{M}}}\underline{\underline{\boldsymbol{s}}}\underline{\boldsymbol{h}} \tag{3.84}$$

$$\text{with } \underline{\underline{\boldsymbol{M}}} = \text{diag}(0, 1, \ldots, kN-1) \tag{3.85}$$

As previously stated, this CRB does not take into account the BEM modeling error and so it is not always relevant. We also point out that in the specific case of TIV channel, we fall back in the CRB developed in Chapter 2 and that in this case, no modeling error is present.

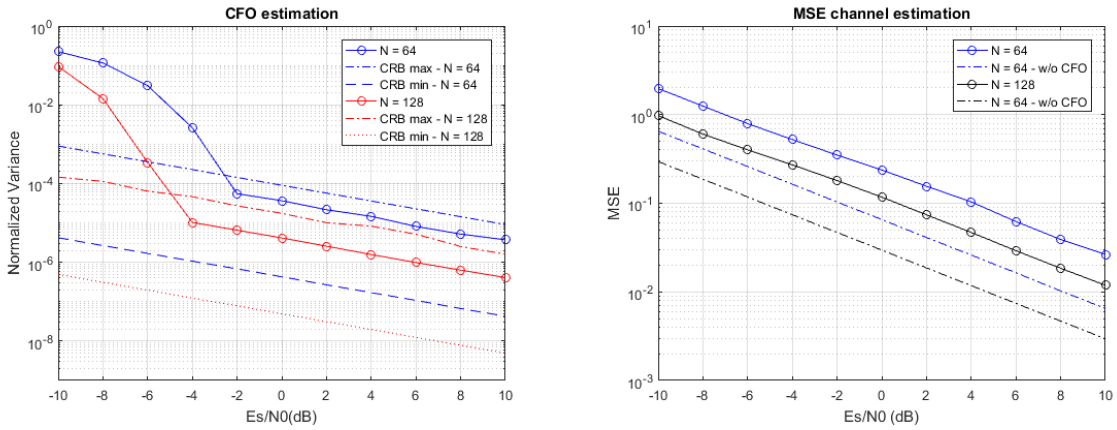

Figure 3.13 – Carrier Recovery for CE-BEM channel

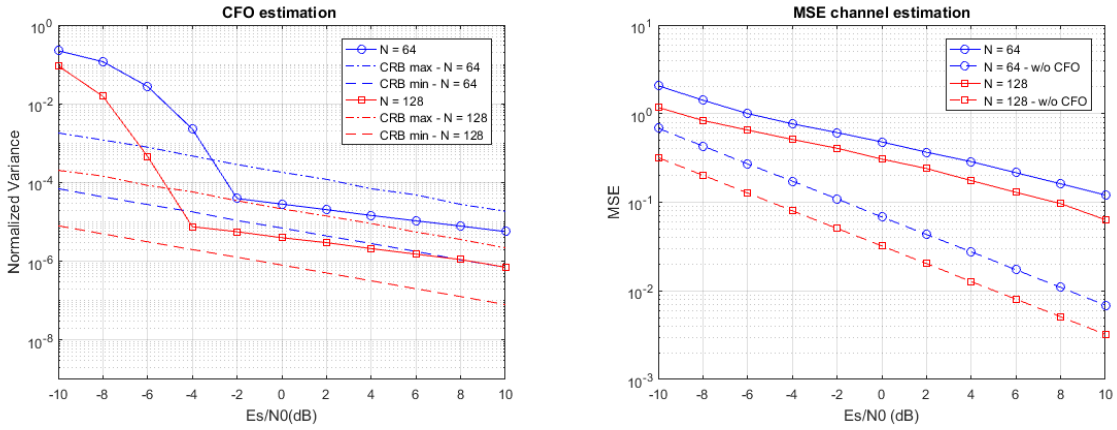

Figure 3.14 – Carrier Recovery for OCE-BEM channel

3.5.4 Results and Discussion

In this section, we present some simulation results for the proposed joint CFO and channel estimator in case of TV channels, which capitalizes on the BEM representation of the channel.

We consider a binary CPM with a Mixed RC-REC pulse shape (mixing factor of 0.75), a memory of $L_{\text{CPM}} = 2$ and a modulation index of $h = 1/2$. A random sequence preamble is used in the following.

First, we simulate a channel which is a CE-BEM channel. In this case, no BEM modeling error is present in our system. In Fig.3.13, we can see that the variance of our CFO estimator lies between the minimum and maximum CRB as expected. However, we can observe that our channel estimation suffers from the presence of the residual CFO.

Similar observations can be made over a OCE-BEM channel (with an oversampling factor of 2) with fig.3.14.

Further investigations are needed to validate our proposed joint CFO and TV channel estimation method.

3.6 Conclusion

In this chapter, we have extended our work to the case of a transmission over doubly-selective channels.

Concerning channel equalization, only the authors of [Dar+16] [Dar+18] considered CPM transmission over TV channels. They have proposed a Linear Time Varying Equalizer in the Time-Domain. We have shown that by exploiting the band structure of the channel matrix in the Frequency Domain, we can design an approximate block MMSE-FDE.

Moreover, by using the well-known BEM, we have presented a method to perform channel estimation and also how to perform joint channel and carrier frequency estimation. However, it seems that the last does not present convincing performance and further studies must be investigated.

Chapter 4

Application to the aeronautical link by satellite

Contents

Résumé

Dans ce chapitre, nous présentons brièvement les modulations CPM considérées à la standardisation pour les communications avec des drones par satellite. Après une analyse asymptotique, nous montrons la limitation des schémas proposés et proposons des pistes d'amélioration (qui ne seront pas étudiées en détail ici).

Enfin, nous évaluons les méthodes d'égalisation et de synchronisation proposées dans cette thèse (quand elles sont applicables) et montrons que celles-ci permettent d'atteindre des performances acceptables dans le contexte des communications aéronautiques.

4.1 Introduction

In this chapter, we will discuss on the use cases of CPM transmissions over an aeronautical channel by satellite. The choice of CPM for this application is due to its use for the terrestrial

Modulation Order	$M = 4$
Pulse Shape	RC
CPM Memory	$L = 2$
Modulation index	$h = 1/3$
Preamble Size	$N = 128$
UW Size	$N = 32$
Block of Interest	$N = 512$
Number of Block	69

Table 4.1 – FWD Link parameters

link as recommended in [RCT16]. Hence, by using the same modulation, we can reduce the weight of the UAV and the use of Commercial off-the-shelf equipment ($COTS$). Moreover, the satellite will introduce non-linearities due to embedded amplifiers and CPM are known to be robust to this kind of impairments.

First, we will present the two systems considered for the Forward Link (FWD) and for the Return Link (RTN). We will also introduce the model used for the aeronautical channel. Then, some simulation results will be presented to assess the performance of our proposed equalization and synchronization methods in this context and conclusions will be drawn.

4.2 System Description

In the proposed MOPS [RCT16], two CPM schemes are proposed: one for the Forward (FWD) link and one for the Return (RTN) link.

4.2.1 Forward Link

We present the CPM parameters and framing in Table 4.1 for the FWD link. The phase response function is rectangular (REC pulse shape), as shown in Fig.4.6.

We have computed, by simulations, the maximum achievable Rate of this CPM modulation. As seen in Fig.4.4, there is no perceptible degradation in case where the receiver capitalizes on the PAM decomposition to reduce its overall complexity and therefore we recommend to use this low-complexity detector. The components of the PAM decomposition are given in Fig.4.3.

Moreover, even if it is a well-known property of CPM signals, we emphasize on the relevance of a turbo-detection at the receiver. Indeed, for a targeted code rate of $R = 0.5$, there is a degradation of 3dB in terms of minimum SNR. In other words, at 0dB the maximum achievable rate is 0.5 if a turbo-detection is used between this code and the CPM detection. If no turbo-detection is used, this rate cannot be obtained for an Es/N0 lower than 3dB.

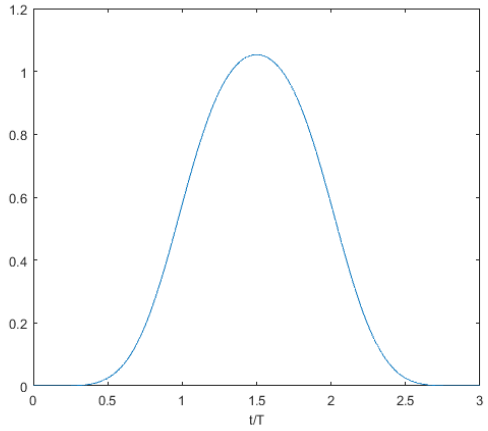

Figure 4.1 – $g_0(t)$

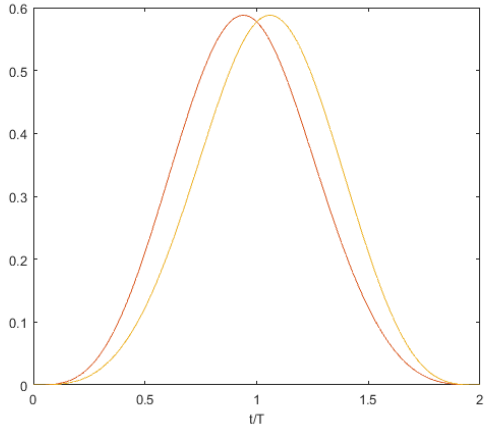

Figure 4.2 – $g_1(t)$ and $g_1(t)$

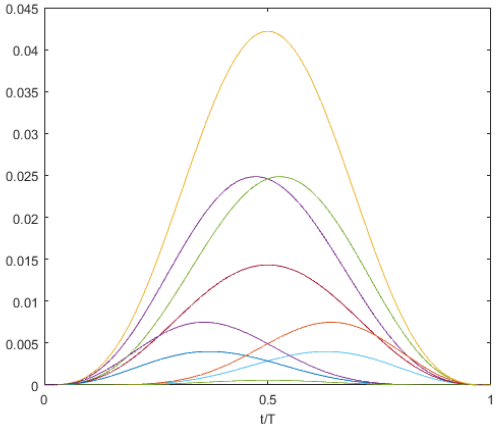

Figure 4.3 – $\{g_i(t)\}$, for $2 \leq i \leq 11$

We assess the performance of the FWD link with a serial concatenation of a 1/2 rate convolutional code with polynomial generators $(5, 7)_8$ given in octal. We iterate 10 times between the CPM detector and the outer code. We plot the BER in Fig. 4.5 and we can see that if the decoding threshold does not change, the size of the packet does have an impact on the BER (the bigger the packet is, the better is the BER).

4.2.2 Return Link

We present the CPM parameters and framing in Table 4.2 for the RTN link. The phase response function is a mixture of the REC and the RC type with a mixing factor $\alpha = 0.75$, as shown in Fig.4.6 (readers may refer to Chapter 1 for the definition of this pulse shape). As for the FWD link, the data is separated in blocks and an UW is added in order to ensure the circularization of the signal.

We have evaluated the maximum achievable rates for the RTN link and results are pre-

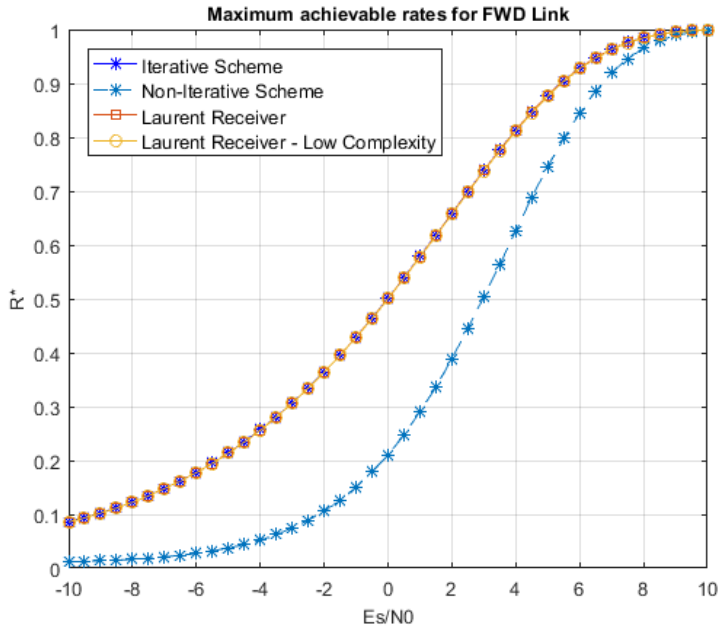

Figure 4.4 – Information Rate for FWD Link

Modulation Order	$M = 2$
Pulse Shape	Averaged REC/RC ($\alpha = 0.75$)
CPM Memory	$L = 2$
Modulation index	$h = 1/2$
Preamble Size	$N = 128$
UW Size	$N = 32$
Block of Interest	$N = 512$
Number of Block	9

Table 4.2 – RTN Link parameters

sented in Fig.4.7.

As previously, the approximation of the Laurent Decomposition at the receiver side does not result in a degradation in terms of performance. Indeed, using this representation, the CPM signal can be represented as the sum of 2 PAM $g_0(t)$ and $g_1(t)$ (given in Fig.4.8):

$$s_b(t) = \sum_{n=0}^{N-1} a_{0,n} g_0(t - nT) + \sum_{n=0}^{N-1} a_{1,n} g_1(t - nT) \tag{4.1}$$

$$\approx \sum_{n=0}^{N-1} a_{0,n} g_0(t - nT) \tag{4.2}$$

Therefore, we advice to capitalize on the Laurent Decomposition at the receiver in order to reduce the complexity of the MAP detection.

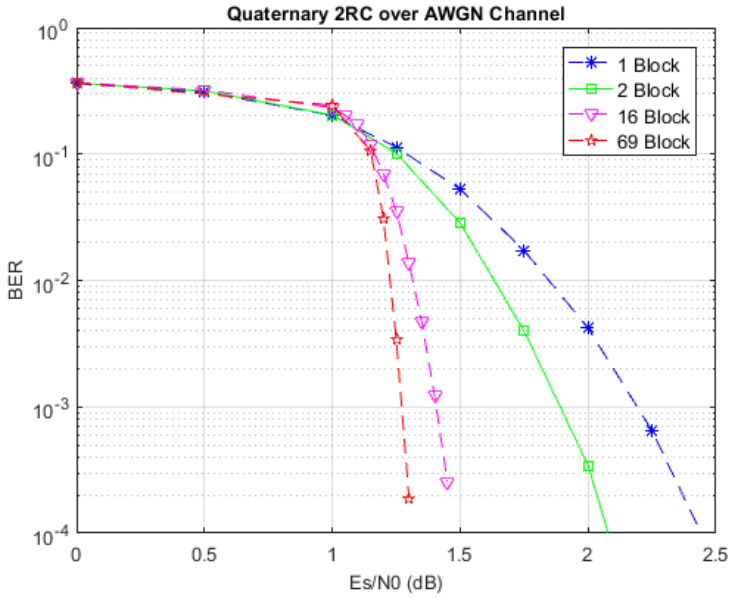

Figure 4.5 – Influence of the size of the packet on the BER for the FWD link

Moreover, we still can see the importance of the iteration between the CPM detector and the channel decoder as it can result in a loss of 2.5dB for a targeted rate of 1/2 and 3.5dB for a targeted rate of 1/3. Without iteration, a rate of 1/3 cannot be obtained for a Es/N0 lower than -2.15dB

Let us now consider the serial concatenation of a 1/2 rate convolutional code $(4, [15, 17])_8$, given in octal, with this CPM. We provide in the following an asymptotic analysis of the RTN link. We can interpret the convergence threshold of the system as the lowest SNR such as the EXIT charts of the CPM and the code do not intersect [Bri01]. In this case, the threshold is around $Es/N0 = -1.8$dB as shown in Fig.4.9.

We have plotted some BER curves obtained by simulations with the same outer code for different packet sizes in Fig.4.10. We iterate 10 times between the CPM detector and the outer code. Our simulations confirm the previous analysis as the decoding threshold corresponds to the one obtained with the EXIT chart analysis. As previously, and without surprise, the BER decreases with larger packet sizes.

4.2.3 Discussion

As specified in the previous section, we can see that the size of a block of interest (Data + UW) does not depend on the link, as does the size of the preamble or the size of an UW. Hence, at the receiver, the DFT size will not depend on the link.

To sum up, we can say that the main difference in the implementation between those systems is only within the CPM detector (if the same outer code is used).

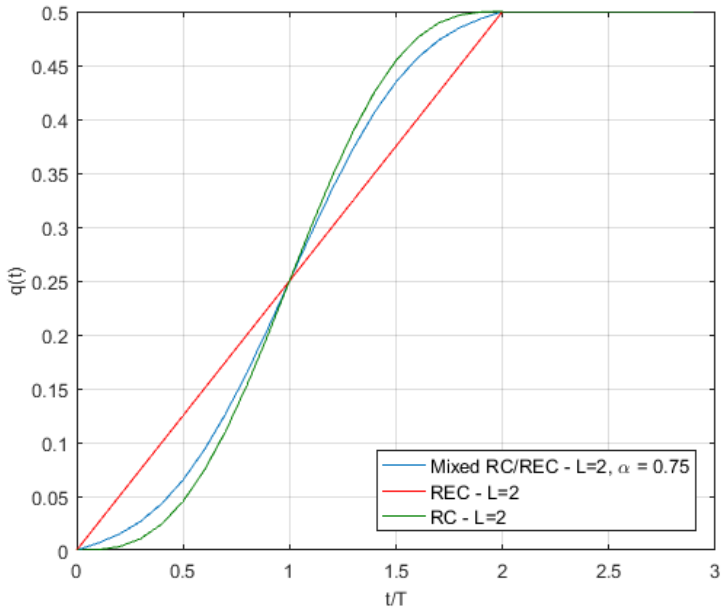

Figure 4.6 – Pulse shapes for the FWD and RTN links

For instance, the preamble is almost the same as it is composed of 32 data symbols "M-1", 64 data symbols "1-M" and 32 data symbols "M-1". It corresponds to the optimal preamble for CPM over AWGN channel regarding timing, phase and carrier recovery [HP13b]. Therefore, the Carrier Recovery (for transmissions over an AWGN channel) presents almost the same performance for the FWD and the RTN schemes, as we will see in the following.

In this chapter, we do not consider the case of a turbo code as an outer code. Indeed, the use of a Turbo Code does not improve automatically the overall performance of the system (as for linear modulations) as no turbo-detection is made (we previously saw that this results in a non-negligible loss in terms of maximum achievable rate). However, this disadvantage can be easily corrected with the use of a precoder. In [LNJP17], it is shown that the use of the precoder described in [Per+10] (which has been briefly introduced in Chapter 1) in the case of binary CPM makes the EXIT Charts flat while keeping the achievable Information Rate unchanged, and therefore making the use of a turbo-detection useless. If a turbo-code is to be used, we strongly recommend the use of the precoder of [Per+10].

4.3 Aeronautical Channel

The aeronautical channel by satellite is a doubly-selective channel which is modelled by only two paths as depicted in Fig.4.11. The first path corresponds to a Line of Sight (LOS) signal

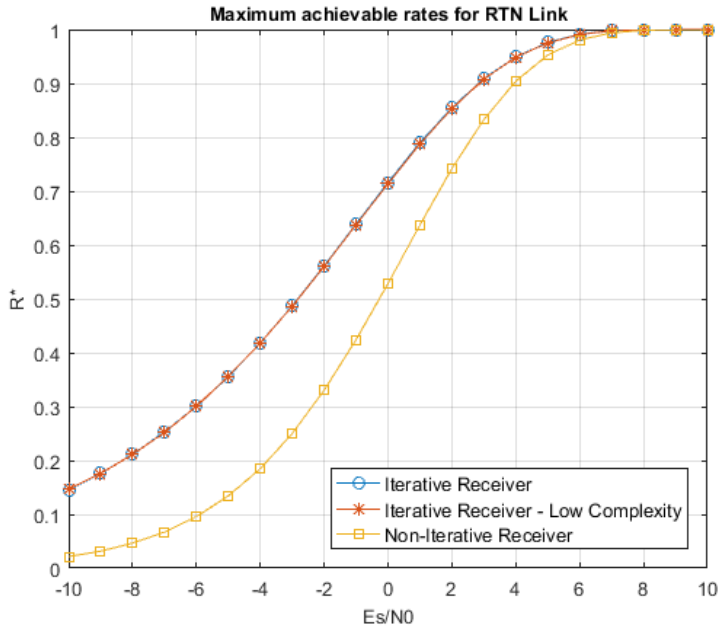

Figure 4.7 – Information Rate for RTN Link

and the second corresponds to the Ground Reflection (GR) signal:

$$h(t) = h_0(t)\delta(t) + h_1(t)\delta(t-\tau) \tag{4.3}$$

The LOS path is divided into two components: a direct LOS ($DLOS$) path and some Local Scatters (LS) due to the reflection of the signal on the UAV structure. The second component is composed of delayed and attenuated Ground Reflections (GR), which are particularly strong over oceans. The local scatters and the ground reflections are modulated by two different complex colored Gaussian processes, h_{SC} and h_{GR} respectively. The absolute values of these Gaussians correspond to a Rayleigh amplitude fading.

In the following, we give the procedure to simulate the aeronautical channel:

- The total power of the LOS path (DLOS and LS paths) is attenuated by a factor α_{LOS}

- The power of the DLOS path (resp. the LS path) is attenuated by a factor k_1 (resp. k_2) such as:

$$k_{\mathrm{LOS}} = k_1/k_2 \tag{4.4}$$
$$k_1 + k_2 = 1 \tag{4.5}$$

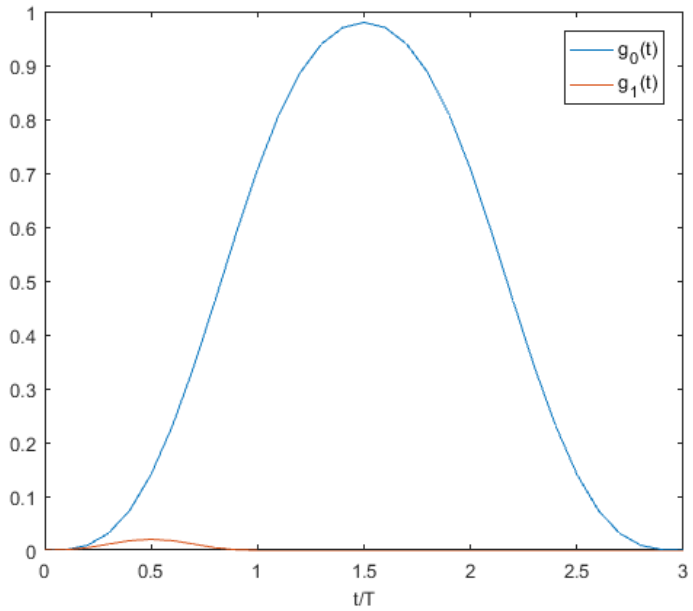

Figure 4.8 – Laurent Pulses for RTN Link

Chan. Number	C/M(dB)	Delay (μs)	GR Doppler Spread (Hz)	k_{LOS} (dB)	LS Doppler Spread (Hz)
chan 3	35.6	37.27	278.46	14	1
chan 9	20.6	25.09	187.5	14	1
chan 13	11.6	0.87	17.35	14	1
chan 16	11.7	11.62	243.09	14	1

Table 4.3 – Use cases

- the GR path is attenuated by a factor α_{GR} and delayed by τ_{GR} such as:

$$\frac{C}{M} = \frac{\alpha_{\text{LOS}}}{\alpha_{\text{GR}}} \tag{4.6}$$

$$\alpha_{\text{LOS}} + \alpha_{\text{GR}} = 1 \tag{4.7}$$

$$\tau_{\text{GR}} = \frac{2H\sin(\epsilon)}{c} \tag{4.8}$$

  where $\frac{C}{M}$ is the power ratio between the first path and the second path.

- Doppler Spread is applied on the LS and the GR paths, according to the speed of the aircraft. We can see that the parameters corresponding to the LS component remain unchanged as they do no depend on the UAV position or speed.

In our simulations, we will only consider a few cases which depend on the position and speeds of the UAV. Those use cases are summarized in Table.4.3.

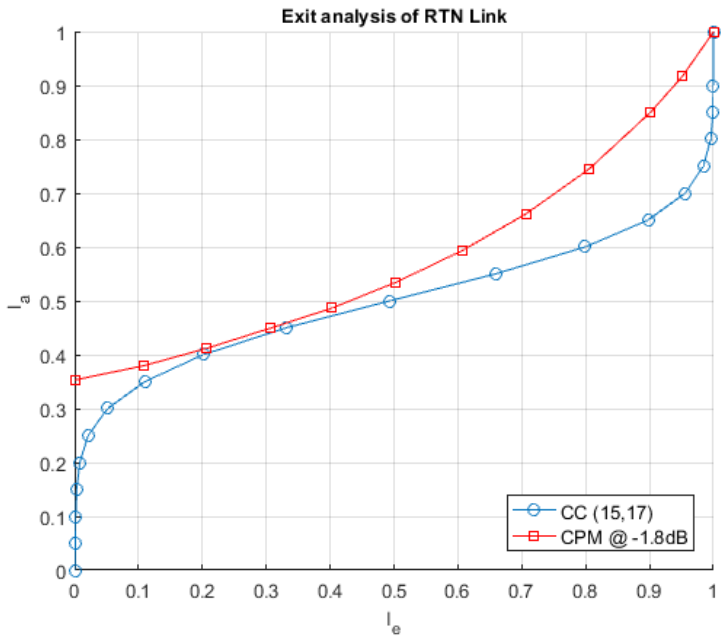

Figure 4.9 – EXIT analysis of the RTN Link CPM concatenated with a (4,[15,17]) convolutional code

4.4 Simulation Results

4.4.1 Simulations over AWGN channel

First, we present the performance of the FWD and RTN links when CPM signals are transmitted over an AWGN channel. For carrier-recovery, we compare two CFO estimators: the R&B estimation [RB74] (designed for a transmission over an AWGN channel and therefore optimal in this case) and the one we developed in Section 2.5.3. Results are given in Fig.4.12. As the chosen preamble is optimal for transmission over AWGN channel, without a genuine surprise, both methods present the (almost) same performance; the Carrier Frequency Offset (CFO) estimation has a variance close to the Cramér Rao Bound (CRB).

In terms of Bit Error Rate, as we explained deeply why turbo-code should not be used "directly", we use a 1/2 rate convolutional code with polynomial generator (15,17) given in octal. In this case, no equalization is used and results are presented later in Fig.4.16 for the FWD link and in Fig.4.15 for the RTN link, along with the performance over the aeronautical channel.

4.4.2 Simulations over the aeronautical channel

We have evaluated the performance of our joint channel and carrier frequency estimation for both links over a time-invariant (TIV) aeronautical channel in Fig.4.13. We can see that our

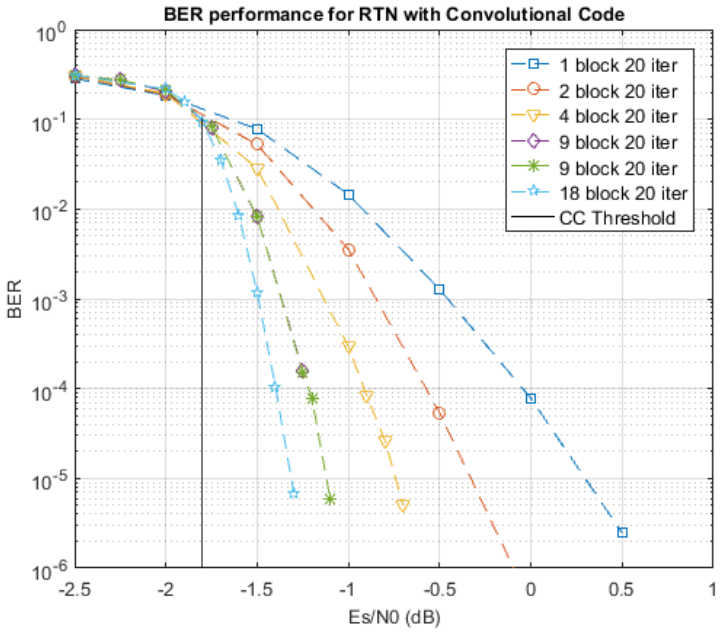

Figure 4.10 – Influence of the size of the packet on the BER

estimation does not present any genuine surprise in terms of performance: first, both schemes present a threshold, and after reaching it, our CFO estimation lies between the maximum and minimum CRB.

We now assess the performance of our improved channel estimation using *a priori* knowledge on the delays of the paths (by GPS positioning) for both channel 3 and channel 13 (see Table.4.3), considered constant here, in Fig.4.14. The classical Least Squares (LS) estimator supposes that the channel to estimate has a length of 32 symbols (corresponding to the size of the UW) whereas our proposed parametric LS has to estimate only 2 coefficients (reducing the number of coefficients to estimate by a factor $32 * 2/2 = 32$ as we work here at a sample rate of $2R_s$). We can see that the parametric knowledge only improves the threshold of the CFO estimation as asymptotically both CFO estimations reach the CRB. However, the parametric LS estimation outperforms the LS estimation in terms of Mean Square Error for the channel estimation as already observed in Chapter 2.

Let us now plot the Bit Error Rate obtained by simulation. For simulation reason, we considered smaller packets for the FWD link (only 5 data blocks instead of 69) which will degrade the overall performance (we do make a fair comparison as we will also consider 5 data blocks for a transmission over an AWGN channel). We first consider TIV aeronautical channel for both FWD (in Fig.4.16) and RTN (in Fig.4.15) links, which is justified as for the case of the FWD link the duration of a frame is shorter than the channel coherence time in most cases. We can see that the waterfall region of our receiver is still distant from the AWGN case. This can be explained as our proposed MMSE-FDE is biased (as the others presented in the literature). Further investigation should be conducted to correct this bias in

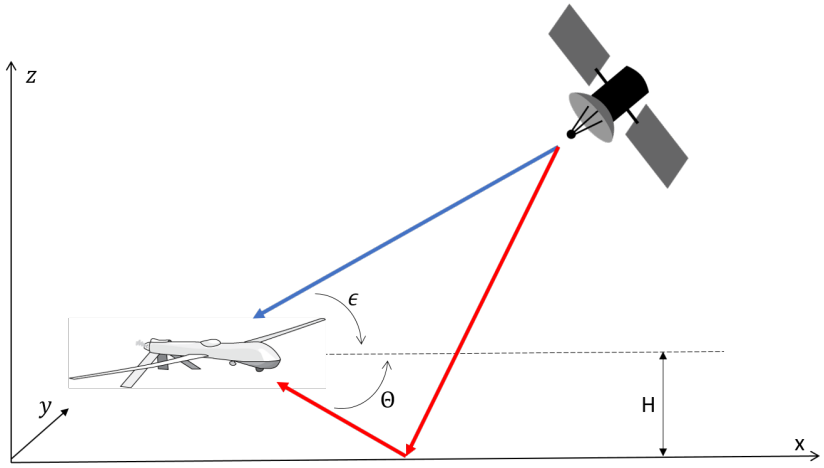

Figure 4.11 – Aeronautical channel model

order to improve the BER.

Finally, we now consider the RTN link over a TV aeronautical channel as it is the most challenging case due to its lower data rate (for the same Doppler spread). 10 iterations are made between the CPM detector and the outer code decoder. Different observations can be made. In the case of channel 3, even if the Doppler is 'high', as the C/M is very high, we cannot see any difference in terms of BER when we take into account one or more diagonals in our proposed band MMSE-FDE (see Chapter 3). In the case where the Doppler Spread is relatively low, the same result is observed without surprise (we can approximate the channel as a TIV channel over a data block). Last, for channel 16 which has one of the lowest C/M with a 'high' Doppler spread, we can see that our band MMSE-FDE improves the BER by considering more and more diagonals. All those results tend to validate the comments already made in Chapter 3. However, it allows us to conclude that in most cases, the aeronautical channel by satellite is a simple channel to deal with and that our most advanced methods for TV channels are needed in only a few cases.

4.5 Conclusion

In this chapter, we have assessed our equalization and synchronization methods in the context of UAV communications by a satellite link.

We have seen that in most cases we can consider the channel constant over the duration of a data block and therefore methods proposed in Chapter 2 can be used and performs well in this context.

Last, in the few cases where the channel is time-variant over the data block, we have assessed the equalizer proposed in Chapter 3 and we reach reasonable performance.

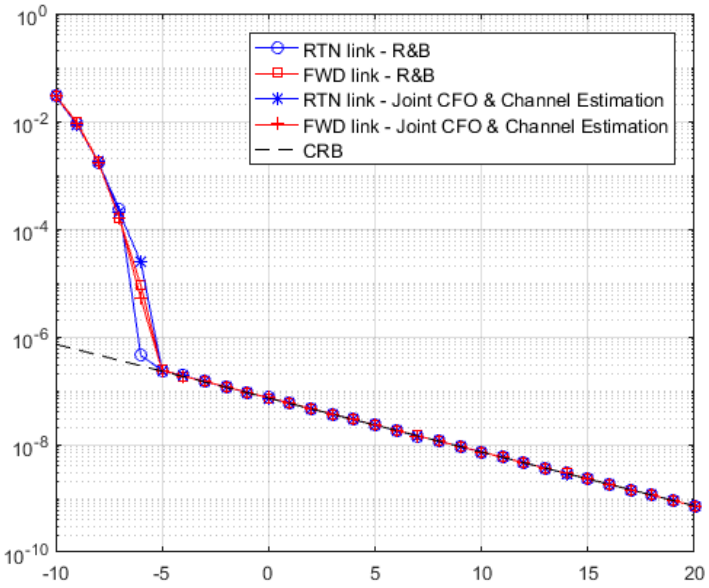

Figure 4.12 – CFO Estimation over AWGN channel

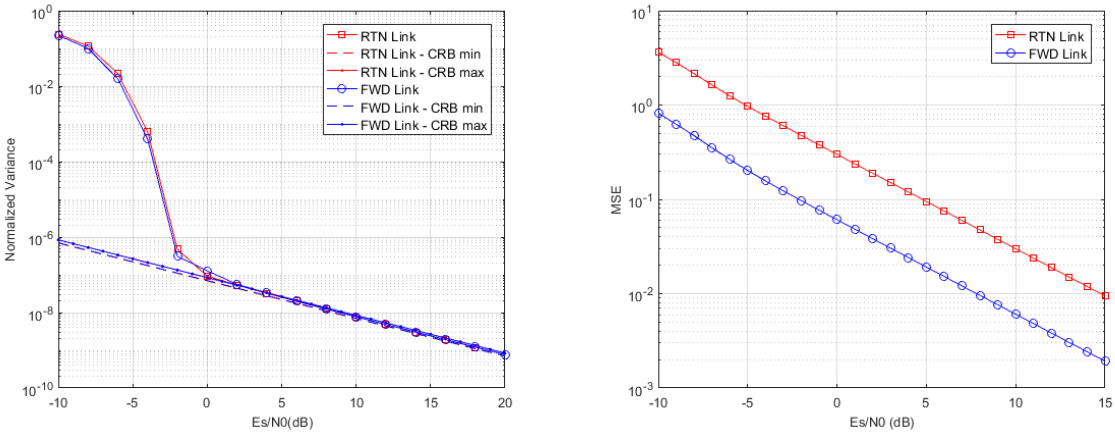

Figure 4.13 – Carrier Recovery for FWD and RTN Link over a TIV aeronautical channel

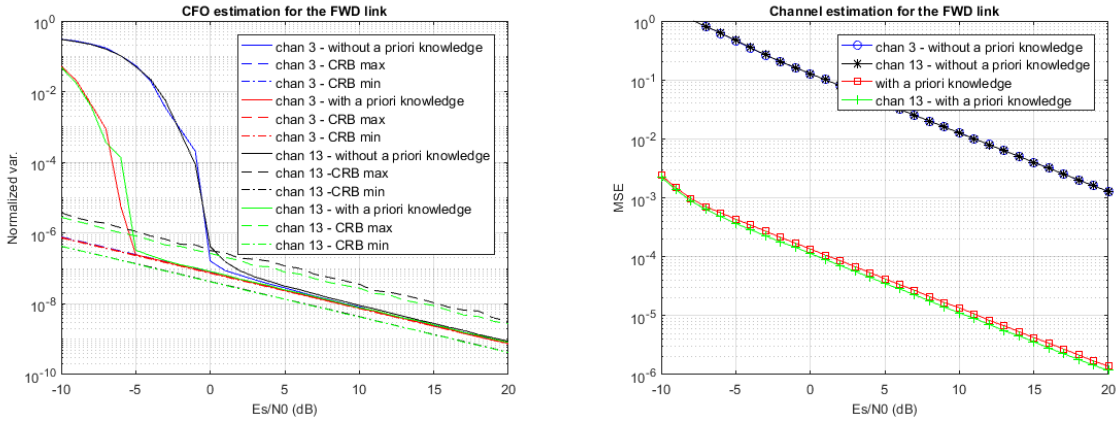

Figure 4.14 – Carrier Recovery for 4-ary CPMs over AWGN channel

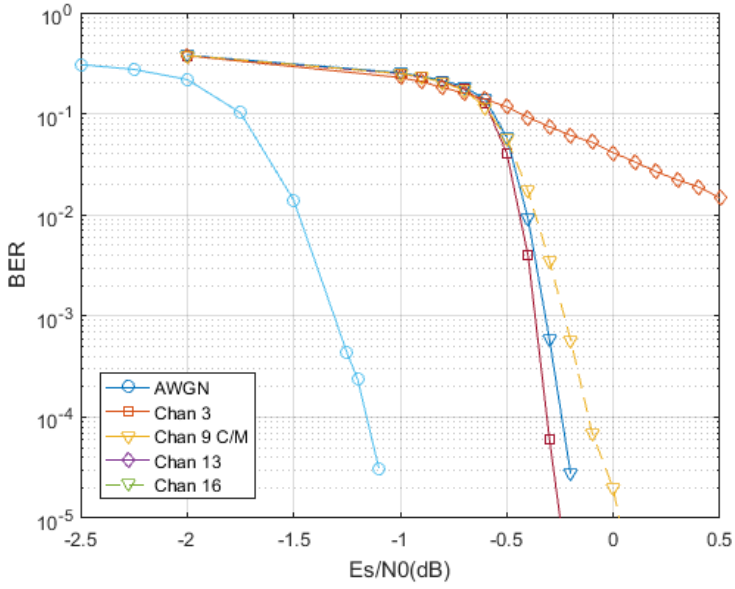

Figure 4.15 – BER over aeronautical channel for the RTN link

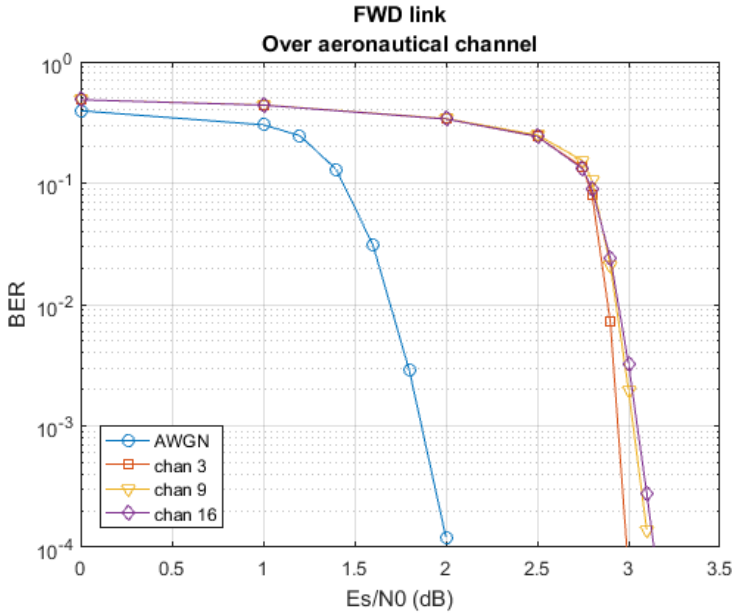

Figure 4.16 – BER over aeronautical channel for the FWD link

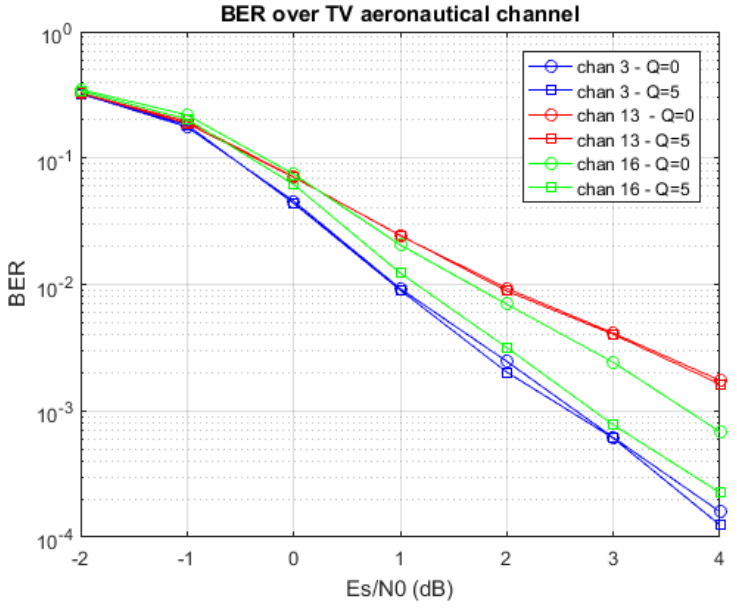

Figure 4.17 – BER over TV aeronautical channel for the RTN link

Conclusion and perspectives

Conclusions

In this thesis, we have studied detection, equalization and synchronization techniques for Continuous Phase Modulation (*CPM*) over frequency-selective channels and over doubly-selective channels. The choice of CPM has been made in order to answer to the growing demand in terms of frequency allocation and also for its robustness to the non-linearities introduced by the satellite embedded amplifiers. The ITU and ICAO recommended the use of CPM for the satellite link for UAV, and CPM are also considered for other applications such the Internet of Things, or the telemetry application. The methods proposed in the literature have, in most cases, a high computational complexity, and generally lack to study the properties of circular extended block based transmission to enable low-complexity approach.

In Chapter 1, we have introduced CPM signals and also a receiver structure based on the Laurent decomposition. The use of the PAM decomposition allows us to design low-complexity detection. Moreover, we have also presented some precoding techniques which in the first case increase the Spectral Efficiency of a CPM scheme without increasing the computational complexity of the CPM detector, and in the second case, make the EXIT charts of the CPM flat, making useless the need to iterate between the outer channel decoder and the CPM detector at the receiver.

Chapter 2 analyzed CPM receiver structure over frequency-selective channels. Thanks to the exploitation of the periodic statistical properties of block-based CPM, we have developed a low-complexity MMSE Frequency Domain Equalizer, without making any approximation. Hence, it reaches the same performance than the other State of the Art MMSE-FDE but with a significant lower complexity. We have also proposed channel estimation techniques and a joint channel and carrier frequency estimation in case of transmission over a frequency-selective channel. In this last case, Cramér Rao Bounds have been derived.

Chapter 3 proposed the extension of those previous methods for frequency-selective channel to doubly-selective channels. By exploiting the band structure of the channel matrix in the Frequency Domain, we have designed an approximate low-complexity equalizer. We also proposed a channel estimation method based on the Basis Expansion Model and we have shown how to implement it in our block-based system.

Finally, Chapter 4 gave some simulation results in the context of the UAV link by satellite. We have shown that our proposed methods lead to good results in this aeronautical context.

Perspectives

Decision Feedback Equalization and Turbo Equalization

As we have now proposed a low-complexity equalizer for CPM over frequency-selective channels, we can improve the overall performance of the equalization scheme by using a Decision Feedback Equalizer (*DFE*) or a Turbo-Equalizer. [OKD09] proposes an approximate turbo-equalization scheme that does not take into account the time-averaged auto-correlation of a CPM signal whereas [PV06] proposes a DFE and a turbo equalizer, both capitalizing on the Laurent Decomposition. As for its linear equalizer, it does take into account both channel and Laurent Pulses contributions. It could be improved by using our FS representation of the over-sampled received signal and by only take into account the channel equalization.

Timing recovery

In order to finalize our system, we need to investigate frame detection and timing synchronization for CPM over doubly-selective channels. [HP13b] has studied such algorithms for CPM signals but only in the case of a transmission over an AWGN channel.

Preamble design

[Hos13] proposes an optimal preamble for timing and carrier recovery for CPM signals over AWGN channels. To our knowledge, only [LGC18] studies the preamble for CPM over a frequency-selective channel. The main idea is to design a sequence with auto-correlation side-lobes close to zero, improving the performance of a LS channel estimation (compared to a random sequence or the preamble proposed in [Hos13]).

Optimal BEM model for the aeronautical channel

In Chapter 3, we introduce the BEM model to perform channel estimation. The main idea is that the channel space is reduced to a few basis functions, known at the receiver. If the optimal model is known in the case of the Doppler has a Jakes' Spectrum, no study has been done for the aeronautical channel by satellite. As we have shown, the performance of channel estimation is highly dependant on the chosen basis, and so the use of an optimal BEM would outperform the presented results.

Conclusion et perspectives

Conclusions

Dans cette thèse, nous avons étudié des techniques de détection, d'égalisation et de synchronisation pour des signaux CPM transmis sur des canaux sélectifs en fréquence ou doublement sélectifs. Le choix des Modulations à Phase Continue a été fait pour répondre à la demande croissante en termes d'allocation fréquentielle mais aussi pour leurs robustesses face aux non-linéarités indroduites par les amplificateurs embarqués dans les satellites. L'ITU et l'ICAO recommandent ainsi l'utilisation des CPM pour le lien des communications des drones par satellite, et les CPMs sont aussi considérées pour de nombreuses autres applications comme l'Internet des Objets ou la télémesure. Les méthodes proposées dans la littérature ont, la plupart du temps, une complexité calculatoire élevée et n'ont pas réussi à exploiter la structure cyclique du signal pour développer des méthodes à complexité réduite.

Dans le Chapitre 1, nous avons présenté les signaux CPM et également un récepteur basé sur la décomposition de Laurent. L'utilisation de cette décomposition en PAM permet de concevoir un détecteur avec une faible complexité. De plus, nous avons également introduit quelques pré-codeurs qui permettent dans le premier cas d'augmenter l'efficacité spectrale du système sans en augmenter la complexité, et dans le second cas de rendre les graphes EXIT plats et ainsi rendant la nécessité d'itérer entre le code correcteur d'erreur et le détecteur CPM inutile en réception.

Le Chapitre 2 donne une analyse des récepteurs CPM dans le cas de transmissions sur des canaux sélectifs en fréquence. En exploitant les propriétés statistiques périodiques du signal obtenues par une extension circulaire de ce dernier, nous avons développé un égaliseur MMSE dans le domaine fréquentiel à complexité faible, sans faire aucune approximation. Ainsi, il atteint les mêmes performances que les autres égaliseurs de la littérature mais avec une complexité significativement plus faible. De plus, nous avons également proposé des méthodes d'estimation canal et un estimateur conjoint du canal et de l'erreur résiduelle de fréquence. Dans ce dernier cas, la borne de Cramér Rao a été calculée.

Dans le Chapitre 3, nous avons étendu ces méthodes en considérant un canal doublement sélectifs. En exploitant la structure en bande de la matrice canal dans le domaine fréquentiel, nous avons conçu un égaliseur faible complexité mais qui présente des approximations. Ainsi, ce dernier possède un classique compromis entre sa complexité et ses performances. Nous avons également présenté des méthodes d'estimation canal reposant sur les Basis Expansion Models et avons montré comment les utiliser dans le cadre de notre système de communication.

Enfin, le Chapitre 4 donne des résultats de simulation dans le contexte de lien de communications des drones par satellite. Nous avons ainsi pu montrer que les méthodes proposées dans cette thèse donnent des résultats convenables dans ce contexte aéronautique.

Perspectives

Egalisation non linéaire et turbo égalisation

Dans cette thèse, nous avons proposé un égaliseur à faible complexité pour CPM. Les performances d'un tel égaliseur peuvent être améliorées en utilisant un schéma d'égalisation non-linéaire comme un DFE (*Decision Feedback Equalizer*) ou un turbo égaliseur. [OKD09] a proposé un turbo égaliseur approximé qui ne prend pas en compte l'autocorrélation du signal CPM tandis que [PV06] a proposé un DFE et un turbo égaliseur capitalisant sur la décomposition de Laurent. Comme pour son égaliseur linéaire, ces égaliseurs prennent en compte les contributions du canal et des composantes de Laurent. Ces schémas peuvent donc être améliorés en utilisant une représentation FS du signal et en suivant le modèle du signal reçu présenté en détail dans le Chapitre 2.

4.5.1 Synchronisation temporelle

Pour rendre notre étude plus complète, une étude de la détection des trames et de la synchronisation temporelle pour les signaux CPM transmis sur canaux sélectifs en fréquence ou doublement sélectifs doit être menée. [HP13b] a étudié ces méthodes dans le cas d'un canal AWGN.

Conception de préambule

[Hos13] a proposé un préambule optimal pour la synchronisation temporelle et fréquentielle pour des signaux CPM transmis sur des canaux AWGN. A notre connaissance, seulement [LGC18] a étudié la conception de préambule dans le cas de canaux sélectifs en fréquence. L'idée principale est alors d'obtenir une séquence dont les lobes secondaires de l'autocorrélation sont proches de zéro, améliorant ainsi les performances de l'estimation du canal (en utilisant un critère des moindres carrés) comparé au préambule de [Hos13].

Modèle BEM optimal pour le canal aéronautique

Dans le Chapitre 3, nous avons introduit les modèles BEM pour estimer le canal. L'idée principale est que l'espace canal est réduit à un petit nombre de fonctions de bases (famille génératrice), connues à la réception. Dans le cas d'un Doppler avec un Spectre de Jakes, le modèle est connu. Cependant, aucune étude n'a été faite pour le cas du canal aéronautique par satellite. Comme nous avons pu le voir, les performances de l'estimation canal dépendent fortement du modèle choisi, et ainsi l'utilisation d'une base optimale est nécessaire.

Appendix A

CPM with duo-M-ary encoder

In this section, we study the extension of the work of [Mes+16] and [OSL17] for M-ary CPM signals. The main idea is to use the same precoder and evaluate the Spectral Efficiency of such precoded CPM signals.

Let $\underline{\boldsymbol{\alpha}} = \{\alpha_0, \alpha_1, \ldots, \alpha_{N-1}\} \in \{\pm 1, \pm 3, \ldots, \pm(M-1)\}^N$ coded data symbols (as given by the BICM described in Chapter 1). The considered duo-M-ary encoder is given by:

$$\widetilde{\alpha}_n = \frac{\alpha_n + \alpha_{n-1}}{2} \tag{A.1}$$

The symbols $\underline{\widetilde{\boldsymbol{\alpha}}} = \{\widetilde{\alpha}_n\}_{0 \leq n \leq N-1} \in \{0, \pm 1, \ldots, \pm 2(M-1)\}^N$ is then given to the CPM modulator. The CPM has a memory L_{cpm} and a pulse shape $q(t)$.

As in the case of the duo-binary encoder, we can separate the information phase in two:

$$\begin{aligned}
\theta(t, \underline{\widetilde{\boldsymbol{\alpha}}}) &= 2\pi h \sum_{n=0}^{N-1} \frac{\widetilde{\alpha}_n}{2} q(t - nT_s) && \text{(A.2)} \\
&= 2\pi h \sum_{n=0}^{N-1} \frac{\alpha_n}{2} q(t - nT_s) + 2\pi h \sum_{n=0}^{N-1} \frac{\alpha_{n-1}}{2} q(t - nT_s) && \text{(A.3)} \\
&= 2\pi h \sum_{n=0}^{N-1} \frac{\alpha_n}{2} q(t - nT_s) + 2\pi h \sum_{n=0}^{N-2} \frac{\alpha_n}{2} q(t - (n+1)T_s) && \text{(A.4)} \\
&= 2\pi h \sum_{n=0}^{N-1} \alpha_n \frac{q(t - nT_s) + q(t - (n+1)T_s)}{2} && \text{(A.5)}
\end{aligned}$$

By defining, $\widetilde{q}(t) = \frac{q(t) + q(t - T_s)}{2}$, we obtain the following phase information:

$$\theta(t, \underline{\widetilde{\boldsymbol{\alpha}}}) = 2\pi h \sum_{n=0}^{N-1} \alpha_n \widetilde{q}(t - nT_s) \tag{A.6}$$

which corresponds to the information phase of a M-ary CPM with a memory $L_d = L_{\text{cpm}} + 1$ with a pulse shape $\widetilde{q}(t)$.

Hence, as for duo-binary encoder, we have increased the modulation order (and therefore the minimal distance), but we also have limited the phase hopping (and therefore limiting the bandwidth increase). Moreover, this proposed scheme does not imply an important compu-

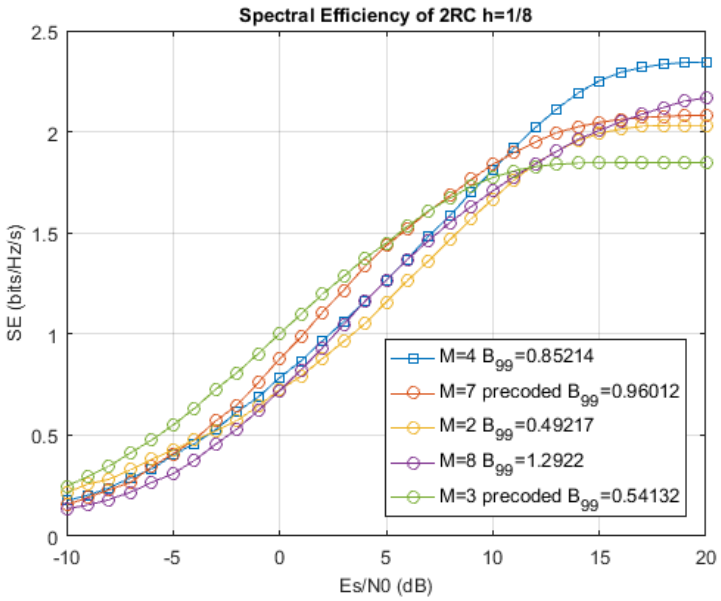

Figure A.1 – SE for h = 1/8

tational complexity increase at the receiver as we can still design a CPM detector for M-ary CPM signals (and capitalizing on the PAM decomposition to further decrease the overall computational complexity).

We have assessed this duo-Mary encoder for a CPM signal with an index modulation of $h = 1/8$ and $h = 1/10$ for a Raised Cosine (RC) CPM scheme and a memory of $L_{\text{CPM}} = 2$ in Fig.A.1 and Fig.A.2.

As for the binary case, at 'low' SNR, the Spectral Efficiency of our proposed scheme is better than the traditional one.

In Fig.A.1, we can see that the ternary precoded CPM achieve a better SE up to 3dB, and the precoded $7 - ary$ has a better SE than the other schemes from 3dB to 15dB.

Those results confirm the interest of the duo-binary encoder proposed in [OSL17] and that those results can be extended to higher modulation order. However, it seems that the increased SE will suffer from a high modulation index.

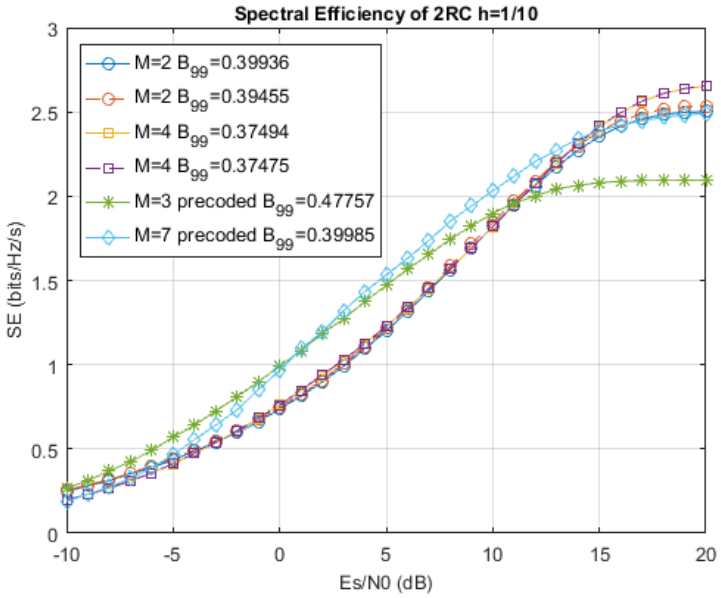

Figure A.2 – SE for h = 1/10

Appendix B

Baud Rate MMSE-FDE [TS05]

In the following, we present the two-baud rate equalizers of [TS05]. The authors made the hypothesis that the delays of paths of the channel are multiple of T_s. In practical case, this hypothesis does not hold true and results in a degradation of the performance.

B.1 Baud Rate MMSE-FDE using orthogonal representation

In [TS05], the authors propose a symbol rate equalizer based on the received signal filtered by an orthonormal bank filters derived from the Rimoldi representation of CPM signals.

In this section, we will first present their work using their hypothesis of a T_s-spaced channel. Then, we will show that this hypothesis on the channel is too restrictive to be applied, limiting its practical interest.

The Rimoldi representation [Rim88] of CPM signals is an other trellis representation, widely used in the field. The receiver signal space is generated by pM^L pulses. But, as discussed in [Ben15], the receiver signal space as a dimension $J \leq M^L$. By using the Gram-Schmidt orthogonalization procedure on those pulse, we define the orthonormal basis $\{f_p(t)\}_p$ of support T_s and we denote by $s_{p,n}$ the projection of the CPM signal $s_b(t), nT_s \leq t \leq (n+1)T_s$:

$$s_{p,n} =< s_n(t), f_p(t) > \tag{B.1}$$

$$= \int_{nT_s}^{(n+1)T_s} s(t) f_p^*(t - nT_s) dt \tag{B.2}$$

and therefore the transmitted signal is given by

$$s_b(t) = \sum_{n=0}^{N-1} \sum_{p=0}^{P-1} s_{p,n} f_p(t - nT_s) \tag{B.3}$$

We consider the case of a frequency-selective channels where the delays of the paths are multiple of T_s, i.e.:

$$h_c(t) = \sum_{l=0}^{L_c-1} h_l \delta(t - lT_s) \tag{B.4}$$

We will see later that this hypothesis is the major drawback of this method.

We recall that the received signal, using a FS representation, is given by :

$$r(t) = h_c(t) * s_b(t) + w(t) \tag{B.5}$$

$$= \sum_{l=0}^{L_c-1} h_l s_b(t - lT_s) + w(t) \tag{B.6}$$

We now filter this received filter by the orthogonal basis. Hence, the projection of the received signal at nT_s on $f_p(t)$ gives:

$$r_{p,n} = \int_{nT_s}^{(n+1)T_s} r(t) f_p^*(t - nT_s) dt \tag{B.7}$$

$$= \sum_{l=0}^{L_c-1} h_l \int_{nT_s}^{(n+1)T_s} s_b(t - lT_s) f_p^*(t - nT_s) dt + \underbrace{\int_{nT_s}^{(n+1)T_s} w(t) f_p^*(t - nT_s) dt}_{=w_{p,n}} \tag{B.8}$$

$$= \sum_{l=0}^{L_c-1} h_l \int_{(n-l)T_s}^{(n-l+1)T_s} s_b(t) f_p^*(t - (n+l)T_s) dt + w_{p,n} \tag{B.9}$$

$$= \sum_{l=0}^{L_c-1} h_l s_{p,n-l} + w_{p,n} \tag{B.10}$$

The orthogonal representation yields to J independents equalizers (one for each basis function) and therefore J independents equalizers should be implemented at the receiver.

By exploiting the circular block-based structure of the signal thanks to the use of an UW or a CP, this linear convolution in Eq.Eq.(B.10) can be re-written as a discrete circular convolution of the channel impulse response and the projection of the CPM signal:

$$\underline{\boldsymbol{r}}_p = \begin{bmatrix} r_{p,0} \\ r_{p,1} \\ \vdots \\ \vdots \\ \vdots \\ r_{p,N-1} \end{bmatrix} = \begin{bmatrix} h_0 & 0 & \dots & h_{L_c-1} & \dots & h_1 \\ h_1 & h_0 & 0 & \dots & h_{L_c-1} & \ddots \\ \ddots & \ddots & \ddots & \ddots & \ddots & \ddots \\ h_{L_c-1} & \dots & h_0 & 0 & \dots & 0 \\ \ddots & \ddots & \ddots & \ddots & \ddots & \ddots \\ 0 & \dots & h_{L_c-1} & \dots & h_1 & h_0 \end{bmatrix} \begin{bmatrix} s_{p,0} \\ s_{p,1} \\ \vdots \\ \vdots \\ \vdots \\ s_{p,N-1} \end{bmatrix} + \begin{bmatrix} w_{p,0} \\ w_{p,1} \\ \vdots \\ \vdots \\ \vdots \\ w_{p,N-1} \end{bmatrix} \tag{B.11}$$

$$= \underline{\underline{\boldsymbol{h}}} \underline{\boldsymbol{s}}_p + \underline{\boldsymbol{w}}_p \tag{B.12}$$

In this FD, this equation becomes:

$$\underline{\boldsymbol{R}}_p = \underline{\underline{\boldsymbol{F}}}_N \underline{\boldsymbol{r}}_p \tag{B.13}$$

$$= \underbrace{\underline{\underline{\boldsymbol{F}}}_N \underline{\underline{\boldsymbol{h}}} \underline{\underline{\boldsymbol{F}}}_N^H}_{=\underline{\underline{\boldsymbol{H}}}} \underbrace{\underline{\underline{\boldsymbol{F}}}_N \underline{\boldsymbol{s}}_p}_{=\underline{\boldsymbol{S}}_p} + \underbrace{\underline{\underline{\boldsymbol{F}}}_N \underline{\boldsymbol{w}}_p}_{=\underline{\boldsymbol{W}}_p} \tag{B.14}$$

$$= \underline{\underline{\boldsymbol{H}}} \underline{\boldsymbol{S}}_p + \underline{\boldsymbol{W}}_p \tag{B.15}$$

where $\underline{\underline{\boldsymbol{F}}}_N$ is the unitary Fourier Matrix of size $N \times N$ with generic term $[\underline{\underline{\boldsymbol{F}}}_N]_{l,m} = \exp(-j2\pi/(N))^{lm}/\text{sqrt}(N)$. By DFT properties, $\underline{\underline{\boldsymbol{H}}}$ is a diagonal matrix and so this equation can be further reduced in closed-form given by:

$$R_{p,k} = H_k S_{p,k} + W_{p,k} \tag{B.16}$$

Hence, for the p^{th} channel, the MMSE Equalizer is [TS05]:

$$G_k = \frac{H_k^*}{|H_k|^2 + N_0} \tag{B.17}$$

$$\text{and } \widetilde{S}_{p,k} = G_k R_{p,k} \tag{B.18}$$

We can note that all the channels have the same equalizer which therefore can be synthesize only once. The overall architecture of this receiver is given in Fig.B.1.

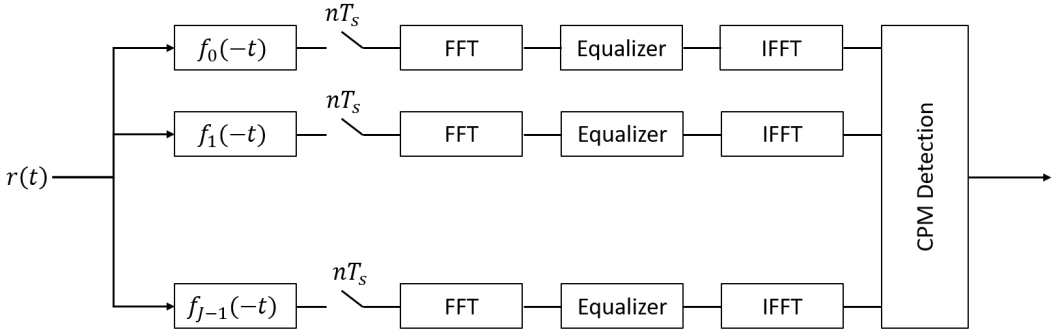

Figure B.1 – MMSE-FDE with orthogonal representation from [TS05]

The main advantage of this equalizers remains into its computational complexity. Indeed, we need:

- one DFT, one IDFT per channel;
- one 'one-tap' equalizer per channel;

Hence, the overall complexity is dominated by the DFT/IDFT operations, and so is in $O(2JNlog(N))$ where N is the number of symbols in the block.

However, as stated earlier, this equalizer suffers from a very restrictive hypothesis on the

channel. The authors made the hypothesis that the channel is a T_s-spaced tapped delayed line, which is not true in practical scenario.

Without any hypothesis on the delays, the channel is is given by

$$h_c(t) = \sum_l h_l \delta(t - \tau_l) \tag{B.19}$$

The received signal in Eq.B.6 becomes:

$$r(t) = \sum_l h_l s_b(t - \tau_l) + w(t) \tag{B.20}$$

$$= \sum_l h_l \sum_m \sum_q s_{q,m} f_q(t - mT_s - \tau_l) + w(t) \tag{B.21}$$

Hence, the projection of the received signal on the p^{th} basis function is given by:

$$r_{p,n} = \int_{nT_s}^{(n+1)T_s} r(t) f_p^*(t - nT_s) + w_{p,n} \tag{B.22}$$

$$= \sum_l h_l \sum_m \sum_q s_{q,m} \int_{nT_s}^{(n+1)T_s} f_q(t - mT_s - \tau_l) f_p^*(t - nT_s) dt + w_{p,n} \tag{B.23}$$

Let us now observe the term $\int_{nT_s}^{(n+1)T_s} f_q(t - mT_s - \tau_l) f_p^*(t - nT_s) dt$. Using the authors' hypothesis $\tau_l = lT_s$, we obtain:

$$\int_{nT_s}^{(n+1)T_s} f_q(t - mT_s - \tau_l) f_p^*(t - nT_s) dt \tag{B.24}$$

$$= \int_{nT_s}^{(n+1)T_s} f_q(t - (m+l)T_s) f_p^*(t - nT_s) dt \tag{B.25}$$

$$= \int_0^{T_s} f_q(t + (n - m - l)T_s) f_p^*(t) dt \tag{B.26}$$

$$= \begin{cases} 1, \text{if } p = q \text{ and } n - m - l = 0 \\ 0, \text{elsewhere} \end{cases} \tag{B.27}$$

Therefore, the received signal in Eq.(B.23) becomes:

$$r_{p,n} = \sum_l h_l s_{p,n-l} + w_{p,n} \tag{B.28}$$

which corresponds to the Eq.(B.31).

However, in the case where τ_l is not a multiple of T_s, some interference terms appear between the function of the basis and we do not have J independent channel anymore. By not taking into account this interference, the proposed equalizer does not perform well in most of the practical scenarios as shown by simulation in Section 2.3.5.

B.2 Baud Rate MMSE-FDE using the Laurent Decomposition

In [TS05], the authors propose a symbol rate equalizer based on the received signal which has been filtered by the matched filters of the Laurent Pulses (LPs). They do not use the polyphase/multi-channel or the FS representation to design their equalizer as they directly work on the received filtered signal. First, we will present their work using their hypothesis and notation. Then, we will show its limitation due to some hypothesis on the channel.

Let us consider that the frequency-selective channel can be modeled by a T_s-spaced tapped delay line such as:

$$h_c(t) = \sum_{l=0}^{L_c-1} h_l \delta(t - lT_s) \tag{B.29}$$

Therefore, the received signal becomes:

$$r(t) = \sum_{l=0}^{L_c-1} h_l s_b(t - lT_s) + w(t) \tag{B.30}$$

We consider now at the receiver a bank filters composed by the matched filters of the Laurent Pulses. The pth matched filter output is:

$$\begin{aligned} r_{p,n} &= \int r(t) g_p^*(t - nT_s) dt \\ &= \int (\sum_{l=0}^{L_c-1} h_l s(t - lT_s) + w(t)) g_p(t - nT_s) dt \\ &= \sum_{l=0}^{L_c-1} \int h_l s(t - lT_s) g_p(t - nT_s) dt + \int w(t) g_p(t - nT_s) dt \\ &= \sum_{l=0}^{L_c-1} h_l s_{p,n-l} + z_{p,n} \end{aligned} \tag{B.31}$$

where

$$s_{p,n} = \int s(t) g_p(t - nT_s) dt \tag{B.32}$$

$$\text{and } z_{p,n} = \int w(t) g_p(t - nT_s) dt \tag{B.33}$$

Therefore, as for linear modulation, in case of a T_s-spaced channel model, we can obtain a discrete *equivalent* channel at symbol rate working on the $\{s_{n,p}\}$ as we have in case of the AWGN channel the following:

$$r_{n,p} = s_{n,p} + z_{n,p} \tag{B.34}$$

In this system, we also consider a circular block based transmission of the CPM signals.

Denoting G the guard interval (with $L_c < G$), we have:

$$\text{for } -G < n < 0, s_{p,n} = s_{p,N+n} = s_{p,\text{mod}(n,N)} \tag{B.35}$$

where mod(.,.) is the modulo operator. Hence, the output of the p^{th} matched filter can be re-written as:

$$r_{p,n} = \sum_{l=0}^{L_c-1} h_l s_{p,\text{mod}(n-l,N)} + w_{p,n} \tag{B.36}$$

which is a discrete circular convolution.

Matrix-wise, the received vector is given by

$$\underline{\boldsymbol{r}}_p = \left[r_{p,0}, r_{p,1}, \ldots, r_{p,N-1}\right]^T \tag{B.37}$$

$$= \begin{bmatrix} h_0 & 0 & \ldots & h_{L_c-1} & \ldots & h_1 \\ h_1 & h_0 & 0 & \ldots & h_{L_c-1} & \ddots \\ \ddots & \ddots & \ddots & \ddots & \ddots & \ddots \\ h_{L_c-1} & \ldots & h_0 & 0 & \ldots & 0 \\ \ddots & \ddots & \ddots & \ddots & \ddots & \ddots \\ 0 & \ldots & h_{L_c-1} & \ldots & h_1 & h_0 \end{bmatrix} \begin{bmatrix} s_{p,0} \\ s_{p,1} \\ \vdots \\ \vdots \\ \vdots \\ s_{p,N-1} \end{bmatrix} + \begin{bmatrix} w_{p,0} \\ w_{p,1} \\ \vdots \\ \vdots \\ \vdots \\ w_{p,N-1} \end{bmatrix} \tag{B.38}$$

$$= \underline{\underline{\boldsymbol{h}}}\,\underline{\boldsymbol{s}}_p + \underline{\boldsymbol{w}}_p \tag{B.39}$$

Hence, using this representation, there is K channels (one for each Laurent Pulse), and each model is an ISI channel with correlated noise. In the Frequency-Domain, the received signal is

$$\underline{\boldsymbol{R}}_p = \underline{\underline{\boldsymbol{F}}}_N \underline{\boldsymbol{r}}_p \tag{B.40}$$

$$= \underbrace{\underline{\underline{\boldsymbol{F}}}_N \underline{\underline{\boldsymbol{h}}} \underline{\underline{\boldsymbol{F}}}_N^H}_{=\underline{\underline{\boldsymbol{H}}}} \underbrace{\underline{\underline{\boldsymbol{F}}}_N \underline{\boldsymbol{s}}_p}_{=\underline{\boldsymbol{S}}_p} + \underbrace{\underline{\underline{\boldsymbol{F}}}_N \underline{\boldsymbol{w}}_p}_{=\underline{\boldsymbol{W}}_p} \tag{B.41}$$

$$= \underline{\underline{\boldsymbol{H}}}\,\underline{\boldsymbol{S}}_p + \underline{\boldsymbol{W}}_p \tag{B.42}$$

where $\underline{\underline{\boldsymbol{F}}}_N$ is the unitary Fourier Matrix of size $N \times N$ with generic term $[\underline{\underline{\boldsymbol{F}}}_N]_{l,m} = \exp(-j2\pi/(N))^{lm}/\text{sqrt}(N)$. By Discrete Fourier Transform (DFT), as the matrix $\underline{\underline{\boldsymbol{h}}}$ is circulant, its FD counterpart $\underline{\underline{\boldsymbol{H}}}$ is diagonal and we obtain Eq.(B.42) can be reduced to the following closed-form, for $0 \leq k \leq N$:

$$R_p[k] = H[k]S_p[k] + W_p[k] \tag{B.43}$$

Therefore, using this equation, [TS05] designs a MMSE-FDE working on those K parallel

channels. For each channel, we therefore apply first a whitening filter given by:

$$W_p[k] = \frac{1}{\sqrt{C(p,p;k)}} \tag{B.44}$$

where $C(p,p;k)$ is the FD counterpart of the discrete auto-correlation of the Laurent Pulse $g_p(t)$ given by:

$$c(p,p;k) = \int_{\mathbb{R}} c_p(t+nT_s)c_p^*(t)dt \tag{B.45}$$

Then we apply the MMSE-FDE given by:

$$G_p[k] = \frac{H[k]^* W_p[k]}{|H[k]W_p[k]|^2 + N_0} \tag{B.46}$$

Hence, the equalized signal is:

$$\widehat{S}_p[k] = G_p[k]W_p[k]R_p[k] \tag{B.47}$$

$$= \frac{H[k]^*}{|H[k]|^2 + N_0 C(p,p;k)} R_p[k] \tag{B.48}$$

The overall equalizer is presented in Fig.B.2.

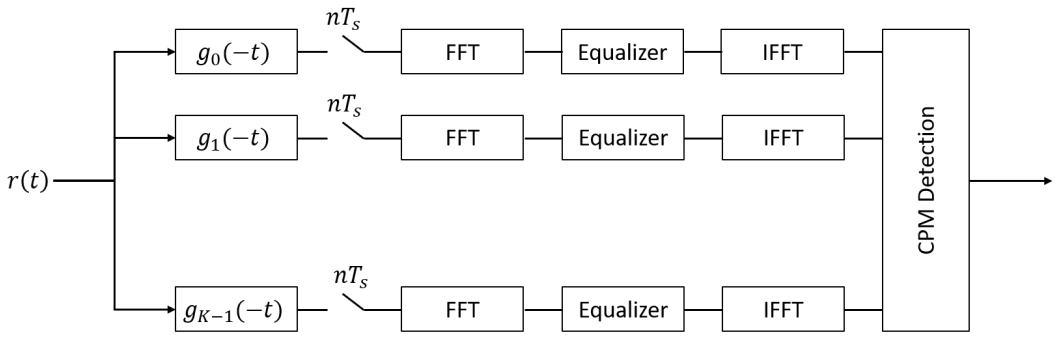

Figure B.2 – MMSE-FDE from [TS05]

As seen in Eq.B.31, we use the hypothesis of a T_s-spaced channel model to develop this equalizer, however this hypothesis is rarely true in practical case.

We can remark that this model does not hold when a delay is fractional of T_s and we cannot obtain the model in Eq.(B.36). This is a major drawback of this solution. Indeed, in the case, we have also interference coming from the others matched filters and the signal cannot be seen as K independent channel". However, if we consider only the main Laurent Pulse (i.e. $g_0(t)$), the equalizer does not suffer from those interference. This approximation can be only considered in the case of a binary CPM signal with a non-integer modulation index. In case of M-ary CPM signals, for instance, we have to consider the first '$M-1$'

Laurent Pulses, and so this equalizer cannot be used.

Furthermore, we can see that this equalizer does not consider the auto-correlation function of the signal. In their use case, [TS05] applies their equalization method on a binary CPM with a modulation index of $h = 1/2$. In this particular case, the auto-correlation matrix of the pseudo-symbols is the identity matrix and their equalizer is therefore exact. In Section 2.3.2.2, we present an other MMSE-FDE method proposed by [PV06] which can be seen as the exact version of this one.

Appendix C

Preamble Design and Carrier Recovery for CPM over AWGN channel [HP13b]

In his thesis [Hos13], Hosseini presents a carrier recovery techniques based on his optimum preamble.

Let us recall the LLF for timing and carrier synchronization is given by:

$$\Gamma(\underline{\boldsymbol{r}}; f, \theta, \epsilon) \approx \Re\Big[\sum_{n=0}^{kN-1} e^{-j(2\pi n f+\theta)} r[n] s_\epsilon[n]\Big] \tag{C.1}$$

where f is the CFO, θ the initial carrier offset, ϵ the timing offset, $r[n]$ the sampled received signal, and $s_\epsilon[n]$ the sampled version of $s(t-\epsilon)$.

It is shown that the designed optimal preamble can be approximated with a delayed 1REC CPM at the same h. The approximated phase response is:

$$\text{For } T_l \leq t < \frac{T_0}{4} + T_l, \phi(t, \boldsymbol{\alpha}) = -(M-1)\pi h \frac{(t-T_l)}{Ts} \tag{C.2}$$

$$\text{For } \frac{T_0}{4} + T_l \leq t < \frac{3T_0}{4} + T_l, \phi(t, \boldsymbol{\alpha}) = (M-1)\pi h \frac{(t-T_l-T_0/2)}{Ts} \tag{C.3}$$

$$\text{For } \frac{3T_0}{4} + T_l \leq t < T_0 + T_l, \phi(t, \boldsymbol{\alpha}) = -(M-1)\pi h \frac{(t-T_l-T_0)}{Ts} \tag{C.4}$$

$$\text{with } T_l = \frac{L-1}{2} T_s \text{ when the pulse shape is symmetric} \tag{C.5}$$

For the rest of this discussion, we assume that the channel observation starts at T_L and hence ignore it ($T_L = 0$). Our preamble can now be written :

$$\text{For } 0 \leq n < \frac{NL_0}{4} + T_l, s[n] = exp\Big(-j(M-1)\pi h(\frac{n}{N} - \epsilon)\Big) \tag{C.6}$$

$$\text{For } \frac{NL_0}{4} \leq t < \frac{3NL_0}{4}, s[n] = exp\Big(j(M-1)\pi h(\frac{n}{N} - \frac{L_0}{2} - \epsilon)\Big) \tag{C.7}$$

$$\text{For } \frac{3NL_0}{4} \leq t < NL_0, s[n] = exp\Big(j(M-1)\pi h(\frac{n}{N} - L_0 - \epsilon)\Big) \tag{C.8}$$

Hence, we can use this apprixmation, LLF Γ becomes:

$$\begin{aligned}\Gamma(\underline{\boldsymbol{r}};f,\theta,\epsilon) = \Re(e^{-j\widetilde{\theta}}[&\sum_{n=0}^{NL_0/4-1} e^{-j2\pi h\widetilde{f}n} r[n] exp\Big(j(M-1)\pi h(\frac{n}{N}-\epsilon)\Big) \\ &+ \sum_{n=NL_0/4}^{3NL_0/4-1} e^{-j2\pi h\widetilde{f}n} r[n] exp\Big(-j(M-1)\pi h(\frac{n}{N}-\frac{L_0}{2}-\epsilon)\Big) \\ &+ \sum_{n=3NL_0/4}^{NL_0} e^{-j2\pi h\widetilde{f}n} r[n] exp\Big(j(M-1)\pi h(\frac{n}{N}-L_0-\epsilon)\Big)]) \end{aligned} \tag{C.9}$$

Let us define:

$$\lambda_1(\widetilde{f}) = \sum_{n=0}^{NL_0/4} e^{-j2\pi h\widetilde{f}n} r[n]s^*[n] + \sum_{n=3NL_0/4}^{NL_0} e^{-j2\pi h\widetilde{f}n} r[n]s^*[n] \tag{C.10}$$

$$\begin{aligned} &= \sum_{n=0}^{NL_0/4} e^{-j2\pi h\widetilde{f}n} r[n] exp\Big(j(M-1)\pi h(\frac{n}{N})\Big) \\ &\quad + e^{-j(M-1)\pi hL_0} \sum_{n=3NL_0/4}^{NL_0} e^{-j2\pi h\widetilde{f}n} r[n] exp\Big(j(M-1)\pi h(\frac{n}{N})\Big) \end{aligned} \tag{C.11}$$

$$\lambda_2(\widetilde{f}) = \sum_{n=NL_0/4}^{3NL_0-1} e^{-j2\pi h\widetilde{f}n} r[n]s^*[n] \tag{C.12}$$

$$= e^{j(M-1)\pi hL_0/2} \sum_{n=NL_0/4}^{3NL_0-1} e^{-j2\pi h\widetilde{f}n} r[n] exp\Big(-j(M-1)\pi h(\frac{n}{N})\Big) \tag{C.13}$$

By using those equations in Eq. C.9, we obtain:

$$\Gamma(\underline{\boldsymbol{r}};f,\theta,\epsilon) = \Re\Big(e^{-j\widetilde{\theta}}[e^{-j(M-1)\pi h\widetilde{\epsilon}}\lambda_1(\widetilde{f}) + e^{j(M-1)\pi h\widetilde{\epsilon}}\lambda_2(\widetilde{f})]\Big) \tag{C.14}$$

We can see that the estimation of the different parameters are decoupled. Indeed, we define the following:

$$\Gamma(\underline{\boldsymbol{r}};f,\epsilon) = e^{-j(M-1)\pi h\widetilde{\epsilon}}\lambda_1(\widetilde{f}) + e^{j(M-1)\pi h\widetilde{\epsilon}}\lambda_2(\widetilde{f}) \tag{C.15}$$

The LLF becomes in a closed form:

$$\Gamma(\underline{\boldsymbol{r}};f,\theta,\epsilon) = \Re\Big(e^{-j\widetilde{\theta}}\Gamma(\underline{\boldsymbol{r}};f,\epsilon)\Big) \tag{C.16}$$

For any values of f and ϵ, the estimation of the initial carrier phase θ is simply:

$$\widehat{\theta} = \arg(\Gamma(\underline{\boldsymbol{r}};f,\epsilon)) \tag{C.17}$$

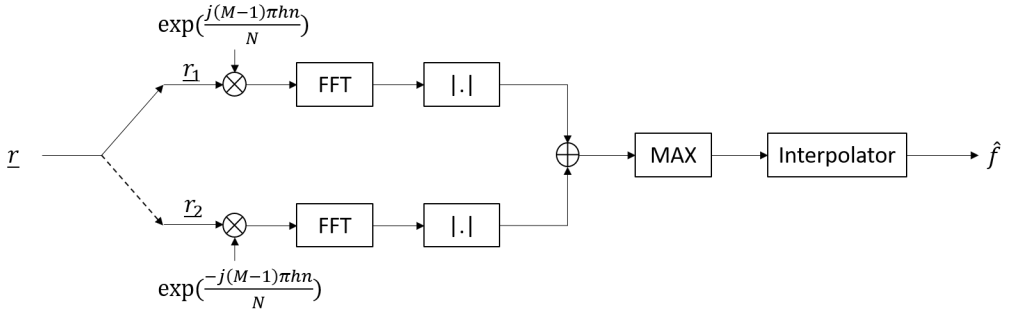

Figure C.1 – CFO Recovery from [Hos13]

It turns out that this reduced the ML estimation to maximizing:

$$|\Gamma(\underline{\boldsymbol{r}}; f, \epsilon)|^2 = |\lambda_1(\widetilde{f})|^2 + |\lambda_2(\widetilde{f})|^2 + 2\Re\{e^{-j2(M-1)\pi h\widetilde{\epsilon}}\lambda_1(\widetilde{f})\lambda_2(\widetilde{f})^*\} \tag{C.18}$$

Once again, by fixing $\widetilde{f}$, this function is maximize when the the function inside the real part is a real pure, which means:

$$\widehat{\epsilon} = \frac{\arg(\lambda_1(\widetilde{f})\lambda_2^*(\widetilde{f}))}{2(M-1)\pi h} \tag{C.19}$$

Finally, the ML estimation of the CFO f is given by the maximization of:

$$|\Gamma(\underline{\boldsymbol{r}}; f, \epsilon)|^2 = |\lambda_1(\widetilde{f})|^2 + |\lambda_2(\widetilde{f})|^2 + 2|\lambda_1(\widetilde{f})||\lambda_2(\widetilde{f})| \tag{C.20}$$

$$= |\lambda_1(\widetilde{f}) + \lambda_1(\widetilde{f})|^2 \tag{C.21}$$

which is equivalent to maximizing the square root of this function as each term is real and positive. Therefore, the ML estimation of the CFO is given by:

$$\widehat{f_d} = \underset{\widetilde{f}}{\text{argmax}}\Big(|\lambda_1(\widetilde{f})| + |\lambda_2(\widetilde{f})|\Big) \tag{C.22}$$

The computation of $\lambda_1(\widetilde{f})$ and $\lambda_2(\widetilde{f})$ for different values $\widetilde{f}$ by a grid search, done efficiently with a DFT operation where $\widetilde{f}$ are trial discrete frequency.

We obtain the frequency estimator in Fig. C.1.

Bibliography

[AAS13] John B Anderson, Tor Aulin, and Carl-Erik Sundberg. *Digital phase modulation*. Springer Science & Business Media, 2013 (cit. on pp. 16, 21).

[AKB04] Alexei Ashikhmin, Gerhard Kramer, and Stephan ten Brink. "Extrinsic information transfer functions: model and erasure channel properties". In: *IEEE Transactions on Information Theory* 50.11 (2004), pp. 2657–2673 (cit. on p. 30).

[ARS81a] Tor Aulin, Nils Rydbeck, and C-E Sundberg. "Continuous phase modulation–Part I: Full response signaling". In: *IEEE Transactions on Communications* 29.3 (1981), pp. 196–209 (cit. on pp. 15, 16).

[ARS81b] Tor Aulin, Nils Rydbeck, and C-E Sundberg. "Continuous phase modulation–Part II: partial response signaling". In: *IEEE Transactions on Communications* 29.3 (1981), pp. 210–225 (cit. on pp. 15, 16, 20).

[AS06] John B Anderson and Arne Svensson. *Coded modulation systems*. Springer Science & Business Media, 2006 (cit. on p. 16).

[Bah+74] Lalit Bahl et al. "Optimal decoding of linear codes for minimizing symbol error rate (corresp.)" In: *IEEE Transactions on information theory* 20.2 (1974), pp. 284–287 (cit. on pp. 18, 26).

[Ben+10] Nevio Benvenuto et al. "Single carrier modulation with nonlinear frequency domain equalization: An idea whose time has come—Again". In: *Proceedings of the IEEE* 98.1 (2010), pp. 69–96 (cit. on p. 44).

[Ben15] Tarik Benaddi. "Sparse graph-based coding schemes for continuous phase modulations". Thèse de doctorat dirigée par Poulliat, Charly et Boucheret, Marie-Laure Réseaux, Télécommunications, Systèmes et Architecture Toulouse, INPT 2015. PhD thesis. 2015 (cit. on pp. 2, 3, 8, 9, 17, 29, 30, 139).

[BM96] N. Benvenuto and R. Marchesani. "The Viterbi algorithm for sparse channels". In: *IEEE Transactions on Communications* 44.3 (1996), pp. 287–289 (cit. on pp. 65, 105).

[Boc+16] Carsten Bockelmann et al. "Massive machine-type communications in 5G: Physical and MAC-layer solutions". In: *IEEE Communications Magazine* 54.9 (2016), pp. 59–65 (cit. on pp. 3, 9).

[Bri01] Stephan ten Brink. "Code characteristic matching for iterative decoding of serially concatenated codes". In: *Annales des télécommunications*. Vol. 56. 7-8. Springer. 2001, pp. 394–408 (cit. on p. 121).

[BV] C Brown and PJ Vigneron. "Equalisation for continuous phase modulation using basis functions". In: *presented at SPIE 2011, Orlando, Florida, April 2011.* (Cit. on p. 61).

[BV11] C Brown and PJ Vigneron. “Channel estimation and equalisation for single carrier continuous phase modulation”. In: *IEEE Military Communications Conference (MILCOM) , Baltimore, MD*. 2011, pp. 334–340 (cit. on pp. 61, 67).

[CB05] G. Colavolpe and A. Barbieri. “Simplified iterative detection of serially concatenated CPM signals”. In: *IEEE Global Telecommunications Conference (GLOBECOM), St. Louis, MO* 3 (2005) (cit. on pp. 5, 10, 21, 26, 50, 53).

[CFC10] Enrico Casini, Dario Fertonani, and Giulio Colavolpe. “Advanced CPM receiver for the NATO tactical narrowband waveform”. In: *MILITARY COMMUNICATIONS CONFERENCE, 2010-MILCOM 2010*. IEEE. 2010, pp. 1725–1730 (cit. on pp. 3, 9, 16).

[Cha+04] Ridha Chaggara et al. “Continuous phase modulations for future satellite communication systems”. In: *2004 12th European Signal Processing Conference*. IEEE. 2004, pp. 1083–1086 (cit. on p. 21).

[Cha+17a] R. Chayot et al. “Channel estimation and equalization for CPM with application for aeronautical communications via a satellite link”. In: *MILCOM 2017 - 2017 IEEE Military Communications Conference*. 2017 (cit. on pp. 3, 10, 46, 59, 61, 105, 107).

[Cha+17b] R. Chayot et al. “Joint channel and carrier frequency estimation for M-ary CPM over frequency-selective channel using PAM decomposition”. In: *2017 IEEE International Conference on Acoustics, Speech and Signal Processing (ICASSP)*. 2017, pp. 3789–3793 (cit. on p. 71).

[Cha+18] R. Chayot et al. “A New Exact Low-Complexity MMSE Equalizer for Continuous Phase Modulation”. In: *IEEE Communications Letters* 22.11 (2018), pp. 2218–2221 (cit. on p. 59).

[CRR14] Arlene Cole-Rhodes and Michael Rice. “A block processing approach to CMA equalization of SOQPSK for aeronautical telemetry”. In: *Military Communications Conference (MILCOM), 2014 IEEE*. IEEE. 2014, pp. 440–444 (cit. on p. 88).

[CVM07] Cecilia Carbonelli, Satish Vedantam, and Urbashi Mitra. “Sparse channel estimation with zero tap detection”. In: *IEEE Transactions on Wireless Communications* 6.5 (2007) (cit. on pp. 65, 105).

[CW14] Shih Yu Chang and Hsiao-Chun Wu. “Innovative parallel equalizer design for continuous phase modulation systems”. In: *Communications (ICC), 2014 IEEE International Conference on*. IEEE. 2014, pp. 4372–4377 (cit. on p. 46).

[Dar+16] Donatella Darsena et al. “LTV equalization of CPM signals over doubly-selective aeronautical channels”. In: *Metrology for Aerospace (MetroAeroSpace), 2016 IEEE*. IEEE. 2016, pp. 75–80 (cit. on pp. 4, 6, 10, 11, 88, 90, 92, 93, 115).

[Dar+17] Donatella Darsena et al. “Second-order statistics of one-sided cpm signals”. In: *IEEE Signal Processing Letters* 24.10 (2017), pp. 1512–1516 (cit. on p. 25).

[Dar+18] D. Darsena et al. “Equalization techniques of control and non-payload communication links for unmanned aerial vehicles”. In: *IEEE Access* PP.99 (2018), pp. 1–1 (cit. on pp. 88, 90, 92, 93, 98, 99, 101, 106, 115).

[DCTS97] Modulation (GSM 05.04) Digital Cellular Telecommunications System. *ETSI standard ETS 300959*. 1997 (cit. on pp. 3, 9).

[DHJ07] Robert C Daniels and Robert W Heath Jr. “60 GHz wireless communications: Emerging requirements and design recommendations”. In: *IEEE Vehicular technology magazine* 2.3 (2007) (cit. on pp. 3, 9).

[DL12] Luc Deneire and Jerome Lebrun. “Continuous phase modulation and space-time coding: A candidate for wireless robotics”. In: *Wireless Personal Communications* 64.3 (2012), pp. 473–487 (cit. on p. 16).

[DMR94] Aldo N D’Andrea, Umberto Mengali, and Ruggero Reggiannini. “The modified Cramer-Rao bound and its application to synchronization problems”. In: *IEEE Transactions on Communications* 42.234 (1994), pp. 1391–1399 (cit. on p. 81).

[GT98] Georgios B Giannakis and Cihan Tepedelenlioglu. “Basis expansion models and diversity techniques for blind identification and equalization of time-varying channels”. In: *Proceedings of the IEEE* 86.10 (1998), pp. 1969–1986 (cit. on p. 102).

[GVL12] Gene H Golub and Charles F Van Loan. *Matrix computations*. Vol. 3. JHU Press, 2012 (cit. on p. 97).

[Haa02] Erik Haas. “Aeronautical channel modeling”. In: *IEEE transactions on vehicular technology* 51.2 (2002), pp. 254–264 (cit. on p. 98).

[Hag04] Joachim Hagenauer. “The EXIT chart-introduction to extrinsic information transfer in iterative processing”. In: *Signal Processing Conference, 2004 12th European*. IEEE. 2004, pp. 1541–1548 (cit. on pp. 31, 60, 61).

[Has+09] Emad S Hassan et al. “A continuous phase modulation single-carrier wireless system with frequency domain equalization”. In: *Computer Engineering & Systems, 2009. ICCES 2009. International Conference on*. IEEE. 2009, pp. 599–604 (cit. on p. 46).

[HL03] Xiaojing Huang and Yunxin Li. “The PAM decomposition of CPM signals with integer modulation index”. In: *IEEE Trans. Comm.* 51.4 (2003), pp. 543–546 (cit. on p. 23).

[HMV95] Michael Honig, Upamanyu Madhow, and Sergio Verdu. “Blind adaptive multiuser detection”. In: *IEEE Trans. Inf. Theory* 41.4 (1995), pp. 944–960 (cit. on p. 56).

[Hos13] Seyed Mohammad Ehsan Hosseini. “Synchronization Techniques for Burst-Mode Continuous Phase Modulation”. PhD thesis. University of Kansas, 2013 (cit. on pp. 4, 10, 132, 134, 147, 149).

[HP13a] E. Hosseini and E. Perrins. “The Cramer-Rao Bound for Training Sequence Design for Burst-Mode CPM”. In: *IEEE Transactions on Communications* 61.6 (2013), pp. 2396–2407 (cit. on pp. 70, 81, 82).

[HP13b] Ehsan Hosseini and Erik Perrins. “Timing, carrier, and frame synchronization of burst-mode CPM”. In: *IEEE Transactions on Communications* 61.12 (2013), pp. 5125–5138 (cit. on pp. 70, 75, 79, 82, 122, 132, 134, 147).

[IRI17] IRIG. *Telemetry Standards IRIG Standard 106-17 (Part 1) Chapter 2*. 2017 (cit. on pp. 3, 9, 16).

[Kal89] Ghassan Kawas Kaleh. “Simple coherent receivers for partial response continuous phase modulation”. In: *IEEE Journal on Selected Areas in Communications* 7.9 (1989), pp. 1427–1436 (cit. on pp. 21, 24, 26).

[Lau86] P. Laurent. “Exact and Approximate Construction of Digital Phase Modulations by Superposition of Amplitude Modulated Pulses (AMP)”. In: *IEEE Transactions on Communications* 34.2 (1986), pp. 150–160 (cit. on pp. 5, 10, 11, 21, 25, 50, 56, 71, 96).

[Leu04] Geert Leus. “On the estimation of rapidly time-varying channels”. In: *Signal Processing Conference, 2004 12th European*. IEEE. 2004, pp. 2227–2230 (cit. on pp. 100, 104).

[LGC18] Zilong Liu, Yong Liang Guan, and Chee-Cheon Chui. “CPM Training Waveforms With Autocorrelation Sidelobes Close To Zero”. In: *IEEE Transactions on Vehicular Technology* (2018) (cit. on pp. 132, 134).

[LNJP17] Adrien Le Naour, Elie Janin, and Charly Poulliat. “New perspectives for coded continuous phase modulations for narrowband waveforms: Iterative versus non-iterative solutions”. In: *Military Communications Conference (MILCOM), MILCOM 2017-2017 IEEE*. IEEE. 2017, pp. 489–494 (cit. on pp. 34, 35, 122).

[LSL06] Gottfried Lechner, Jossy Sayir, and Ingmar Land. “Optimization of LDPC codes for receiver frontends”. In: *Information Theory, 2006 IEEE International Symposium on*. IEEE. 2006, pp. 2388–2392 (cit. on p. 31).

[LTB11] Geert Leus, Zijian Tang, and Paolo Banelli. “Estimation of time-varying channels–a block approach”. In: *Wireless communications over rapidly time-varying channels*. Elsevier, 2011, pp. 155–197 (cit. on pp. 100, 106, 108–110).

[MA01] Pär Moqvist and Tor M Aulin. “Serially concatenated continuous phase modulation with iterative decoding”. In: *IEEE Transactions on Communications* 49.11 (2001), pp. 1901–1915 (cit. on p. 16).

[MD97] Umberto Mengali and Aldo N. D’Andrea. *Synchronization Techniques for Digital Receivers*. Springer Science & Business Media, 1997 (cit. on pp. 4, 10).

[Mes+16] Malek Messai et al. “Binary CPMs with improved spectral efficiency”. In: *IEEE communications letters* 20.1 (2016), pp. 85–88 (cit. on pp. 5, 10, 32, 33, 135).

[MFG97] P. A. Murphy, G. E. Ford, and M. Golanbari. “MAP symbol detection of CPM bursts”. In: *Proc. Virginia Tech. Symp. Wireless Pers. Commun.* (1997), pp. 1–12 (cit. on pp. 53, 93).

[MM00] M. Morelli and U. Mengali. “Carrier-frequency estimation for transmissions over selective channels”. In: *IEEE Transactions on Communications* 48.9 (2000), pp. 1580–1589 (cit. on pp. 71, 72, 80, 81, 113).

[MM95] Umberto Mengali and Michele Morelli. “Decomposition of M-ary CPM signals into PAM waveforms”. In: *IEEE Transactions on Information Theory* 41.5 (1995), pp. 1265–1275 (cit. on pp. 23, 71).

[NS01] Antonio Napolitano and Chad M Spooner. “Cyclic spectral analysis of continuous-phase modulated signals”. In: *IEEE Transactions on Signal Processing* 49.1 (2001), pp. 30–44 (cit. on p. 25).

[Nse+07] Jimmy Nsenga et al. “Comparison of OQPSK and CPM for communications at 60 GHz with a nonideal front end”. In: *EURASIP Journal on Wireless Communications and Networking* 2007.1 (2007), pp. 51–51 (cit. on pp. 3, 9, 16).

[OKD09] Baris Ozgul, Mutlu Koca, and Hakan Deliç. “Double turbo equalization of continuous phase modulation with frequency domain processing”. In: *IEEE Transactions on Communications* 57.2 (2009), pp. 423–429 (cit. on pp. 46, 55, 58, 59, 61, 132, 134).

[OLS18] Rami Othman, Yves Louët, and Alexandre Skrzypczak. “Joint Channel Estimation and Detection of SOQPSK Using the PAM Decomposition”. In: *2018 25th International Conference on Telecommunications (ICT)*. IEEE. 2018, pp. 154–158 (cit. on pp. 4, 10, 88).

[OSL17] Rami Othman, Alexandre Skrzypczak, and Yves Louët. “PAM Decomposition of Ternary CPM With Duobinary Encoding”. In: *IEEE Transactions on Communications* 65.10 (2017), pp. 4274–4284 (cit. on pp. 5, 10, 32, 33, 88, 135, 136).

[Per+10] Alberto Perotti et al. “Capacity-achieving CPM schemes”. In: *IEEE Transactions on Information Theory* 56.4 (2010), pp. 1521–1541 (cit. on pp. 5, 10, 34, 122).

[PHR09] Cheol-Hee Park, Robert W Heath, and Theodore S Rappaport. “Frequency-domain channel estimation and equalization for continuous-phase modulations with superimposed pilot sequences”. In: *IEEE Transactions on Vehicular Technology* 58.9 (2009), p. 4903 (cit. on p. 61).

[PR05] Erik Perrins and Michael Rice. “PAM decomposition of M-ary multi-h CPM”. In: *IEEE Transactions on Communications* 53.12 (2005), pp. 2065–2075 (cit. on p. 23).

[PT87] A-N Premji and D Taylor. “A practical receiver structure for multi-h CPM signals”. In: *IEEE transactions on communications* 35.9 (1987), pp. 901–908 (cit. on p. 19).

[PV06] Fabrizio Pancaldi and Giorgio Matteo Vitetta. “Equalization algorithms in the frequency domain for continuous phase modulations”. In: *IEEE Transactions on Communications* 54.4 (2006), pp. 648–658 (cit. on pp. 3, 5, 10, 11, 38, 46, 50, 52, 53, 55, 59–61, 91, 93, 132, 134, 146).

[Rad+15] Bilel Raddadi et al. “Channel estimation with a priori position for aeronautical communications via a satellite link”. In: (2015), pp. 532–537 (cit. on pp. 65, 105).

[Ran15] N. M. Range. *Commanders Council White Sands Missile Range IRIG Standard 106–15: Telemetry Standards Secretariat*. 2015 (cit. on p. 16).

[RB74] DCBP Rife and Robert Boorstyn. “Single tone parameter estimation from discrete-time observations”. In: *IEEE Transactions on information theory* 20.5 (1974), pp. 591–598 (cit. on pp. 69, 70, 79, 125).

[RBL05] Luca Rugini, Paolo Banelli, and Geert Leus. “Simple equalization of time-varying channels for OFDM”. In: *IEEE communications letters* 9.7 (2005), pp. 619–621 (cit. on p. 97).

[RBL06] Luca Rugini, Paolo Banelli, and Geert Leus. “Low-complexity banded equalizers for OFDM systems in Doppler spread channels”. In: *EURASIP Journal on Applied Signal Processing* 2006 (2006), pp. 248–248 (cit. on pp. 96, 100, 102).

[RCT16] RCTA. *Command and Control (C2) Data Link Minimum Operational Performance Standards (MOPS) (Terrestrial)*. 2016 (cit. on pp. 1, 7, 16, 118).

[Rim88] Bixio E Rimoldi. “A decomposition approach to CPM”. In: *IEEE Transactions on Information Theory* 34.2 (1988), pp. 260–270 (cit. on pp. 20, 34, 139).

[RP17] Michael Rice and Erik Perrins. “A comparison of frequency-domain equalization techniques in aeronautical telemetry”. In: *Proc. IEEE LATINCOM* (2017), pp. 1–6 (cit. on p. 46).

[RPT95] Riccardo Raheli, Andreas Polydoros, and Ching-Kae Tzou. “Per-survivor processing: A general approach to MLSE in uncertain environments”. In: *IEEE Transactions on Communications* 43.234 (1995), pp. 354–364 (cit. on p. 88).

[Sim05] Marvin K Simon. *Bandwidth-efficient digital modulation with application to deep space communications*. Vol. 2. John Wiley & Sons, 2005 (cit. on pp. 3, 9).

[SS08] Matthew Sharp and Anna Scaglione. “Estimation of sparse multipath channels”. In: *Military Communications Conference, 2008. MILCOM 2008. IEEE*. IEEE. 2008, pp. 1–7 (cit. on pp. 65, 105).

[Tan07] Zijian Tang. “Ofdm transmissions over rapidly changing channels”. PhD thesis. TU Delft, Delft University of Technology, 2007 (cit. on p. 104).

[TG96] Michail K Tsatsanis and Georgios B Giannakis. “Modelling and equalization of rapidly fading channels”. In: *Int. J. on Adapt. Control* 10.2-3 (1996), pp. 159–176 (cit. on pp. 100, 104).

[Thi+09] W. Van Thillo et al. “Training Sequence Versus Cyclic Prefix for CPM with Frequency Domain Equalization”. In: *IEEE Global Telecommunication Conference (GLOBECOM), Honolulu, HI*. 2009, pp. 1–5 (cit. on pp. 42, 43).

[TO05] Kok Ann Donny Teo and Shuichi Ohno. “Optimal MMSE finite parameter model for doubly-selective channels”. In: *IEEE GLOBECOM*. Vol. 6. IEEE. 2005, 5–pp (cit. on pp. 100, 104).

[TS05] Jun Tan and Gordon L Stuber. “Frequency-domain equalization for continuous phase modulation”. In: *IEEE Transactions on Wireless Communication*. Vol. 4. 5. 2005, pp. 2479–2490 (cit. on pp. 3, 5, 10, 11, 46, 60, 139, 141, 143–146).

[TV00] Timothy A Thomas and Frederick W Vook. “Multi-user frequency-domain channel identification, interference suppression, and equalization for time-varying broadband wireless communications”. In: *Sensor Array and Multichannel Signal Processing Workshop. 2000. Proceedings of the 2000 IEEE*. IEEE. 2000, pp. 444–448 (cit. on p. 104).

[Vis96] M. Visintin. “Karhunen-Loeve expansion of a fast Rayleigh fading process”. In: *Electronics Letters* 32.18 (1996), pp. 1712– (cit. on pp. 100, 104).

[Vit67] Andrew Viterbi. “Error bounds for convolutional codes and an asymptotically optimum decoding algorithm”. In: *IEEE transactions on Information Theory* 13.2 (1967), pp. 260–269 (cit. on p. 26).

[VKG14] Martin Vetterli, Jelena Kovačević, and Vivek K Goyal. *Foundations of signal processing*. Cambridge University Press, 2014 (cit. on p. 44).

[VT+09] Wim Van Thillo et al. “Low-complexity linear frequency domain equalization for continuous phase modulation”. In: *IEEE Transactions on Wireless Communications* 8.3 (2009), pp. 1435–1445 (cit. on pp. 3, 5, 10, 11, 38, 46, 49, 50, 53–61, 91, 96).

[WGPS11] Marilynn P Wylie-Green, Erik Perrins, and Tommy Svensson. “Introduction to CPM-SC-FDMA: A novel multiple-access power-efficient transmission scheme”. In: *IEEE transactions on communications* (2011) (cit. on pp. 3, 9).

[Wit+02] Harald Witschnig et al. “A different look on cyclic prefix for SC/FDE”. In: *Personal, Indoor and Mobile Radio Communications, 2002. The 13th IEEE International Symposium on*. Vol. 2. IEEE. 2002, pp. 824–828 (cit. on pp. 41, 42).

[Xu+09] X. Xu et al. “Low-complexity fractional-spaced equalization approach in the frequency domain for CPM”. In: *2009 9th International Symposium on Communications and Information Technology*. 2009, pp. 1301–1306 (cit. on p. 46).

[Yue06] Joseph H Yuen. *Autonomous software-defined radio receivers for deep space applications*. Vol. 13. John Wiley & Sons, 2006 (cit. on pp. 3, 9).

[ZM05] Thomas Zemen and Christoph F Mecklenbrauker. “Time-variant channel estimation using discrete prolate spheroidal sequences”. In: *IEEE Trans. on Signal Processing* 53.9 (2005), pp. 3597–3607 (cit. on p. 104).

Résumé — Si les drones militaires connaissent un développement important depuis une quinzaine d'année, suivi depuis quelques années par les drones civiles dont les usages ne font que se multiplier, en réalité les drones ont un siècle avec le premier vol d'un avion équipé d'un système de pilotage automatique sur une centaine de kilomètre en 1918. La question des règles d'usage des drones civiles sont en cours de développement malgré leur multiplication pour des usages allant de l'agriculture, à l'observation en passant par la livraison de colis. Ainsi, leur intégration dans l'espace aérien reste un enjeu important, ainsi que les standards de communication avec ces drones dans laquelle s'inscrit cette thèse.

Cette thèse vise en effet à étudier et proposer des solutions pour les liens de communications des drones par satellite. L'intégration de ce lien de communication permet d'assurer la fiabilité des communications et particulièrement du lien de Commande et Contrôle partout dans le monde, en s'affranchissant des contraintes d'un réseau terrestre (comme les zones blanches). En raison de la rareté des ressources fréquentielles déjà allouées pour les futurs systèmes intégrant des drones, l'efficacité spectrale devient un paramètre important pour leur déploiement à grande échelle et le contexte spatiale demande l'utilisation d'un système de communication robuste aux non-linéarités. Les Modulations à Phase Continue permettent de répondre à ces problématiques. Cependant, ces dernières sont des modulations non-linéaire à mémoire entrainant une augmentation de la complexité des récepteurs.

Du fait de la présence d'un canal multi-trajet (canal aéronautique par satellite), le principal objectif de cette thèse est de proposer des algorithmes d'égalisation (dans le domaine fréquentiel pour réduire leur complexité) et de synchronisation pour CPM adaptés à ce contexte tout en essayant de proposer une complexité calculatoire raisonnable. Dans un premier temps, nous avons considéré uniquement des canaux sélectifs en fréquence et avons étudier les différents égaliseurs de la littérature. En étudiant leur similitudes et différences, nous avons pu développer un égaliseur dans le domaine fréquentiel qui proposant les mêmes performances a une complexité moindre. Nous proposons également des méthodes d'estimation canal et une méthode d'estimation conjointe du canal et de la fréquence porteuse. Dans un second temps nous avons montré comment étendre ces méthodes à des canaux sélectifs en temps et fréquence permettant ainsi de conserver une complexité calculatoire raisonnable.

Mots clés : Continuous Phase Modulation, Détection, Égalisation, Synchonisation, Estimation canal, Canaux sélectif en fréquence, Canaux sélectifs en temps et en fréquence

Abstract — If the use of Unmanned Aerial Vehicles (UAV) has been booming for military applications since a decade, followed by civil applications since a few years (with a lot of completely different purposes), the first UAV has been developed and tested in 1918 with the first flight of a fight with the first autopilot system. The issue of a complete and safe integration in the existing air traffic aircraft system is currently being studied as the multiple use cases of UAV are growing exponentially from agriculture, observation and package delivery. Hence, the integration of UAV in the air traffic system is a global issue, and so are the communication standard in which the thesis take place.

This thesis aims to study and propose solutions for the communication link by satellite for UAV. This satellite link would ensure the reliability of the system, and above all of the Command and Control Link, by avoiding the issue of a terrestrial communication network (such as over the ocean, where no terrestrial network is available). Due to spectral resource lack already allocated for the UAV, the spectral efficiency of the communication link is a critical issue, as its robustness to non-linearity due to the spatial context. Continuous Phase Modulation is a potential solution to answer to those issues. However, this will lead to an increased computational complexity at the receiver compared to linear modulation scheme.

The aeronautical channel by satellite is characterized by a doubly-selective channels due to Ground Reflections of the signal, and in this thesis, we proposed equalization algorithms and synchronization techniques for CPM in this context while trying to keep a reasonable computational complexity. First, we have only considered transmission over frequency-selective channels. We have made a study of the equalizers proposed by the literature and by studying their similitudes and differences, we have been able to propose a new equalizer with a lower computational complexity but having the same performance. We also have proposed a channel estimation method and a joint channel and carrier frequency estimation for CPM over frequency-selective channels. In a second time, we have extended our method to doubly-selective channel (as there is Doppler Spread in our communication system due to the UAV speed) which allows us to have an overall receiver structure with a reasonable computational complexity.

Keywords: Continuous Phase Modulation, Detection, Equalization, Synchronization, Channel estimation, frequency selective channels, frequency and time selective channels

TéSA/Toulouse INP, 7 Boulevard de la Gare
31500 Toulouse